12-2010

DEVELOPMENT AND CHARACTERIZATION OF NOVEL SUB-COATINGS WITH POLYMORPHIC BROOKITE TITANIA NANOPARTICLES: ENHANCED UV/VIS PHOTOCATALYTIC ANTIBACTERIAL AND ANTICANCER PROPERTIES

Donna Weinbrenner
Clemson University, drweinbrenner@gmail.com

DEVELOPMENT AND CHARACTERIZATION OF NOVEL SUB-COATINGS WITH POLYMORPHIC BROOKITE TITANIA NANOPARTICLES: ENHANCED UV/VIS PHOTOCATALYTIC ANTIBACTERIAL AND ANTICANCER PROPERTIES

A Dissertation
Presented to
the Graduate School of
Clemson University

In Partial Fulfillment
of the Requirements for the Degree
Doctor of Philosophy

---

by
Donna Ruth Armstrong Weinbrenner
December 2010

Accepted by:
Dr. Tzuen-Rong Jeremy Tzeng, Committee Chair
Dr. Burtrand Lee
Dr. Yong Huang
Dr. Lisa Bain

ABSTRACT

Nosocomial and community infections and biofilm formation from bacteria has increased significantly through adaptation combined with overuse of broad spectrum antibiotics. Because the world population continues to escalate, hospitals and long-term managed care will also escalate, thereby increasing transmission of infections, lowering patients' quality of health. Another disease on the rise throughout the world is skin cancer. A treatment modality that would cause less deleterious effects on the patient would be ideal. These two seemingly different issues could be solved with one product. First an inexpensive, safe, and non-selective antimicrobial surface coating would enhance the hospital arena and a coating that would treat skin cancer like wearing a band-aid would be patient friendly. We proposed two novel sub-coatings containing polymorphic Titanium dioxide, Br200 and BrNMP. Titanium dioxide is versatile, non-selective, and degrades compounds through photocatalytic oxidation.

The antibacterial sub-coating made of Poly(diallyldimethylammonium chloride) solution (PDDA) and Poly(4-styrenesulfonic acid) solution (PSS) in a 1:1 ratio of 0.1M PDDA/PSS as a 25 layer-by-layer coating on glass cover slips is known as the P sub-coating. It contains Nitrogen and Sulfur molecules that were associated via low temperature liquid deposition with Br200 or BrNMP Titania. XRD and XPS evaluations of these P sub-coatings containing the polymorphic Br200 and BrNMP confirmed a match with the original properties of the loose nanoparticles. P sub-coating with these Titania under long range ultraviolet light and visible light were evaluated for Methyl Orange oxidative-degradation to quantify photocatalytic activity. UVA irradiation of

Br200 and BrNMP on the P sub-coating degraded Methyl Orange approximately two times faster than the same Titania on the control B sub-coating. The B sub-coating consisted of five mol of 3-glycidoxypropyl-trimethoxysilane mixed with 3 mol of Tetramethyl orthosilicate, prehydrolyzed with Ethanol and brought to pH 3 with Nitric acid.

Light intensity, wavelength, surface material characteristics, and bacterial load affect efficiency of photo-oxidation. The super-hydrophilic nature of the polyelectrolyte-Titania coating may attract and enhance photo-oxidative activity due to bacterial adherence via hydrophilic fimbriae that attach to biotic and abiotic surfaces. Br200 demonstrated a stable working pH range including pH 3 to 4. The broad absorption edge of the polymorphic Brookite Titania Br200 and BrNMP enhanced by the N and S molecule surface interactions, and a narrowing of the band-gap, of the P sub-coating exhibited superior photocatalytic oxidative degradation on bacteria compared to the commercial P25 and vlp7000 Titania, or binder sub-coating with Titania. The polymorphic nature of Br200 and BrNMP may delay the electron/hole recombination centers due to electron transfer to different phases of crystallites.

The LB sub-coating provided the polymorphic Titania with superior photocatalytic activity as compared to the P25 commercial product in vitro on HT-29 human colon cancer cells and HTB-67 Human Melanoma cells. The novel P sub-coating with polymorphic Brookite Titania can provide a low cost, effective method for decreased transmission of bacterial infections and biofilm formation in the healthcare arena and community setting. The novel format of using FDA approved liquid band-aid

coated with Br200 non-selective Titania coating can provide lower pain and scarring in a topical format cancer treatment.

DEDICATION

I dedicate my dissertation to both my adoptive and natural parents, and my children, respectively. E. Donald and Wilma I. Armstrong, who through their love and upbringing provided me with the opportunity to explore my physical, artistic, and academic interests. Lee and Ann Hunt who through their love, support, and encouragement got me through these final years of effort. To my eldest daughter Jordan Ashley, I give thanks for her love, understanding, support, and constant belief in me over the years to achieve my goals. To my youngest daughter Jessica Marie and my son Steven Matthew, I hope that they are proud of me for my dedication and perseverance to attain my doctoral degree.

ACKNOWLEDGMENTS

First, I would like to thank Dr. Tzuen-Rong Jeremy Tzeng, my advisor and mentor. He offered me the opportunity to work on this project. He allowed me to design this project and carry it out, giving guidance and suggestions when needed. He has encouraged me to voice my opinions giving me confidence in my knowledge and skills. I am deeply appreciative of his insight that has allowed me to flourish. I realize that it takes someone who is secure with himself in his knowledge and expertise to offer this type of guidance and mentorship.

I give many thanks to Dr. Alfred P. (Hap) Wheeler, the Biological Sciences Department Chair. He was supportive of everything I needed to help me attain my degree. His suggestions and problem-solving skills were appropriate and helpful.

I would like to acknowledge my committee members: Dr. Burtrand Lee, Dr. Yong Huang, and Dr. Lisa Bain for their time, effort, expertise, for the different areas of knowledge each one represents aiding me in the successful completion of my research and dissertation.

I have special thanks and acknowledgement to Dr. Diana Ivankovic, who gave me constant encouragement, helped support this research monetarily, and provided me with students, Isaac Stovall, Raychel Holtel, Brittany Hall, and Sierra Davis to aid in experiments.

I give many thanks to Dr. George Huang, for his expertise and countless hours of tissue culture maintenance and experimental preparations.

I acknowledge and give special thanks to Sujaree Kaewgun for providing me with all of the Titanium dioxide samples with in which to perform this research.

I acknowledge and thank Kim Ivey for her expertise, time, and effort to perform the FT-IR samples.

I also acknowledge and thank Don Van Derveer for his expertise, time and effort to perform the XRD measurements on my samples.

I also wish to thank Jonathan Boguski for his polite manner and many hours of superb, efficient work. And, my friend Lee Bryson for coming in during the summer to aid in experiments and grammar review of my dissertation.

TABLE OF CONTENTS

Page

TITLE PAGE i

ABSTRACT ii

DEDICATION v

ACKNOWLEDGMENTS vi

LIST OF TABLES xi

LIST OF FIGURES xii

CHAPTER

I. INTRODUCTION 1

1.1 Uses and Characteristics of Titania as a Photocatalyst 1

1.2 Significance of Bacteria, Biofilm, and Overuse of Antibiotics 3

1.3 Significance of Skin Cancer and Current Treatments 6

1.4 Relevant Previous Research by Our Collaborators 8

1.5 Relevant Previous Research by Our Lab 8

1.6 Significance of This Research to the Scientific Community 9

1.7 Research Objectives 10

1.8 References 13

II. LITERATURE REVIEW 20

2.1 Titania, Characteristics, Current Products, and Uses 20

2.2 Bacteria, Biofilm, and Overuse of Antibiotics 22

2.3 Skin Cancer 25

2.4 References 27

TABLE OF CONTENTS (Continued)

Page

III. DEVELOPMENT, CHARACTERIZATION, AND PHOTOCATALYTIC ACTIVITY OF LIGHT ACTIVATED POLYMORPHIC BROOKITE TITANIA ENHANCED VIA NOVEL SUB-COATTINGS ON *Escherichia coli*.....34
3.1 Abstract.....34
3.2 Introduction.....37
3.3 Results.....46
3.4 Discussion.....58
3.5 Conclusions.....62
3.6 Experimental.....66
3.7 References.....75

IV. EFFECTS OF PHOTOCATALYTICALLY ACTIVATED POLYMORPHIC BROOKITE TITANIA NANOPARTICLE WITH ENHANCED VIA NOVEL SUB-COATTINGS ON CANCER CELL VIABILITY *in vitro*.....107
4.1 Abstract.....107
4.2 Introduction.....108
4.3 Results.....111
4.4 Discussion.....112
4.5 Conclusions.....112
4.6 Experimental.....113
4.7 References.....117

V. CONCLUSIONS AND RECOMMENDATIONS.....134

TABLE OF CONTENTS (Continued)

Page

APPENDICES……140

A: LAMP WAVELENGTH SPECTRA……141

A.1 Visible Wavelength Spectra..... 142

A.2 UVA Wavelength Spectra 143

B: XPS SPECTRA GRAPHS OF TITANIA ON P OR B SUB-COATINGS 144

C: XRD SPECTRA GRAPHS OF TITANIA ON P OR B SUB-COATINGS 212

D. P SUB-COATING STRUCTURES AND COMPONENTS 223

LIST OF TABLES

Table Page

3.9.1 Surface chemical analysis P25 or Br200 Titania in powder Form 104

3.9.2 Surface chemical [Mass] % analysis of P or B Sub-coatings with or without Titania..... 105

3.9.3 Hydrophilicity measured by contact angle on P or B Sub-Coatings with or without Titania 106

LIST OF FIGURES

Figure		Page
3.8.1 A	[a]XPS spectra graph of PSS/PDDA sub-coating	82
3.8.1 B	[b]XPS spectra graph of PSS/PDDA sub-coating with commercial P25 Titania	83
3.8.1 C	[c]XPS spectra graph of PSS/PDDA sub-coating with Br200 Titania	84
3.8.1 D	[c]XPS spectra graph of PSS/PDDA sub-coating with BrNMP Titania	85
3.8.1 E	[c]XPS spectra graph of PSS sub-coating with vlp7000 Titania	86
3.8.2	X-ray diffraction spectra of the PDDA/PSS sub-coating with or without Titania	87
3.8.3	X-ray diffraction spectra of the Binder sub-coating with or without Titania	88
3.8.4	Hydrophilicity of PDDA/PSS and Binder sub-coating with and without Titania	89
3.8.5	Photocatalytic Activities of Titania Coatings Under UVA	90
3.8.6	Photocatalytic Activities of Titania Coatings Under Visible Light	91
3.8.7	Activated TiO_2 exposed to *Escherichia coli* B at pH 7.4 in water or PBS for 120 Minutes	92
3.8.8	TiO_2 Degradation of *Escherichia coli* B with or without UV at 0, 30, 75, or 120 Minutes in Water at pH 4.0	93
3.8.9	Static Contact Angle	94

LIST OF FIGURES (Continued)

Figure		Page
3.8.10	BacLight Fluorescent Assay Linearity Range on *Escherichia coli* B with p values less than 0.05	95
3.8.11	Bac-Titer-Glo™ Luminescent Assay Linearity Range on *Escherichia coli* B with p values less than 0.05	96
3.8.12	Effects of UVA Activated P25, Br200 and BrNMP Titania 1 mg/mL in Free Suspension on *E. coli* B: *Bac*Light ™Assay with p values less than 0.01	97
3.8.13	Effects of UVA Activated P25 and Br200 Titania 1 mg/mL in Free Suspension on *E. coli* B	98
3.8.14	Effects of Visible Light Activated VLP7000, Br200 and BrNMP Titania 1mg/mL in Free Suspension on *E. coli* B	99
3.8.15	Effects of UVA Light Activated P-25, Br200 and BrNMP Titania (2mg) on the PDDA/PSS Sub-coating on *E. coli* B for 0-60 Minutes	100
3.8.16	Effects of UVA Light Activated P-25, Br200 and BrNMP Titania (2mg) on the Binder Sub-coating on *E. coli* B for 0-60 Minutes	101
3.8.17	Effects of Visible Light Activated VLP7000, Br200 and BrNMP Titania (2mg) with PDDA/PSS Sub-coating on *E. coli* B for 0-60 Minutes	102
3.8.18	Effects of Visible Light Activated VLP7000, Br200 and BrNMP Titania (2mg) with Binder Sub-coating on *E. coli* B for 0-60 Minutes	103
4.8.1	FT-IF Spectral Graphs of P25 with and without Liquid Band-Aid	128
4.8.2	FT-IF Spectral Graphs of Br200 with and without Liquid Band-Aid	129

LIST OF FIGURES (Continued)

Figure Page

4.8.3 Representative Photos of Live/Dead Cytocompatibility HTB-67 Human Malignant Melanoma Cells exposed to Dark *in vitro* 130

4.8.4 Representative Photos of Live/Dead Cytocompatibility HTB-67 Human Malignant Melanoma Cells with and without Titania exposed to UVA *in vitro* 131

4.8.5 Effects of UVA photoactivation on HTB-67 Melanoma cells by Br200 or P25 with or without Liquid Band-Aid with p values ranging from 0.01 to 0.00003..... 132

4.8.6 Effects of UVA photoactivation on HT-29 Colon Cancer cells by Br200 or P25 with or without Liquid Band-Aid with p values ranging from 0.02 to 0.00003..... 133

CHAPTER ONE

INTRODUCTION

1.1 Uses and Characteristics of Titania as a Photocatalyst

Titanium dioxide is a versatile compound that is used in many applications, industries, materials, and products throughout the world. It is used in pigments due to its extremely high refractive index of n = 2.7 [1]. The Huntsman Pigments Company, (Billingham, England) produces Rutile phase pigments for architectural paints for use in highly opaque surface coatings, powder coatings, plastics, inks, and paper applications. Anatase phase pigment is used for delustring synthetic fibers such as polyester and optical brighteners in ceramics. Photovoltaic solid-state hetero-junctions comprising a dense TiO_2 film electrode as an electron conductor is another product [2]. In a medical application, a high compressive strength (>2 MPa) titanium oxide scaffold may be used in bone [3]. Hair dye, sun screens, and cosmetics are popular Titania containing products [4]. Chemical vapor deposition using Anatase phase for self-cleaning, super hydrophilic, antimicrobial glass [5]. Photomineralization with air and water purification, photoelectrodes as a hydrolysis catalyst, and photosterilization in sterilizing, deodorizing, and anti-fouling methods and products are all applications of Titania [6-7].

Characteristics of Titania or Titanium (IV) dioxide exhibit three polymorphic lattice phases, Rutile, Anatase, and Brookite. The most thermodynamically stable phase is Rutile because it has minimal electrostatic repulsive energy. Rutile is formed in a linear structure that is tetragonal and two of the twelve edges are shared in the octahedron [8]. Anatase phase is also tetragonal and shares four edges per octahedron without corner

oxygen sharing. Brookite is unique with three shared edges per octahedron in an orthorhombic composure. Zallen and Moret measured the optical absorption edge of Brookite Titania and saw that its phase extends throughout the visible light range [9]. Brookite was observed to have a broad absorption edge in contrast to the steep absorption edges of Anatase and Rutile. No evidence of a direct gap was observed in the evaluated spectral range. It was proposed that Brookite phase Titania is an indirect-gap semiconductor with an approximate bandgap of 1.9 eV [9]. In contrast, calculations using the self-consistent orthogonalized linear-combination-of-atomic-orbitals method, Mo and Ching, 1995 approximated a direct bandgap for Brookite [10]. Other researchers have determined that all three phases of Titania have similar direct bandgap energies (~3.1 $\pm$ 0.1 eV) [11]. Banerjee and colleagues report different bandgap values for each phase, Anatase (3.2 eV), Rutile (3.02 eV), and Brookite (2.96 eV) [12]. Whether direct or indirect, Brookite phase Titania exhibits the lowest bandgap energy.

Characteristics of a photocatalyst were described as its ability to simultaneously adsorb two reactants [12]. Then efficiently absorb light ($h\nu \geq E_g$) to reduce and oxidize the adsorbed reactants. In order to excite the electron (e^-) from the valence band to the conduction band producing an e^--h^+ pair, the absorbed light energy must be equal or larger than the bandgap without being consumed. The produced hydroxyl radicals oxidize holes in the cells walls / membranes allowing the contents to leak out and also be degraded. Superoxide anions ($\cdot O_2^-$) can enter the cells through the holes in the cell walls and produce Reactive oxygen species (ROS), such as H_2O_2 molecules that will decompose DNA via the Fenton Reaction.

Ions such as Phosphate have a very high affinity for Titania and can significantly decrease the photocatalytic activity. The substrate, ions, diluent, surface roughness, hydrophilicity or hydrophobicity, morphology, particle size, surface area, and crystal structure, absorption edge type, direct or indirect bandgap, bandgap size, number of exposed active sites, are all factors that influence the amount of photocatalytic activity on Titania [12].

1.2 Significance of Bacteria, Biofilm, and Overuse of Antibiotics

Significant overuse of broad spectrum antibiotics has escalated the emergence of bacterial resistance. These Multi-Drug Resistant (MDR) bacterial infections increase the morbidity and mortality of patients. Therefore, nosocomial infections of bacteria such as *Staphylococcus aureus, Acinetobacter baumannii, Escherichia coli* are expected to rise. The CDC states that approximately 65% of infections are found in biofilms.

Currently, antibiotics provide a selective method of bacterial elimination, but are losing the battle against emerging resistant pathogens. A rising problem consists of bacteria sharing plasmids, crossing specie boundaries. In Brooklyn, New York three hospitals isolated *E. coli* from UTIs that possessed 23-kb plasmid encoding *Klebsiella pneumonia* carbapenemase type 2 (KPC-2) and increasingly containing the gene $bla_{\text{KPC-2}}$ [13]. The gram-negative multi-drug-resistant (MDR) bacteria *Acinetobacter baumannii* is ubiquitous and can be isolated from water, soil, animals, humans, and other environmental sources [14]. It is aerobic and an opportunistic pathogen escalating nosocomial outbreaks in intensive-care-units (ICU) and burn units [15] [16] [17]. The

mechanisms which allow for such MDR in *A. baumannii* could be that they amass quickly and exchange genetic information easily [16, 18]. Recently a clinical isolate of that produced extended-spectrum β-lactamase but was carbapenem-susceptible, contained more than 40 identified resistance genes [19]. This unique class of Gram-negative bacteria may easily share genetic pools where prevalent clonal groups of *A. baumannii* co-exist via horizontal gene transfer [16, 18, 20]. Clonal expansion may work additionally to increase resistance [20].

Another method of resistance is chromosomal cassette transfer [21]. DNA damaging antibiotics depress SOS-regulated polymerases via LexA cleavage inducing resistant mutations [22]. SOS-independent response increased frameshift mutations when exposed to β-lactam antibiotics [23]. *A. baumannii* contains an over-expressed efflux pump affecting many type of antibiotics [24]. Sub-lethal levels of antibiotics induce mutagenesis via reactive oxygen species (ROS). The bacteria remained sensitive to the utilized antibiotic, but increased mutant strains that were resistant to other antibiotics [25].

Another mechanism that bacteria use to protect themselves is by creating and living in biofilms [26]. Bacteria change from planktonic to sessile existence through attachment to surfaces. Generating a gooey matrix and signaling (quorum sensing (QS)) one another to proliferate into a microcolony, offers a selective advantage to increase their survival rate. [27]. Other species of bacteria may join the colony due to QS signals released into the environment. These chemical gradients allow for a diverse species to coexist. Lastly, some cells escape from the colony and return to the planktonic state

moving and landing in a different location to start the process of biofilm formation again. Biofilms are ubiquitous and the CDC estimates that biofilms are involved in at least 65% of all infections [28].

Reisner and colleagues determined that biofilm formation was significantly dependent on growth medium composition [29]. Specific adhesion to $_{D}$-mannose demonstrated direct binding of FimH type 1 pili which is serologically conserved throughout Enterobacteriaceae [30]. EC and many other species of bacteria contain hydrophilic fimbriae that attach to biotic and abiotic surfaces [31-32].

E. coli B was chosen as the model bacteria in this work was for the following reasons. First, *E. coli* B contains the *fimH* gene, which codes for the hydrophilic FimH subunit of type 1 pili conferring attachment to biotic and abiotic surfaces. QS in *E. coli* is capable of binding to and responding to exogenous Acetylhomoserine lactone (AHL), and regulate target gene expression and adjust cellular functions to match the environment [33].

When microorganisms attach to a surface and grow as biofilm, they become less susceptible to antimicrobials than the same microbes in planktonic growth. Several factors are responsible for biofilm resistance including restricted penetration of antimicrobials into a biofilm, decreased growth rate, and expression of resistance genes [34-36].

Exopolymer matrix of biofilms can restrict diffusion of drugs. Diffusion rate in a biofilm is approximately 20 to 80 percent of that in free floating planktonic state [37]. The negatively charged exopolysaccharide is also effective against positively charged

antibiotics retarding permeation [38-39]. Another biofilm-reduced susceptibility could be contributed to the slower growing rate or non-growing status, or increased stress responses of microbial cells in biofilm due to limited diffusion of oxygen, nutrients, or starvation protecting the biofilm from environmental stresses [40] [41].

Different strategies [26] to prevent or eradicate bacteria biofilms include: prevention of attachment or QS [42-45]. A super-hydrophilic surface with a contact angle of $<5^{o}$ is used and may attract the hydrophilic heads of bacterial fimbriae to the surface [46]. Hydroxyl radicals would successively attack the bacterial cell walls and membranes through the photocatalytic activity of the UVA or visible light (VL) irradiated surface. Titanium dioxide water structure at the TiO_2/aqueous interface is significantly dependent on the specific nature of the ions present in the diluent and the pH for optimized photocatalytic activity.

1.3 Significance of Skin Cancer and Current Treatments

In the United States Skin cancer is the most common form of cancer with basal cell and squamous cell carcinomas being the two highest common types. Malignant Melanoma is highly dangerous among younger people. Exposure to ultraviolet (UV) light or sunlight, or tanning beds, or other sources of man-made UV such as fingernail polish curing with UV causes approximately 65%–90% of melanomas [47]. In the U.S. in 2006, 53,919 people were diagnosed with skin melanomas and 8,441 people in the United States died from skin melanomas [48]. Protection from UV light will prevent most skin cancers [47]. People living in areas of the earth that receive high levels of UV radiation

are at higher risk developing skin cancer [49]. Skin cancer is an accumulative phenomenon and is related to lifetime exposure to UV radiation. The time of day such as midday presents a higher chance of cancer. Normal skin or in an existing mole can becomes cancerous; Melanoma can develop anywhere on your body. Indicators of Melanoma include moles with irregular borders and different colors, lesions on palms of hands or feet, large multicolored spots with darker speckles, a mole that changes color, size, or bleeds.

Exposure to photocatalytically activated Anatase phase Titanium dioxide resulted in a dose-dependent decrease of cell-viability in goldfish cells [50]. With similar results, another research group used TiO_2 nanoparticles (DeGussa) that were 75% Rutile and 25% Anatase crystalline phase in free suspension [51].

In human hepatoma Bel-7402 cells, apoptosis induced by the photocatalytically activated TiO_2 nanoparticles was determined to be the primary mechanism of cell death [52]. The small size with large surface area and unique characteristics of TiO_2 nanoparticles may facilitate absorption and transport across the barriers of mammalian epithelium (skin, lungs, and gut) followed with systemic entry to the circulatory system to secondary target organs and may even cross the blood-brain barrier to reside in the brain [53-54].

Opposing the above theory, Kiss and colleagues (2008) investigated the possibility of TiO_2 particles penetrating through the stratum corneum in human skin xenografts onto nude mice [55]. The stratum corneum funtioned to keep the TiO_2

nannoparticles from traveling further through intact skin. Photocatalytically activated Titania may prove to be a treatment modality for skin cancer.

1.4 Relevant Previous Research by Our Collaborators

The minimization of lattice defects and influennce of hydroxyl content were evaaluated. Water-based Ambient Condition Sol (WACS) post-treated by a Solvent-based Ambient Condition Sol (SACS) process in sec-butanol (sec-BuOH), processed primarily Brookite phase Titania. A polar solvent, N-methylpyrrolidone (NMP), was used to alter polymorphic Titania nanoparticles to increase photocatalytic activity by extracting lattice hydroxyls and adorn nitrogen on the surface of the Titania nanoparticles. The nanoparticles were well characterized and the photocatalytic activity was evaluated via Methyl orange oxidative degradation by exposure to either a 182 Watt UVA lamp or a 150 Watt Halogen lamp. Two types of polymorphic Titania were produced, Br200 and BrNMP.

1.5 Relevant Previous Research by Our Lab

A free suspension assay was developed and evaluated Titania nanoparticles under UVA (365 nm) exposure on bacteria. A working concentration of Titania in free suspension was established. While the method is accurate and highly reproducible, it used a lot of material, time, money, and labor. A preliminary coating study with Titania suspended and mixed in the Binder was undertaken.

Previous research was deficient in the following items. A complete death curve was never identified. Only UVA (365 nm) provided useable data. Titania was mixed with Binder provided by our collaborators. The method used, coated all sides of the crystal lattice, and cells numbers were not significantly reduced in 30 minutes of UVA exposure. A fast miniaturized assay was not created. Visible light exposure of Br200 and P25 in a free suspension assay only gained a 3 log reduction difference after 8 hours of exposure. BrNMP was not evaluated. From the above it is evident that the Specific Aims and Objectives of my research are different and advance the knowledge of this line of research.

1.6 Significance of This Research to the Scientific Community

The significance of the proposed research is to aid in the prevention of transmission of bacteria in the nosocomial and community settings. Developing a suitable coating for hospitals and long-term managed care facilities would enhance the patients' lives by preventing bacterial infections that can easily cause death, and increase the length of the patients' lives. The surface coating must be safe, effective, inexpensive, durable, and easy to install and care for. Therefore, two different types of polymorphic Brookite will be evaluated under UVA and VIS light separately, comparing them to the appropriate controls and commercial samples. Developing a sub-coating with the above characteristics, that will enhance the photocatalytic activity of the Titania, for work under VIS light irradiation in a timely manner. The success of this new research would

significantly enhance the well-being of people's lives in the nosocomial and community settings.

Even more differently, examination of these Titania with coatings for cancer treatments will be evaluated. Proving these novel methods and coatings work well would help cancer patients have less scarring and deleterious effects from cancer treatment. This new research would significantly enhance cancer patients' lives. Therefore, this research is different from prior work and has the possibility of significantly impacting the body of Science and increasing the quality of life significantly for many people.

Current Status

We have the two types of polymorphic Brookite Titania graciously provided to us by our collaborators, Dr. Lee and Dr. Kaewgun. Through prior evaluations with the free suspension bioassay, we have a partial death curve and a working concentration with in which to start our new and further developing research.

1.7 Research Objectives

Therefore my objectives for my research include the following:

- Modify and miniaturize the free suspension assay
- Adapt the modified and miniaturized assay for use with coatings
- Develop a sub-coating for the Titania, and characterize it to confirm a match with the original properties of the loose nanoparticles.

- Determine the death curve of each appropriate type of Titania under UVA in free suspension
- Determine the death curve of each appropriate type of Titania under VL in free suspension
- Evaluate the photocatalytic ability of free suspension Titania under UVA light on Methyl Orange oxidative-degradation to verify activity in the new assay format
- Evaluate the photocatalytic ability of free suspension Titania under VL light on Methyl Orange oxidative-degradation to verify activity in the new assay format
- Determine the death curve of each appropriate type of Titania under UVA on novel sub-coating with Titania
- Determine the death curve of each appropriate type of Titania under VL on novel sub-coating with Titania
- Evaluate the photocatalytic ability of sub-coating with appropriate Titania under UVA light on Methyl Orange oxidative-degradation to verify activity
- Evaluate the photocatalytic ability of sub-coating with appropriate Titania under VL light on Methyl Orange oxidative-degradation to verify activity in the new assay format
- Based upon those results, choose the best candidate for evaluation of the most active form of free suspension Titania on cancer cells *in vitro* as a feasibility proof of concept model

- Based upon those results, choose the best candidate for evaluation of a second novel sub-coating containing the most active form of Titania on cancer cells *in vitro* as a feasibility proof of concept model

1.8 References

1. Pigments, H., *Pigments.* 2010.
2. Johansson, E.M.J., et al., *Photovoltaic and Interfacial Properties of Heterojunctions Containing Dye-Sensitized Dense TiO2 and Tri-arylamine Derivatives.* Chemistry of Materials, 2007. **19**(8): p. 2071-2078.
3. Sabetrasekh, R. and et al., *Impact of trace elements on biocompatibility of titanium scaffolds.* Biomedical Materials, 2010. **5**(1): p. 015003.
4. Popov, A., et al. *Interaction of sunscreen TiO[sub 2] nanoparticles with skin and UV light: penetration, protection, phototoxicity.* 2009. Munich, Germany: SPIE.
5. Evans, P., et al., *A comparative study of three techniques for determining photocatalytic activity.* Journal of Photochemistry and Photobiology A: Chemistry, 2007. **188**(2-3): p. 387-391.
6. Srinivasan, C., et al,, *Bactericidal and detoxification effects of irradiated semiconductor catalyst, TiO2.* Current Science, 2003. **85**(10): p. 1431-1438.
7. News, T.B.T., *Titanium-Oxide Photocatalyst.* Three Bond Technical News, 2004. **62**: p. 1-8.

8. Watson, S., et al.,, *Preparation of nanosized crystalline TiO2 particles at low temperature for photocatalysis.* Journal of Nanoparticle Research, 2004. **6**(2): p. 193-207.

9. Zallen, R. and M.P. Moret, *The optical absorption edge of brookite TiO2.* Solid State Communications, 2006. **137**(3): p. 154-157.

10. Mo, S.-D. and W.Y. Ching, *Electronic and optical properties of three phases of titanium dioxide: Rutile, anatase, and brookite.* Physical Review B, 1995. **51**(19): p. 13023.

11. Watson, S., et al., *Preparation of nanosized crystalline TiO2 particles at low temperature for photocatalysis.* Journal of Nanoparticle Research, 2004. **6**(2): p. 193-207.

12. Banerjee, S., et al., *Physics and chemistry of photocatalytic titanium dioxide: Visualization of bactericidal activity using atomic force microscopy* Current Science, 2006. **90**(10).

13. Bratu, S., Steven Brooks, Sibte Burney, Sandeep Kochar, Jyoti Gupta, David Landman, and John Quale, *Detection and Spread of Escherichia coli Possessing the Plasmid-Borne Carbapenemase KPC-2 in Brooklyn, New York.* Clinical Infectious Diseases, 2007. 44: p. 972-975.

14. Jawad, A., et al., *Survival of Acinetobacter baumannii on Dry Surfaces: Comparison of Outbreak and Sporadic Isolates.* J. Clin. Microbiol., 1998. **36**(7): p. 1938-1941.

15. Savini, V., et al., *Misidentification of ampicillin-sulbactam heteroresistance in Acinetobacter baumannii strains from ICU patients.* Journal of Infection, 2009. In Press, Corrected Proof.

16. Giamarellou, H., A. Antoniadou, and K. Kanellakopoulou, *Acinetobacter baumannii: a universal threat to public health?* International Journal of Antimicrobial Agents, 2008. **32**(2): p. 106-119.

17. Wendt, C., et al., *Survival of Acinetobacter baumannii on dry surfaces.* J. Clin. Microbiol., 1997. **35**(6): p. 1394-1397.

18. Perez, F., et al., *Global Challenge of Multidrug-Resistant Acinetobacter baumannii.* Antimicrob. Agents Chemother., 2007. **51**(10): p. 3471-3484.

19. Fournier, P.-E., et al., *Comparative Genomics of Multidrug Resistance in <italic>Acinetobacter baumannii</italic>*. PLoS Genet, 2006. **2**(1): p. e7.

20. Nemec, A., et al., *Diversity of aminoglycoside-resistance genes and their association with class 1 integrons among strains of pan-European Acinetobacter baumannii clones.* J Med Microbiol, 2004. **53**(12): p. 1233-1240.

21. Oliveira, D.C., A. Tomasz, and H. de Lencastre, *Secrets of success of a human pathogen: molecular evolution of pandemic clones of meticillin-resistant Staphylococcus aureus.* The Lancet Infectious Diseases, 2002. **2**(3): p. 180-189.

22. Cirz, R.T., et al., *Inhibition of Mutation and Combating the Evolution of Antibiotic Resistance.* PLoS Biol, 2005. **3**(6): p. e176.

23. Perez-Capilla, T., et al., *SOS-Independent Induction of dinB Transcription by {beta}-Lactam-Mediated Inhibition of Cell Wall Synthesis in Escherichia coli.* J. Bacteriol., 2005. **187**(4): p. 1515-1518.

24. Magnet, S., P. Courvalin, and T. Lambert, *Resistance-Nodulation-Cell Division-Type Efflux Pump Involved in Aminoglycoside Resistance in Acinetobacter baumannii Strain BM4454.* Antimicrob. Agents Chemother., 2001. **45**(12): p. 3375-3380.

25. Kohanski, M.A., M.A. DePristo, and J.J. Collins, *Sublethal Antibiotic Treatment Leads to Multidrug Resistance via Radical-Induced Mutagenesis.* Molecular Cell, 2010. **37**(3): p. 311-320.

26. Costerton, J.W., and P.H. Stewart, *Battling Biofilms.* Scientific American: Special Supplement 2006: p. 2-11.

27. Schembri, M.A., D. Dalsgaard, and P. Klemm, *Capsule shields the function of short bacterial adhesins.* J Bacteriol, 2004. **186**(5): p. 1249-57.

28. Mehrotra, A., *Bacterial Biofilms.* Pediatric Asthma, Allergy & Immunology, 2007. **20**(3): p. 191-195.

29. Reisner, A., et al., *In Vitro Biofilm Formation of Commensal and Pathogenic Escherichia coli Strains: Impact of Environmental and Genetic Factors.* J. Bacteriol., 2006. **188**(10): p. 3572-3581.

30. Jones, C.H., *FimH adhesin of type 1 pili is assembled into a fibrillar tip structure in the Enterobacteriaceae.* Proc. Natl. Acad. Sci. , 1995. **92**: p. 2081-2085.

31. Bower, J.M., D.S. Eto, and M.A. Mulvey, *Covert Operations of Uropathogenic Escherichia coli within the Urinary Tract.* Traffic, 2005. **6**(1): p. 18-31.

32. Das, M., et al., *Hydrophilic Domain II of Escherichia coli Dr Fimbriae Facilitates Cell Invasion.* Infect. Immun., 2005. **73**(9): p. 6119-6126.

33. Ahmer, B.M.M., *Cell-to-cell signalling in Escherichia coli and Salmonella enterica*. Molecular Microbiology, 2004. **52**(4): p. 933-945.

34. Costerton, J.W., P.S. Stewart, and E.P. Greenberg, *Bacterial biofilms: a common cause of persistent infections.* Science, 1999. **284**(5418): p. 1318-22.

35. Maira-Litran, T., D.G. Allison, and P. Gilbert, *An evaluation of the potential of the multiple antibiotic resistance operon (mar) and the multidrug efflux pump acrAB to moderate resistance towards ciprofloxacin in Escherichia coli biofilms.* J Antimicrob Chemother, 2000. **45**(6): p. 789-95.

36. Genevaux, P., S. Muller, and P. Bauda, *A rapid screening procedure to identify mini-Tn10 insertion mutants of Escherichia coli K-12 with altered adhesion properties.* FEMS Microbiol Lett, 1996. **142**(1): p. 27-30.

37. Stewart, P.S., *A review of experimental measurements of effective diffusive permeabilities and effective diffusion coefficients in biofilms.* Biotechnol Bioeng, 1998. **59**(3): p. 261-72.

38. Ishida, H., et al., *In vitro and in vivo activities of levofloxacin against biofilm-producing Pseudomonas aeruginosa.* Antimicrob Agents Chemother, 1998. **42**(7): p. 1641-5.

39. Shigeta, M., et al., *Permeation of antimicrobial agents through Pseudomonas aeruginosa biofilms: a simple method.* Chemotherapy, 1997. **43**(5): p. 340-5.

40. Brown, M.R. and J. Barker, *Unexplored reservoirs of pathogenic bacteria: protozoa and biofilms.* Trends Microbiol, 1999. **7**(1): p. 46-50.

41. de Beer, D., et al., *Effects of biofilm structure on oxygen distribution and mass transport.* Biotechnol. Bioeng., 1994. **43**: p. 1131-1138.

42. Darouiche, R.O., et al., *Efficacy of antimicrobial-impregnated bladder catheters in reducing catheter-associated bacteriuria: a prospective, randomized, multicenter clinical trial.* Urology, 1999. **54**(6): p. 976-81.

43. Raad, I. and H. Hanna, *Intravascular catheters impregnated with antimicrobial agents: a milestone in the prevention of bloodstream infections.* Support Care Cancer, 1999. **7**(6): p. 386-90.

44. Spencer, R.C., *Novel methods for the prevention of infection of intravascular devices.* J Hosp Infect, 1999. **43 Suppl**: p. S127-35.

45. Woo, G.L., M.W. Mittelman, and J.P. Santerre, *Synthesis and characterization of a novel biodegradable antimicrobial polymer.* Biomaterials, 2000. **21**(12): p. 1235-46.

46. Kallio, T., et al., *Antifouling properties of TiO2: Photocatalytic decomposition and adhesion of fatty and rosin acids, sterols and lipophilic wood extractives.* Colloids and Surfaces A: Physicochemical and Engineering Aspects, 2006. **291**(1-3): p. 162-176.

47. Prevention, C.f.D.C.a., *Guidelines for school programs to prevent skin cancer.* MMWR 2002. **51**((RR-4)): p. 1-16.

48. Group, U.S.C.S.W., *United States Cancer Statistics: 1999–2006 Incidence and Mortality Web-based Report.* . United States Cancer Statistics:, 2010.

49. America, C.T.C.o., *Learn more about skin cancer treatments.* 2010.

50. James F. Reeves, S.J.D., Nicholas J.F. Dodd, Awadhesh N. Jha, *Hydroxyl radicals (•OH) are associated with titanium dioxide (TiO2) nanoparticle-induced cytotoxicity and oxidative DNA damage in fish cells.* Mutation Research, 2007. **640**: p. 113-122.

51. Vevers, W.F. and A.N. Jha, *Genotoxic and cytotoxic potential of titanium dioxide (TiO2) nanoparticles on fish cells in vitro.* Ecotoxicology, 2008. **17**(5): p. 410-20.

52. Xia, C.-H., et al., *The Primary Mechanism of Photoexcited TiO2 Nanoparticles-induced Apoptosis in Human Hepatoma Bel-7402 Cells.* bmei BioMedical Engineering and Informatics, International Conference on International Conference on BioMedical Engineering and Informatics 2008. **2**: p. 698-702.

53. Holsapple, M.P., et al., *Research Strategies for Safety Evaluation of Nanomaterials, Part II: Toxicological and Safety Evaluation of Nanomaterials, Current Challenges and Data Needs.* Toxicol. Sci., 2005. **88**(1): p. 12-17.

54. Liang, X.-J., et al., *Biopharmaceutics and Therapeutic Potential of Engineered Nanomaterials.* Current Drug Metabolism, 2008. **9**: p. 697-709.

55. Kiss, B., et al., *Investigation of micronized titanium dioxide penetration in human skin xenografts and its effect on cellular functions of human skin-derived cells.* Experimental Dermatology, 2008. **17**(8): p. 659-667.

CHAPTER TWO

LITATURE REVIEW

2.1 Titania, Characteristics, Current Products, and Uses

Titania or Titanium dioxide (TiO_2) degrades compounds through photo-oxidation making it a versatile non-selective compound with photocatalytic properties. Titanium dioxide exists in three different polymorphic lattice phases, Anatase, Brookite, and Rutile. Rutile phase has minimal electrostatic repulsive energy, and is the most thermodynamically stable due to its abridged in a linear structure with two of the twelve edges shared in the octahedron [8]. Anatase phase shares four edges per octahedron without corner oxygen sharing. Uniquely, Brookite phase is composed orthorhombically with three shared edges per octahedron. Zallen and Moret measured the optical absorption edge of Brookite Titania [9]. The optical absorption edge of Brookite phase extends throughout the visible light range. Brookite was observed to have a broad absorption edge in contrast to the steep absorption edges of Anatase and Rutile. No evidence of a direct gap was observed in the evaluated spectral range. It was proposed that Brookite phase Titania is an indirect-gap semiconductor with an approximate bandgap of 1.9 eV [9]. In contrast, calculations using the self-consistent orthogonalized linear-combination-of-atomic-orbitals method, Mo and Ching, 1995 approximated a direct bandgap for Brookite [10]. Other researchers have determined that all three phases of Titania have similar direct bandgap energies (~3.1 $\pm$ 0.1 eV) [11]. Banerjee and colleagues report different bandgap values for each phase, Anatase (3.2 eV), Rutile (3.02

eV), and Brookite (2.96 eV) [12]. Whether direct or indirect, Brookite phase Titania exhibits the lowest bandgap energy.

Characteristics of a photocatalyst were described as its ability to simultaneously adsorb two reactants [12]. Then efficiently absorb light ($h\nu \geq E_g$) to reduce and oxidize the adsorbed reactants. In order to excite the e^- from the valence band to the conduction band producing an e^--h^+ pair, the absorbed light energy must be equal or larger than the bandgap without being consumed. The produced hydroxyl radicals oxidize holes in the cells walls / membranes allowing the contents to leak out and also be degraded. Superoxide anions ($\cdot O_2^-$) eventually produce Reactive oxygen species (ROS), H_2O_2 molecules decomposing DNA via the Fenton Reaction.

Ions such as Phosphate have a very high affinity for the Titania and can significantly decrease the photocatalytic activity. The substrate, ions, diluent, surface roughness, hydrophilicity or hydrophobicity, morphology, particle size, surface area, and crystal structure are factors that influence the amount of photocatalytic activity [12].

Titanium dioxide is a versatile compound that is used in many applications, industries, materials, and products throughout the world. It is used in pigments due to it extremely high refractive index of n = 2.7 [1]. The Huntsman Pigments Company, (Billingham, England) produces Rutile phase pigments for architectural paints for use in highly opaque surface coatings, powder coatings, plastics, inks, and paper applications. Huntsman produces Anatase phase pigment for delustring synthetic fibers such as polyester and optical brighteners in ceramics. Another company makes photovoltaic solid-state hetero-junctions comprising a dense TiO_2 film electrode as an electron

conductor [2]. In a medical application, a high compressive strength (>2 MPa) titanium oxide scaffold may be used in bone [3]. Hair dye, sun screens, and cosmetics are popular Titania containing products [4]. Chemical vapor deposition using Anatase phase for self-cleaning, super hydrophilic, antimicrobial glass [5]. Photomineralization with air and water purification, photoelectrodes as a hydrolysis catalyst, and photosterilization in sterilizing, deodorizing, and anti-fouling methods and products [6-7].

2.2 Bacteria, Biofilm, and Overuse of Antibiotics

Significant overuse of broad spectrum antibiotics has escalated the emergence of bacterial resistance. These Multi-Drug Resistant (MDR) bacterial infections increase the morbidity and mortality of patients. Therefore, nosocomial infections of bacteria such as *Staphylococcus aureus, Acinetobacter baumannii, Escherichia coli* are expected to rise.

Currently, antibiotics provide a selective method of bacterial elimination, but are losing the battle against emerging resistant pathogens. A rising problem consists of bacteria sharing plasmids, crossing specie boundaries. In Brooklyn, New York three hospitals isolated *E. coli* from UTIs that possessed 23-kb plasmid encoding *Klebsiella pneumonia* carbapenemase type 2 (KPC-2) and increasingly containing the gene $bla_{\text{KPC-2}}$ [13]. The gram-negative multi-drug-resistant (MDR) bacteria *Acinetobacter baumannii* is ubiquitous and can be isolated from water, soil, animals, humans, and other environmental sources [14]. It is aerobic and an opportunistic pathogen escalating nosocomial outbreaks in intensive-care-units (ICU) and burn units [15] [16] [17]. The mechanisms which allow for such MDR in *A. baumannii* could be that they amass

quickly and exchange genetic information easily [16, 18]. Recently a clinical isolate of that produced extended-spectrum β-lactamase but was carbapenem-susceptible, contained more than 40 identified resistance genes [19]. This unique class of Gram-negative bacteria may easily share genetic pools where prevalent clonal groups of *A. baumannii* co-exist via horizontal gene transfer [16, 18, 20]. Clonal expansion may work additionally to increase resistance [20].

Another method of resistance is chromosomal cassette transfer [21]. DNA damaging antibiotics depress SOS-regulated polymerases via LexA cleavage inducing resistant mutations [22]. SOS-independent response increased frameshift mutations when exposed to β-lactam antibiotics [23]. *A. baumannii* contains an over-expressed efflux pump affecting many type of antibiotics [24]. Sub-lethal levels of antibiotics induce mutagenesis via reactive oxygen species (ROS). The bacteria remained sensitive to the utilized antibiotic, but increased mutant strains that were resistant to other antibiotics [25].

Another mechanism that bacteria use to protect themselves is by creating and living in biofilms [26]. Bacteria change from planktonic to sessile existence through attachment to surfaces. Generating a gooey matrix and signaling (quorum sensing (QS)) one another to proliferate into a microcolony, offers a selective advantage to increase their survival rate. [27]. Other species of bacteria may join the colony due to QS signals released into the environment. These chemical gradients allow for a diverse species to coexist. Lastly, some cells escape from the colony and return to the planktonic state moving and landing in a different location to start the process of biofilm formation again.

Biofilms are ubiquitous and the CDC estimates that biofilms are involved in at least 65% of all infections [28].

Reisner and colleagues determined that biofilm formation was significantly dependent on growth medium composition [29]. Specific adhesion to D-mannose demonstrated direct binding of FimH type 1 pili which is serologically conserved throughout Enterobacteriaceae [30]. EC and many other species of bacteria contain hydrophilic fimbriae that attach to biotic and abiotic surfaces [31-32].

E. coli B was chosen as the model bacteria in this work was for the following reasons. First, *E. coli* B contains the *fimH* gene, which codes for the hydrophilic FimH subunit of type 1 pili conferring attachment to biotic and abiotic surfaces. QS in *E. coli* is capable of binding to and responding to exogenous Acetylhomoserine lactone (AHL), and regulate target gene expression and adjust cellular functions to match the environment [33].

When microorganisms attach to a surface and grow as biofilm, they become less susceptible to antimicrobials than the same microbes in planktonic growth. Several factors are responsible for biofilm resistance including restricted penetration of antimicrobials into a biofilm, decreased growth rate, and expression of resistance genes [34-36].

Exopolymer matrix of biofilms can restrict diffusion of drugs. Diffusion rate in a biofilm is approximately 20 to 80 percent of that in free floating planktonic state [37]. The negatively charged exopolysaccharide is also effective against positively charged antibiotics retarding permeation [38-39]. Another biofilm-reduced susceptibility could be

contributed to the slower growing rate or non-growing status, or increased stress responses of microbial cells in biofilm due to limited diffusion of oxygen, nutrients, or starvation protecting the biofilm from environmental stresses [40] [41].

Different strategies [26] to prevent or eradicate bacteria biofilms include: prevention of attachment or QS [42-45]. A super-hydrophilic surface with a contact angle of $<5^{o}$ is used and may attract the hydrophilic heads of bacterial fimbriae to the surface [46]. Hydroxyl radicals would successively attack the bacterial cell walls and membranes through the photocatalytic activity of the UVA or visible light (VL) irradiated surface. As Titanium dioxide water structure at the TiO2/aqueous interface is significantly dependent on the specific nature of the ions present in the diluent and the pH for optimized photocatalytic activity.

2.3 Skin Cancer

In the United States Skin cancer is the most common form of cancer with basal cell and squamous cell carcinomas being the two highest common types. Melanoma is highly dangerous among younger people. Exposure to ultraviolet (UV) light or sunlight, or tanning beds, or other sources of man-made UV such as fingernail polish curing with UV causes approximately 65%–90% of melanomas [47]. In the U.S. in 2006, 53,919 people were diagnosed with skin melanomas and 8,441 people in the United States died from skin melanomas [48]. Protection from UV light will prevent most skin cancers [47]. People living in areas of the earth that receive high levels of UV radiation are at higher risk developing skin cancer [49]. Skin cancer is an accumulative phenomenon and is

related to lifetime exposure to UV radiation. The time of day such as midday presents a higher chance of cancer. Normal skin or in an existing mole can becomes cancerous; Melanoma can develop anywhere on your body. Indicators of Melanoma include moles with irregular borders and different colors, lesions on palms of hands or feet, large multicolored spots with darker speckles, a mole that changes color, size, or bleeds.

Skin Cancer Research

Exposure to photocatalytically activated Anatase phase Titanium dioxide resulted in a dose-dependent decrease of cell-viability in goldfish cells [50]. With similar results, another research group used TiO_2 nanoparticles (DeGussa) that were 75% Rutile and 25% Anatase crystalline phase in free suspension [51].

In human hepatoma Bel-7402 cells, apoptosis induced by the photocatalytically activated TiO_2 nanoparticles was determined to be the primary mechanism of cell death [52]. The small size with large surface area and unique characteristics of TiO_2 nanoparticles may facilitate absorption and transport across the barriers of mammalian epithelium (skin, lungs, and gut) followed with systemic entry to the circulatory system to secondary target organs and may even cross the blood-brain barrier to reside in the brain [53-54].

Opposing the above theory, Kiss and colleagues (2008) investigated the possibility of TiO_2 particles penetrating through the stratum corneum in human skin xenografts onto nude mice [55]. The stratum corneum funtioned to keep the TiO_2 nannoparticles from traveling further through the intact skin. Titania may prove to be a treatment modality for skin cancer.

2.4 References

1. Pigments, H., *Pigments.* 2010.
2. Johansson, E.M.J., et al., *Photovoltaic and Interfacial Properties of Heterojunctions Containing Dye-Sensitized Dense TiO2 and Tri-arylamine Derivatives.* Chemistry of Materials, 2007. **19**(8): p. 2071-2078.
3. Sabetrasekh, R. and et al., *Impact of trace elements on biocompatibility of titanium scaffolds.* Biomedical Materials, 2010. **5**(1): p. 015003.
4. Popov, A., et al. *Interaction of sunscreen TiO[sub 2] nanoparticles with skin and UV light: penetration, protection, phototoxicity.* 2009. Munich, Germany: SPIE.
5. Evans, P., et al., *A comparative study of three techniques for determining photocatalytic activity.* Journal of Photochemistry and Photobiology A: Chemistry, 2007. **188**(2-3): p. 387-391.
6. Srinivasan, C., et al,, *Bactericidal and detoxification effects of irradiated semiconductor catalyst, TiO2.* Current Science, 2003. **85**(10): p. 1431-1438.
7. News, T.B.T., *Titanium-Oxide Photocatalyst.* Three Bond Technical News, 2004. **62**: p. 1-8.
8. Watson, S., et al.,, *Preparation of nanosized crystalline TiO2 particles at low temperature for photocatalysis.* Journal of Nanoparticle Research, 2004. **6**(2): p. 193-207.
9. Zallen, R. and M.P. Moret, *The optical absorption edge of brookite TiO2.* Solid State Communications, 2006. **137**(3): p. 154-157.

10. Mo, S.-D. and W.Y. Ching, *Electronic and optical properties of three phases of titanium dioxide: Rutile, anatase, and brookite.* Physical Review B, 1995. **51**(19): p. 13023.

11. Watson, S., et al., *Preparation of nanosized crystalline TiO2 particles at low temperature for photocatalysis.* Journal of Nanoparticle Research, 2004. **6**(2): p. 193-207.

12. Banerjee, S., et al., *Physics and chemistry of photocatalytic titanium dioxide: Visualization of bactericidal activity using atomic force microscopy* Current Science, 2006. **90**(10).

13. Bratu, S., Steven Brooks, Sibte Burney, Sandeep Kochar, Jyoti Gupta, David Landman, and John Quale, *Detection and Spread of Escherichia coli Possessing the Plasmid-Borne Carbapenemase KPC-2 in Brooklyn, New York.* Clinical Infectious Diseases, **2007**. **44**: p. 972-975.

14. Jawad, A., et al., *Survival of Acinetobacter baumannii on Dry Surfaces: Comparison of Outbreak and Sporadic Isolates.* J. Clin. Microbiol., 1998. **36**(7): p. 1938-1941.

15. Savini, V., et al., *Misidentification of ampicillin-sulbactam heteroresistance in Acinetobacter baumannii strains from ICU patients.* Journal of Infection, 2009. In Press, Corrected Proof.

16. Giamarellou, H., A. Antoniadou, and K. Kanellakopoulou, *Acinetobacter baumannii: a universal threat to public health?* International Journal of Antimicrobial Agents, 2008. **32**(2): p. 106-119.

17. Wendt, C., et al., *Survival of Acinetobacter baumannii on dry surfaces.* J. Clin. Microbiol., 1997. **35**(6): p. 1394-1397.

18. Perez, F., et al., *Global Challenge of Multidrug-Resistant Acinetobacter baumannii.* Antimicrob. Agents Chemother., 2007. **51**(10): p. 3471-3484.

19. Fournier, P.-E., et al., *Comparative Genomics of Multidrug Resistance in <italic>Acinetobacter baumannii</italic>*. PLoS Genet, 2006. **2**(1): p. e7.

20. Nemec, A., et al., *Diversity of aminoglycoside-resistance genes and their association with class 1 integrons among strains of pan-European Acinetobacter baumannii clones.* J Med Microbiol, 2004. **53**(12): p. 1233-1240.

21. Oliveira, D.C., A. Tomasz, and H. de Lencastre, *Secrets of success of a human pathogen: molecular evolution of pandemic clones of meticillin-resistant Staphylococcus aureus.* The Lancet Infectious Diseases, 2002. **2**(3): p. 180-189.

22. Cirz, R.T., et al., *Inhibition of Mutation and Combating the Evolution of Antibiotic Resistance.* PLoS Biol, 2005. **3**(6): p. e176.

23. Perez-Capilla, T., et al., *SOS-Independent Induction of dinB Transcription by {beta}-Lactam-Mediated Inhibition of Cell Wall Synthesis in Escherichia coli.* J. Bacteriol., 2005. **187**(4): p. 1515-1518.

24. Magnet, S., P. Courvalin, and T. Lambert, *Resistance-Nodulation-Cell Division-Type Efflux Pump Involved in Aminoglycoside Resistance in Acinetobacter baumannii Strain BM4454.* Antimicrob. Agents Chemother., 2001. **45**(12): p. 3375-3380.

25. Kohanski, M.A., M.A. DePristo, and J.J. Collins, *Sublethal Antibiotic Treatment Leads to Multidrug Resistance via Radical-Induced Mutagenesis.* Molecular Cell, 2010. **37**(3): p. 311-320.

26. Costerton, J.W., and P.H. Stewart, *Battling Biofilms.* Scientific American: Special Supplement 2006: p. 2-11.

27. Schembri, M.A., D. Dalsgaard, and P. Klemm, *Capsule shields the function of short bacterial adhesins.* J Bacteriol, 2004. **186**(5): p. 1249-57.

28. Mehrotra, A., *Bacterial Biofilms.* Pediatric Asthma, Allergy & Immunology, 2007. **20**(3): p. 191-195.

29. Reisner, A., et al., *In Vitro Biofilm Formation of Commensal and Pathogenic Escherichia coli Strains: Impact of Environmental and Genetic Factors.* J. Bacteriol., 2006. **188**(10): p. 3572-3581.

30. Jones, C.H., *FimH adhesin of type 1 pili is assembled into a fibrillar tip structure in the Enterobacteriaceae.* Proc. Natl. Acad. Sci. , 1995. **92**: p. 2081-2085.

31. Bower, J.M., D.S. Eto, and M.A. Mulvey, *Covert Operations of Uropathogenic Escherichia coli within the Urinary Tract.* Traffic, 2005. **6**(1): p. 18-31.

32. Das, M., et al., *Hydrophilic Domain II of Escherichia coli Dr Fimbriae Facilitates Cell Invasion.* Infect. Immun., 2005. **73**(9): p. 6119-6126.

33. Ahmer, B.M.M., *Cell-to-cell signalling in Escherichia coli and Salmonella enterica.* Molecular Microbiology, 2004. **52**(4): p. 933-945.

34. Costerton, J.W., P.S. Stewart, and E.P. Greenberg, *Bacterial biofilms: a common cause of persistent infections.* Science, 1999. **284**(5418): p. 1318-22.

35. Maira-Litran, T., D.G. Allison, and P. Gilbert, *An evaluation of the potential of the multiple antibiotic resistance operon (mar) and the multidrug efflux pump acrAB to moderate resistance towards ciprofloxacin in Escherichia coli biofilms.* J Antimicrob Chemother, 2000. **45**(6): p. 789-95.

36. Genevaux, P., S. Muller, and P. Bauda, *A rapid screening procedure to identify mini-Tn10 insertion mutants of Escherichia coli K-12 with altered adhesion properties.* FEMS Microbiol Lett, 1996. **142**(1): p. 27-30.

37. Stewart, P.S., *A review of experimental measurements of effective diffusive permeabilities and effective diffusion coefficients in biofilms.* Biotechnol Bioeng, 1998. **59**(3): p. 261-72.

38. Ishida, H., et al., *In vitro and in vivo activities of levofloxacin against biofilm-producing Pseudomonas aeruginosa.* Antimicrob Agents Chemother, 1998. **42**(7): p. 1641-5.

39. Shigeta, M., et al., *Permeation of antimicrobial agents through Pseudomonas aeruginosa biofilms: a simple method.* Chemotherapy, 1997. **43**(5): p. 340-5.

40. Brown, M.R. and J. Barker, *Unexplored reservoirs of pathogenic bacteria: protozoa and biofilms.* Trends Microbiol, 1999. **7**(1): p. 46-50.

41. de Beer, D., et al., *Effects of biofilm structure on oxygen distribution and mass transport.* Biotechnol. Bioeng., 1994. **43**: p. 1131-1138.

42. Darouiche, R.O., et al., *Efficacy of antimicrobial-impregnated bladder catheters in reducing catheter-associated bacteriuria: a prospective, randomized, multicenter clinical trial.* Urology, 1999. **54**(6): p. 976-81.

43. Raad, I. and H. Hanna, *Intravascular catheters impregnated with antimicrobial agents: a milestone in the prevention of bloodstream infections.* Support Care Cancer, 1999. **7**(6): p. 386-90.

44. Spencer, R.C., *Novel methods for the prevention of infection of intravascular devices.* J Hosp Infect, 1999. **43 Suppl**: p. S127-35.

45. Woo, G.L., M.W. Mittelman, and J.P. Santerre, *Synthesis and characterization of a novel biodegradable antimicrobial polymer.* Biomaterials, 2000. **21**(12): p. 1235-46.

46. Kallio, T., et al., *Antifouling properties of TiO2: Photocatalytic decomposition and adhesion of fatty and rosin acids, sterols and lipophilic wood extractives.* Colloids and Surfaces A: Physicochemical and Engineering Aspects, 2006. **291**(1-3): p. 162-176.

47. Prevention, C.f.D.C.a., *Guidelines for school programs to prevent skin cancer.* MMWR 2002. **51**((RR-4)): p. 1-16.

48. Group, U.S.C.S.W., *United States Cancer Statistics: 1999–2006 Incidence and Mortality Web-based Report.* . United States Cancer Statistics:, 2010.

49. America, C.T.C.o., *Learn more about skin cancer treatments.* 2010.

50. James F. Reeves, S.J.D., Nicholas J.F. Dodd, Awadhesh N. Jha, *Hydroxyl radicals (•OH) are associated with titanium dioxide (TiO2) nanoparticle-induced cytotoxicity and oxidative DNA damage in fish cells.* Mutation Research, 2007. **640**: p. 113-122.

51. Vevers, W.F. and A.N. Jha, *Genotoxic and cytotoxic potential of titanium dioxide (TiO2) nanoparticles on fish cells in vitro.* Ecotoxicology, 2008. **17**(5): p. 410-20.

52. Xia, C.-H., et al., *The Primary Mechanism of Photoexcited TiO2 Nanoparticles-induced Apoptosis in Human Hepatoma Bel-7402 Cells.* bmei BioMedical Engineering and Informatics, International Conference on International Conference on BioMedical Engineering and Informatics 2008. **2**: p. 698-702.

53. Holsapple, M.P., et al., *Research Strategies for Safety Evaluation of Nanomaterials, Part II: Toxicological and Safety Evaluation of Nanomaterials, Current Challenges and Data Needs.* Toxicol. Sci., 2005. **88**(1): p. 12-17.

54. Liang, X.-J., et al., *Biopharmaceutics and Therapeutic Potential of Engineered Nanomaterials.* Current Drug Metabolism, 2008. **9**: p. 697-709.

55. Kiss, B., et al., *Investigation of micronized titanium dioxide penetration in human skin xenografts and its effect on cellular functions of human skin-derived cells.* Experimental Dermatology, 2008. **17**(8): p. 659-667.

CHAPTER THREE

DEVELOPMENT, CHARACTERIZATION, AND PHOTOCATALYTIC ACTIVITY OF LIGHT ACTIVATED POLYMORPHIC BROOKITE TITANIA ENHANCED VIA NOVEL SUB-COATTINGS ON *Escherichia coli*

(As a manuscript formatted for submission to the Journal of Nanobiotechnology)

3.1 Abstract

Nosocomial infections are rising due to bacterial adaptation combined with overuse of broad spectrum antibiotics which significantly increased emergence of resistant pathogens. Because about sixty-five percent of all bacterial infections are biofilm associated, an inexpensive, durable, safe, visible-light activated, and non-selective antimicrobial surface coating is ideal. Titanium dioxide, a versatile non-selective compound with photocatalytic properties, degrades compounds through photo-oxidation. Titanium dioxide exists in three lattice phases, Anatase, Brookite, and Rutile, with Anatase used extensively. Without doping or close atomic association with another specific atom causing band-gap narrowing, Titanium dioxide is active under long wave ultraviolet light (365 nm) and not visible light. Studies incorporating doping of atoms into the crystal lattice structure can only be performed at temperatures higher than the phase transition temperature for Brookite, causing Anatase or Rutile lattice configurations. In order to maintain the Brookite phase of the Titanium dioxide, this study evaluated a novel super hydrophilic polyelectrolyte sub-coating. Room temperature deposition maintained the Brookite lattice phase and provided atomic surface associations between the sub-

coating and the Titania. The sub-coating contained Nitrogen and Sulfur molecules. With their surface associations to the Titania, it was proposed to narrow the band-gap, causing visible-light photocatalytic activity. In conjunction with the sub-coating, two types of polymorphic Brookite phase Titania were evaluated, Br200 and BrNMP.

PDDA/PSS sub-coatings were successfully attached to glass cover-slips in a 25 layer-by-layer room temperature liquid deposition method. Each type of Titania evaluated was attached to the PDDA/PSS sub-coated cover-slips by room temperature liquid phase deposition via XPS analysis. Appropriate molecules of O 1s, N 1s, S 2P and Ti 2p were found on the surface of the cover-slips. XRD analysis determined that predominantly Brookite phase with some Anatase phase and a small amount of Rutile phase Titania lattice structures remained on the surface of the cover-slips matching peaks with the powder Titania samples. The PDDA/PSS sub-coating was found to be photocatalytically active under visible light on Methyl orange degradation and had bactericidal activity on *E. coli* B. Visible-light photocatalytically activated super hydrophilic polyelectrolyte sub-coating with vlp7000, Br200, or BrNMP Titania killed all *E. coli* B in 40, 8, or 30 minutes, respectively, or with binder sub-coating plus each type of Titania eliminated all *E. coli* B in 60, 50, or 50 minutes, respectively.

Light intensity, wavelength, amount of surface area, size of each crystallite, surface material characteristics, pH, band gap, efficiency of hole-electron recombination, amount of dissolved oxygen, broad absorption edge (indirect bandgap) versus sharp absorption edge (direct bandgap), number of available active surface sites, and bacterial load affect efficiency of photo-oxidation. The super-hydrophilic nature of the

polyelectrolyte-Titania coating attracts and enhances photo-oxidative activity due to bacterial adherence via hydrophilic fimbriae that attach to biotic and abiotic surfaces. Br200 demonstrated a stable working pH range including pH3 to 4. The 5-8nm diameter crystallite size range provides a large surface area, changing the characteristics from a monolithic nature to Nitrogen and Sulfur molecules being able to associate with the crystal lattice structures on the surface of each surface crystallite, and significantly increasing target contact probability. We suggest that the association of the Nitrogen and Sulfur molecules on the sub-coating interact with the surface of the lattice structures on each nanoparticle surface, enhancing visible light photo activity by narrowing the band-gap and slowing the electron/hole recombination. Br200 and BrNMP Titania on the polyelectrolyte sub-coating provided superior photo-oxidative activity on both Methyl orange degradation and bacterial decomposition compared to the commercial P25 and vlp7000 Titania, or binder sub-coating with Titania. Further characterization and evaluation of these PDDA/PSS sub-coatings with Br200 or BrNMP are warranted. Furthermore, the Br200 may have been more photocatalytically active than the BrNMP in association with the sub-coatings on *E. coli* B. This phenomenon may be caused by the low manufacturing and calcination temperatures of BrNMP. Some charred NMP residue may have remained on the Titania surface and blocked some of the photoactive sites and aided in electron/hole recombination. Also the bacteria may not have been as attracted to the residue covered surface of BrNMP. These novel polyelectrolyte-Br200 or polyelectrolyte-BrNMP non-selective Titania coatings would provide a low cost, visible-light active, safe, and effective non-selective method to aid in preventing transmission of

bacterial infections and in prevention of biofilm formation in the nosocomial and community settings.

3.2 Introduction

Worldwide exploitation of broad spectrum antibiotics significantly increased emergence of bacterial resistance. Bacterial infections increase the morbidity and mortality of patients in war zones, acute or long-term care hospitals. As the world population increases and people travel further and live longer, they will require more hospital and long-term managed care. Therefore, nosocomial infections of bacteria such as *Escherichia coli* are expected to rise.

Currently, antibiotics provide a selective method of bacterial elimination, but are losing the battle against emerging resistant pathogens. A rising problem consists of bacteria sharing plasmids, crossing specie boundaries. Hospitals isolated *E. coli* from UTIs that possessed 23-kb plasmid encoding *Klebsiella pneumonia* carbapenemase type 2 (KPC-2) and increasingly containing the gene $bla_{\text{KPC-2}}$ [13]. The gram-negative multi-drug-resistant (MDR) bacteria *Acinetobacter baumannii* is ubiquitous and can be isolated from water, soil, animals, humans, and other environmental sources [14]. It is aerobic and an opportunistic pathogen escalating nosocomial outbreaks in intensive-care-units (ICU) and burn units [15] [16] [17]. The mechanisms which allow for such MDR in *A. baumannii* could be that they amass quickly and exchange genetic information easily [16, 18]. *A. baumannii* extended-spectrum β-lactamase isolates containing more than 40 identified resistance genes have been identified [19]. This unique class of Gram-negative

bacteria may easily share genetic pools where prevalent clonal groups of *A. baumannii* co-exist via horizontal gene transfer [16, 18, 20]. Clonal expansion may work additionally to increase resistance [20].

Another method of resistance is chromosomal cassette transfer. *Staphylococcus aureus* contains the staphylococcal chromosomal cassette (SCC*mec*), in which the gene *mecA* encodes for PBP2a causing low binding affinity to β-lactam antibiotics thus rendering them ineffective on cell wall synthesis disruption [21]. DNA damaging antibiotics such as ciprofloxacin depresses SOS-regulated polymerases via LexA cleavage inducing resistant mutations [22]. SOS-independent response by induction of DinB increased frameshift mutations when exposed to β-lactam antibiotics [23]. *A. baumannii* contains an over-expressed efflux pump affecting fluoroquinolones, tetracyclines, aminoglycosides, erythromycin, cefotaxime, and trimethoprim [24]. Kohanski and colleagues recently identified an increase in reactive oxygen species (ROS) due to exposure to sub-lethal levels of antibiotics induce mutagenesis. The bacteria remained sensitive to the utilized antibiotic, but increased mutant strains that were resistant to other antibiotics [25].

Another mechanism that bacteria use to protect themselves is by creating and living in biofilms. Costerton and Stewart (2006) put together a theory of how biofilms develop [26]. Within natural, medical, and engineered environments, free-swimming (planktonic) bacteria land on a surface, aggregate and affix to living and abiotic surfaces, causing the bacteria to change from its planktonic state to a sessile existence. Generating a gooey matrix and signaling (quorum sensing) one another to proliferate into a

microcolony, offers a selective advantage to increase their survival rate. Although not adhered directly to the surface, some bacteria in the matrix may grow a polysaccharide capsule for protection, remaining dormant until favorable environmental conditions arise [27]. Other species of bacteria may join the colony due to chemical auto-induced signals released into the environment. These chemical gradients allow different metabolic states and diverse species to coexist. Lastly, some cells escape from the colony and return to the planktonic state moving and landing in a different location to start the process of biofilm formation again. Biofilms are ubiquitous and implicated in several infectious processes including nosocomial infections such as indwelling devices and chronic infections. The CDC estimates that biofilms are involved in at least 65% of all infections [28].

Reisner and colleagues determined that biofilm formation was significantly dependent on growth medium composition, rather than the association between pathogenic *E. coli*, increased biofilm formation, to commensal *E. coli* K-12 strains that normally reside within the mucus layer without colonizing the epithelium [29]. Krogfelt and researchers (1990) used a carrier protein attached to $_{D}$-mannose to demonstrate direct binding of FimH the mannose-specific adhesion. FimH was visualized by electron microscopy. The FimH adhesin of the type 1 pilus is serologically conserved throughout Enterobacteriaceae [30]. Electron Microscopy depicted a 16 nm fibrillar tip structure joined end to end on the pilus rod with structural design matching the FimG-FimH complex. . EC and many other species of bacteria contain hydrophilic fimbriae that attach to biotic and abiotic surfaces [31-32].

E. coli B was chosen as the model bacteria in this work was for the following reasons. First, *E. coli* B contains the *fimH* gene, which codes for the hydrophilic FimH subunit of type 1 pili conferring attachment to biotic and abiotic surfaces. In the Vandemaele study, greater than ninety nine percent homology was indicated among strains from either bovine (B), avian (A), or porcine (P) species. Of the 24 strains tested, all contained the *fimH* gene except strain P3. Secondly, Quorum Sensing was examined. *E. coli* contains the signal receptor protein SdiA of the luxR family. The SdiA receptor protein is capable of binding to and responding to exogenous AHLs, but not producing them, therefore regulating target gene expression [33]. SdiA also responds to endogenous indole, allowing the bacteria to adjust cellular functions correctly in the biofilm environment [56]. The signal generating enzyme was found to be a LuxS homologue producing AI-2.

When microorganisms attach to a surface and grow as biofilm, they become less susceptible to antimicrobials than the same microbes in planktonic growth. Several factors are responsible for biofilm resistance including restricted penetration of antimicrobials into a biofilm, decreased growth rate, and expression of resistance genes [34-36].

Biofilms are enclosed in a self-produced exopolymer matrix that can restrict simple diffusion of drugs. Diffusion rate in a biofilm is approximately 20 to 80 percent of that in free floating planktonic state [37]. The negatively charged exopolysaccharide is also effective against positively charged antibiotics, e.g. aminoglycoside, retarding their permeation [38-39]. Another biofilm-reduced susceptibility could be contributed to the

slower growing rate or non-growing status of microbial cells in biofilm due to limited diffusion of oxygen, nutrients, or starvation. Slow growing or starved microorganisms are less susceptible to the action of antimicrobials [41]. There may also be increased stress responses which result in physiological changes that help protect the biofilm from environmental stresses [40].

Different strategies [26] to prevent or eradicate bacteria include: prevention of attachment by molecules through surface coatings that block adhesion via repressing expression of genes involved in adhesion and matrix production. Use signal inhibitors or within a biofilm, or some type of signal or chemical to cause release of cells back to their more susceptible planktonic state for exposure to antibodies and other antibiotics. Antibiofilm therapies based on incorporation of antibiotics into the medical materials have been reported [42-45]. Due to these many avenues of bacterial resistance towards antibiotics and through biofilm formation to enhance protection, a different approach to killing bacteria is warranted, especially in the nosocomial settings. A non-selective, safe, durable, controllable, coating that would kill bacteria and prevent biofilm formation should be investigated. One promising compound is Titanium dioxide, however alone requires photoactivation via long range ultra violet light which is not safe over time to humans. Exposure to long range ultra violet light can cause cancer in humans. Therefore, altering the Titania, or associating the Titania with something to cause it to be photocatalytically active in a coating format in visible light is investigated in this work.

Titania or Titanium dioxide (TiO_2), is a versatile non-selective compound with photocatalytic properties, degrades compounds through photo-oxidation. Titanium

dioxide exists in three different polymorphic lattice phases, Anatase, Brookite, and Rutile. Rutile phase is the most thermodynamically stable due to its minimal electrostatic repulsive energy; it is abridged in a linear structure with two of the twelve edges of the octahedron are shared [8]. Anatase phase shares four edges per octahedron without corner oxygen sharing. Uniquely, Brookite phase is composed orthorhombically with three shared edges per octahedron. Zallen and Moret measured the optical absorption edge of Brookite Titania [9]. Extending throughout the visible light range, Brookite was observed to have a broad absorption edge in contrast to the steep absorption edges of Anatase and Rutile. In the evaluated spectral range, no evidence of a direct gap was observed. They propose the Brookite phase Titania is an indirect-gap semiconductor with an approximate bandgap of 1.9 eV [9]. In contrast, calculations using the self-consistent orthogonalized linear-combination-of-atomic-orbitals method, Mo and Ching, 1995 approximated a direct bandgap for Brookite [10]. Other researchers have determined that all three phases of Titania have similar direct bandgap energies (~3.1 $\pm$ 0.1 eV) [11]. Banerjee and colleagues report the bandgap values for each phase is Anatase (3.2 eV), Rutile (3.02 eV), and Brookite (2.96 eV) [12]. Whether direct or indirect, Brookite phase Titania exhibits the lowest bandgap energy.

Chang and colleagues concluded that the optimal experimental conditions on degradation of salicylic acid were irradiation with intensity of 2.9mWcm^{-2} on at concentration of 250mgL−1 by both agitation and aeration processes (dissolved oxygen level = 8.2 mg O_2 L^{-1}) at pH 5 [57] achieving optimal hydroxyl radical yield of 5.1×10^{-17} M. The pH, dissolved oxygen content, and irradiation intensity are important factors to

consider. Also the rate of recombination of hole–electron pairs is within nanoseconds [58-59]. Additives such as Pt, Pd and Au may improve the photocatalytic efficiency of TiO_2 by slowing down the recombination of the hole-electron pair. Plus, a single photon can activate two oxygen molecules [58]. All of these parameters affect the photocatalytic efficiency of TiO_2.

Banerjee's work used and Atomic Force Microscope (AFM) to visualize the antimicrobial photocatalytic activity of photo-activated Titania on bacteria [12]. They described the characteristics of a photocatalyst as its ability to simultaneously adsorb two reactants. Then efficiently adsorb light ($h\nu \geq E_g$) to reduce and oxidize the adsorbed reactants. The adsorbed light energy must be enough to excite the e^- from the valence band to the conduction band producing an e^--h^+ pair. In the presence of water and dissolved oxygen (H_2O/O_2), the positive holes oxidize water splitting it into $^{\cdot}OH$ and H^+. The dissolved oxygen is reduced by the photo electron of the conduction band, generating superoxide anions ($^{\cdot}O_2^-$). H+ combines with the ($^{\cdot}O_2^-$) generating a hydroperoxyl radical, eventually producing a reactive oxygen species (ROS) H_2O_2 molecule. The photo induced ROS hydroxyl radical and hydrogen peroxide cause biocidal catalysis by penetrating cell walls and cutting DNA strands. The super oxide anion can enter the cell after oxidizing holes are made. Once inside, hydrogen peroxide and the super oxide anion may become hydroxyl radical precursors. Once inside the cell wall (Fe2+) may activate hydrogen peroxide via the Fenton reaction producing more damaging hydroxyl radicals.

$$Fe^{+2} + H_2O_2 \rightarrow OH\bullet + OH^{-1} + Fe^{+3}$$

After the photocatalytic source is turned off, residual hydrogen peroxide within the cell would interact with the iron compounds generating additional hydroxyls also through the Fenton reaction. There is a second reaction pathway forming additional hydroxyl radicals. The Haber-Weiss iron-catalyzed reaction occurs when both H_2O_2 and superoxide ion are present [60-61].

$$Fe^{+3} + O_2^{-} \rightarrow Fe^{+2} + O_2$$

$$Fe^{+2} + H_2O_2 \rightarrow Fe^{+3} + OH^{-} + OH\bullet.$$

Because the outer surface of the cell is the initial target of these reactive oxygen species (ROS), the chemical arrangements and rigidity of the each cell's surface structure will determine the effectiveness of the photocatalytic activity of each type of Titania.

The efficiency of the photocatalytic activity of Titania is also dependent on the surrounding environment. Phosphate ions from Phosphate Buffered Saline have a very high affinity for the Titania. Phosphate ions bind to the substrate surface causing the isoelectric point of the TiO_2/aqueous interface to significantly shift downward to pH2.0 and increasing the $3400cm^{-1}$ peak-intensity measured by vibrational sum-frequency spectroscopy (VSFS). [62]. The isoelectric point was ~5.5 in the presence of Cl ions. However, the Langmuir binding constant of phosphate onto TiO_2 at pH 2.3 is $(3.8 \pm 0.8) \times 10^4$ dm^3 mol^{-1} [63]. Adsorption kinetics depicting fast adsorption with very slow release confirmed that phosphate binds in a bidentate manner to Ti(IV) ions at the TiO_2 surface [63].

In commercial applications, hydrophobicity or hydrophilicity characteristics of a surface is important. A super-hydrophilic surface with a contact angle of $<5^o$ is used

commercially in antifogging and antifouling products and in self cleaning products [46]. The hydrophilicity of the surface could attract the hydrophilic heads of bacterial fimbriae. The fimbriae would attach to the surface where the hydroxyl radicals would successively attack the bacterial cell walls and membranes through the photocatalytic activity of the UVA or visible light (VL) irradiated surface. As Titanium dioxide water structure at the TiO_2/aqueous interface is significantly dependent on the specific nature of the ions present in the diluent and the pH for optimized photocatalytic activity.

The type of coating chosen was made layer-by-layer and contained super-hydrophilic surface characteristics. One component of the sub-coating, Poly(4-styrenesulfonic acid) solution (PSS) (~75,000 Mw, 18%wt. in H_2O, Sigma Aldrich, St. Louis, MO) has excellent film-forming and coating capabilities along with good conductive properties throughout an expansive range of relative humidity. The PSS polyelectrolyte is electroconductive and is used for antistatic resin in electrographic and electrophotographic substrates. It strongly interacts with electropositive active sites, and produces polyanions when it is dissolved in water. Due to the polyanionic nature of PSS, it has some tendency to also adsorb at the (100) crystal planes, but preferentially adsorbs to the {111) crystal planes of Brookite [64]. Charge and steric stabilization decrease coagulation effects in colloidal particles by these polyelectrolyte films. The second component of the sub-coating was Poly(diallyldimethylammonium chloride) solution (PDDA) (average Mw 200,000-350,000, 20 wt. % in H2O, Sigma Aldrich, St. Louis, MO) a polyelectrolyte, PDDA, produces polycations when it is dissolved in water. It strongly interacts with electronegative active sites. PDDA contains Nitrogen molecules.

This work investigated two types of Brookite phase Titania, Br200 and BrNMP on a pH dependent polyelectrolyte sub-coating. They with be evaluated under UVA 365 nm and Visible Light (VL) irradiation on Methyl orange (MO) photo-oxidation degradation. The hydrophilicity, surface chemical analysis via X-ray Photoelectron Spectroscopy (XPS), and X-ray Diffraction (XRD) of the Titania coatings will be characterized. The Titania coatings will be evaluated for the photo-oxidative biocidal effectiveness on *Escherichia coli* B.

3.3 Results

The chemical analyses of the PDDA/PSS (P) sub-coating surfaces with or without Titania nanoparticles and nanoparticle coatings confirm the presence of the sub-coating molecules and Titania on the surface (Table 1). XPS spectra graphs of P or B sub-coating with and without Br200, P25, BrNMP, vlp7000, Anatase, or vlp7001 are depicted in Appendix B. Surface elemental chemical analysis numerical results are exhibited in Table 1.

The x-ray diffraction spectra of the glass cover slips with either P or Binder (B) sub-coatings with or without TiO2 nanoparticle coatings are depicted in Figures 2 and 3, respectively. The spectra graphs acquired were confirmed by comparison with the original spectra graphs from the nanoparticle powders that were used to make the coatings [65-66]. Kaewgun and colleagues reported considerably small (6-8mm) crystallite sized particles of their prepared Titania broadened the XRD peaks and

calculated phase composition of TiO2 from XRD data. The Br200 (WACS-200) calculated phase composition was 45 wt% Anatase, 53 wt% Brookite, and 2 wt% Rutile.

The P and B sub-coatings were different in surface hydrophilicity characteristics shown in Figure 4. The P coatings with or without various Titania depicted super-hydrophilicity as the 10 µL drop of nanopure water instantly flattened out and disappeared from view with the naked eye. All P sub-coatings exhibited a contact angle measurement of $< 1^{o}$. In contrast the B sub-coatings with or without various Titania displayed strong hydrophobic characteristics as the 10 µL drop of 18Ω nanopure water remained rounded. The B sub-coating alone exhibited a contact angle of 62.5^{o}, B+P25 51.5^{o}, B+Br200 52.5^{o}, B+BrNMP 67.5^{o}, and B+vlp7000 at 105^{o} indicating that the B sub-coating is a material significantly more hydrophobic than the P sub-coating. For comparison, the hydrophilicity contact angle results are located in Table 3.

Significance of difference was evaluated with a student T-Test with an alpha of 0.05. All P Sub-Coatings with or without all Types of Titania compared to all P Sub-coatings with or without all Types of Titania at an alpha of 0.05 were not significantly different from each other (p=0.35). P Sub-Coating with or without all types of Titania are significantly different at an alpha of 0.05 from all B Sub-Coatings with or without all types of Titania with a range of p values from 2.36×10^{-5} to 6.93×10^{-6}. All B Sub-Coatings with or without all Types of Titania compared to all B Sub-coatings with or without all Types of Titania at an alpha of 0.05 were all significantly different from each other (p=0.016 to 3.15×10^{-6}).

The statistics of Figures 9 and 10 results were determined using a student T-Test with alpha equal to 0.05. *E. coli* B in PBS pH 7.4 or water at pH 7.4 exposed to UV light in the absence or presence of TiO_2 P-25 or TiO_2 Brookite did not significantly reduce the bacterial population in 120 minutes. In contrast, *E. coli* B in water at pH 4.0 exposed to UV in the presence of TiO_2 P-25 and TiO_2 Brookite had a significant seven log drop in 120 ($p=0.004$) or 30 ($p=0.001$) minutes, respectively. *E. coli* B in the absence of TiO_2 in water at pH 4.0 depicted no significant reduction of the bacterial population in 120 minutes. The pH of the water at 120 minutes dropped from pH 7.4 to pH 6.0, while the water beginning at pH 4.0 remained at pH 4.0 ($\pm$ 0.2) throughout 120 minutes.

The earlier version of the Free Suspension Bioassay [67], was on a large scale format. It is good and accurate, but used large amounts of materials, was labor intensive, and only one test variable could be evaluated at a time. The assay was miniaturized with the option of two different assays in combination with a third. Dilution curves of *E. coli* B (n=8) were evaluated. Based on the results, the LIVE/DEAD® *Bac*Light™ Bacterial Viability Kit (Molecular Probes®, Invitrogen™,USA) was found to be linear in the range of 1×10^3 to 1×10^8 CFU/mL in the presence of 1 mg/mL Titania. The second assay evaluated was the BacTiter-Glo™ Microbial Cell Viability Assay (Promega, Madison, WI). Based on the results, the BacTiter-Glo™ Microbial Cell Viability Assay was found to be linear in the range of 1×10^2 to 1×10^7 CFU/mL in the presence of 1 mg/mL Titania.

The six well – six mL volume free suspension assay was miniaturized to a 24 well format using a 1 mL volume assay. Many testing variables were tested at the same time

under this new assay format. An optically clear film was used to prevent evaporation during testing. After testing, 100 µL aliquots (n=4) from each sample well was dispensed into a 96 well black or white plate for fluorescence or luminescence assay, respectively. The 24 well testing assay in combination with either the fluorescent LIVE/DEAD® *Bac*Light™ Bacterial Viability Kit or the luminescent BacTiter-Glo™ Microbial Cell Viability Assay provided excellent results after subtracting the background. Although, greater than the suggested cell concentration or greater than the suggested Titania concentration of 1 mg/mL gave erroneous or non-linear results with either assay.

The UVA generated photocatalytic activities of P25, Br200, or BrNMP Titania powder (1mg TiO_2 / 1 mL) were evaluated by MO oxidative degradation as shown in Figure 5. BrNMP and Br200 on P sub-coating completed the MO degradation in 10 and 14 h, respectively. BrNMP and Br200 on B sub-coating completed the MO degradation in 18 and 22 h, respectively. The commercial P25 on P sub-coat attained approximately 80% degradation at 26 h and the P25 on B sub-coat achieved about 43% MO degradation at 26 h. The sub-coatings alone did not have much effect on MO degradation. MO alone did not degrade and remained at 0%.

The Visible Light generated photocatalytic activities of the P or B sub-coatings alone or with P25, Br200, or BrNMP Titania coatings (2 mg TiO_2 / 22 mm diameter cover slip) were evaluated by MO oxidative degradation as shown in Figure 6. Titania coated onto the P sub-coat degraded the MO significantly faster than its counterpart on B sub-coating. Br200 and BrNMP on P sub-coating completed the MO degradation in 12-14 h. Br200 and BrNMP on B sub-coating completed the MO degradation in 16-18 h and

20 h, respectively. The commercial vlp7000 on P sub-coat attained approximately 95% degradation at 26 h and on B sub-coat it achieved about 55% MO degradation at 26 h. The sub-coatings alone had little effect on MO degradation. MO alone did not degrade and remained at 0%.

The UVA generated photocatalytic activities of the P or B sub-coatings alone or with P25, Br200, or BrNMP Titania coatings (2mg TiO_2 / 38mm^2 cover slip) were evaluated by MO oxidative degradation as shown in Figure 5. All Titania coated onto the P sub-coat degraded the MO significantly faster than its counterpart on B sub-coating. BrNMP and Br200 on P sub-coating completed the MO degradation in 10 and 14 h, respectively. BrNMP and Br200 on B sub-coating completed the MO degradation in 18 and 22 h, respectively. The commercial P25 on P sub-coat attained approximately 80% degradation at 26 h and the P25 on B sub-coat achieved about 43% MO degradation at 26 h. The sub-coatings alone did not have much effect on MO degradation. MO alone did not degrade and remained at 0%. Statistics were determined using a student T-Test with alpha equal to 0.05. P or B Sub-Coating with MO (20 µM) in water at pH 4.0 exposed to UV light (365nm) with a (363-364 µW/cm2) intensity in with or without P- P-25 26+ h and P-Br200 14 h, or P-BrNMP 10 h, B- P-25 28+ h and B-Br200 22 h, or B-BrNMP 18 h oxidative degradation of MO. Br200 and BrNMP were significantly different from 2 h - 26 h ($p= 0.02 – 0.005$); P25 was significantly different from16 h-28 h (0.044 – 0.032). MO alone or on P or B- Sub-Coating was not significantly different throughout the 26 h evaluated ($p=0.35$).

The Visible Light generated photocatalytic activities of the P or B sub-coatings alone or with P25, Br200, or BrNMP Titania coatings (2 mg TiO_2 / 22 mm diameter cover slip) were evaluated by MO oxidative degradation as shown in Figure 6. Titania coated onto the P sub-coat degraded the MO significantly faster than its counterpart on B sub-coating. Br200 and BrNMP on P sub-coating completed the MO degradation in 12-14 h. Br200 and BrNMP on B sub-coating completed the MO degradation in 16-18 h and 20 h, respectively. The commercial vlp7000 on P sub-coat attained approximately 95% degradation at 26 h and on B sub-coat it achieved about 55% MO degradation at 26 h. The sub-coatings alone had little effect on MO degradation. MO alone did not degrade and remained at 0%. Percent survival of *E. coli* B (EC) CFU/mL with and without VLP 7000, Br200, and BrNMP Titania on B Sub-Coating exposed to a cool white 8 Watt bulb for either 0, 1, 2, 4, 6, 8, 10, 20, 30, 40, 50, or 60 minutes or the dark for 0, 30, or 60 minutes. (Error bars may be too small to see.)

Student T-Test indicated significant difference at an alpha of 0.05 between EC at 0 min to vlp7000, not significantly different at 0 or 10 min VL or 30 – 60 min D; significantly different at 20 – 60 min VL (p= 0.005 – 0.001); between EC at 0 min to Br200, not significantly different at 0, 2, 4, or 6, min VL or 30 – 60 min D (p= 0.3 – 0.2), but significantly different at 8 – 60 min VL (p= 0.01 – 0.0002); and between EC at 0 min to BrNMP, not significantly different at 0 min VL or 30 – 60 min D, but significantly different at 10 – 60 min VL (p= 0.04 – 0.0002).

Preliminary studies were performed with Titania in modified, miniaturized free suspension assays to determine a starting concentration of Titania for the coating studies.

Dilution curves indicate linear results with minimal background in the 10^3 to 10^8 CFU/mL range using the Live/Dead® *Bac*Light™ Bacterial Viability fluorescent based Assay (L-7012, Molecular Probes, Eugene, OR) as shown in Figure 7.

Evaluation of the second assay dilution curve results indicate linearity with minimal background in the 10^2 to 10^7 CFU/mL range using the Luminescent Assay Bac Titer-Glo™ Microbial Cell Viability Assay (Promega: Madison, WI, USA) depicted in Figure 8.

Effects of UVA activated P25, Br200 and BrNMP Titania 1 mg/mL using the miniaturized free suspension on *E. coli* B (EC) with the *Bac*Light ™Assay over a 2 h time period were evaluated (Figure 12). Results indicated that Br200 yielded an 8 log drop in 30 minutes. BrNMP and P25 required 2 h to yield the 8 log drop. P25 in the dark incurred an approximate 0.5 log drop during the 2 h, while Br200, BrNMP, and EC in both UVA and dark remained the same.

Evaluation of the lower count (1×10^4) bacteria using either the Spiral Plater or manual cell spreading yielded a 4 log drop in 60 or 90 seconds with P25 and Br200, respectively (Figure 13). EC in both UV and Dark along with P25 and Br200 in the dark results yielded the same as time zero. Student T-Test indicated significant difference at an alpha of 0.05 between EC at 0 sec to P25, not significantly different at 0, or 90-120 sec in the dark, but significantly different at 30 – 120 sec in UVA ($p= 0.004 – 0.002$); between EC at 0 min sec to Br200, not significantly different at 0 min UVA or 90 - 120 sec D or at 30 sec in UVA; but significantly different at 60 – 120 sec in UVA ($p= 0.006 – 0.002$).

The effects of visible light (VL) activated Br200, BrNMP, or vlp7000 Titania nanoparticles on EC were evaluated as shown in Figure 14. Br200 results yielded a 4 log drop in EC within 30 minutes; vlp7000 completed the 4 log drop in 60 minutes while BrNMP results yielded a ~2.5 log drop in 60 minutes. EC under light or in the dark, Br200, BrNMP, and vlp7000 with EC cultures in the dark remained viable.

The results of exposing free suspension Titania nanoparticles (VLP 7000, Br200, and BrNMP) to visible light using a fluorescent 8 Watt cool white bulb at 100 $\mu W/cm^2$ intensity on *E. coli* B for 0, 10, 20, 30, 40, 50, or 60 minutes yielded the results shown in Figure X. Dark measurements were also recorded at 0, 30, and 60 minutes. Three separate experiments were performed in triplicate with the results normalized in a percent survival curve and recorded.

Br200 EC under visible light dropped to zero percent alive within 30 minutes for all experiments and within 20 minutes for two of the three experiments. VLP7000 EC and BrNMP EC dropped to 0% within 60 minutes for two of the three experiments.

Student T-Tests were performed with an alpha of 0.05. At zero minutes all variables were not significantly different and results were normalized at 100%. At ten minutes of exposure to visible light Br200 EC (51%) and BrNMP EC (59%) were significantly different to EC alone (88%) with p values of 0.0014 and 0.0001, respectively. VLP700 EC dropped to 79%. VLP7000 EC was significantly different to Br200 EC (p=0.0275). Other variables were not significantly different at 10 minutes. At 20 minutes exposure, Br200 EC (13%) and BrNMP EC (54%) were significantly different to EC alone (78%) with p values of 0.0016 and 0.0214, respectively. VLP7000

EC (65%) was significantly different to Br200 EC (p=0.0105). Br200 EC was significantly different to BrNMP EC (p=0.0003). Other variables were not significantly different at 20 minutes. At 30 minutes exposure to visible light, VLP7000 EC (54%), Br200 EC (0%) and BrNMP EC (52%) were significantly different to EC alone (88%) with p values of 0.0109, $3.9x10^{-6}$ and 0.0009, respectively. VLP7000 EC was significantly different to Br200 EC (p=0.0001). Br200 EC was significantly different to BrNMP EC ($p=3.06x10^{-6}$). Other variables were not significantly different at 30 minutes. At 40 minutes exposure to visible light, VLP7000 EC (38%), Br200 EC (0%) and BrNMP EC (53%) were significantly different to EC alone (75%) with p values of 0.0001, $1.4x10^{-6}$ and 0.0296, respectively. VLP7000 EC was significantly different to Br200 EC (p=0.0004). Br200 EC was significantly different to BrNMP EC ($p=2.69x10^{-5}$). Other variables were not significantly different at 40 minutes. At 50 minutes exposure to visible light, VLP7000 EC (22%), Br200 EC (0%) and BrNMP EC (45%) were significantly different to EC alone (80%) with p values of 0.0007, $1.92x10^{-8}$ and 0.0024, respectively. VLP7000 EC was significantly different to Br200 EC (p=0.0365) and BrNMP EC (p=0.0056). Br200 EC was significantly different to BrNMP EC (p=0.0003). At 60 minutes exposure to visible light, VLP7000 EC (2.7%), Br200 EC (0%) and BrNMP EC (10%) were significantly different to EC alone (65%) with p values of 4.36x10-5, $2.86x10^{-8}$ and 0.0006, respectively. Other variables with visible light exposure were not significantly different at 60 minutes.

EC alone samples that remained in the dark throughout 30 (98%) or 60 minutes (103%) were not significantly different from EC alone (100%) at zero minutes. VLP7000

EC was significantly different at both 30 (77%) and 60 minutes (66%) when compared to it zero time point (100%) with p values of 0.0237 and 0.0145 respectively. Br200 EC was not significantly different to the zero time point (100%) from either the 30 (95%) or 60 minute (95%) time points. BrNMP EC was significantly different to the 30 (80%) and 60 minute (80%) time points with p values of $6.78x10^{-5}$ and 0.0056, respectively.

Comparing EC alone under visible light at 30 minutes (88%) to EC alone in the dark 30 minutes (98%) was significantly different with a p value of 0.0333. EC alone at 60 minutes comparing visible light (65%) to dark (103%) exposure was also significantly different (p=0.0042). VLP EC at 60 minutes comparing visible light (2.7%) to dark (66%) exposure was significantly different (p=0.0013). Comparing Br200 EC under visible light at 30 minutes (0%) to Br200 EC in the dark at 30 minutes (95%) was significantly different with a p value of $9.996x10^{-9}$. Br200 EC at 60 minutes comparing visible light (0%) to dark (95%) exposure was also significantly different ($p=2.48x10^{-8}$). Comparing BrNMP EC under visible light at 30 minutes (52%) to BrNMP EC in the dark at 30 minutes (80%) was significantly different with a p value of 0.0002. BrNMP EC at 60 minutes comparing visible light (10%) to dark (80%) exposure was also significantly different (p=0.0003). Br200 results indicated a much stronger killing capability than either VLP7000 or BrNMP under visible light.

P or B sub-coatings with or without Br200, BrNMP, or P25 Titania ($2mg/38mm^2$ surface) were evaluated every 10 minutes under UVA irradiation for 0-60 minutes. Depicted in Figure 15, are the photocatalytic activity results with the P sub-coating. Br200, P25, and BrNMP results yielded a 4 log drop in viable cells within 30, 40, or 50

minutes, respectively. EC alone or on the P sub-coating exposed to UVA remained viable. All samples exposed to the dark for 1 h remained viable. Student T-Test indicated significant difference at an alpha of 0.05 between EC at 0 min to P25, not significantly different at 0 or 10 min UVA; significantly different at 20 – 60 min VL ($p= 2.5 \times 10^{-5}$ – 1.3×10^{-6}), and at 30 – 60 min D (p= 0.039 – 0.002); between EC at 0 min to Br200, not significantly different at 0 or 10 min UVA or 30 – 60 min D (p= 0.3 – 0.2), but significantly different at 20 – 60 min UVA ($p= 5 \times 10^{-4}$ – 1. X 10^{-6}); and between EC at 0 min to BrNMP, not significantly different at 0 or 10 min UVA, or 30 – 60 min D, but significantly different at 20 – 60 min UVA ($p= 0.001 – 1.3 \times 10^{-6}$).

Figure 16 shows the results of the UVA activation (365 nm, 363-364 $\mu W/cm^2$) of Br200, BrNMP, or P25 on the B sub-coating. Br200 killed the total EC with a 4 log drop in 40 minutes. BrNMP or P25 completely reduced the viable count to 0 at 50 and 60 minutes, respectively. Binder under UVA irradiation and P25 in the dark reduced the cell population by ~20%. EC alone and all variable dark exposed samples except P25 in the dark maintained the viable population of cells. Student T-Test indicated significant difference at an alpha of 0.05 between EC at 0 min to P25, not significantly different at 0 min UVA; significantly different at 10 – 60 min UVA (p= 0.01 – 0.001), and at 30 – 60 min D (p= 0.04– 0.002); between EC at 0 min to Br200, not significantly different at 0 min UVA or 30 – 60 min D (p= 0.3 – 0.2), but significantly different at 10 – 60 min UVA (p= 0.001 – 0.01); and between EC at 0 min to BrNMP, not significantly different at 0 min UVA or 60 min D, but significantly different at 10 – 60 min UVA (p= 0.04 – 0.001), or 30 min D (p= 0.01).

P or B sub-coatings with or without Br200, BrNMP, or vlp7000 Titania (2mg/38mm^2 surface) were evaluated every 10 minutes under VL (Cool White 8 Watt lamp, 0.1mW/cm^2) for 0-60 minutes (Figures 17 and 18). Additionally, Br200 was tested at 0, 1, 2, 4, 6, 8, and 10 minutes separately with the proper controls to determine the survival curve. Depicted in Figure 17, are the photocatalytic activity results using the P sub-coating. Br200, BrNMP, and vlp7000 results yielded a 4 log drop in viable cells within 8, 30, or 40 minutes, respectively. EC alone or EC on the P sub-coating exposed to VL irradiation remained viable. All samples exposed to the dark for 1 h remained viable. Student T-Test indicated significant difference at an alpha of 0.05 between EC at 0 min to P25, not significantly different at 0 min VL or 30 – 60 min D; significantly different at 10 – 60 min VL (p= 0.01 – 0.003); between EC at 0 min to Br200, not significantly different at 0, 2, 4, or 6 min VL or 30 – 60 min D (p= 0.3 – 0.2), but significantly different at 8 – 60 min VL (p= 0.002 – 4 x 0^{-11}); and between EC at 0 min to BrNMP, not significantly different at 0 min VL or 30 – 60 min D, but significantly different at 10 – 60 min VL (p= 0.02 – 0.002).

Figure 18 shows the results of the VL activation of Br200, BrNMP, or vlp7000 on the B sub-coating. Br200 killed the total EC with a 4 log drop in 40 minutes. BrNMP or vlp7000 completely reduced the viable count to 0 at 50 or 60 minutes, respectively. Binder under VL irradiation reduced the cell population by ~20%. EC alone exposed to VL and all variable samples in the dark maintained the viable population of cells. Student T-Test indicated significant difference at an alpha of 0.05 between EC at 0 min to vlp7000, not significantly different at 0 or 10 min VL or 30 – 60 min D; significantly

different at 20 – 60 min VL (p= 0.005 – 0.001); between EC at 0 min to Br200, not significantly different at 0, 2, 4, or 6, min VL or 30 – 60 min D (p= 0.3 – 0.2), but significantly different at 8 – 60 min VL (p= 0.01 – 0.0002); and between EC at 0 min to BrNMP, not significantly different at 0 min VL or 30 – 60 min D, but significantly different at 10 – 60 min VL (p= 0.04 – 0.0002).

3.4 Discussion

X-ray Photoelectron Spectroscopy (XPS) verified that Titanium molecules were present on the surface of the coatings, allowing the Titania to have direct contact with the organic substance to be oxidatively degraded. TiO_2 P-25 was free of Cl 2p while Brookite contained 2.31% mass concentration. This may have contributed to the increased oxidative efficacy of the Brookite. Both contained small amounts C 1s which may have come from atmospheric pressure rather than as a consequence of the precursor [62].

X-ray Diffraction (XRD) confirmed the peaks of Br200 and BrNMP to the original powder sample peaks [66, 68]. This verified that the Br200 and BrNMP Titania coatings should have the same percent of TiO_2 phases meaning the specific type of crystal lattice structure contained within each sample as the nanoparticle powders with approximately 44-45% Anatase, 53% Brookite, and 2-3% Rutile.

Low temperature calcination of 200^{o}C for 2 h on both Br200 and BrNMP Titania produced crystallite sizes ranging from 5-8 nm, therefore, providing a very high surface area ranging from (BET) 138 - 157 m^2/g [65]. This provides a significantly greater surface area per particle than the Degussa commercial P25 reference standard at (BET)

56 m^2/g with 79% Anatase and 21% Rutile phase TiO_2. The Kronos vlp7000 has an approximate 15 nm crystallite size with a surface area of (BET) 225 m^2/g and a stable working pH range of 4 – 9. The Kronos vlp7000 has a much larger surface area than the Brookite samples. The crystal lattice structure of Br200 and BrNMP contains Brookite phase which is orthorhombic and Anatase phase which is tetragonal. Kaewgun and colleagues proposed that the mixture of orthorhombic phase and tetragonal phase in Br200 or BrNMP caused a slower electron/hole recombination due to the transfer between the two phases of crystallites [69]. Even though the Kronos vlp7000 has a much larger surface area of (BET) 225 m^2/g than the polymorphic Brookite (BET) 157 m^2/g [66], it is made with pure Anatase and the single phase product may contribute to a faster electron/hole recombination, decreasing the photocatalytic efficiency.

The two different sub-coatings displayed different hydrophilic properties. The P sub-coating exhibited extreme hydrophilic surfaces as shown in Figure 4, while the B sub-coatings exhibited hydrophobic surfaces. The P coatings contained strong polyelectrolytes and were rinsed in neutral pH nanopure 18Ω water between each layer and after completion. In contrast, the B sub-coating is finalized at pH3. The surface tack and surface gloss were both observed to be low in the P sub-coating and both were observed to be high in the B sub-coating. After the liquid phase deposition of the Titania followed by air drying, the surface gloss of the P sub-coating remained lower than the surface gloss of the B sub-coating. Bacteria are attracted to the hydrophilic surface of the P sub-coatings with Titania. Therefore the bacteria can interact more quickly with the Titania and its free radicals causing oxidative death more quickly. The hydrophobicity of

the B sub-coating can repel the negative charge of the bacteria. This could be the factor that causes the P sub-coating to provide faster killing. The distance and orientation of the bacteria to the active sites of the Titania are also factors affecting the photocatalytic activity.

Other considerations that may increase the enhancement effect of the P sub-coating over the B sub-coating include the following. According to mindat.org, it was named for Henry James Brooke (1771-1857), who was an English crystallographer and mineralogist. The length of edges on the orthorhombic crystallite of Brookite phase Titania are, a=5.4558 Å, b=9.1819 Å, and c= 5.1429 Å, where 1 nm = 10 Å [70]. The OHBA crystal structure site labeled the Brookite Space group as Pbca and the Pearson symbol as oP24 [71]. OHBA reported that it contains approximately two atoms thick with four layers on one edge, boding well for surface adsorption of N and S. Because the crystallite particle sizes are 5-8 nm in diameter, bulk properties break down, surface area and surface tension to volume significantly increases causing surface effects to dictate properties [71]. Light absorption and re-emission properties change. Due to ionic bonding, the ion size of the Sulfur in either the +4 state (0.37 Å), or the +6 state (0.29 Å) or ion size of the Nitrogen in either the +3 state (0.16 Å) or the +5 state (0.13 Å), indicates that either one could easily adsorb to the surface [72]. This would aid in broadening the absorption edge, narrowing the band-gap, causing the photocatalytic activity of Br200 and BrNMP to significantly increase.

Buffer composition and pH play a strong role in the oxidative ability of TiO_2 to kill bacteria. The PBS contained phosphate anions which strongly adsorb to TiO_2 forming

bidentate complexes, shifting the isoelectric point down towards pH 2.0 [62, 73-74]. This may have caused a lack of adjacent sites to the oxide, hence, preventing the formation of tetrahedrally coordinated water. pH values below the isoelectric point of the TiO_2 may possibly flip the water dipoles [62]. The TiO_2 in water at pH 4.0 proved to have more efficient results in killing the bacteria than pH 7.4 whether in water or PBS. These results indicate that photocatalytically activated TiO_2 P-25 or Brookite at pH 4.0, optimum pH and diluent, can provide a non-selective modality for decreasing the transmission of pathogenic bacteria

MO oxidative degradation occurred in significantly less time with the Br200 and BrNMP Titania on either the P or B sub-coatings than the commercial P25 or vlp7000 Titania. Both the Br200 and BrNMP Titania on the P sub-coating was significantly faster than the B sub-coating to complete the MO degradation by 2 – 4 h under both UVA and VL irradiation. Neither P nor B sub-coating alone significantly degraded MO over the 26 h time period.

Using the *Bac*Light™ Assay, UVA irradiation on suspended Br200 Titania was 90 minutes faster than BrNMP, or P25 Titania in AW. While in the lower cell population, enumerating with viable cell counts, the commercial P25 was faster by 30 seconds at completing the 4 log kill of cells than Br200. That was the first time in this study that the commercial P25 was faster than Br200.

Evaluating the effects of VL irradiation to photocatalytically activate the suspended Br200, BrNMP or vlp7000 Titania on bacterial killing resulted in Br200 displaying a complete elimination of viable bacteria within 30 minutes. P25 Titania

required twice the amount of time and BrNMP did not complete the elimination in the 60 minute time period.

Br200 Titania on either P or B sub-coating, with either UVA or VL irradiation eliminated all viable cells from 10 – 22 minutes faster than the next fastest Titania type. With either UVA or VL irradiation, Br200, BrNMP, and P25 (UVA) or vlp7000 (VL) on the P sub-coating averaged total elimination of viable cells 10 minutes faster than with the Titania on the B sub-coating. VL irradiation (0.1mW/cm^2) activated all appropriate types of Titania equally or better than UVA irradiation at 363-364 μW/cm^2 on appropriate Titania samples.

3.5 Conclusions

Light intensity, wavelength, surface material characteristics, pH, band gap, efficiency of hole-electron recombination, amount of dissolved oxygen, broad edge (indirect bandgap) versus sharp edge (direct bandgap), number of available active surface sites, and bacterial load affect efficiency of photo-oxidation. Based on the results obtained in this study, Br200 Titania on the P Sub-Coating provided superior oxidative activity on both MO degradation and EC bacterial killing. One explanation is reported by Zallen and Moret, 2006. At ambient temperature, natural Brookite TiO_2 crystals were examined via optical-absorption ranging from 2.1 to 3.54 eV. The Brookite TiO_2 absorption edge is broad, continuing throughout the visible range with no direct gap [9]. In contrast to tetragonal forms, the orthorhombic structure encompasses a larger range of bond lengths from the six unique nearest-neighbor Ti-O bond lengths. They suggest that

Brookite TiO_2 is an indirect-gap semiconductor with a bandgap approximating 1.9 eV [9].

The low temperature method in which the Br200 or BrNMP were formed and calcined, produced small crystallite sizes ranging from 5 – 8 nm in diameter, and a large surface area, approximately (BET) 157 m^2/g [66]. The monolith bulk properties give way to surface effect characteristics as the crystallites are four layers on one edge and two atoms thick enabling N and S surface adsorption [70-72]. This large surface area would provide more opportunities for contact with molecules. The smaller crystallite sizes allow for more particles to make up a specific mass, hence providing more surface area due to higher numbers of particles. vlp7000 contains a larger surface area to volume ratio of (BET) 225 m^2/g than Brookite. Therefore, the higher activities of the Br200 or BrNMP may be from the polymorphic composition in the combination of Brookite and Anatase. This combination may cause the electron/holes to recombine more slowly since the electrons must travel from one type of lattice structure to a different type of lattice structure, while vlp7000, made of pure Anatase, produced efficient electron/hole recombination. Thus, the Br200 and BrNMP in conjunction with the P sub-coating were superior to vlp7000 in visible light.

Based on our results, Br200 on P Sub-Coating consistently had stronger photocatalytic activity than BrNMP on P or B Sub-Coating. Theory suggested it should have been the opposite since BrNMP is associated with a Nitrogen containing compound, N-methylpyrrolidone at 168^{o}Celsius for 4 h (4g/200mL) as described in [65]. Charred organic residue of NMP remaining on the surface covered up or was bound to active sites

on the Brookite, providing less photocatalytically active sites to oxidize bacteria. It was found that temperatures of 420^{o}C were required to remove all of the extraneous NMP, and these high temperatures caused phase changes to a more Anatase product and sintering which caused reduction in surface area to volume ratio, decreasing the photocatalytic activity [68]. Since bacteria are much larger than the Titania crystal particles whether in suspension or bound onto a surface, distance and orientation effects would be more pronounced for bacteria than for Methyl orange [61].

Also one may propose that the hydrophobic nature of the B Sub-coating may have delayed the BrNMP activity, but all samples were exposed to the B Sub-coating and Br200 was more active than BrNMP, again due to residual charred organic residue and blockage of potential photocatalytic active sites. However, each Titania on the P coating performed complete biocidal killing 10 minutes faster than its counterpart on the B Sub-coating. This may be the difference in the effect of the P Sub-coating super-hydrophilicity attracting the bacteria versus the B Sub-coating hydrophobic characteristics repelling the bacteria. The P sub-coating containing N and S molecules in different ionic states, through surface interaction affect the Titania. These effects lengthened the absorption edge into the visible range, narrowed the band-gap, thereby increasing the photocatalytic activity of the Titania.

Br200 results indicate that it has a stable pH working range that includes pH 3-4. The B sub-coating has a pH of 3 and the AW that was used in the experiments was at pH of ~4. The super hydrophilic surface characteristics of the P sub-coating aid in attracting the bacteria to adhere while hydrophobic coatings may even repel the bacteria somewhat.

EC and many other species of bacteria contain hydrophilic fimbriae that attach to biotic and abiotic surfaces [31-32].

After the bacteria adhere to the surface of the photocatalytically activated Br200 Titania surface, bacterial death ensues via two main mechanisms. First, consecutive oxidative attacks to the cell wall / membrane via the hydroxyl radical ($HO^{\cdot}$) [75] destabilize the cell wall. Secondly, the oxygen located on the TiO_2 surface can act in its molecular form as an electron acceptor in the superoxide anion radical form. When the adhered bacteria have direct contact with the photo-generated holes, their cell walls / membranes are further destabilized and decomposition ensues via irreversible loss of electrons and direct bond disruption at the TiO_2 surface [75-77]. After the cell wall is disrupted, the presence of superoxide anions and hydrogen peroxide, the Fenton and Haber-Weiss Reactions continue to produce hydroxyl radicals inside the bacteria, oxidizing the DNA. Chen and colleagues observed a correlation between the decomposition of bacteria and organics such as MO [78]. Therefore, based on this research, P sub-coatings with Br200 Titania displays a superior non-selective method of killing bacteria. This novel P Sub-Coating with bound Br200 Titania could provide non-selective surface coatings in the hospital, surgical, and long term care arenas to aid in prevention of transmission of pathogens and prevention of biofilm formation. In fact, because this coating is turned "on" when light is on (10^{-9} seconds) [59], and turned "off" when light is off, it could be used in many nosocomial settings, community settings, and on appliances, cars, and a vast number of other surfaces.

This work provided new evidence of low temperature association between the P sub-coating molecules and surface characteristic effects of the Titania showing superior photocatalytic activity on MO degradation and bactericidal properties.

3.6 Experimental

Titanium dioxide Br200 and BrNMP nanoparticles samples were generously given to our lab by Dr. B. I. Lee and Dr. S. Kaewgun of Clemson University. Br200 nanoparticles were made by the WACS process as described in [66]. This sample was calcined at 200^{o}Celsius for 2 hours (h) in air. SACS-NMP (BrNMP) was made by the WACS process with a SACS post treatment carried out in N-methylpyrrolidone at 168^{o}Celsius for 4 h (4g/200mL) as described in [65]. This BrNMP sample was calcined in air at 200^{o}Celsius for 2 h. For the long wave ultraviolet light (UVA) (365nm) comparisons, the commercial TiO_2, P25 from Degussa, (Evonik Industries AG, Germany) was used. For the Visible Light comparisons, the commercial Kronos vlp7000 (KRONOS, Inc., Dallas, TX) was used.

A super hydrophilic layer-by-layer (LBL) polyelectrolyte sub-coating using 0.1M Poly (diallyldimethylammonium chloride) (PDDA) and 0.1M Poly(styrenesulfonic acid) in nanopure water, separately, modifying the method from Tsuge et al. 2008 [79]. PDDA, Mw ~200,000–350,000, 20 wt.% aqueous solution), and PSS, Mw ~75,000, 18 wt.% aqueous solution) were purchased from Sigma-Aldrich. Due to the strong polyelectrolytic nature of PDDA and PSS, the pH was not adjusted.

At ambient room temperature #2 micro-cover-glass slips (22 mm diameter) (Electron Microscopy Sciences, Hatfield, PA) were prepared to receive the polyelectrolytes via Tsuge *et al.* 2008 method [79]. The 25-LBL coatings were made beginning with PDDA and ending with PSS and air dried. In this publication, the PDDA/PSS sub-coated slides will be labeled P. Another binder graciously provided by Dr. B.I. Lee was used, GPTS:TEOS (5:3) with HNO_3 and EtOH at pH = 3 to compare and test the effectiveness of the two sub-coatings. Aliquots (50 µL) of the binder (B) was deposited onto the glass cover slips and air dried. The glass cover slips sub-coated with either P or B were placed on a clean baking sheet.

Five mol of 3-glycidoxypropyl-trimethoxysilane (Gelest) was mixed with 3 mol of Tetramethyl orthosilicate (Alfa Aesar). Ethanol prehydrolyzed the solution (Alfa Aesar) at room temperature with constant stirring for 3h. Nitric acid was added to bring the pH to 3. Two aliquots of 50 µL of Binder were aseptically pipetted onto sterile glass cover slips with drying at room temperature in between. Then the coated slides were aseptically stored in a 24 well plate for further use.

Each Titania, Br200, Br-NMP, P25, or vlp7000 was mixed into nanopure water containing 2mL of 0.1M HCl per 100mL of water pH ~4. The acidic water is referred to as AW. The final Titania concentration was 6.67mg Titania/mL water. The liquid Titania suspensions were sonicated (Sonicator FS30H; Fisher Scientific) for 1 h and vortexed. Each sub-coated cover slip received 2 aliquots of 150 µL of Br200, Br-NMP, P25, or vlp7000 suspension, ($2mg/38mm^2$) with ambient air drying between aliquots. The Titania cover-slips were heated in a toaster oven at 60^oC for 1 h prior to use.

X-ray Photoelectron Spectroscopy (XPS) (Axis 165, Kratos; 20mA, Anode HT (12kV) was performed on the P sub-coating with and without Titania (pass energy of 40 with 0.5eV step, 120ms-dwell time and 3 sweeps per sample). Both general and high-resolution scans were performed. The XPS evaluation will identify elements on the surface of the sample. An X-ray powder diffractometer was used to determine phase composition and crystallite size of the TiO2 samples using a Rigaku ULTIMA IV with CuKα radiation at 1.5418Å, continuous scans with a sampling width of 0.020° over a range of 20 to 35^0 (2θ). Hydrophilicity was determined by dropping 10 µL of nanopure water onto the surface of the coating. A close up picture was taken from the direct side view for evaluation of the hydrophilic properties of each surface.

Contact angle of a surface will identify the wet-ability of a surface as shown in Figure 2. A hydrophilic surface is more difficult for hydrophobic walled bacteria to attach, therefore, decreasing bacterial attachment and biofilm formation. Using a macro-digital camera, we will determine the hydrophobic/hydrophilic characteristics of each sample's surface via contact angle measurement. Each coating type will receive a 10 µL drop of 18 Ω nanopure water.

Assuming a spherical or ellipsoid liquid droplet surrounded by gas resting on a solid surface, we will measure the hydrophilicity of the surface on our samples (n=4). Using a high resolution micro-lens camera, pictures will be taken of the three phase boundary where the liquid, gas, and solid intersect. The contact angle, θ_C, is the angle formed by a liquid at this three phase boundary and can be expressed by Young's Relation depicted in Figure 11 and Equation 1 below.

$$\gamma_{SG} = \gamma_{SL} + \gamma_{LG} \cos\theta \quad (1)$$

Where: γ_{SG} = Interfacial tension between the solid and gas

γ_{LG} = Interfacial tension between the solid and liquid

γ_{LG}= Interfacial tension between the liquid and gas

The B or P sub-coatings with or without Br200, Br-NMP, P25, or VLP7000 Titania were evaluated for photocatalytic activity. An empty well with Methyl Orange (MO) was used for the control. A multiple ray lamp (MRL, Model 58; Fisher Scientific) with different 8 Watt tubes UVA (365nm) at 363-364 μW/cm^2) and visible light (Cool White) at 0.100 mW/cm^2) was utilized as the source for photoactivation. The intensity of light was verified with a UVX Digital Radiometer, (Model-UVX, UVP, Inc., Upland, CA) and an ACCU- CAL-50-V (Dymax Corporation, CT) for UVA and visible light, respectively. Polystyrene plates (24-well) containing the Titania coated cover slips were secured onto a microplate orbital mixer (Microplate Genie, Model SI-0400, VWR). One milliliter of 20 μM MO solution was added to each well. A non-fluorescing optically clear film (TemPlate® RT Optical Film, 2978-2700, USA Scientific, Inc.) was adhered to the polystyrene plate to prevent evaporation of the MO. The lamp intensity was adjusted to accommodate the film.

Uniform samples were removed at 2 h intervals (0-26 h). Each sample containing Titania was filtered through a Puradisc™ 25 AS Disposable Filter Device with a 0.2 μm Polyethersulfone Membrane (Whatman, USA) to remove any possible free Titania, and to prevent false positive absorbance via scattering. Quantitative spectral results were

obtained with a Genesys 20 Thermo Spectronic spectrophotometer at 490 nm (Model 4001/4, Thermo Scientific, USA). The percent of MO oxidative degradation, D, was plotted against time in hours shown in Equation 2, where A_0 is the initial peak intensity at 490 nm, and A is the instantaneous peak intensity at 490 nm.

$$D = \frac{C_0 - C}{C_0} \times 100\% = \frac{A_0 - A}{A_0} \times 100\% \quad (2)$$

Escherichia coli B (*E. coli* B) (ATCC 11303, Manassas, VA) was purchased from the American Tissue Culture Collection (ATCC). Cultures incubated in Tryptic Soy Broth (TSB) for 12-14 h in an Environmental Incubator Shaker (Model G24, New Brunswick Scientific) were harvested and centrifuged at 7,000 x g in a microcentrifuge (Eppendorf Centrifuge, Model 5417R). Stock cultures of *E. coli* B were frozen in TSP + 5% Glycerol and stored at -80^{o}C till further use.

Because Phosphate has a very high affinity to TiO_2, acidic sterile water (AW) at ~pH4 (2mL of 0.1M HCl / 100mL water) was used for these assays instead of Phosphate Buffered Saline. Cells were washed three times in AW with centrifugation. Upon re-suspension, the cells were standardized at an Optical Density (OD) of 600 n using a BioRad Smart Spec 3000 (BioRad, USA). A result of 0.2 at OD600 is roughly equivalent 10^9 CFU/mL of *E. coli* B as calculated from replicate dilution curves. All experiments were performed three times in $\geq$ triplicate each.

E. coli B (ATCC 11303, Manassas, VA) were maintained in Tryptic Soy Broth medium for 12-16h at 37^{o}C and examined in a direct contact model using the Free Suspension Assay [67] for 0-2h with or without TiO_2 (1mg/mL) P-25 or Brookite-200,

separately. TiO_2 nanoparticles were activated under long range ultra violet (UV) light (365nm; 364µW/cm^2) at time points of 0, 30, 75, and 120 minutes in sterile water at pH 4 or pH 7.4, or in Phosphate buffered saline (PBS) at pH 7.4. Quantification of bacterial culture by Optical Density (OD) 600nm was verified prior to each experiment. Quantification of *E. coli* B was performed in triplicate by dilution plating with a Spiral Plater (Spiral Biotech, Norwood, MA) on Tryptic Soy Agar and incubated 24 h at 37^{o}C and counted.

To reduce the amount of material, time, labor, and cost, two different assay types were evaluated in order to miniaturize the assays. Dilution curves of *E. coli* B (n=8) were evaluated. The Live/Dead® *Bac*Light™ Bacterial Viability Assay (L-7012, Molecular Probes, Eugene, OR) is a fluorescence based assay for distinguishing live and dead bacteria in a mixed population. SYTO® 9 green-fluorescent nucleic acid stain (480/500 nm) penetrates healthy bacterial cells labeling all bacteria in a population; propidium iodide (490/635 nm) penetrates only bacteria with damaged membranes, causing a reduction in the SYTO 9 stain fluorescence when both dyes are present.

A second assay was also evaluated. The Luminescent Assay Bac Titer-Glo™ Microbial Cell Viability Assay (Promega: Madison, WI, USA) quantitates the amount of ATP present in metabolically active cells. It is based on the luciferase reaction. Mono-oxygenation of luciferin is catalyzed by luciferase in the presence of Mg2+, ATP, and molecular oxygen.

Because Phosphate has a very high affinity to TiO_2, acidic sterile water (AW) at ~pH4 (2mL of 0.1M HCl / 100mL water) was used for these assays instead of Phosphate

Buffered Saline. Cells were washed three times in AW with centrifugation. Upon re-suspension, the cells were standardized at an Optical Density (OD) of 600 n using a BioRad Smart Spec 3000 (BioRad, USA). A result of 0.2 at OD600 is roughly equivalent 10^9 CFU/mL of *E. coli* B as calculated from replicate dilution curves.

The six well – six mL volume free suspension assay was miniaturized to a 24 well format using a 1 mL volume assay. Many testing variables could evaluated at the same time under this new assay format. A non-fluorescing optically clear film (TemPlate® RT Optical Film, 2978-2700, USA Scientific, Inc.) was adhered to the polystyrene plate to prevent evaporation of the bacterial suspension in AW. The lamp intensity was adjusted to accommodate the film via the Radiometers.

After testing, 100 µL aliquots (n=4) from each sample well was dispensed into a 96 well black or white plate for fluorescence or luminescence assay, respectively. The 24 well testing assay in combination with either the fluorescent LIVE/DEAD® *Bac*Light™ Bacterial Viability Kit or the luminescent BacTiter-Glo™ Microbial Cell Viability Assay was evaluated after subtracting the background and to determine if the background was too large. Different Titania concentrations were evaluated, 0.1 mg/mL, 1 mg/mL or 10 mg/mL in both assays.

Miniaturized, modified free suspension assays were performed to determine a starting point for the amount of TiO_2 to use in the coatings. Because preliminary dilution curve results indicated linearity with minimal background in the 10^3 to 10^8 CFU/mL or 10^2-10^7 CFU/mL range with the LIVE/DEAD® *Bac*Light™ Bacterial Viability Kit or the luminescent BacTiter-Glo™ Microbial Cell Viability Assay, respectively, these assays

were used for higher bacterial loads in experiments, specifically the *Bac*Light™ as it conserved time better than the cTiter-Glo™ with similar results. All modified free suspension assay Titania concentrations were 1 mg/mL.

To determine the lower viable range (10^0-10^4 CFU/mL) of *E. coli* B, either Spiral Plating (Spiral Biotech Autoplate, Model 4000) or manual cell spreading on Tryptic Soy Agar petri dishes were performed in triplicate. The bacteria were incubated at 37°C for ~24 h and enumerated. Results from these assays are normalized and plotted as Time (x-axis) versus % Survival (y- axis). Calculations were based on the number of viable cell counts at various time points as percentages described in Equation 3. All experiments were replicated for reproducibility.

$$\frac{\text{Number of Viable Cells (CFU/mL) at Time t}}{\text{Number of Viable Cells (CFU/mL) at Time } t_0} \times 100 \qquad (3)$$

E. coli B cultures were incubated in TSB for 12-14 h in an Environmental Incubator Shaker (Model G24, New Brunswick Scientific). The cultures were harvested and centrifuged at 7,000 x g in a microcentrifuge (Eppendorf Centrifuge, Model 5417R) in AW. The coated cover slips (22 mm in diameter) (#72227-01, No2 Micro Coverglass; Electron Microscopy Sciences, Hatfield, PA) were aseptically inserted into 24 well plates. Because the 24 well plates used had a 22.2 mm diameter bottom, a secure ring was not needed to retain the bacteria on the coated cover slip.

Because Phosphate has a very high affinity to TiO_2, acidic sterile water (AW) at ~pH4 (2mL of 0.1M HCl / 100mL water) was used for these assays instead of Phosphate Buffered Saline. Cells were washed three times in AW with centrifugation. Upon re-

suspension, the cells were standardized at an Optical Density (OD) of 600 n using a BioRad Smart Spec 3000 (BioRad, USA). A result of 0.2 at OD600 is roughly equivalent 10^9 CFU/mL of *E. coli* B as calculated from replicate dilution curves.

E. coli B cells at 1 x 10^4 CFU/mL AW were aliquoted 1 mL per well into a 24 well plate containing various coated cover slips. Exposure times of 0, 2, 4, 6, 8, 10, 20, 30, 40, 50, or 60 minutes were evaluated. At the end of each time period, the samples of *E. coli* B (50 µL), using either Spiral Plating (Spiral Biotech Autoplate, Model 4000) or manual cell spreading on Tryptic Soy Agar petri dishes were performed in triplicate. The bacteria were incubated at 37^{o}C for ~24 h and enumerated. Results from these assays are normalized and plotted as Time (x- axis) versus log 10 Survival (y- axis). Calculations were based on the number of viable cell counts at various time points as percentages described in Equation 3.

The B or P sub-coatings with or without Br200, Br-NMP, P25, or VLP7000 Titania were evaluated for photocatalytic activity. Sub-coatings alone without Titania were used for the controls. A multiple ray lamp (MRL, Model 58; Fisher Scientific) with different 8 Watt tubes UVA (365nm) at 363-364 µW/cm^2) and visible light (Cool White) at 0.100 mW/cm^2) was utilized as the source for photoactivation. The intensity of light was verified with a UVX Digital Radiometer, (Model-UVX, UVP, Inc., Upland, CA) and an ACCU- CAL-50-V (Dymax Corporation, CT) for UVA and visible light, respectively. Polystyrene plates (24-well) containing the Titania coated cover slips were secured onto a microplate orbital mixer (Microplate Genie, Model SI-0400, VWR). One milliliter of 1 x 10^4 E. coli B in AW was added to each well. A non-fluorescing optically clear film

(TemPlate® RT Optical Film, 2978-2700, USA Scientific, Inc.) was adhered to the polystyrene plate to prevent evaporation of the bacterial suspension in AW. The lamp intensity was adjusted to accommodate the film via the Radiometers.

3.7 References

1. Bratu, S., Steven Brooks, Sibte Burney, Sandeep Kochar, Jyoti Gupta, David Landman, and John Quale, *Detection and Spread of Escherichia coli Possessing the Plasmid-Borne Carbapenemase KPC-2 in Brooklyn, New York.* Clinical Infectious Diseases, 2007. 44: p. 972-975.
2. Jawad, A., et al., *Survival of Acinetobacter baumannii on Dry Surfaces: Comparison of Outbreak and Sporadic Isolates.* J. Clin. Microbiol., 1998. 36(7): p. 1938-1941.
3. Savini, V., et al., *Misidentification of ampicillin-sulbactam heteroresistance in Acinetobacter baumannii strains from ICU patients.* Journal of Infection, 2009. In Press, Corrected Proof.
4. Giamarellou, H., A. Antoniadou, and K. Kanellakopoulou, *Acinetobacter baumannii: a universal threat to public health?* International Journal of Antimicrobial Agents, 2008. 32(2): p. 106-119.
5. Wendt, C., et al., *Survival of Acinetobacter baumannii on dry surfaces.* J. Clin. Microbiol., 1997. 35(6): p. 1394-1397.
6. Perez, F., et al., *Global Challenge of Multidrug-Resistant Acinetobacter baumannii.* Antimicrob. Agents Chemother., 2007. 51(10): p. 3471-3484.

7. Fournier, P.-E., et al., *Comparative Genomics of Multidrug Resistance in <italic>Acinetobacter baumannii</italic>*. PLoS Genet, 2006. 2(1): p. e7.

8. Nemec, A., et al., *Diversity of aminoglycoside-resistance genes and their association with class 1 integrons among strains of pan-European Acinetobacter baumannii clones.* J Med Microbiol, 2004. 53(12): p. 1233-1240.

9. Oliveira, D.C., A. Tomasz, and H. de Lencastre, *Secrets of success of a human pathogen: molecular evolution of pandemic clones of meticillin-resistant Staphylococcus aureus.* The Lancet Infectious Diseases, 2002. 2(3): p. 180-189.

10. Cirz, R.T., et al., *Inhibition of Mutation and Combating the Evolution of Antibiotic Resistance.* PLoS Biol, 2005. 3(6): p. e176.

11. Perez-Capilla, T., et al., *SOS-Independent Induction of dinB Transcription by {beta}-Lactam-Mediated Inhibition of Cell Wall Synthesis in Escherichia coli.* J. Bacteriol., 2005. 187(4): p. 1515-1518.

12. Magnet, S., P. Courvalin, and T. Lambert, *Resistance-Nodulation-Cell Division-Type Efflux Pump Involved in Aminoglycoside Resistance in Acinetobacter baumannii Strain BM4454.* Antimicrob. Agents Chemother., 2001. 45(12): p. 3375-3380.

13. Kohanski, M.A., M.A. DePristo, and J.J. Collins, *Sublethal Antibiotic Treatment Leads to Multidrug Resistance via Radical-Induced Mutagenesis.* Molecular Cell, 2010. 37(3): p. 311-320.

14. Costerton, J.W., and P.H. Stewart, *Battling Biofilms.* Scientific American: Special Supplement 2006: p. 2-11.

15. Schembri, M.A., D. Dalsgaard, and P. Klemm, *Capsule shields the function of short bacterial adhesins.* J Bacteriol, 2004. 186(5): p. 1249-57.

16. Mehrotra, A., *Bacterial Biofilms.* Pediatric Asthma, Allergy & Immunology, 2007. 20(3): p. 191-195.

17. Reisner, A., et al., *In Vitro Biofilm Formation of Commensal and Pathogenic Escherichia coli Strains: Impact of Environmental and Genetic Factors.* J. Bacteriol., 2006. 188(10): p. 3572-3581.

18. Jones, C.H., *FimH adhesin of type 1 pili is assembled into a fibrillar tip structure in the Enterobacteriaceae.* Proc. Natl. Acad. Sci. , 1995. 92: p. 2081-2085.

19. Bower, J.M., D.S. Eto, and M.A. Mulvey, *Covert Operations of Uropathogenic Escherichia coli within the Urinary Tract.* Traffic, 2005. 6(1): p. 18-31.

20. Das, M., et al., *Hydrophilic Domain II of Escherichia coli Dr Fimbriae Facilitates Cell Invasion.* Infect. Immun., 2005. 73(9): p. 6119-6126.

21. Ahmer, B.M.M., *Cell-to-cell signalling in Escherichia coli and Salmonella enterica*. Molecular Microbiology, 2004. 52(4): p. 933-945.

22. Venturi, V.a.S.S., *Future research trends in the major chemical languaage of bacteria.* HFSP Journal, 2009. 3(2): p. 105-116.

23. Costerton, J.W., P.S. Stewart, and E.P. Greenberg, *Bacterial biofilms: a common cause of persistent infections.* Science, 1999. 284(5418): p. 1318-22.

24. Maira-Litran, T., D.G. Allison, and P. Gilbert, *An evaluation of the potential of the multiple antibiotic resistance operon (mar) and the multidrug efflux pump acrAB to moderate resistance towards ciprofloxacin in Escherichia coli biofilms.* J Antimicrob Chemother, 2000. 45(6): p. 789-95.

25. Genevaux, P., S. Muller, and P. Bauda, *A rapid screening procedure to identify mini-Tn10 insertion mutants of Escherichia coli K-12 with altered adhesion properties.* FEMS Microbiol Lett, 1996. 142(1): p. 27-30.

26. Stewart, P.S., *A review of experimental measurements of effective diffusive permeabilities and effective diffusion coefficients in biofilms.* Biotechnol Bioeng, 1998. 59(3): p. 261-72.

27. Ishida, H., et al., *In vitro and in vivo activities of levofloxacin against biofilm-producing Pseudomonas aeruginosa.* Antimicrob Agents Chemother, 1998. 42(7): p. 1641-5.

28. Shigeta, M., et al., *Permeation of antimicrobial agents through Pseudomonas aeruginosa biofilms: a simple method.* Chemotherapy, 1997. 43(5): p. 340-5.

29. de Beer, D., et al., *Effects of biofilm structure on oxygen distribution and mass transport.* Biotechnol. Bioeng., 1994. 43: p. 1131-1138.

30. Brown, M.R. and J. Barker, *Unexplored reservoirs of pathogenic bacteria: protozoa and biofilms.* Trends Microbiol, 1999. 7(1): p. 46-50.

31. Darouiche, R.O., et al., *Efficacy of antimicrobial-impregnated bladder catheters in reducing catheter-associated bacteriuria: a prospective, randomized, multicenter clinical trial.* Urology, 1999. 54(6): p. 976-81.

32. Raad, I. and H. Hanna, *Intravascular catheters impregnated with antimicrobial agents: a milestone in the prevention of bloodstream infections.* Support Care Cancer, 1999. 7(6): p. 386-90.

33. Spencer, R.C., *Novel methods for the prevention of infection of intravascular devices.* J Hosp Infect, 1999. 43 Suppl: p. S127-35.

34. Woo, G.L., M.W. Mittelman, and J.P. Santerre, *Synthesis and characterization of a novel biodegradable antimicrobial polymer.* Biomaterials, 2000. 21(12): p. 1235-46.

35. Watson, S., et al.,, *Preparation of nanosized crystalline TiO2 particles at low temperature for photocatalysis.* Journal of Nanoparticle Research, 2004. 6(2): p. 193-207.

36. Zallen, R. and M.P. Moret, *The optical absorption edge of brookite TiO2.* Solid State Communications, 2006. 137(3): p. 154-157.

37. Mo, S.-D. and W.Y. Ching, *Electronic and optical properties of three phases of titanium dioxide: Rutile, anatase, and brookite.* Physical Review B, 1995. 51(19): p. 13023.

38. Watson, S., et al., *Preparation of nanosized crystalline TiO2 particles at low temperature for photocatalysis.* Journal of Nanoparticle Research, 2004. 6(2): p. 193-207.

39. Banerjee, S., et al., *Physics and chemistry of photocatalytic titanium dioxide: Visualization of bactericidal activity using atomic force microscopy* Current Science, 2006. 90(10).

40. Kataoka, S., et al., *Investigation of Water Strcuture at the TiO2/Aqueous Interface.* Langmuir, 2004. 20: p. 1662-6.

41. Kallio, T., et al., *Antifouling properties of TiO2: Photocatalytic decomposition and adhesion of fatty and rosin acids, sterols and lipophilic wood extractives.* Colloids and Surfaces A: Physicochemical and Engineering Aspects, 2006. 291(1-3): p. 162-176.

42. Kaewgun, S., C. Nolph, and B. Lee, *Enhancing Photocatalytic Activity of Polymorphic Titania Nanoparticles by NMP Solvent-based Ambient Condition Process.* Catalysis Letters, 2008. 123(3): p. 173-180.

43. Kaewgun, S., et al., *Influence of hydroxyl contents on photocatalytic activities of polymorphic titania nanoparticles.* Materials Chemistry and Physics, 2009. 114(1): p. 439-445.

44. Kaewgun, S., et al., *Study of visible light photocatalytic activity achieved by NMP solvent treatment of polymorphic titania.* Journal of Photochemistry and Photobiology A: Chemistry, 2009. 202(2-3): p. 154-158.

45. Li, Y., et al., *Photocatalytic degradation of methyl orange by TiO2-coated activated carbon and kinetic study.* Water Research, 2006. 40(6): p. 1119-1126.

46. Kraeutler, B. and A.J. Bard, *Photoelectrosynthesis of ethane from acetate ion at an n-type titanium dioxide electrode. The photo-Kolbe reaction.* Journal of the American Chemical Society, 1977. 99(23): p. 7729-7731.

47. Matos, J., J. Laine, and J.M. Herrmann, *Effect of the Type of Activated Carbons on the Photocatalytic Degradation of Aqueous Organic Pollutants by UV-Irradiated Titania.* Journal of Catalysis, 2001. 200(1): p. 10-20.

48. Chen, F., et al., *Correlation of Photocatalytic Bactericidal Effect and Organic Matter Degradation of TiO2 Part I: Observation of Phenomena.* Environmental Science & Technology, 2009. 43(4): p. 1180-1184.

49. Tsuge, Y., et al., *Fabrication of transparent TiO2 film with high adhesion by using self-assembly methods: Application to super-hydrophilic film.* Thin Solid Films, 2008. 516(9): p. 2463-2468.

3.8 Figures

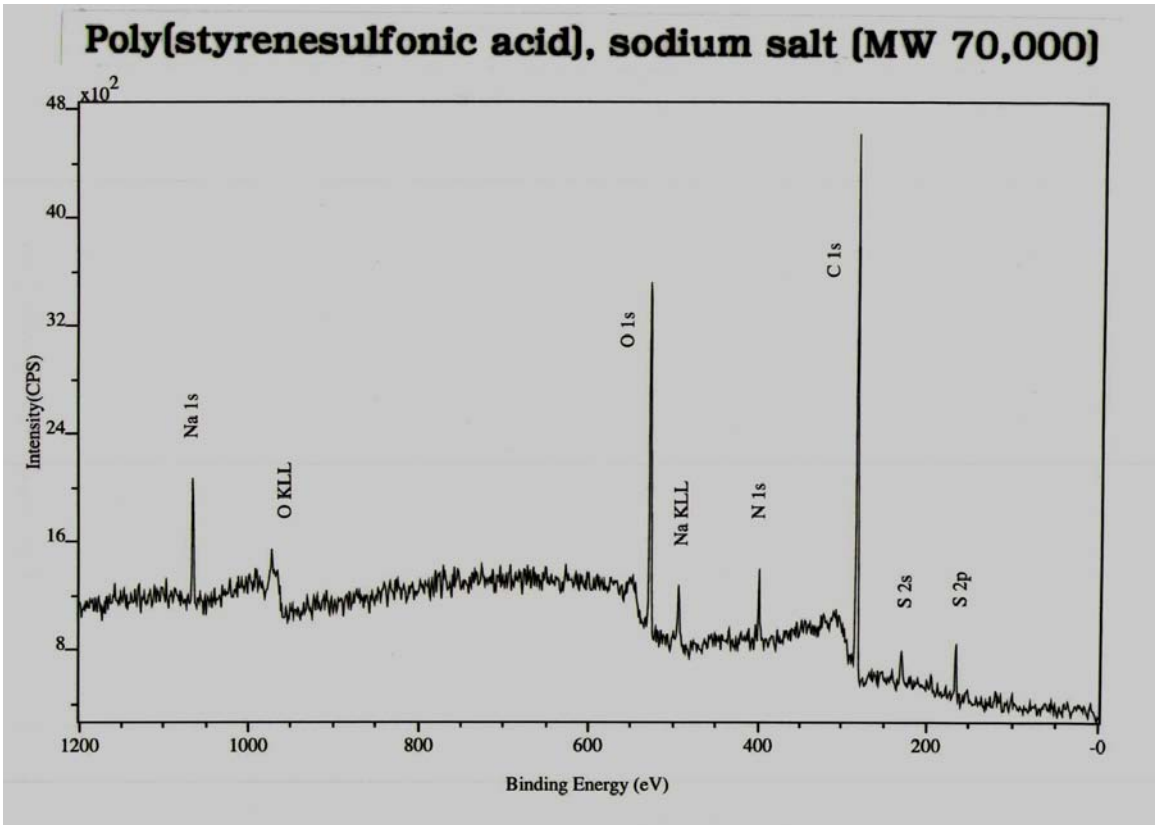

A

Figures 3.8.1. A-E - Surface chemical spectra of sub-coating with and without Titania

Figure 3.8.1. A [a]XPS spectra graph of PSS/PDDA sub-coating

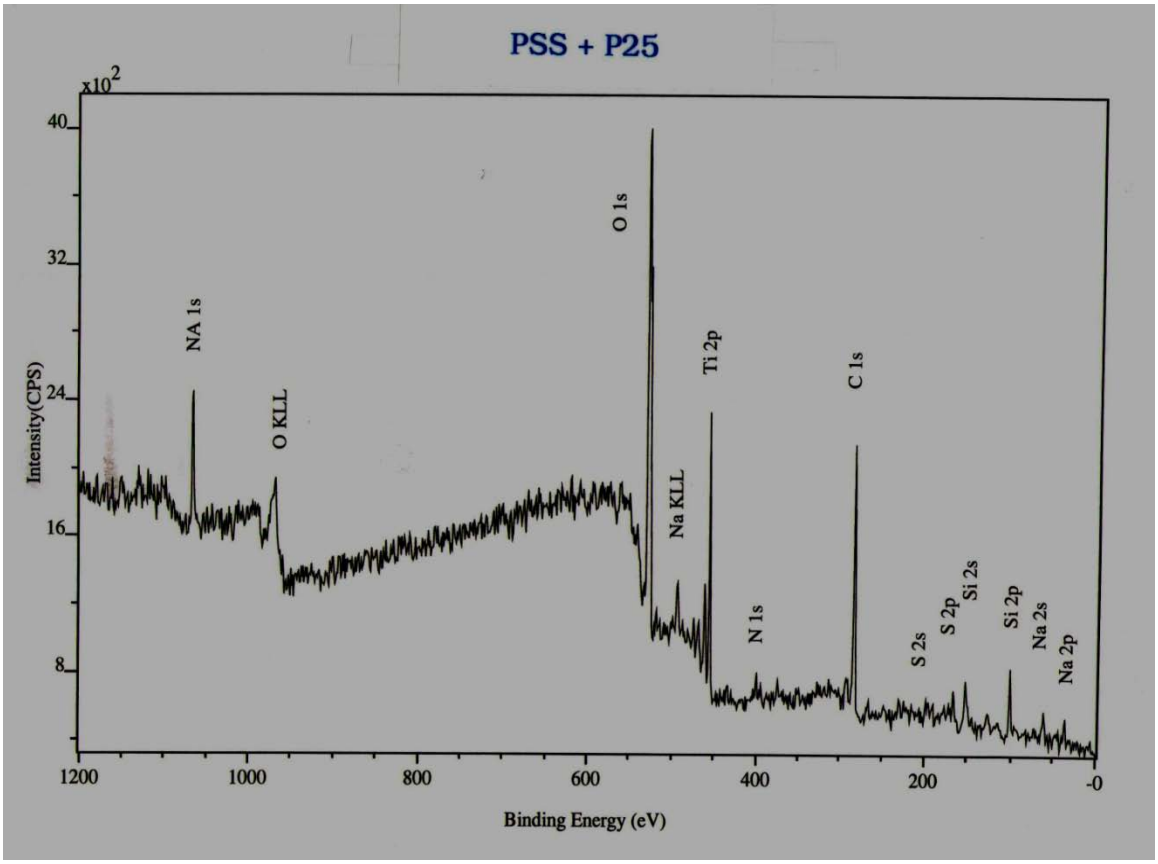

B

Figure 3.8.1. B [b]XPS spectra graph of PSS/PDDA sub-coating with commercial P25 Titania

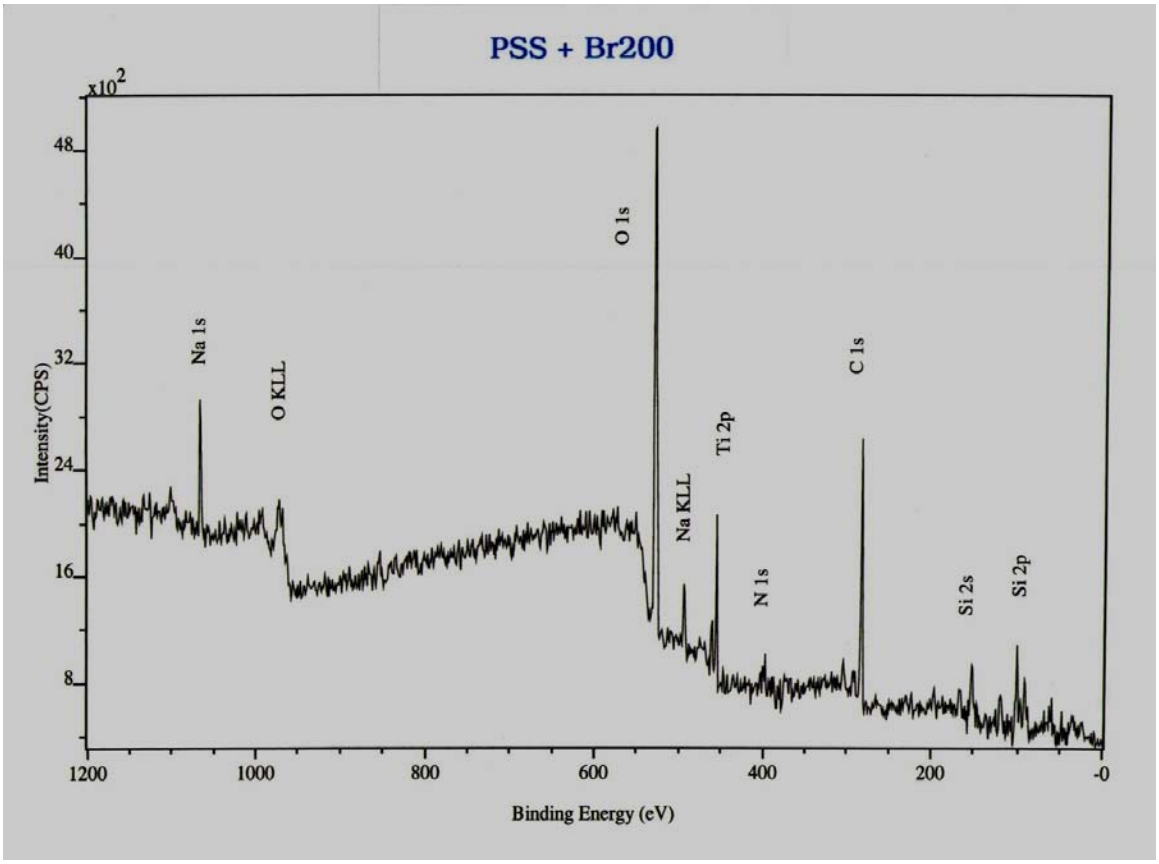

C

Figure 3.8.1 C [c]XPS spectra graph of PSS/PDDA sub-coating with Br200 Titania

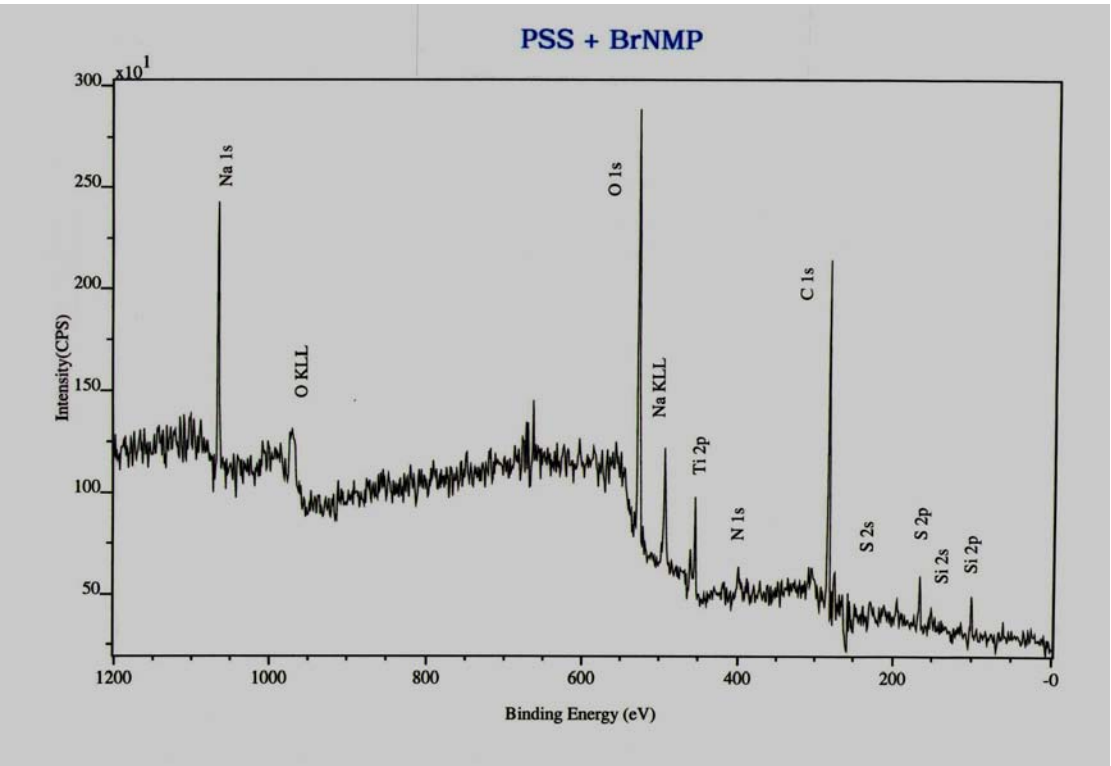

D

Figure 3.8.1 D [c]XPS spectra graph of PSS/PDDA sub-coating with BrNMP Titania

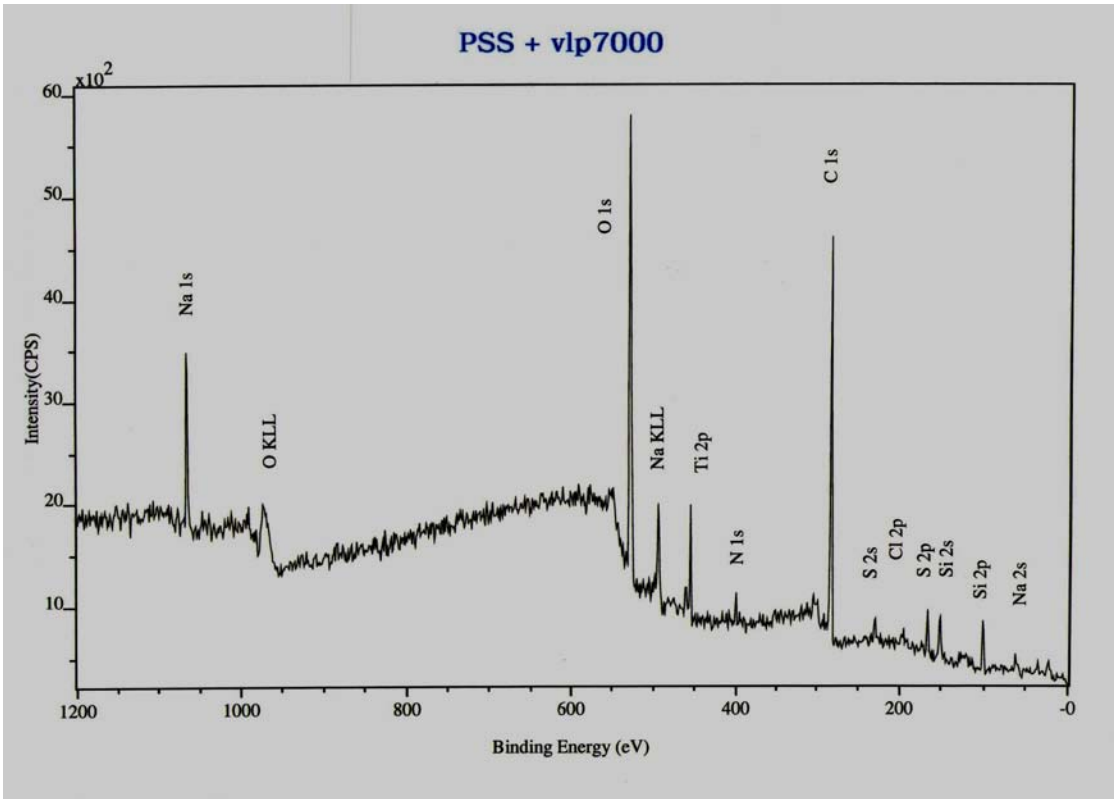

E

Figure 3.8.1 E [c]XPS spectra graph of PSS sub-coating with vlp7000 Titania

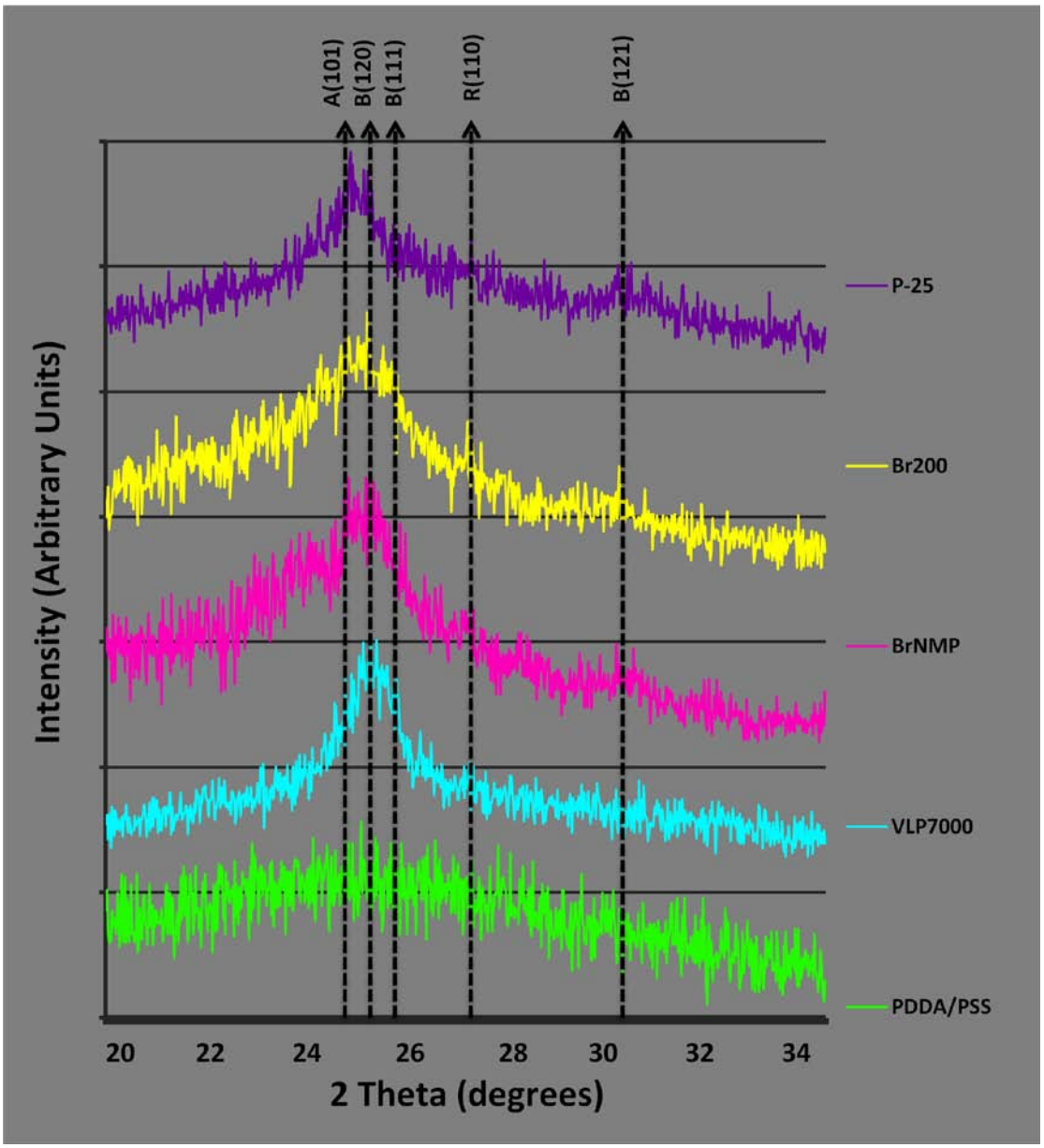

Figure 3.8.2. X-ray diffraction spectra of the PDDA/PSS sub-coating with or without Titania

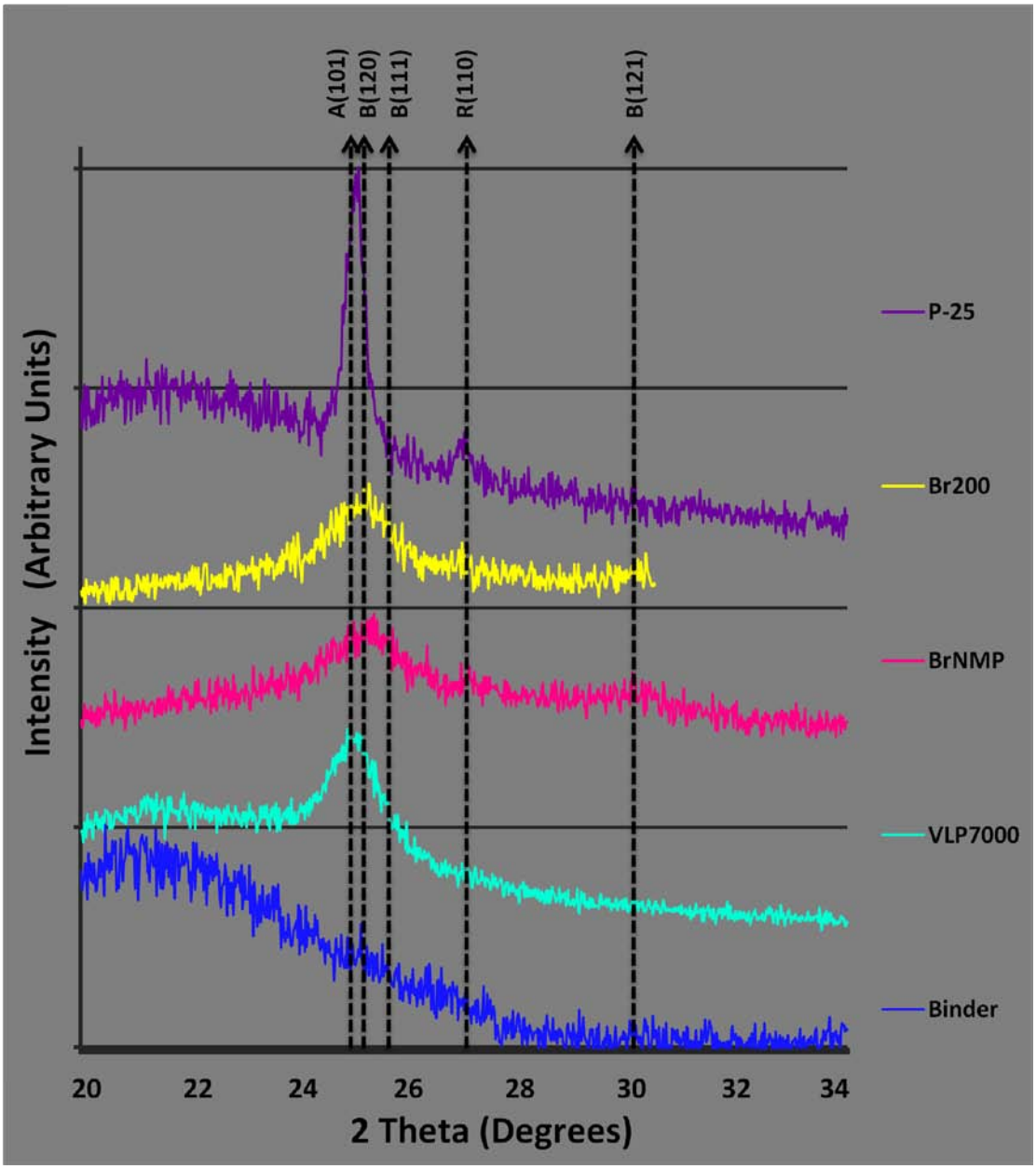

Figure 3.8.3. X-ray diffraction spectra of the Binder sub-coating with or without Titania

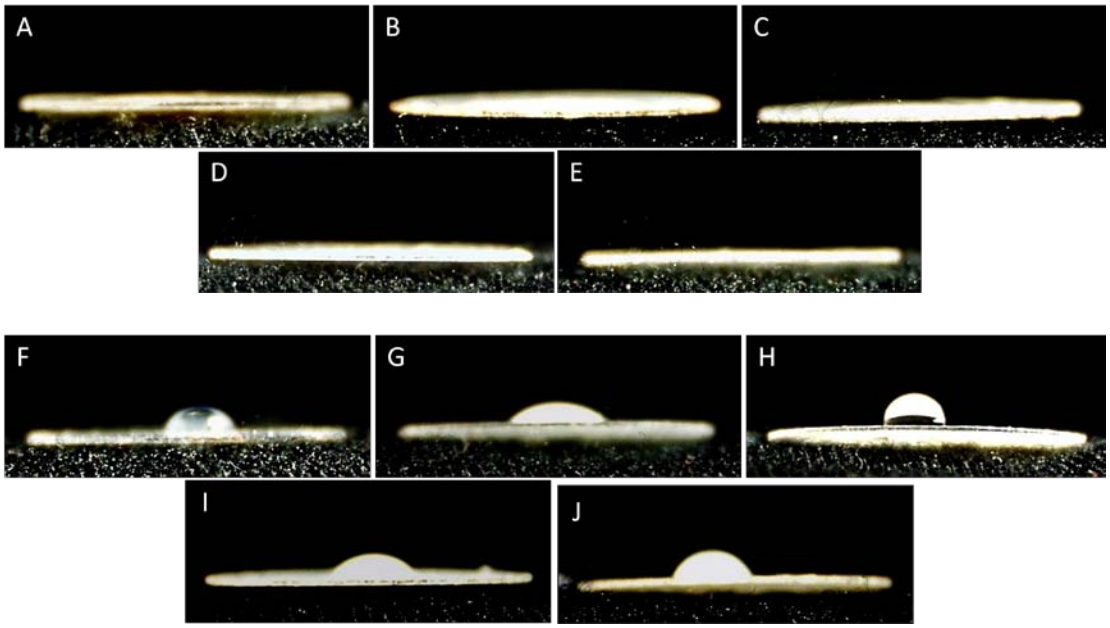

Figure 3.8.4. Hydrophilicity of PDDA/PSS and Binder sub-coating with and without Titania

A) PDDA/PSS
B) PDDA/PSS with P25
C) PDDA/PSS with VLP7000
D) PDDA/PSS with Br200
E) PDDA/PSS with BrNMP
F) Binder
G) Binder with P25
H) Binder with VLP7000
I) Binder with Br200
J) Binder with BrNMP

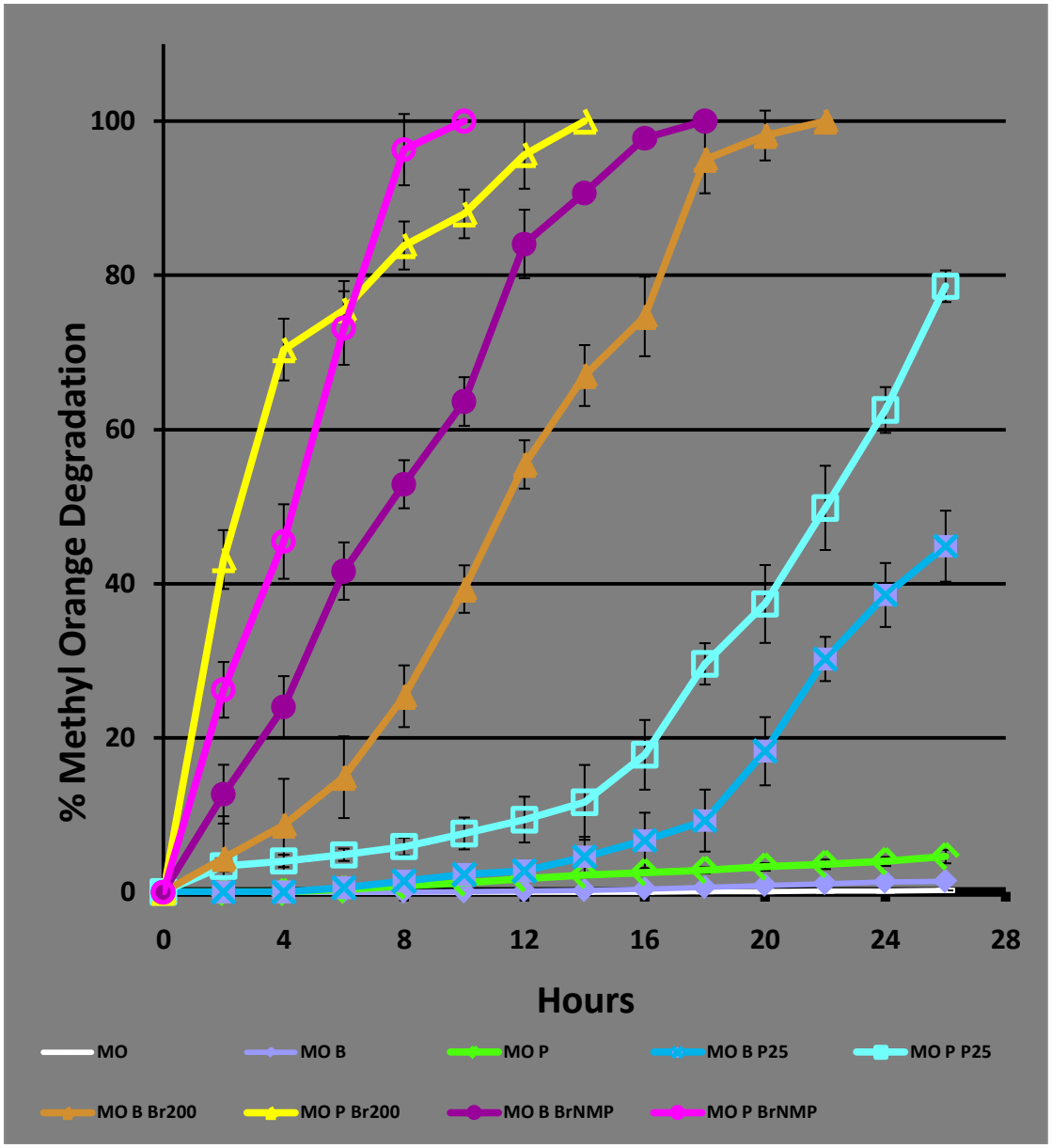

Figure 3.8.5. Photocatalytic Activities of Titania Coatings Under UVA

Statistics were determined using a student T-Test with alpha equal to 0.05. P or B Sub-Coating with MO (20 µM) in water at pH 4.0 exposed to UV light (365nm) with a (363-364 µW/cm2) intensity in with or without P- P-25 26+ h and P-Br200 14 h, or P-BrNMP 10 h, B- P-25 28+ h and B-Br200 22 h, or B-BrNMP 18 h oxidative degradation of MO. Br200 and BrNMP were significantly different from 2 h -26 h (p= 0.02 – 0.005); P25 was significantly different from16 h-28 h (0.044 – 0.032). MO alone or on P or B-Sub-Coating was not significantly different throughout the 26 h evaluated (p=0.35).

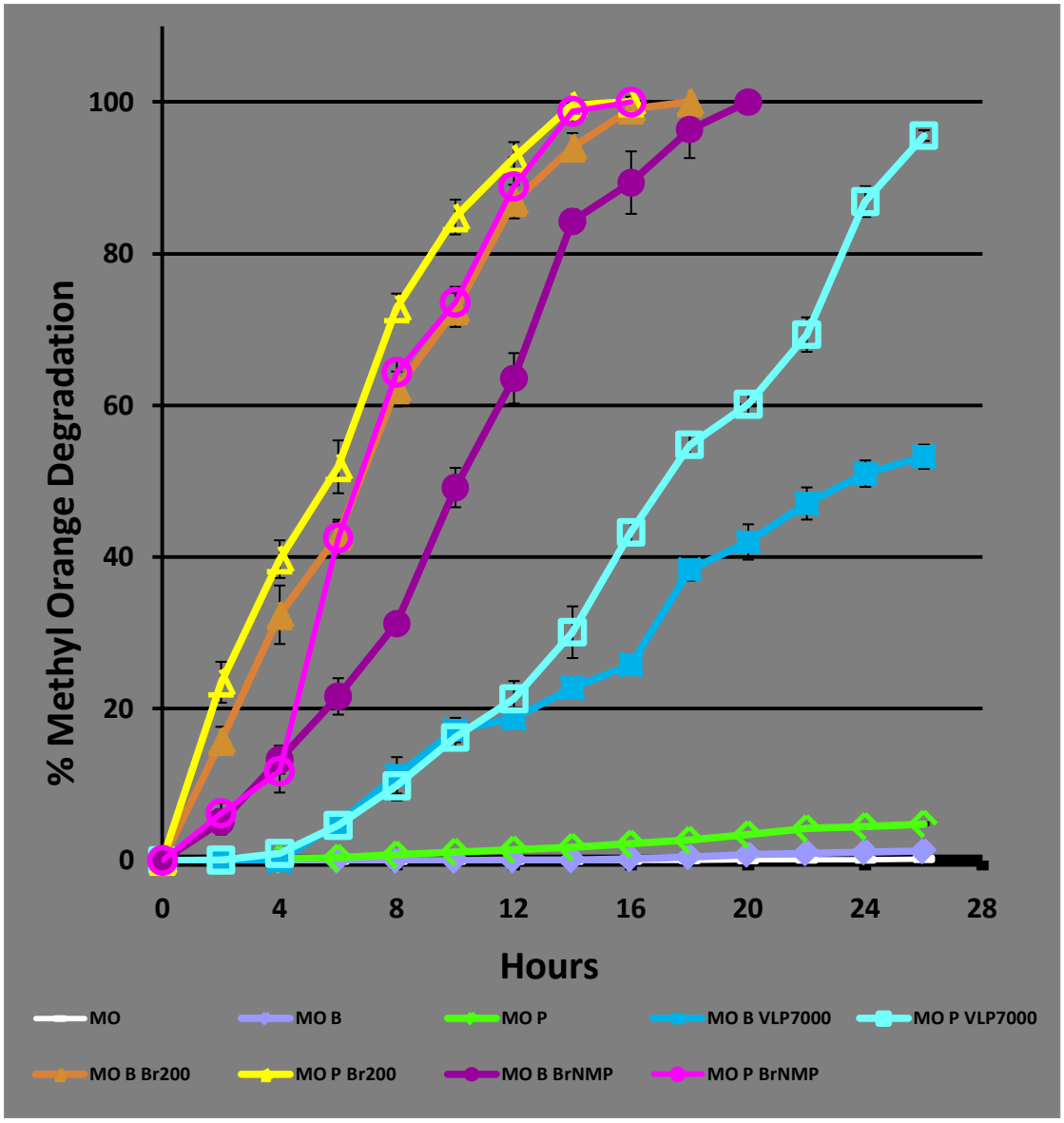

Figure 3.8.6. Photocatalytic Activities of Titania Coatings Under Visible Light

Statistics were determined using a student T-Test with alpha equal to 0.05. P or B Sub-Coating with MO (20 µM) in water at pH 4.0 exposed to VL with a (100 µW/cm2) intensity in with or without P- P-25 26+ h and P-Br200 14 h, or P-BrNMP 14h, B- P-25 28+ h and B-Br200 16 h, or B-BrNMP 20 h oxidative degradation of MO. Br200 and BrNMP were significantly different from 2 h -26 h (p= 0.03 – 0.004); P25 was significantly different from 8 h-28 h (0.03 – 0.01). MO alone or on P or B- Sub-Coating was not significantly different throughout the 26 h evaluated (p=0.35).

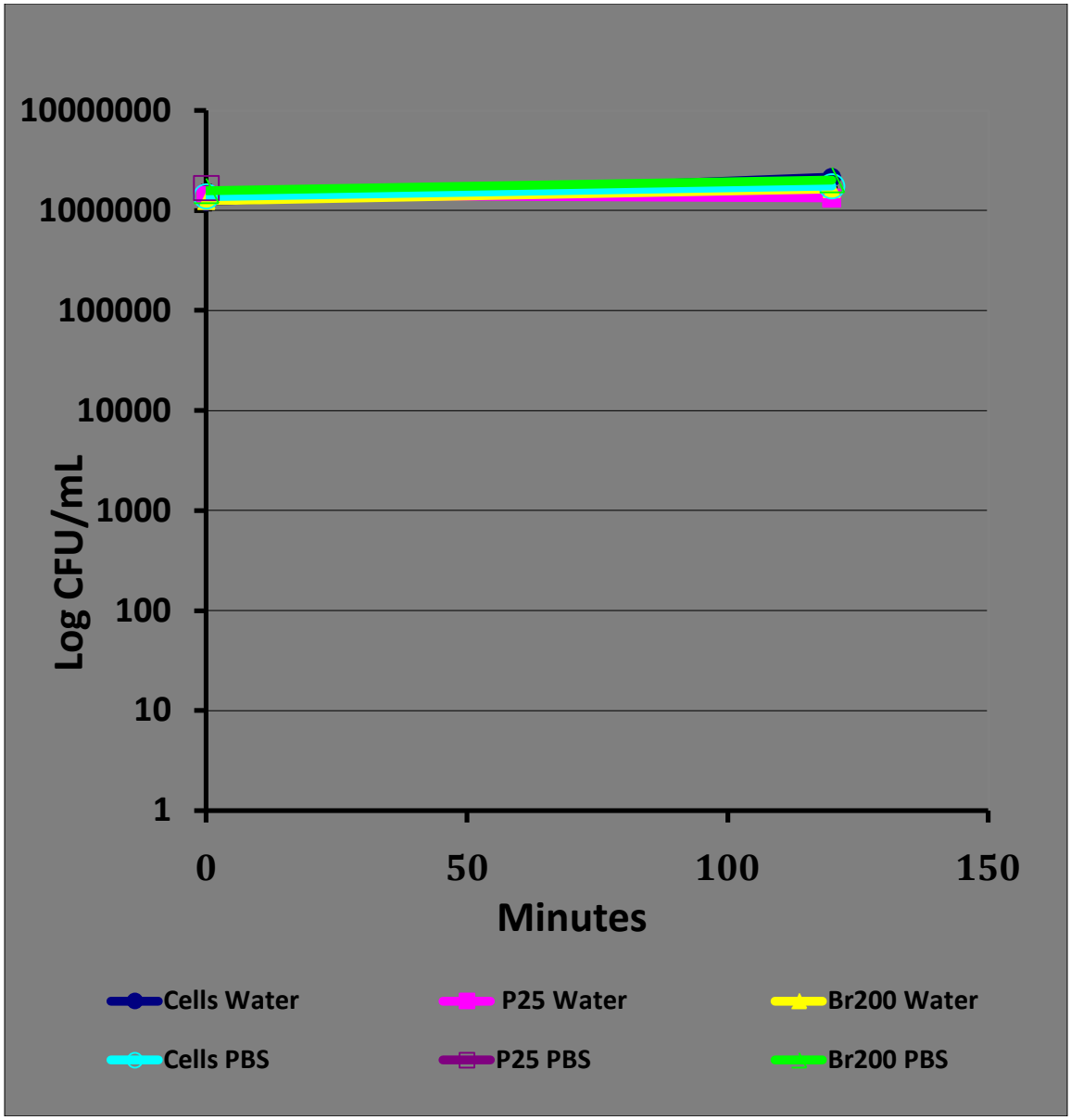

Figure 3.8.7. Activated TiO_2 exposed to *Escherichia coli* B at pH 7.4 in water or PBS for 120 Minutes

Results were determined using a student T-Test with alpha equal to 0.05. E. coli B in PBS pH 7.4 or water at pH 7.4 exposed to UV light (365nm) in the absence or presence of TiO_2 P25 or TiO_2 Brookite maintained the original bacterial population in 120 minutes. The pH of the water at 120 minutes dropped from pH 7.4 to pH 6.0. (Error bars are too small to be seen.)

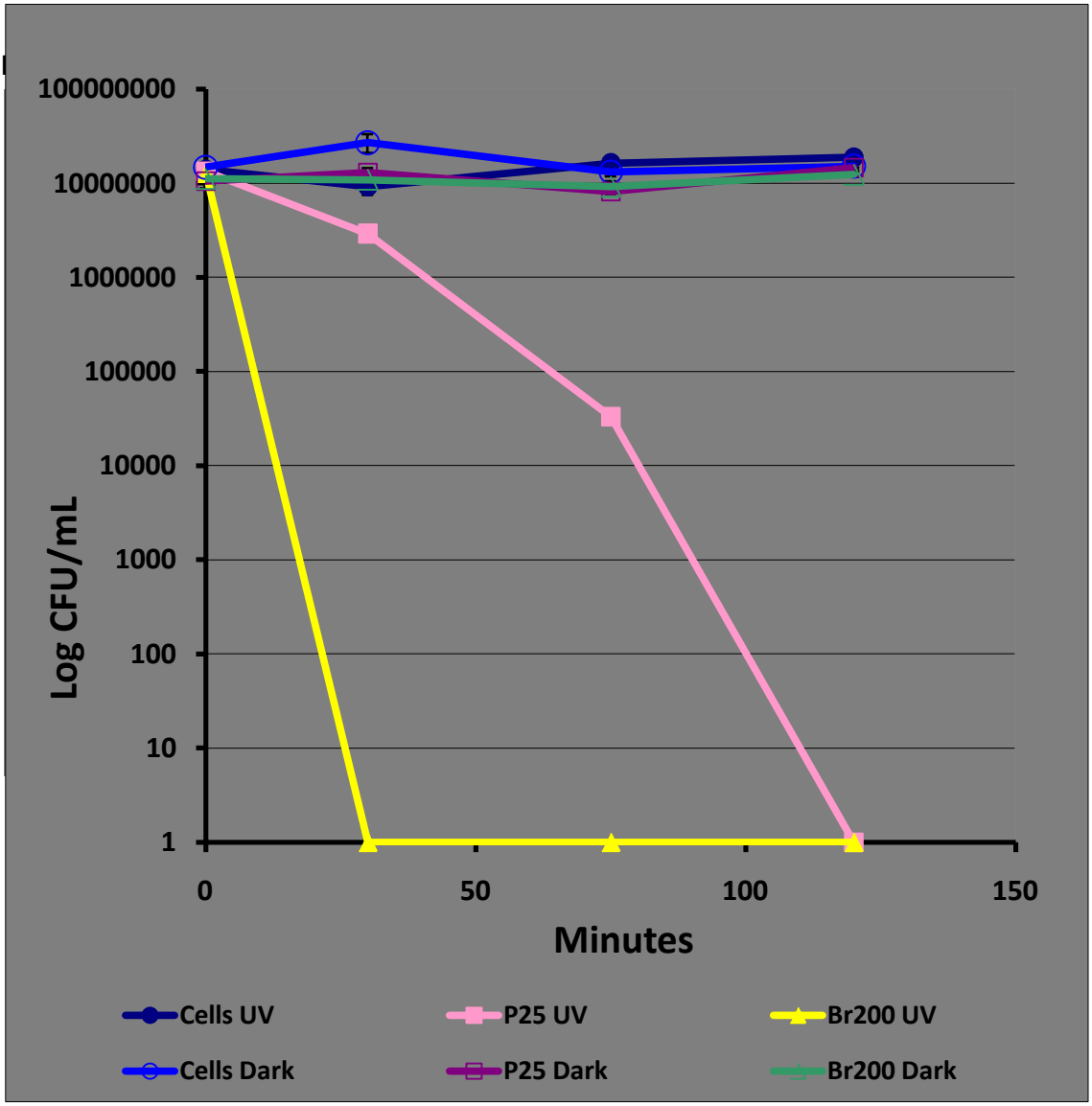

Figure 3.8.8. TiO_2 Degradation of *Escherichia coli* B with or without UV at 0, 30, 75, or 120 Minutes in Water at pH 4.0

Results were determined using a student T-Test with alpha equal to 0.05. *E. coli* B in water at pH 4.0 exposed to UV light (365nm) in the presence of TiO_2 P-25 and TiO_2 Brookite had a significant seven log drop in 120 (p=0.004) or 30 (p=0.001) minutes, respectively. *E. coli* B in the absence of TiO_2 in water at pH 4.0 depicted no significant reduction of the bacterial population in 120 minutes. The water beginning at pH 4.0 remained the same throughout 120 minutes. (Error bars may be too small to be seen.)

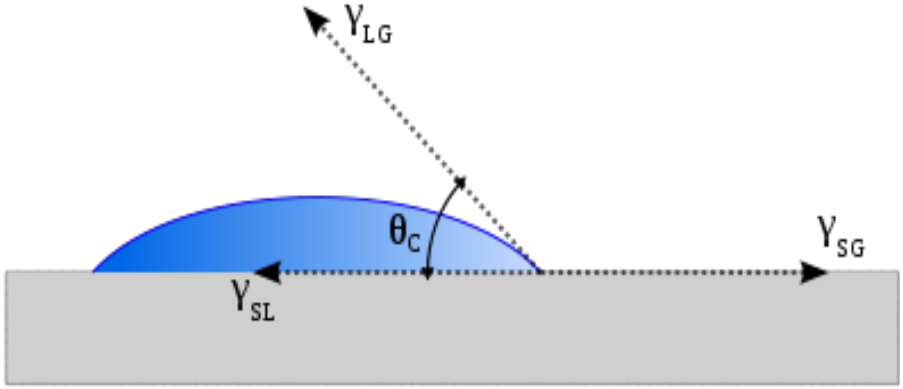

Figure 3.8.9. Static Contact Angle

http://en.wikipedia.org/wiki/Goniometer

$$\gamma_{SG} = \gamma_{SL} + \gamma_{LG} \cos\theta$$

Where: γ_{SG} = Interfacial tension between the solid and gas

γ_{LG} = Interfacial tension between the solid and liquid

γ_{LG}= Interfacial tension between the liquid and gas

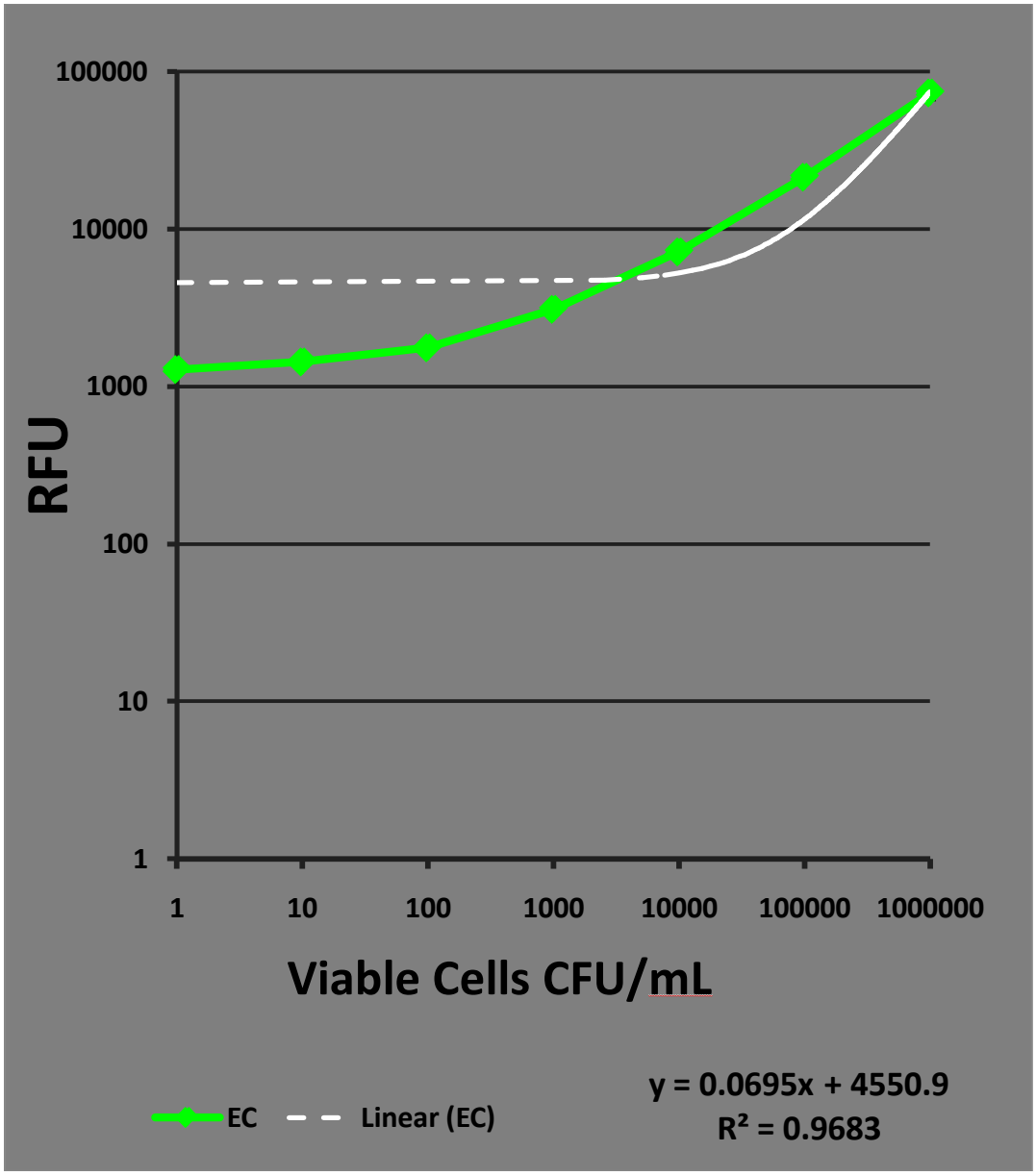

Figure 3.8.10. BacLight Fluorescent Assay Linearity Range on *Escherichia coli* B with p values less than 0.05

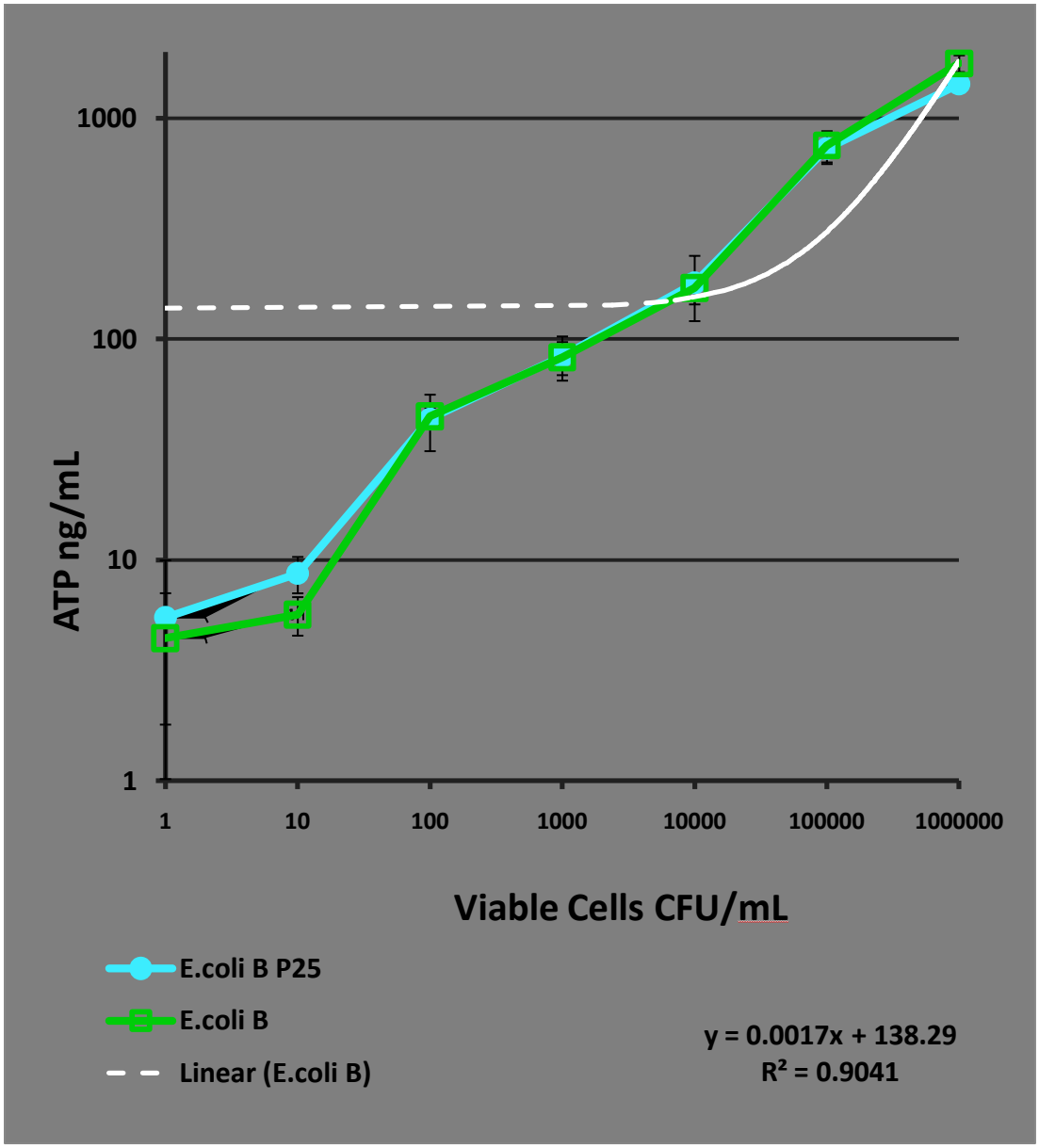

Figure 3.8.11. Bac-Titer-Glo™ Luminescent Assay Linearity Range on *Escherichia coli* B with p values less than 0.05

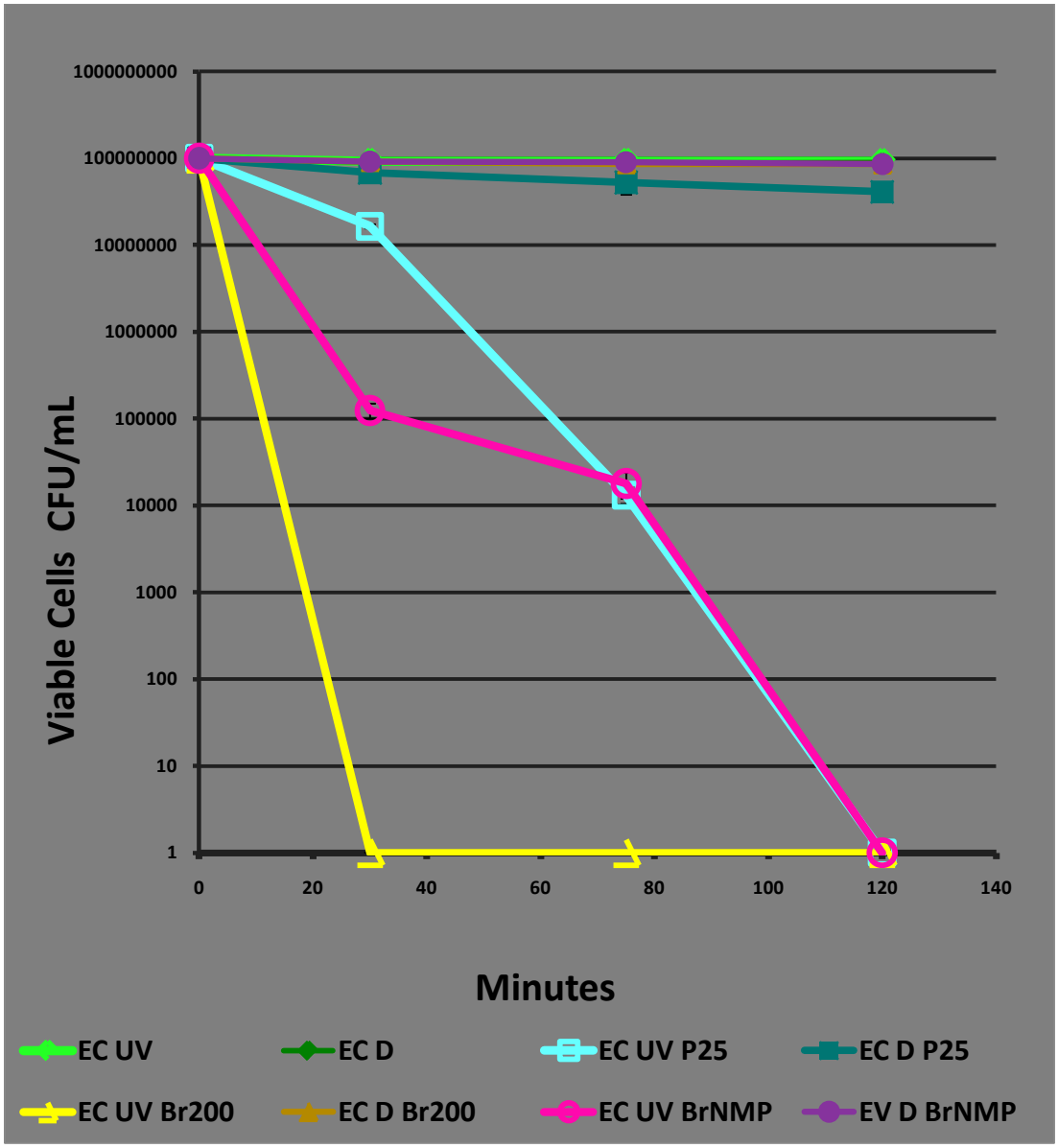

Figure 3.8.12. Effects of UVA Activated P25, Br200 and BrNMP Titania 1 mg/mL in Free Suspension on *E. coli* B: *Bac*Light ™Assay with p values less than 0.01

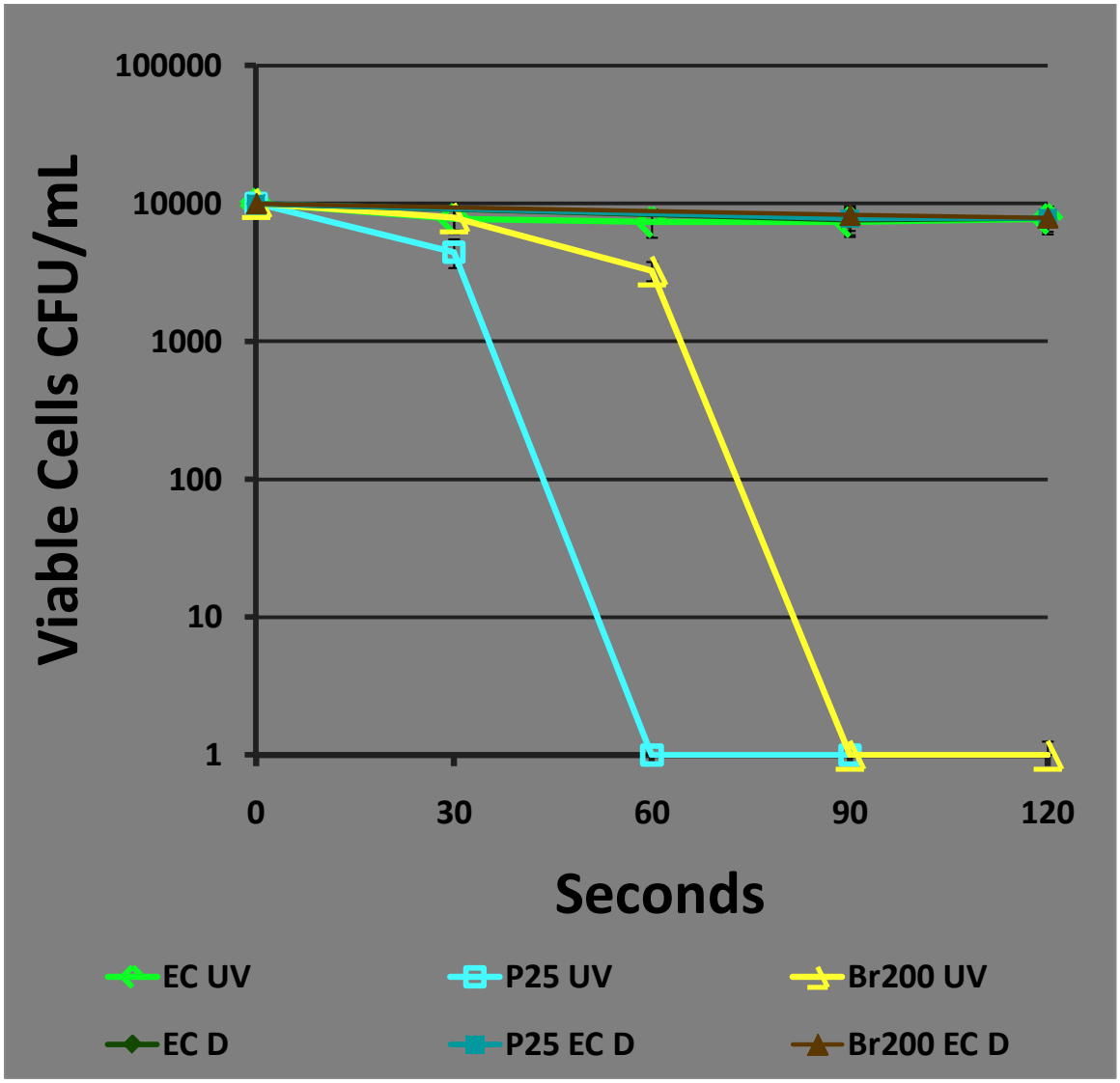

Figure 3.8.13. Effects of UVA Activated P25 and Br200 Titania 1 mg/mL in Free Suspension on *E. coli* B

Percent survival of *E. coli* B (EC) CFU/mL with and without P25 or Br200 Titania exposed to a UVA at 365 nm for either 0, 30, 60, 90, or 120 seconds or the dark for 0, 90, or 120 seconds. Student T-Test indicated significant difference at an alpha of 0.05 between EC at 0 sec to P25, not significantly different at 0, or 90-120 sec in the dark, but significantly different at 30 – 120 sec in UVA (p= 0.004 – 0.002); between EC at 0 min sec to Br200, not significantly different at 0 min UVA or 90 - 120 sec D or at 30 sec in UVA; but significantly different at 60 – 120 sec in UVA (p= 0.006 – 0.002).

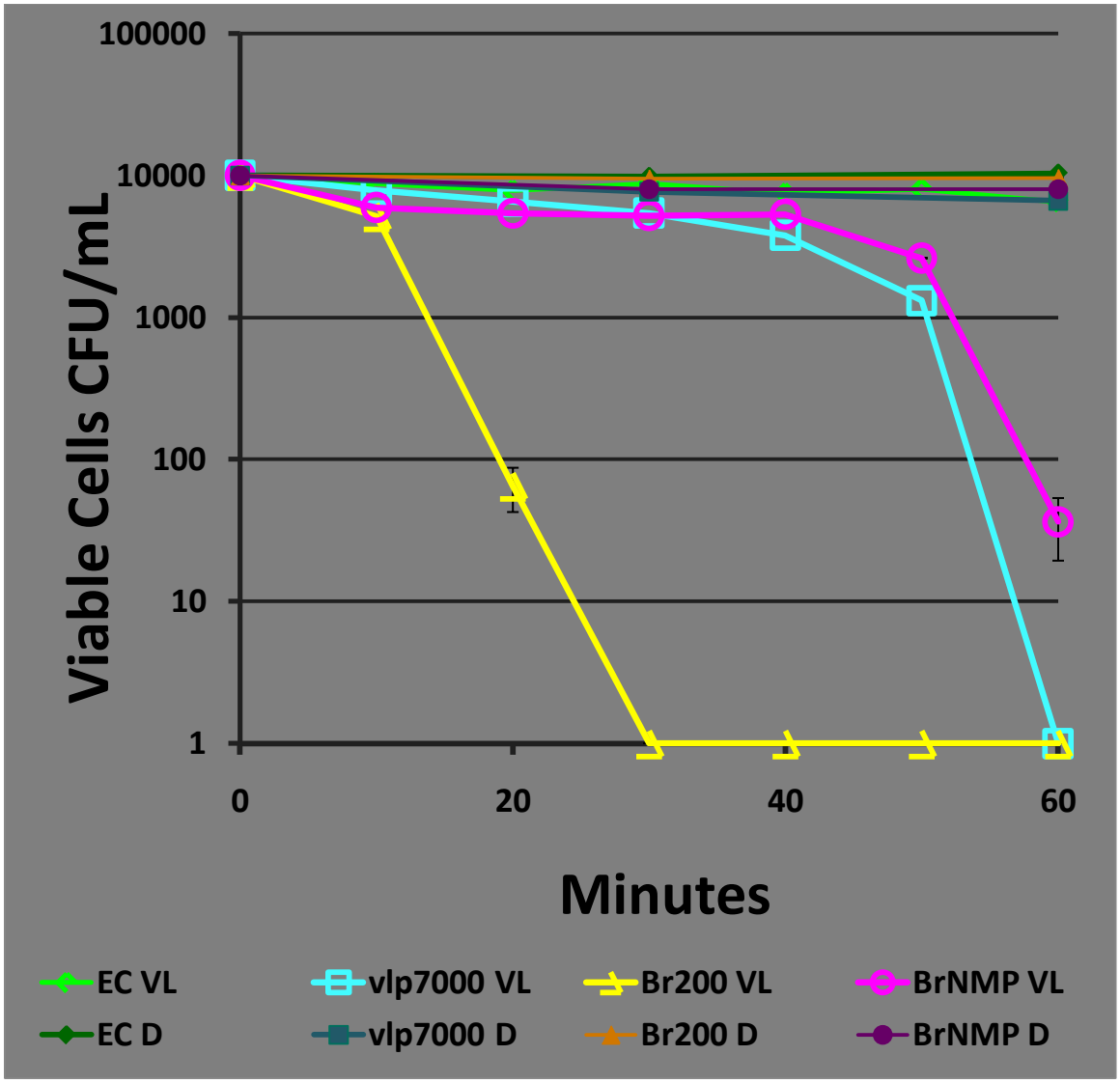

Figure 3.8.14. Effects of Visible Light Activated VLP7000, Br200 and BrNMP Titania 1mg/mL in Free Suspension on *E. coli* B

Percent survival of *E. coli* B (EC) CFU/mL with and without VLP 7000, Br200, and BrNMP Titania exposed to a cool white 8 Watt bulb for either 0, 10, 20, 30, 40, 50, or 60 minutes or the dark for 0, 30, or 60 minutes. Student T-Test indicated significant difference at an alpha of 0.05 between EC at 0 min to P25, not significantly different at 0 or 10 min VL; significantly different at 20 – 60 min VL ($p= 0.01 – 2.5 \times 10^{-5}$), and at 30 – 60 min D ($p= 0.039 – 0.002$); between EC at 0 min to Br200, not significantly different at 0 min VL or 30 – 60 min D ($p= 0.3 – 0.2$), but significantly different at 10 – 60 min VL ($p= 0.001 – 1.9 \times 0^{-8}$); and between EC at 0 min to BrNMP, not significantly different at 0 min VL, but significantly different at 10 – 60 min VL ($p= 0.02 – 8.3 \times 10^{-7}$), or 30 – 60 min D ($p= 0.007 – 0.0005$).

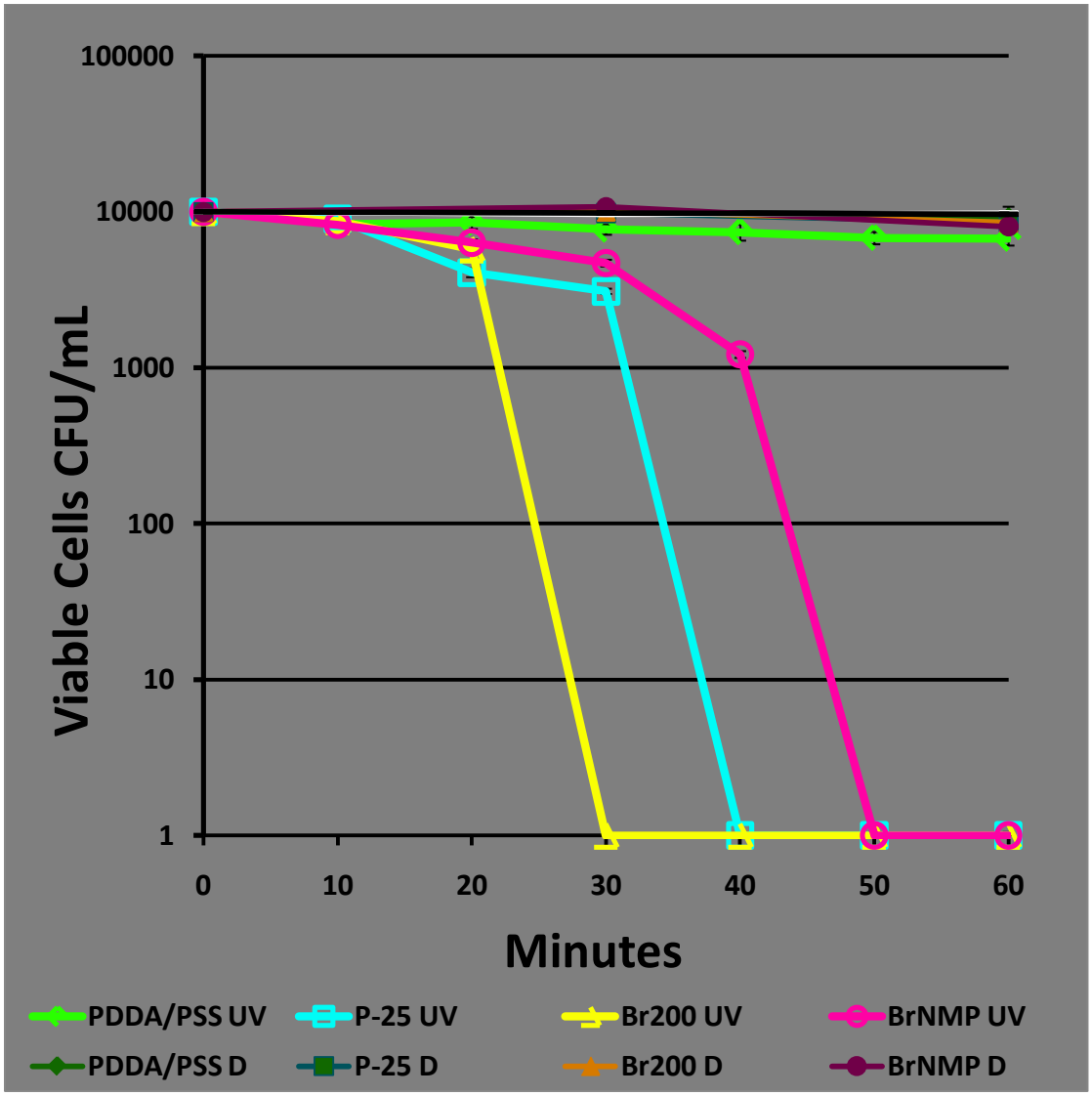

Figure 3.8.15. Effects of UVA Light Activated P-25, Br200 and BrNMP Titania (2mg) on the PDDA/PSS Sub-coating on *E. coli* B for 0-60 Minutes

Percent survival of *E. coli* B (EC) CFU/mL with and without P25, Br200, and BrNMP Titania on P Sub-Coating exposed to a UVA 365 nm lamp for either 0, 10, 20, 30, 40, 50, or 60 minutes or the dark for 0, 30, or 60 minutes. (Error bars may be too small to see.) Student T-Test indicated significant difference at an alpha of 0.05 between EC at 0 min to P25, not significantly different at 0 or 10 min UVA; significantly different at 20 – 60 min VL ($p= 2.5 \times 10^{-5} – 1.3 \times 10^{-6}$), and at 30 – 60 min D ($p= 0.039 – 0.002$); between EC at 0 min to Br200, not significantly different at 0 or 10 min UVA or 30 – 60 min D ($p= 0.3 – 0.2$), but significantly different at 20 – 60 min UVA ($p= 5 \times 10^{-4} – 1. X 10^{-6}$); and between EC at 0 min to BrNMP, not significantly different at 0 or 10 min UVA, or 30 – 60 min D, but significantly different at 20 – 60 min UVA ($p= 0.001 – 1.3 \times 10^{-6}$).

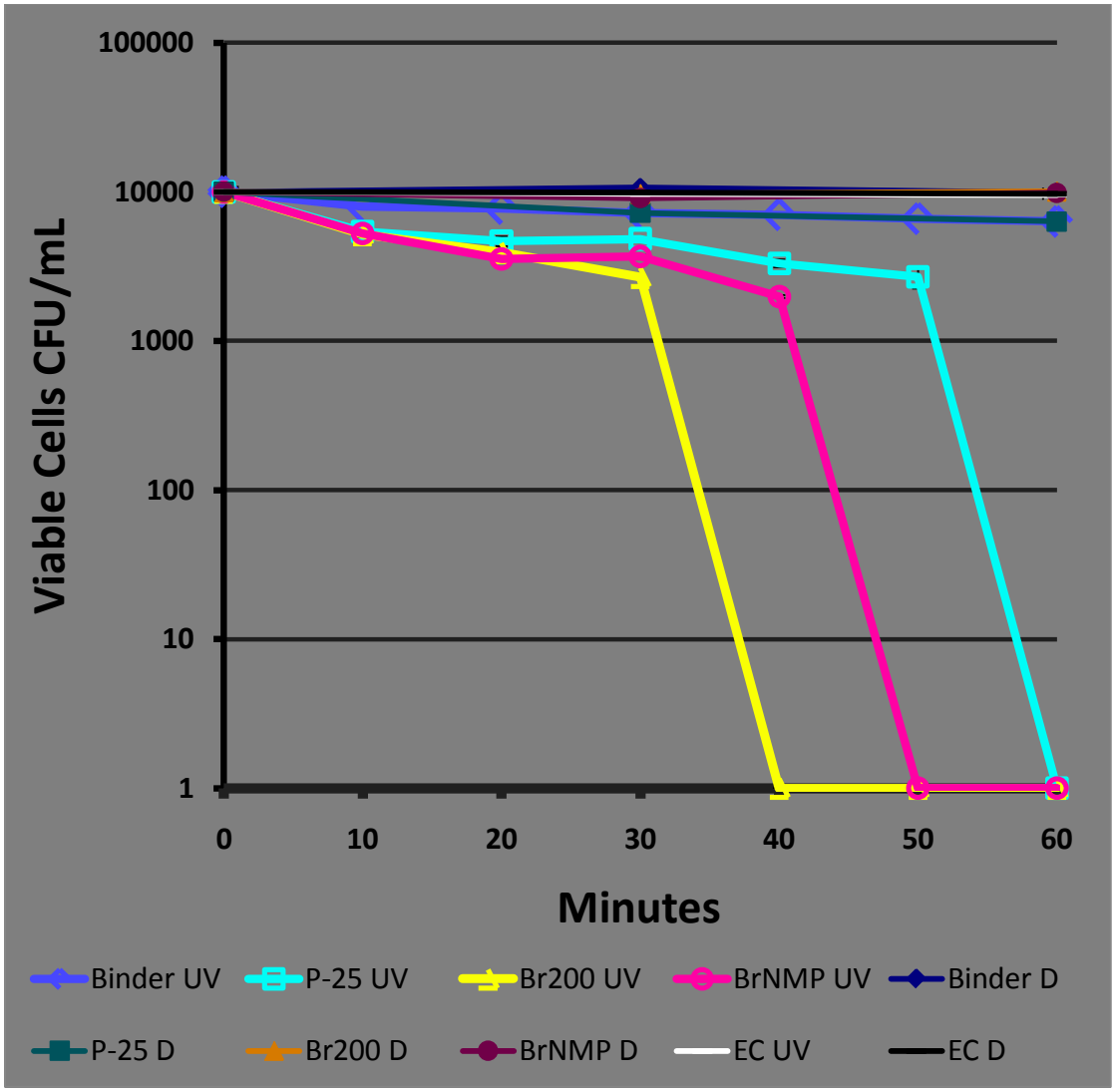

Figure 3.8.16. Effects of UVA Light Activated P-25, Br200 and BrNMP Titania (2mg) on the Binder Sub-coating on *E. coli* B for 0-60 Minutes

Percent survival of *E. coli* B (EC) CFU/mL with and without P25, Br200, and BrNMP Titania on B Sub-Coating exposed to a UVA 365 nm lamp for either 0, 10, 20, 30, 40, 50, or 60 minutes or the dark for 0, 30, or 60 minutes. (Error bars may be too small to see.) Student T-Test indicated significant difference at an alpha of 0.05 between EC at 0 min to P25, not significantly different at 0 min UVA; significantly different at 10 – 60 min UVA (p= 0.01 – 0.001), and at 30 – 60 min D (p= 0.04– 0.002); between EC at 0 min to Br200, not significantly different at 0 min UVA or 30 – 60 min D (p= 0.3 – 0.2), but significantly different at 10 – 60 min UVA (p= 0.001 – 0.01); and between EC at 0 min to BrNMP, not significantly different at 0 min UVA or 60 min D, but significantly different at 10 – 60 min UVA (p= 0.04 – 0.001), or 30 min D (p= 0.01).

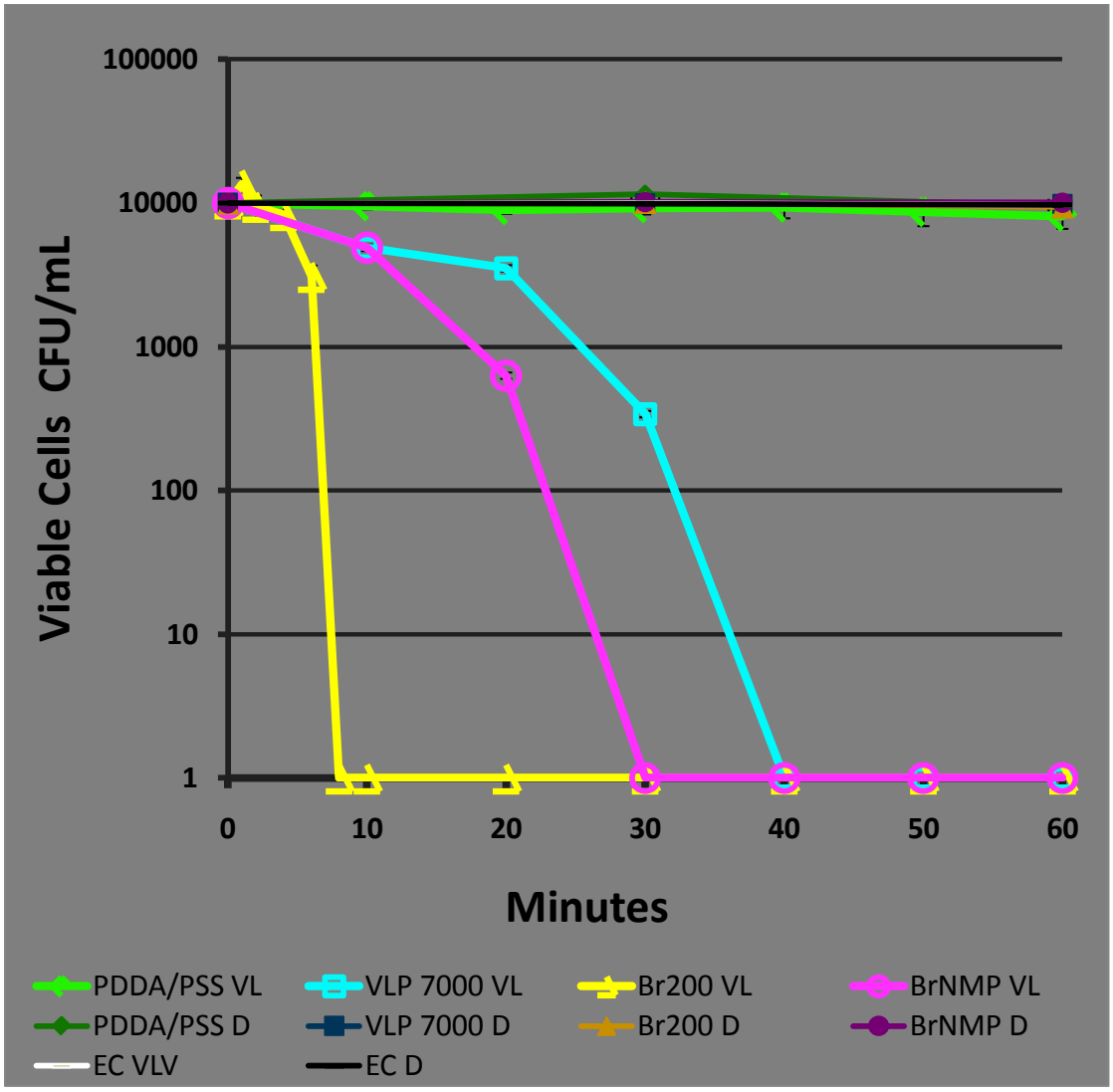

Figure 3.8.17. Effects of Visible Light Activated VLP7000, Br200 and BrNMP Titania (2mg) with PDDA/PSS Sub-coating on *E. coli* B for 0-60 Minutes

Percent survival of *E. coli* B (EC) CFU/mL with and without VLP 7000, Br200, and BrNMP Titania on P Sub-Coating exposed to a cool white 8 Watt bulb for either 0, 10, 20, 30, 40, 50, or 60 minutes or the dark for 0, 30, or 60 minutes. (Error bars may be too small to see.) Student T-Test indicated significant difference at an alpha of 0.05 between EC at 0 min to P25, not significantly different at 0 min VL or 30 – 60 min D; significantly different at 10 – 60 min VL (p= 0.01 – 0.003); between EC at 0 min to Br200, not significantly different at 0, 2, 4, or 6 min VL or 30 – 60 min D (p= 0.3 – 0.2), but significantly different at 8 – 60 min VL (p= 0.002 – 4 x 0^{-11}); and between EC at 0 min to BrNMP, not significantly different at 0 min VL or 30 – 60 min D, but significantly different at 10 – 60 min VL (p= 0.02 – 0.002).

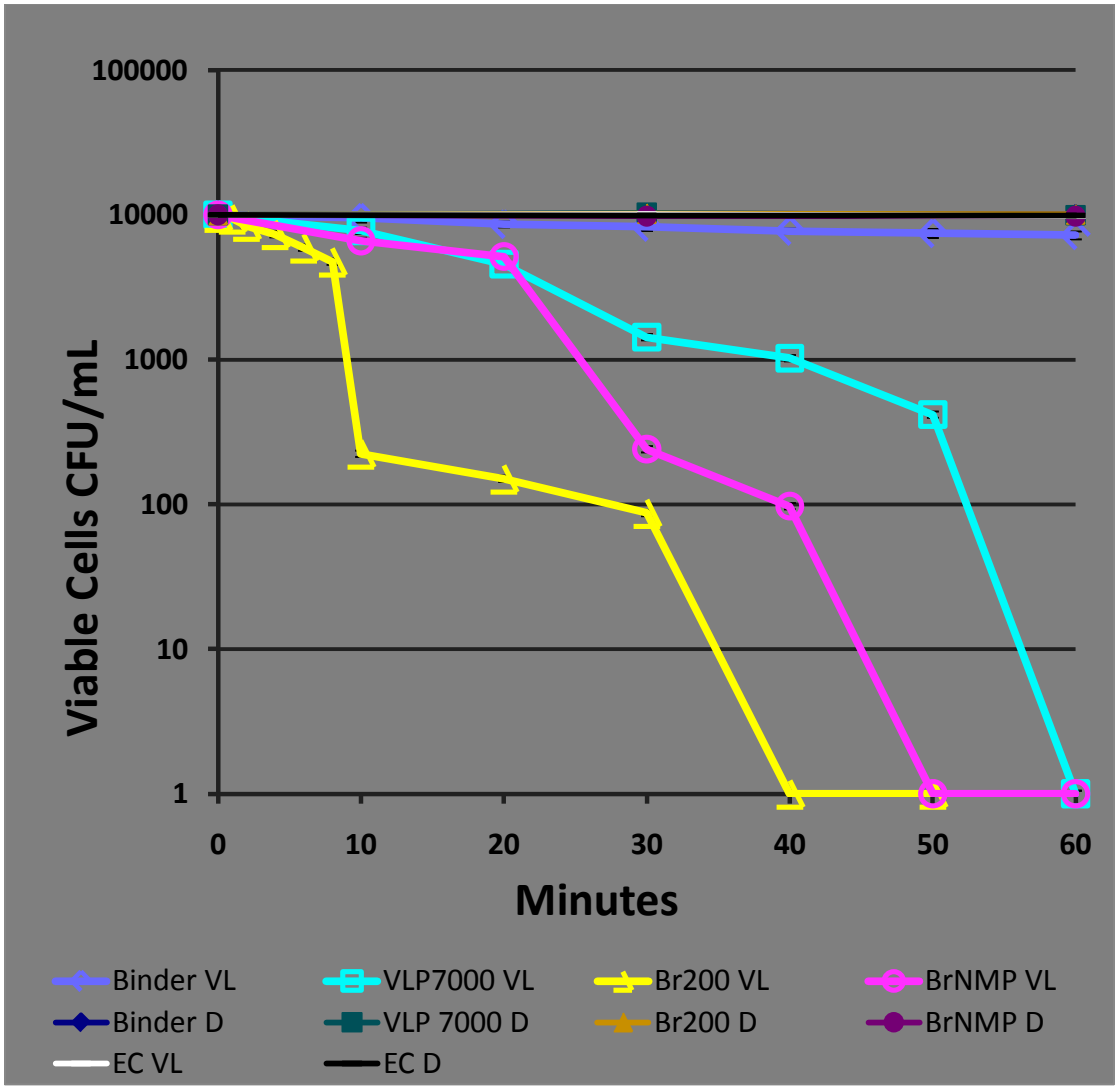

Figure 3.8.18. Effects of Visible Light Activated VLP7000, Br200 and BrNMP Titania (2mg) with Binder Sub-coating on *E. coli* B for 0-60 Minutes

Percent survival of *E. coli* B (EC) CFU/mL with and without VLP 7000, Br200, and BrNMP Titania on B Sub-Coating exposed to a cool white 8 Watt bulb for either 0, 1, 2, 4, 6, 8, 10, 20, 30, 40, 50, or 60 minutes or the dark for 0, 30, or 60 minutes. (Error bars may be too small to see.)
Student T-Test indicated significant difference at an alpha of 0.05 between EC at 0 min to vlp7000, not significantly different at 0 or 10 min VL or 30 – 60 min D; significantly different at 20 – 60 min VL (p= 0.005 – 0.001); between EC at 0 min to Br200, not significantly different at 0, 2, 4, or 6, min VL or 30 – 60 min D (p= 0.3 – 0.2), but significantly different at 8 – 60 min VL (p= 0.01 – 0.0002); and between EC at 0 min to BrNMP, not significantly different at 0 min VL or 30 – 60 min D, but significantly different at 10 – 60 min VL (p= 0.04 – 0.0002).

3.9 Tables

Table 3.9.1. Surface chemical analysis P25 or Br200 Titania in powder form

X-ray Photoelectron Spectroscopy of Titania in Powder Form			
P25		**Brookite-200**	
Peak	**[Mass] %**	**Peak**	**[Mass] %**
O 1s	**39.73**	**O 1s**	**38.97**
Ti 2p	**48.22**	**Ti 2p**	**50.39**
C 1s	**12.06**	**C 1s**	**8.33**
----	**----**	**Cl 2p**	**2.31**

Table 3.9.2. Surface chemical [Mass] % analysis of P or B Sub-coatings with or without Titania

X-ray Photoelectron Spectroscopy of Titania Coatings						
PEAK	**PSS**	**PSS+Br200**	**PSS+P-25**	**PSS+ BrNMP**	**PSS+vlp7000**	**PSS+ Anatase**
Na 1s	**7.94**	**8.68**	**12.93**	**6.56**	**5.88**	**5.88**
O 1s	**24.63**	**32.79**	**28.96**	**21.87**	**32.3**	**34.68**
Ti 2p	**0**	**6.81**	**10.5**	**0**	**5.2**	**9.77**
N 1s	**3.32**	**3.73**	**2.46**	**5.58**	**3.68**	**2.26**
C 1s	**57.24**	**32.12**	**33.01**	**61.6**	**34.21**	**26.67**
S 2p	**6.88**	**4.3**	**5.12**	**4.39**	**5.61**	**3.92**
Si 2p	**0**	**11.57**	**8.02**	**0**	**13.09**	**16.81**

Table 3.9.3. Hydrophilicity measured by contact angle on P or B Sub-coatings with or without Titania

Contact Angle			
P Sub-Coating		**B Sub-Coating**	
Alone	$< 1^o$	**Alone**	62.5^o
P25	$< 1^o$	**P25**	51.5^o
Br200	$< 1^o$	**Br200**	52.5^o
vlp7000	$< 1^o$	**vlp7000**	105.0^o
BrNMP	$< 1^o$	**BrNMP**	67.5^o

P Sub-Coating with or without all types of Titania are significantly different at an alpha of 0.05 from all B Sub-Coatings with or without all types of Titania with a range of p values from 2.36×10^{-5} to 6.93×10^{-6}. All B Sub-Coatings with or without all Types of Titania compared to all B Sub-coatings with or without all Types of Titania at an alpha of 0.05 were all significantly different from each other ($p=0.016$ to 3.15×10^{-6}).

CHAPTER FOUR

EFFECTS OF PHOTOCATALYTICALLY ACTIVATED POLYMORPHIC BROOKITE TITANIA NANOPARTICLE WITH ENHANCED VIA NOVEL SUB-COATTINGS ON CANCER CELL VIABILITY *in vitro*

(As a manuscript formatted for submission to the Journal of Nanobiotechnology)

4.1 Abstract

The most common form of cancer in the U.S. is skin cancer. The most dangerous type of skin cancer is melanoma. Exposure to sunlight or ultraviolet (UV) light causes about 65%-90% of melanoma incidence in the states. Current skin cancer treatments may involve surgery, radiation therapy, photodynamic therapy, hyperthermia therapy, and topical or systemic chemotherapy. For minimal skin cancers, a patient friendly product is needed. Titanium dioxide, a versatile non-selective compound with photocatalytic properties, degrades compounds through photo-oxidation and exists in three lattice phases, Anatase, Brookite, and Rutile. This study evaluated liquid band-aid with liquid phase deposition of polymorphic Brookite phase Titania. Br200 a Water-based Ambient Condition Sol (WACS) was coated onto liquid band-aid and assessed for cytotoxicity on cancer cells *in vitro*.

Long range ultraviolet light (UVA) photocatalytically activated P25 or Br200 Titania with or without liquid band-aid was evaluated for cytotoxicity on HT-29 Human Colon Cancer Cells or HTB-67 Human Malignant Melanoma Cells in vitro. Both cell types resulted in a similar trend. Br200 under UVA without liquid band-aid eliminated

both cell types within 30 minutes. Br200 under UVA with liquid band-aid or P25 under UVA with and without liquid band-aid eliminated all cells within 60 minutes. P25 in the dark with and without liquid band-aid killed approximately 0.5 log of cells. Cells under UVA alone or with liquid band-aid remained at the initial concentration. Except for variables containing P25, all dark exposed cells remained viable at the initial concentration.

Light intensity, wavelength, surface material characteristics, pH, types of ionic molecules in surrounding areas, and target load affect efficiency of photo-oxidation. The Br200 5-8nm diameter crystallite size range provides a greater surface area, significantly increasing target contact probability. Br200 Titania indicated superior photo-oxidative activity when exposed to UVA than the commercial P25 on both HT-29 and HTB-67 cells. This novel format of using FDA approved liquid band-aid coated on one side with Br200 non-selective Titania coating may provide lower pain and scarring for removal of cancer cells.

4.2 Introduction

In the U.S., skin cancer is most prevalent with melanoma the most dangerous type and the third most common. Exposure to ultraviolet (UV) light or sunlight causes about 65%-90% of the melanomas [47]. In the U.S., 2006, melanomas of the skin were diagnosed in 53,919 people and 8,441 people died [48]. Current skin cancer treatments may involve surgery, radiation therapy, external beam radiation, photodynamic therapy, topical, systemic, or fractionated dose chemotherapy, biotherapy, immunotherapy, and

local hyperthermia [49]. These treatments can cause devastation systemically throughout the body along with hair loss and other undesirable effects.

Titania or Titanium dioxide (TiO_2), is a versatile non-selective compound with photocatalytic properties, degrades compounds through photo-oxidation. Titanium dioxide exists in three different polymorphic lattice phases, Anatase, Brookite, and Rutile. Rutile phase is the most thermodynamically stable due to its minimal electrostatic repulsive energy; it is abridged in a linear structure with two of the twelve edges of the octahedron are shared [8]. Anatase phase shares four edges per octahedron without corner oxygen sharing. Uniquely, Brookite phase is composed orthorhombically with three shared edges per octahedron.

Zallen and Moret measured the optical absorption edge of Brookite Titania [9]. Extending throughout the visible light range, Brookite was observed to have a broad absorption edge in contrast to the steep absorption edges of Anatase and Rutile. In the evaluated spectral range, no evidence of a direct gap was observed. They suggest that Brookite phase Titania may function as an indirect-gap semiconductor with an approximate bandgap of 1.9 eV [9]. In contrast, calculations using the self-consistent orthogonalized linear-combination-of-atomic-orbitals method, Mo and Ching, 1995 approximated a direct bandgap for Brookite [10]. Other researchers have determined that all three phases of Titania have similar direct bandgap energies (~3.1 $\pm$ 0.1 eV) [11]. Banerjee and colleagues report the bandgap values for each phase is Anatase (3.2 eV), Rutile (3.02 eV), and Brookite (2.96 eV) [12]. Whether direct or indirect, polymorphic Brookite phase Titania exhibits the lowest bandgap energy.

Researchers have used Atomic Force Microscope (AFM) to visualize the antimicrobial photocatalytic activity of photo-activated Titania [12]. This same phenomenon is expected to work on mammalian cells. The characteristics of a photocatalyst include its ability to simultaneously adsorb two reactants. Then efficiently adsorb light ($h\nu \geq E_g$) to reduce and oxidize the adsorbed reactants. The absorbed light energy must be larger than the bandgap to excite the e^- from the valence band to the conduction band producing an e^--h^+ pair. In the presence of water and dissolved oxygen (H_2O/O_2), the positive holes oxidize water splitting it into $^{\cdot}OH$ and H^+. The dissolved oxygen is reduced by the photo electron of the conduction band, generating superoxide anions ($^{\cdot}O_2^-$). H+ combines with the ($^{\cdot}O_2^-$) generating a hydroperoxyl radical, eventually producing a reactive oxygen species (ROS) H_2O_2 molecule. The photo induced ROS hydroxyl radical and hydrogen peroxide cause biocidal catalysis by penetrating cell walls and cutting DNA strands. The super oxide anion can enter the cell after oxidizing holes are made. Once inside, hydrogen peroxide and the super oxide anion may become hydroxyl radical precursors. Once inside the cell wall (Fe2+) may activate hydrogen peroxide by the Fenton reaction, causing cell death via cell wall destruction and strong DNA damage.

Phosphate ions from Phosphate Buffered Saline have a very high affinity for the Titania. Phosphate ions bind to the substrate surface causing the isoelectric point of the TiO_2/aqueous interface to significantly shift downward to pH 2.0 and increasing the 3400cm^{-1}peak intensity measured by vibrational sum-frequency spectroscopy (VSFS). [62]. The isoelectric point was ~5.5 in the presence of Cl^- ions.

This work investigated one type of polymorphic Brookite phase Titania, Br200, and the commercial Titania P-25 from Degussa, Germany consisting of Anatase phase 79% to the Rutile phase of 21% on liquid band-aid (LB). The samples will be evaluated for their photocatalytic ability with exposure to UVA 365 nm on Human Colon Cancer cells HT-29 and Human Malignant Melanoma Cells HTB-67. The Titania-LB will be examined via Fourier Transform-Infrared Spectrometry.

4.3 Results

Fourier Transform-Infrared Spectrometry verified that Titanium molecules were present in the LB coatings (Figure 1). XPS spectral graphs of the LB sub-coating with and without P25 or Br200 are depicted in Figures 4.8.1 and 4.8.2, respectively.

Long range ultraviolet light (UVA at 365nm) photocatalytically activated P25 or Br200 Titania with or without liquid band-aid were evaluated for cytotoxicity on HT-29 Human Colon Cancer Cells or HTB-67 Human Malignant Melanoma Cells in vitro. Figure 4.8.3 depicts representative photos of the cells. Figures 4.8.4 ($p = 0.01$ to 0.00003) and 4.8.5 ($p = 0.02$ to 0.00003) depict the quantitative graphs of Viable Cells at different time points of treatments. Both cell types resulted in a similar trend. Br200 under UVA without LB eliminated both cell types within 30 minutes. Br200 under UVA with liquid band-aid or P25 under UVA with and without LB eliminated all cells within 60 minutes. P25 in the dark with and without LB killed approximately 0.5 log of cells. Cells under UVA alone or with LB remained at the initial concentration. Except for variables containing P25, all dark exposed cells remained viable at the initial concentration.

4.4 Discussion

Fourier Transform-Infrared Spectrometry verified that Titanium molecules were present in the LB coatings, allowing the Titania to have direct contact with the organic substance to be degraded. Low temperature calcination of 200^{o}C for 2 h on both Br200 Titania produced crystallite sizes ranging from 5-8 nm, therefore, providing a very high surface area ranging from (BET) 138 - 157 m^2/g [65]. This provides a significantly greater surface area per particle than the Degussa commercial P25 reference standard at (BET) 56 m^2/g with 79% Anatase and 21% Rutile phase TiO_2. FT-IR Spectral graphs are shown in Figure 4.8.1 comparing P25 to Figure 4.8.2 Br200 Titania with and without LB.

4.5 Conclusions

According to the results obtained in this study, Br200 Titania with and without LB provided superior oxidative activity on both HT-29 and HTB-67 cancer cell decomposition compared to the commercial P25 TiO_2 from Degussa, (Evonik Industries AG, Germany). One explanation is reported by Zallen and Moret, 2006. At ambient temperature, natural Brookite TiO_2 crystals were examined via optical-absorption ranging from 2.1 to 3.54 eV. The Brookite TiO_2 absorption edge is broad, continuing throughout the visible range with no direct gap [9]. In contrast to tetragonal forms, the orthorhombic structure encompasses a larger range of bond lengths from the six unique nearest-neighbor Ti-O bond lengths. They suggest that Brookite TiO_2 has indirect-band-gap semiconductor properties with a bandgap approximating 1.9 eV. The narrowing off the band gap will shift the absorption edge into the visible range.

Due to the low temperature method in which the Br200 was formed and calcined, provided small crystallite sizes ranging from 5 – 8 nm in diameter, producing a large surface area, approximately (BET) 157 m^2/g [66]. This large surface area would provide more opportunities for contact with molecules or cells. The smaller crystallite size allows for more particles to make up a specific mass, hence providing extremely large surface area for photocatalytic activity.

Therefore, LB coatings with Br200 Titania may provide a non-selective method of killing cancer cells that causes less pain and less scarring, and deliver a patient friendly and effective cancer treatment.

4.6 Experimental

Titanium dioxide Br200 nanoparticles samples were graciously given to our lab by Dr. B. I. Lee and Dr. S. Kaewgun at Clemson University. The donated Br200 nanoparticles were made by the WACS process as described in [66]. This sample was calcined at 200^{o}Celsius for 2 hours (h) in air. The commercial TiO_2, P25 from Degussa, (Evonik Industries AG, Germany) was used for long wave ultraviolet light (UVA) (365nm) comparisons of activity to Br200.

FTIR analysis was performed using a Thermo-Nicolet Magna 550 FTIR spectrometer equipped with a Thermo-Nicolet Nic-Plan FTIR Microscope. Thin films of the gels (New Skin Liquid Band-Aid; Prestige Brands, Inc., USA) with and without Br200 or P25 were cast onto IRTran Plates and dried under an IR heat lamp. Scans (64) at a resolution of 4cm-1 were collected for the sample and also for the background (clean

IRTran Plate) in transmission mode on the microscope. Samples were analyzed over the range of 4000cm-1 to 700cm-1. Data was analyzed using Omnic Data Analysis software and absorbance peaks labeled with wavelength (cm^{-1}).

Each Titania, Br200 or P25, or was mixed into sterile Hanks Balance Salt Solution (HBSS) sonicated for 1 h and vortexed for 1 minute. A thin coat of LB was painted onto wax paper matching the size of the well bottom of the 24-well plate. After drying, 150 µL of the appropriate Titania-HBSS was deposited and air dried for use.

The cell culture assays were conducted using HTB-67 Human Malignant Melanoma Cells and HT-29 Human Colon Cancer Cells (HTB-38; ATCC, Manassas, VA). The cells were shipped cryopreserved at the end of their tertiary culture in the appropriate culture medium and 5% dimethylsulfoxide (DMSO) (Sigma, St. Louis, MO). Based on ATCC's product information sheet, HTB-67 cells were spherical and grew in suspension using 15 mL of medium Eagle's Minimum Essential Medium (EMEM) and 10% Fetal Bovine Serum (FBS). HT-29 cells are epithelial and adherent growing in ATCC-formulated McCoy's 5a Medium Modified, Catalogue No. 30-2007, plus 1% antibiotic solution with FBS to a final concentration of 10%. They were subcultivated in T-75 culture flasks (Corning canted neck flasks with vented caps, (VWR, Atlanta, GA) in a 37°C, 5% CO_2, 95% air, humidified culture incubator with Work was carried out in a class 2 A/B3 biological safety cabinet**.** Hanks' Balanced Salt Solution (HBSS) plus 1% antibiotic solution, modified without calcium chloride, magnesium chloride, or phenol red (ATCC 30-2213) was used for washing cells and the test experiments. For tests, 1 X 10^5 cells/38cm^2 were inoculated and grown to 90% confluency in 24-well tissue culture

treated plates (VWR, Atlanta, GA). Cells were rinsed in HBSS twice prior to testing and HBSS was the testing diluent. HBSS had the least affect on the Titania.

LIVE/DEAD® Viability/Cytotoxicity Kit— (Molecular Probes; Eugene, OR) Calcein AM EX/EM 494/517 is membrane-permeant, cleaved by esterases in live cells resulting in cytoplasmic green fluorescence. Ethidium homodimer-1 EX/EM 517/617 is membrane-impermeant and labels nucleic acids of membrane-compromised cells with red fluorescence. The cells were exposed to either UVA 365nm at 363-364 $\mu W/cm^2$ or dark for different time periods with and without Br200 or P25 Titania, using 1mg/mL free suspension or $2mg/38mm^2$ coatings. Following the Live/Dead product sheet, the cells were incubated for 1 h then observed and photographed under a fluorescent microscope. There were 4 wells per variable with 4 random pictures taken per well. Cells were observed for morphology and life.

The Titania were weighed and mixed into HBSS at either 1mg/ml in free suspension or 14mg Titania/mL HBSS for the coatings. The liquid Titania suspensions were sonicated (Sonicator FS30H; Fisher Scientific) for 1 h and vortexed. Each well received 1mg/mL of either Br200 or P25 Titania. Each treated liquid Band-aid (LB) slip received one aliquot of 150 µL of Br200 or P25 suspension, ($2mg/38mm^2$) and was air dried at ambient temperature between aliquots, then stored aseptically at room temperature for further use.

Phosphate Buffered Saline (PBS) was not used as the diluent because Phosphate ions from Phosphate Buffered Saline have a very high affinity for the Titania. Phosphate ions bind to the substrate surface causing the isoelectric point of the TiO_2/aqueous

interface to significantly shift downward to pH 2.0 and increasing the 3400cm^{-1}peak intensity measured by vibrational sum-frequency spectroscopy (VSFS) [62].

The LB coating with or without Br200 or P25 Titania was evaluated for photocatalytic activity. Cells alone without treatment were the negative control and cells with free suspension Titania were used for the positive controls. A multiple ray lamp (MRL, Model 58; Fisher Scientific) with different 8 Watt tubes UVA (365nm) at 363-364 μW/cm^2) and visible light (Cool White) at 100 μW/cm^2) was utilized as the source for photoactivation. The intensity of light was verified with a UVX Digital Radiometer, (Model-UVX, UVP, Inc., Upland, CA) for UVA light. Polystyrene plates (24-well) containing the cells were secured onto a microplate orbital mixer (Microplate Genie, Model SI-0400, VWR). One milliliter of 1mg/mL Br200 or P25 HBSS solution was added to each well in free suspension. Each coating was placed into well containing 1X10^5 cells in HBSS. A non-fluorescing optically clear film (TemPlate® RT Optical Film, 2978-2700, USA Scientific, Inc.) was adhered to the polystyrene plate to prevent evaporation of the MO. The lamp intensity was adjusted to accommodate the film and the liquid band-aid.

Plates were at 0, 5, 10, 15, 30, and 60 minutes, the experiment was run backward so the times would come due at the same time for each plate. The cells were washed twice in HBSS to remove the free Titania. The wells containing had the coatings removed and cells rinsed twice. The Live/Dead Assay was applied and read after 1 h incubation using a fluorescent microscope. Four random images were taken of each sample and the cells were counted. Calculations were based on the change in viable cells counts at

various time points as percentages described in Equation 1. All experiments were replicated for reproducibility.

$$\frac{\text{Change in Number of Viable Cells}}{\text{Original Cell Concentration}} \times 100\% \quad (1)$$

4.7 References

1. Pigments, H., *Pigments.* 2010.
2. Johansson, E.M.J., et al., *Photovoltaic and Interfacial Properties of Heterojunctions Containing Dye-Sensitized Dense TiO2 and Tri-arylamine Derivatives.* Chemistry of Materials, 2007. **19**(8): p. 2071-2078.
3. Sabetrasekh, R. and et al., *Impact of trace elements on biocompatibility of titanium scaffolds.* Biomedical Materials, 2010. **5**(1): p. 015003.
4. Popov, A., et al. *Interaction of sunscreen TiO[sub 2] nanoparticles with skin and UV light: penetration, protection, phototoxicity.* 2009. Munich, Germany: SPIE.
5. Evans, P., et al., *A comparative study of three techniques for determining photocatalytic activity.* Journal of Photochemistry and Photobiology A: Chemistry, 2007. **188**(2-3): p. 387-391.
6. Srinivasan, C., et al,, *Bactericidal and detoxification effects of irradiated semiconductor catalyst, TiO2.* Current Science, 2003. **85**(10): p. 1431-1438.
7. News, T.B.T., *Titanium-Oxide Photocatalyst.* Three Bond Technical News, 2004. **62**: p. 1-8.

8. Watson, S., et al.,, *Preparation of nanosized crystalline TiO2 particles at low temperature for photocatalysis.* Journal of Nanoparticle Research, 2004. **6**(2): p. 193-207.

9. Zallen, R. and M.P. Moret, *The optical absorption edge of brookite TiO2.* Solid State Communications, 2006. **137**(3): p. 154-157.

10. Mo, S.-D. and W.Y. Ching, *Electronic and optical properties of three phases of titanium dioxide: Rutile, anatase, and brookite.* Physical Review B, 1995. **51**(19): p. 13023.

11. Watson, S., et al., *Preparation of nanosized crystalline TiO2 particles at low temperature for photocatalysis.* Journal of Nanoparticle Research, 2004. **6**(2): p. 193-207.

12. Banerjee, S., et al., *Physics and chemistry of photocatalytic titanium dioxide: Visualization of bactericidal activity using atomic force microscopy* Current Science, 2006. **90**(10).

13. Bratu, S., Steven Brooks, Sibte Burney, Sandeep Kochar, Jyoti Gupta, David Landman, and John Quale, *Detection and Spread of Escherichia coli Possessing the Plasmid-Borne Carbapenemase KPC-2 in Brooklyn, New York.* **Clinical Infectious Diseases**, 2007. **44**: p. 972-975.

14. Jawad, A., et al., *Survival of Acinetobacter baumannii on Dry Surfaces: Comparison of Outbreak and Sporadic Isolates.* J. Clin. Microbiol., 1998. **36**(7): p. 1938-1941.

15. Savini, V., et al., *Misidentification of ampicillin-sulbactam heteroresistance in Acinetobacter baumannii strains from ICU patients.* Journal of Infection, 2009. **In Press, Corrected Proof**.

16. Giamarellou, H., A. Antoniadou, and K. Kanellakopoulou, *Acinetobacter baumannii: a universal threat to public health?* International Journal of Antimicrobial Agents, 2008. **32**(2): p. 106-119.

17. Wendt, C., et al., *Survival of Acinetobacter baumannii on dry surfaces.* J. Clin. Microbiol., 1997. **35**(6): p. 1394-1397.

18. Perez, F., et al., *Global Challenge of Multidrug-Resistant Acinetobacter baumannii.* Antimicrob. Agents Chemother., 2007. **51**(10): p. 3471-3484.

19. Fournier, P.-E., et al., *Comparative Genomics of Multidrug Resistance in <italic>Acinetobacter baumannii</italic>*. PLoS Genet, 2006. **2**(1): p. e7.

20. Nemec, A., et al., *Diversity of aminoglycoside-resistance genes and their association with class 1 integrons among strains of pan-European Acinetobacter baumannii clones.* J Med Microbiol, 2004. **53**(12): p. 1233-1240.

21. Oliveira, D.C., A. Tomasz, and H. de Lencastre, *Secrets of success of a human pathogen: molecular evolution of pandemic clones of meticillin-resistant Staphylococcus aureus.* The Lancet Infectious Diseases, 2002. **2**(3): p. 180-189.

22. Cirz, R.T., et al., *Inhibition of Mutation and Combating the Evolution of Antibiotic Resistance.* PLoS Biol, 2005. **3**(6): p. e176.

23. Perez-Capilla, T., et al., *SOS-Independent Induction of dinB Transcription by {beta}-Lactam-Mediated Inhibition of Cell Wall Synthesis in Escherichia coli.* J. Bacteriol., 2005. **187**(4): p. 1515-1518.

24. Magnet, S., P. Courvalin, and T. Lambert, *Resistance-Nodulation-Cell Division-Type Efflux Pump Involved in Aminoglycoside Resistance in Acinetobacter baumannii Strain BM4454.* Antimicrob. Agents Chemother., 2001. **45**(12): p. 3375-3380.

25. Kohanski, M.A., M.A. DePristo, and J.J. Collins, *Sublethal Antibiotic Treatment Leads to Multidrug Resistance via Radical-Induced Mutagenesis.* Molecular Cell, 2010. **37**(3): p. 311-320.

26. Costerton, J.W., and P.H. Stewart, *Battling Biofilms.* Scientific American: Special Supplement 2006: p. 2-11.

27. Schembri, M.A., D. Dalsgaard, and P. Klemm, *Capsule shields the function of short bacterial adhesins.* J Bacteriol, 2004. **186**(5): p. 1249-57.

28. Mehrotra, A., *Bacterial Biofilms.* Pediatric Asthma, Allergy & Immunology, 2007. **20**(3): p. 191-195.

29. Reisner, A., et al., *In Vitro Biofilm Formation of Commensal and Pathogenic Escherichia coli Strains: Impact of Environmental and Genetic Factors.* J. Bacteriol., 2006. **188**(10): p. 3572-3581.

30. Jones, C.H., *FimH adhesin of type 1 pili is assembled into a fibrillar tip structure in the Enterobacteriaceae.* Proc. Natl. Acad. Sci. , 1995. **92**: p. 2081-2085.

31. Bower, J.M., D.S. Eto, and M.A. Mulvey, *Covert Operations of Uropathogenic Escherichia coli within the Urinary Tract.* Traffic, 2005. **6**(1): p. 18-31.

32. Das, M., et al., *Hydrophilic Domain II of Escherichia coli Dr Fimbriae Facilitates Cell Invasion.* Infect. Immun., 2005. **73**(9): p. 6119-6126.

33. Ahmer, B.M.M., *Cell-to-cell signalling in Escherichia coli and Salmonella enterica*. Molecular Microbiology, 2004. **52**(4): p. 933-945.

34. Costerton, J.W., P.S. Stewart, and E.P. Greenberg, *Bacterial biofilms: a common cause of persistent infections.* Science, 1999. **284**(5418): p. 1318-22.

35. Maira-Litran, T., D.G. Allison, and P. Gilbert, *An evaluation of the potential of the multiple antibiotic resistance operon (mar) and the multidrug efflux pump acrAB to moderate resistance towards ciprofloxacin in Escherichia coli biofilms.* J Antimicrob Chemother, 2000. **45**(6): p. 789-95.

36. Genevaux, P., S. Muller, and P. Bauda, *A rapid screening procedure to identify mini-Tn10 insertion mutants of Escherichia coli K-12 with altered adhesion properties.* FEMS Microbiol Lett, 1996. **142**(1): p. 27-30.

37. Stewart, P.S., *A review of experimental measurements of effective diffusive permeabilities and effective diffusion coefficients in biofilms.* Biotechnol Bioeng, 1998. **59**(3): p. 261-72.

38. Ishida, H., et al., *In vitro and in vivo activities of levofloxacin against biofilm-producing Pseudomonas aeruginosa.* Antimicrob Agents Chemother, 1998. **42**(7): p. 1641-5.

39. Shigeta, M., et al., *Permeation of antimicrobial agents through Pseudomonas aeruginosa biofilms: a simple method.* Chemotherapy, 1997. **43**(5): p. 340-5.

40. Brown, M.R. and J. Barker, *Unexplored reservoirs of pathogenic bacteria: protozoa and biofilms.* Trends Microbiol, 1999. **7**(1): p. 46-50.

41. de Beer, D., et al., *Effects of biofilm structure on oxygen distribution and mass transport.* Biotechnol. Bioeng., 1994. **43**: p. 1131-1138.

42. Darouiche, R.O., et al., *Efficacy of antimicrobial-impregnated bladder catheters in reducing catheter-associated bacteriuria: a prospective, randomized, multicenter clinical trial.* Urology, 1999. **54**(6): p. 976-81.

43. Raad, I. and H. Hanna, *Intravascular catheters impregnated with antimicrobial agents: a milestone in the prevention of bloodstream infections.* Support Care Cancer, 1999. **7**(6): p. 386-90.

44. Spencer, R.C., *Novel methods for the prevention of infection of intravascular devices.* J Hosp Infect, 1999. **43 Suppl**: p. S127-35.

45. Woo, G.L., M.W. Mittelman, and J.P. Santerre, *Synthesis and characterization of a novel biodegradable antimicrobial polymer.* Biomaterials, 2000. **21**(12): p. 1235-46.

46. Kallio, T., et al., *Antifouling properties of TiO2: Photocatalytic decomposition and adhesion of fatty and rosin acids, sterols and lipophilic wood extractives.* Colloids and Surfaces A: Physicochemical and Engineering Aspects, 2006. **291**(1-3): p. 162-176.

47. Prevention, C.f.D.C.a., *Guidelines for school programs to prevent skin cancer.* MMWR 2002. **51**((RR-4)): p. 1-16.

48. Group, U.S.C.S.W., *United States Cancer Statistics: 1999–2006 Incidence and Mortality Web-based Report.* . United States Cancer Statistics:, 2010.

49. America, C.T.C.o., *Learn more about skin cancer treatments.* 2010.

50. James F. Reeves, S.J.D., Nicholas J.F. Dodd, Awadhesh N. Jha, *Hydroxyl radicals (•OH) are associated with titanium dioxide (TiO2) nanoparticle-induced cytotoxicity and oxidative DNA damage in fish cells.* Mutation Research, 2007. **640**: p. 113-122.

51. Vevers, W.F. and A.N. Jha, *Genotoxic and cytotoxic potential of titanium dioxide (TiO2) nanoparticles on fish cells in vitro.* Ecotoxicology, 2008. **17**(5): p. 410-20.

52. Xia, C.-H., et al., *The Primary Mechanism of Photoexcited TiO2 Nanoparticles-induced Apoptosis in Human Hepatoma Bel-7402 Cells.* bmei BioMedical Engineering and Informatics, International Conference on International Conference on BioMedical Engineering and Informatics 2008. **2**: p. 698-702.

53. Holsapple, M.P., et al., *Research Strategies for Safety Evaluation of Nanomaterials, Part II: Toxicological and Safety Evaluation of Nanomaterials, Current Challenges and Data Needs.* Toxicol. Sci., 2005. **88**(1): p. 12-17.

54. Liang, X.-J., et al., *Biopharmaceutics and Therapeutic Potential of Engineered Nanomaterials.* Current Drug Metabolism, 2008. **9**: p. 697-709.

55. Kiss, B., et al., *Investigation of micronized titanium dioxide penetration in human skin xenografts and its effect on cellular functions of human skin-derived cells.* Experimental Dermatology, 2008. **17**(8): p. 659-667.

56. Venturi, V.a.S.S., *Future research trends in the major chemical languaage of bacteria.* HFSP Journal, 2009. **3**(2): p. 105-116.

57. Chang, C.-Y., et al., *Establishment of activity indicator of TiO2 photocatalytic reaction--Hydroxyl radical trapping method.* Journal of Hazardous Materials, 2009. **166**(2-3): p. 897-903.

58. Heller, A., *Chemistry and Applications of Photocatalytic Oxidation of Thin Organic Films.* Accounts of Chemical Research, 1995. **28**(12): p. 503-508.

59. Le, D.D. and et al., *The fabrication of visible light responsive Ag-SiO 2 co-doped TiO 2 thin films by the sol–gel method.* Advances in Natural Sciences: Nanoscience and Nanotechnology, 2010. **1**(1): p. 015007.

60. Youngman, R.J., *Oxygen activation: is the hydroxyl radical always biologically relevant?* Trends in Biochemical Sciences, 1984. **9**(6): p. 280-283.

61. Blake, D.M., et al., *Application of the Photocatalytic Chemistry of Titanium Dioxide to Disinfection and the Killing of Cancer Cells.* Separation and Purification Methods, 1999. **28**(1): p. 1 - 50.

62. Kataoka, S., et al., *Investigation of Water Strcuture at the TiO2/Aqueous Interface.* Langmuir, 2004. **20**: p. 1662-6.

63. Connor, P.A. and A.J. McQuillan, *Phosphate Adsorption onto TiO2 from Aqueous Solutions: An in Situ Internal Reflection Infrared Spectroscopic Study.* Langmuir, 1999. **15**: p. 2916-2921.

64. Bakshi, M.S., et al., *Shape-Controlled Synthesis of Poly(styrene sulfonate) and Poly(vinyl pyrolidone) Capped Lead Sulfide Nanocubes, Bars, and Threads.* The Journal of Physical Chemistry C, 2008. **112**(13): p. 4948-4953.

65. Kaewgun, S., C. Nolph, and B. Lee, *Enhancing Photocatalytic Activity of Polymorphic Titania Nanoparticles by NMP Solvent-based Ambient Condition Process.* Catalysis Letters, 2008. **123**(3): p. 173-180.

66. Kaewgun, S., et al., *Influence of hydroxyl contents on photocatalytic activities of polymorphic titania nanoparticles.* Materials Chemistry and Physics, 2009. **114**(1): p. 439-445.

67. Shah, R.R., *The antibacterial properties of brookite phase titanium dioxide nanoparticles against methicillin-resistant staphylococcus aureus*
A Thesis Presented to the Graduate School of Clemson University, 2007.

68. Kaewgun, S., et al., *Study of visible light photocatalytic activity achieved by NMP solvent treatment of polymorphic titania.* Journal of Photochemistry and Photobiology A: Chemistry, 2009. **202**(2-3): p. 154-158.

69. Kaewgun, S. and B.I. Lee, *Deactivation and regeneration of visible light active brookite titania in photocatalytic degradation of organic dye.* Journal of Photochemistry and Photobiology A: Chemistry, 2010. **210**(2-3): p. 162-167.

70. mindat.org. *Brookite*. Mineral Data 2010 [cited 2010; Available from: +

71. HP, O.s.L. *Crystal Structure*. 2010 2010]; Available from: http://www.geocities.jp/ohba_lab_ob_page/structure6.html.

72. *Ion Sizes of Common Elements*. 2010; Available from: http://www.astro.lsa.umich.edu/~cowley/ionsize.html.

73. Connor, P.A. and A.J. McQuillan, *Phosphate Adsorption onto TiO2 from Aqueous Solutions: An in Situ Internal Reflection Infrared Spectroscopic Study*. Langmuir, 1999. **15**(8): p. 2916-2921.

74. Nelson, B.P., et al., *Control of Surface and ζ Potentials on Nanoporous TiO2 Films by Potential-Determining and Specifically Adsorbed Ions.* Langmuir, 2000. **16**: p. 6094-6101.

75. Li, Y., et al., *Photocatalytic degradation of methyl orange by TiO2-coated activated carbon and kinetic study*. Water Research, 2006. **40**(6): p. 1119-1126.

76. Kraeutler, B. and A.J. Bard, *Photoelectrosynthesis of ethane from acetate ion at an n-type titanium dioxide electrode. The photo-Kolbe reaction.* Journal of the American Chemical Society, 1977. **99**(23): p. 7729-7731.

77. Matos, J., J. Laine, and J.M. Herrmann, *Effect of the Type of Activated Carbons on the Photocatalytic Degradation of Aqueous Organic Pollutants by UV-Irradiated Titania*. Journal of Catalysis, 2001. **200**(1): p. 10-20.

78. Chen, F., et al., *Correlation of Photocatalytic Bactericidal Effect and Organic Matter Degradation of TiO2 Part I: Observation of Phenomena.* Environmental Science & Technology, 2009. **43**(4): p. 1180-1184.

79. Tsuge, Y., et al., *Fabrication of transparent TiO2 film with high adhesion by using self-assembly methods: Application to super-hydrophilic film.* Thin Solid Films, 2008. **516**(9): p. 2463-2468.

4.8 Figures

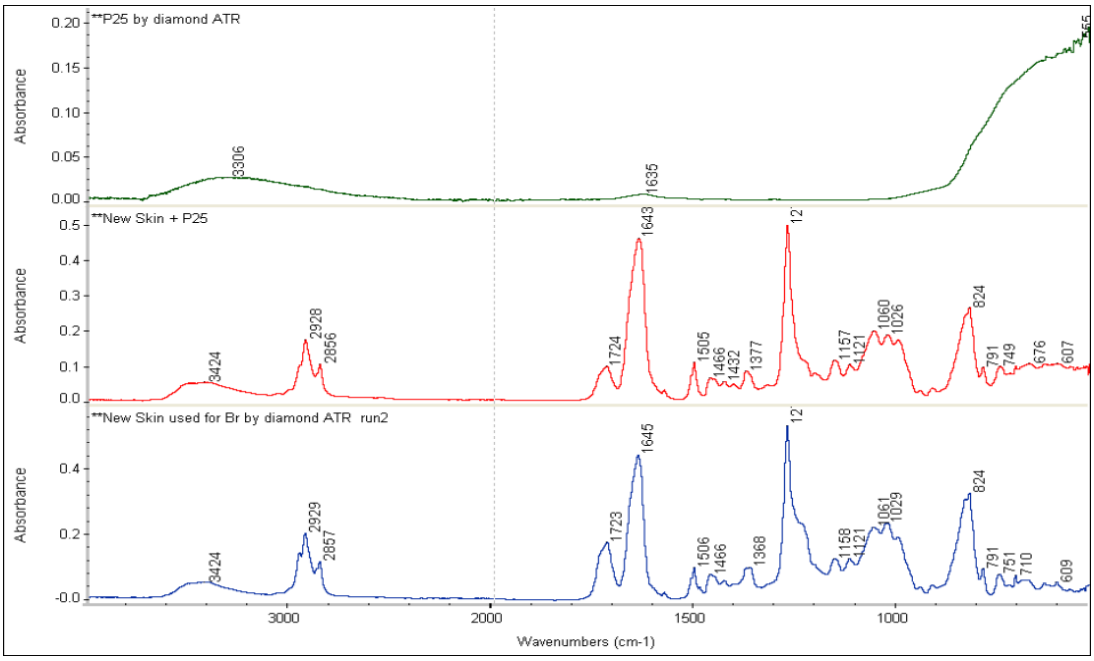

Figure 4.8.1. FT-IF Spectral Graphs of P25 with and without Liquid Band-Aid

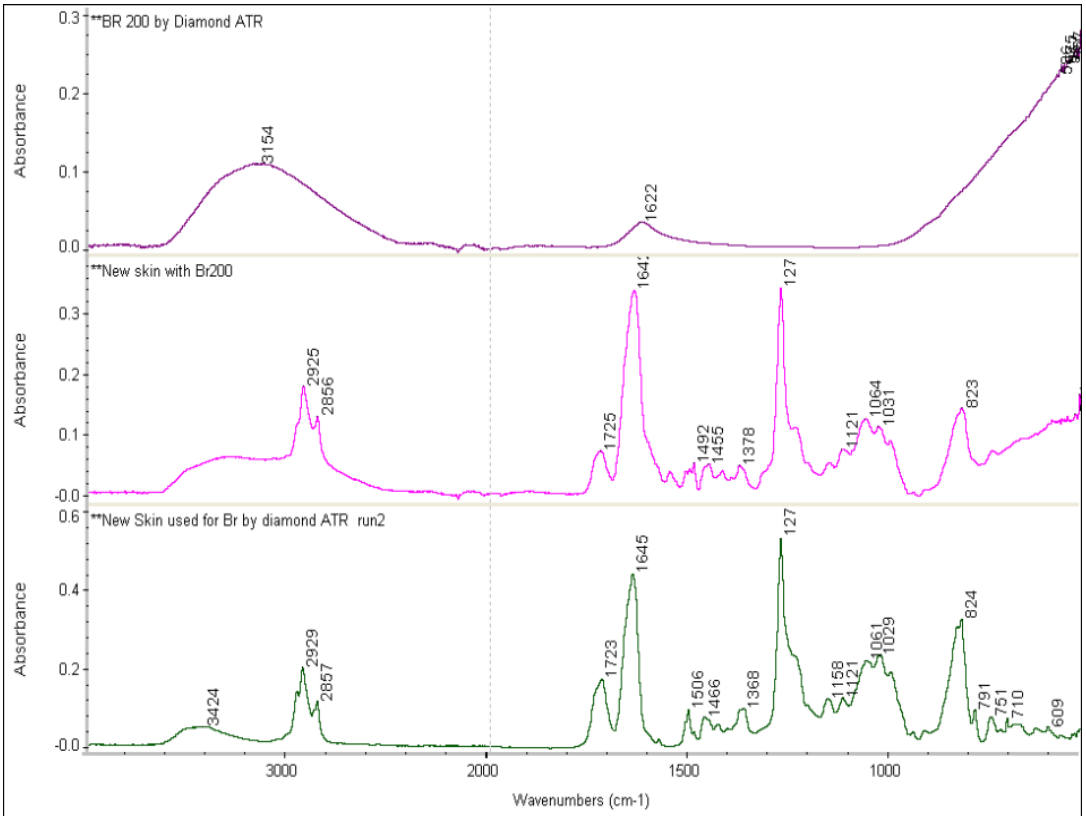

Figure 4.8.2. FT-IF Spectral Graphs of Br200 with and without Liquid Band-Aid

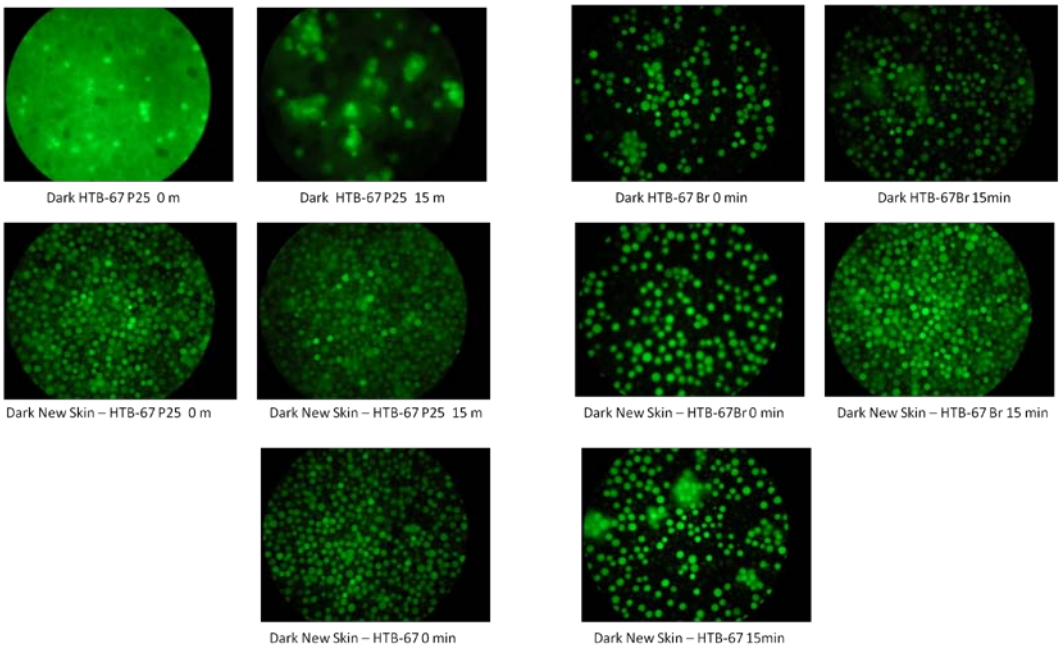

Figure 4.8.3. Representative Photos of Live/Dead Cytocompatibility HTB-67 Human Malignant Melanoma Cells exposed to Dark *in vitro*

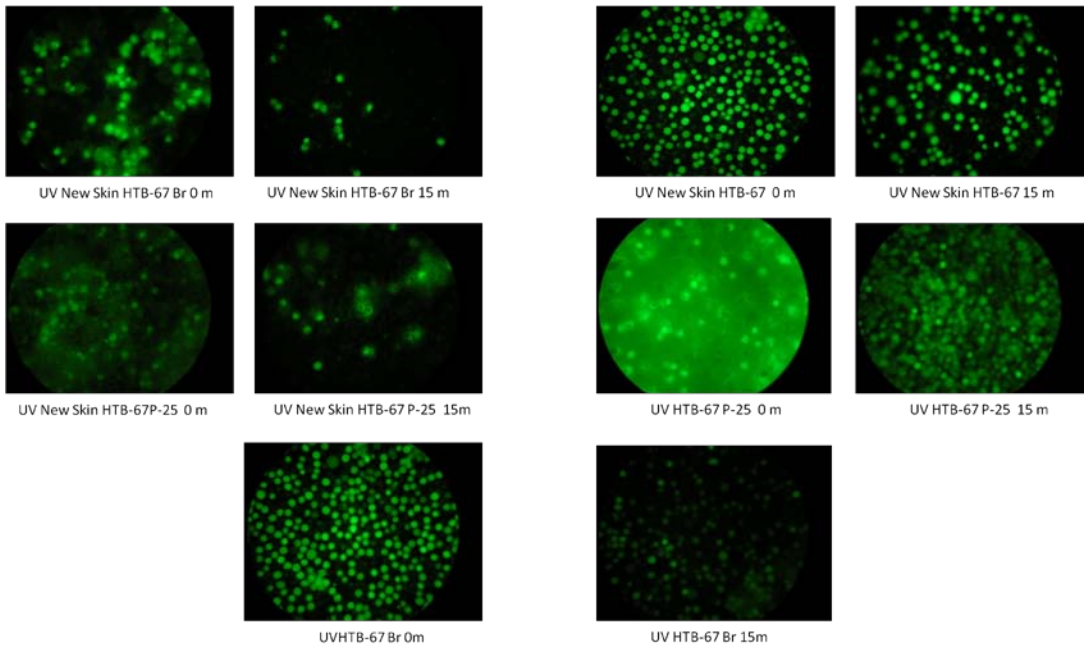

Figure 4.8.4. Representative Photos of Live/Dead Cytocompatibility HTB-67 Human Malignant Melanoma Cells with and without Titania exposed to UVA *in vitro*

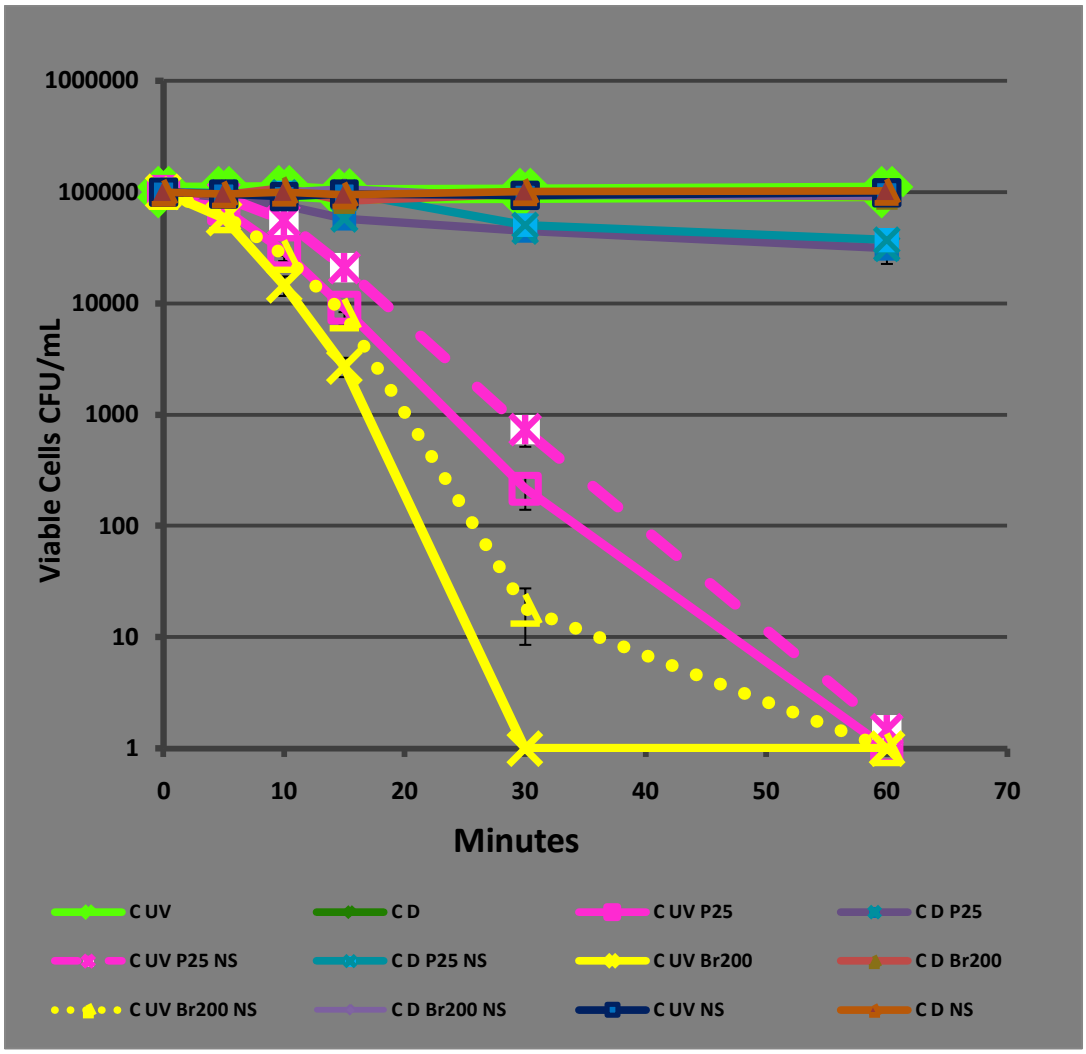

Figure 4.8.5. Effects of UVA photoactivation on HTB-67 Melanoma cells by Br200 or P25 with or without Liquid Band-Aid with p values ranging from 0.01 to 0.00003

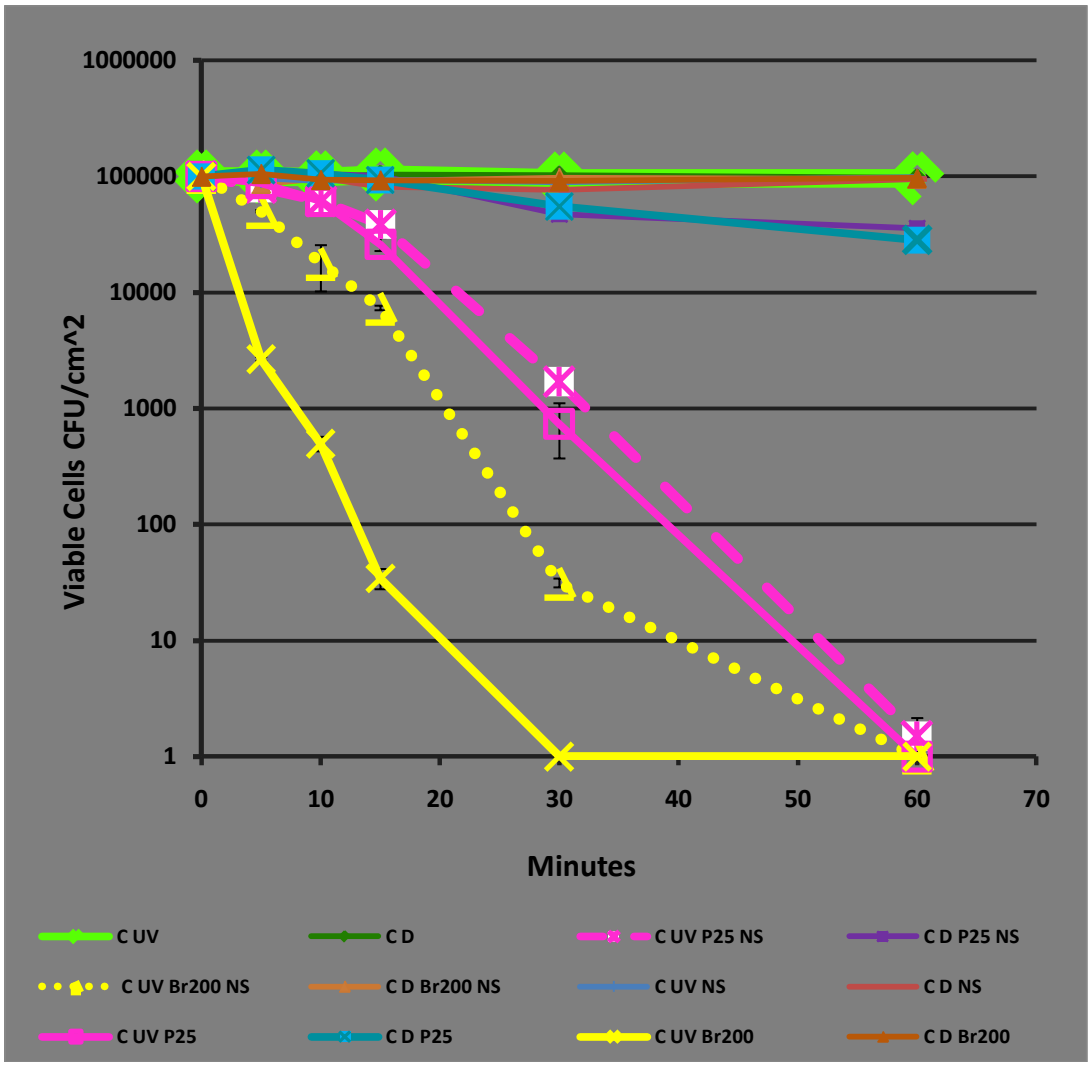

Figure 4.8.6. Effects of UVA photoactivation on HT-29 Colon Cancer cells by Br200 or P25 with or without Liquid Band-Aid with p values ranging from 0.02 to 0.00003

CHAPTER FIVE

CONCLUSIONS

As MDR bacteria and biofilms become more prevalent and resistant in both the nosocomial and community settings, non-selective surface coatings that eradicate these super bugs are truly needed. In our first study, we created a super-hydrophilic-polyelectrolyte-Brookite phase Titania coating. We obtained positive results in characterizing the coatings through surface chemical analysis and XRD. We verified that the polyelectrolyte super-hydrophilic-Brookite phase Titania coating contained the Titania particles on the surface and that the spectra peaks corresponded to the lattice structure in the original Brookite phase nanoparticle powered Titania provided to our lab by Dr. Lee. The polyelectrolyte coatings containing Br200 Titania were superior to BrNMP, the commercial P25 from Degussa, and the commercial Kronos VLP7000 in every evaluation in both UVA and VL light against different loads of bacteria. To our knowledge, this is the first super-hydrophilic-polyelectrolyte-Brookite phase Br200 Titania coating. This novel polyelectrolyte-Br200 non-selective Titania coating can provide a low cost, effective non-selective method of preventing transmission of bacterial infections, or prevention of biofilm formation in the nosocomial and community settings.

The Brookite phase Titania was also evaluated on cancer cells, HT-29 human colon cancer cells and HTB-67 human malignant melanoma cells *in vitro*. Again, the Br200 Titania whether in free suspension or used as a coating with liquid band-aid, it proved significantly superior to the commercial Anatase phase, P25 from Degussa. To our knowledge, this is the first study to evaluate this novel format of using FDA approved

liquid band-aid coated on one side with Br200 non-selective Titania coating and can provide lower pain and scarring for removal of skin cancers in a patient friendly format.

The objectives of this research were obtained. First the free suspension assay was modified and miniaturized with three different methods. For high bacterial loads, the BacLight Live Dead Assay and the BacTiterGlo Assay provide a fast and multiple variable 96-well format for quantitative measurements using fluorescence or luminescence plate reader and qualitatively using fluorescence microscopy. With a lower bacterial load, spread plating from a 24-well plate format provides superior low number counts. The modified and miniaturized assay was adapted for use with coatings. Twenty-two millimeter glass cover slips were used as the coating base and fit in the 22.2 mm diameter wells of the 24-well plates. Twenty-four samples could be evaluated at one time with spread plating techniques for quantification.

The novel P sub-coating was developed and characterized via XRD to confirm a match with the original properties of the loose nanoparticles. XPS further characterized the molecules present on the surface of the coatings, indicating that Ti, O, N, and S were on the surfaces. Complete death curves were quantified for each type of Titania, P25, Br200, BrNMP, and vlp7000 both in free suspension and comparing the new P sub-coating with and without Titania to the B sub-coating with and without Titania. The death curves were performed under UVA or VIS light for the appropriate types of Titania. Br200 remained superior to all other types of Titania evaluated in the coatings under both UVA and VIS light. In fact, Br200 with the P sub-coating killed all bacteria within 8 minutes under VIS light. In previous work by our lab's researchers their coating with

Br200 required over 8 hours of exposure to kill 3 logs of cells difference from the Br200 cells in the dark.

Methyl Orange oxidative-degradation using the P sub-coating with Br200, BrNMP and UVA (P25) or VIS light (vlp7000) with an 8 Watt lamp yielded total degradation. Total degradation occurred under UVA and P sub-coatings with Br200 and BrNMP in 10-12 hours and under VIS light and P sub-coatings with Br200 and BrNMP in 14 hours. These results indicate the uniqueness of the P sub-coating bound with the Br200 and BrNMP Titania.

Because of these results of the P sub-coating with the polymorphic Brookite Br200 and BrNMP, low temperature surface interactions between the P sub-coating N and/ or S molecules and the Titania may occur. These molecules are enhancing the photocatalytic activity of the polymorphic Brookite Br200 and BrNMP by increasing the absorption edge and narrowing the ban-gap. To our knowledge, this is the first time that low temperature interactions via the P sub-coating, positively affecting Titania photocatalytic properties in this manner has been described. Therefore, this work contributes to the scientific body of knowledge. The P sub-coating is novel and has enhancing abilities to increase the photocatalytic activity of polymorphic Brookite, Br200, and BrNMP.

Due to the superior results of Br200, it was chosen for the *in vitro* cancer work as a feasibility proof of concept model. Br200 and P25 were examined with the LB sub-coating to kill cancer cells under UVA irradiation. Again, Br200 with the FDA approved LB sub-coating was found superior. This work may contribute to the enrichment of

cancer patients' lives, by receiving treatment that is less deleterious throughout the body, causes less scarring and pain. Finding a new treatment for cancer also contributes to the scientific body of knowledge.

RECOMMENDATIONS

The super-hydrophilic-Brookite phase Br200 Titania coating should be characterized further by evaluating to verify the coated Titania retains the same characteristics as the original nanoparticle powder. Characterize and verify in detail how the P sub-coating containing the N and S molecules enhance the polymorphic Brookite Br200 and BrNMP Titania.

1. Solid state $_1$H MAS NMR measurements, used to distinguish and analyze the amount of surface hydroxyls and lattice hydroxyls as minimization increases photocatalytic activity
2. N_2 physisorption to verify BET surface area, pore volume, average pore diameter, and pore size distribution of TiO_2 on coatings
3. Fourier-Transform Infrared Spectroscopy (FT-IR) to verify vibrational bands for total water and -OH groups on coatings
4. ATR for the semiquatitative analysis of hydroxyls on coatings
5. Diffuse Reflectance Infrared Fourier Transform (DRIFT) spectroscopy to confirm that the ATR is valid for the semiquatitative analysis of hydroxyls

Because, light intensity, wavelength, surface material characteristics, and bacterial load affect efficiency of photo-oxidation, further evaluation of the novel P sub-coating is warranted.

6. Different loads of and species of bacteria should be evaluated under both UVA and VL light on the novel sub-coatings with Titania

7. Test comparing VL light on the novel sub-coatings with Titania
8. Different strains of human melanomas on the LB novel sub-coatings with Titania
9. Observe the effects in an *in vivo* murine model. The immunohistochemistry marker HMB-45 will stain malignant melanoma.
10. Test more variables and reproducibility in the *in vivo* work for statically significant results
11. Further characterization of the liquid band-aid-Br200 coating to verify the Br200 Titania as listed above with the first coating.
12. File for IP
13. Look into Clinical Trials
14. Work on product development

APPENDICES

APPENDIX A

LAMP WAVELENGTH SPECTRA

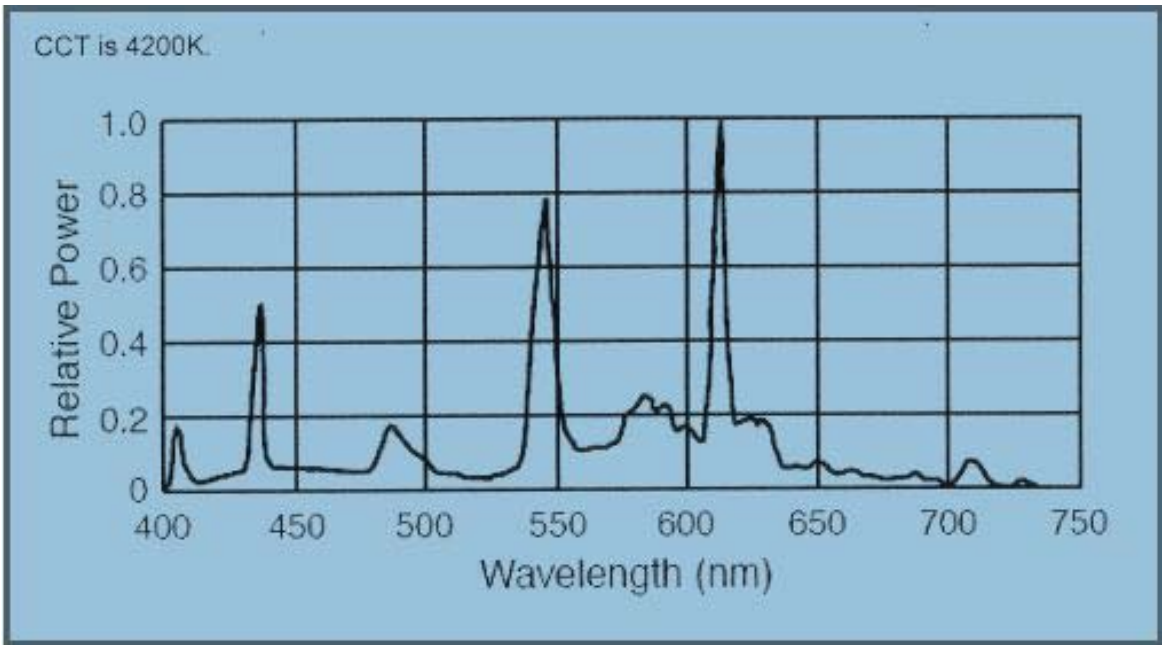

A.1. Visible Wavelength Spectra: Emission range of Cool White 8 Watt Lamp for VL work, UVP, Inc., Upland, CA

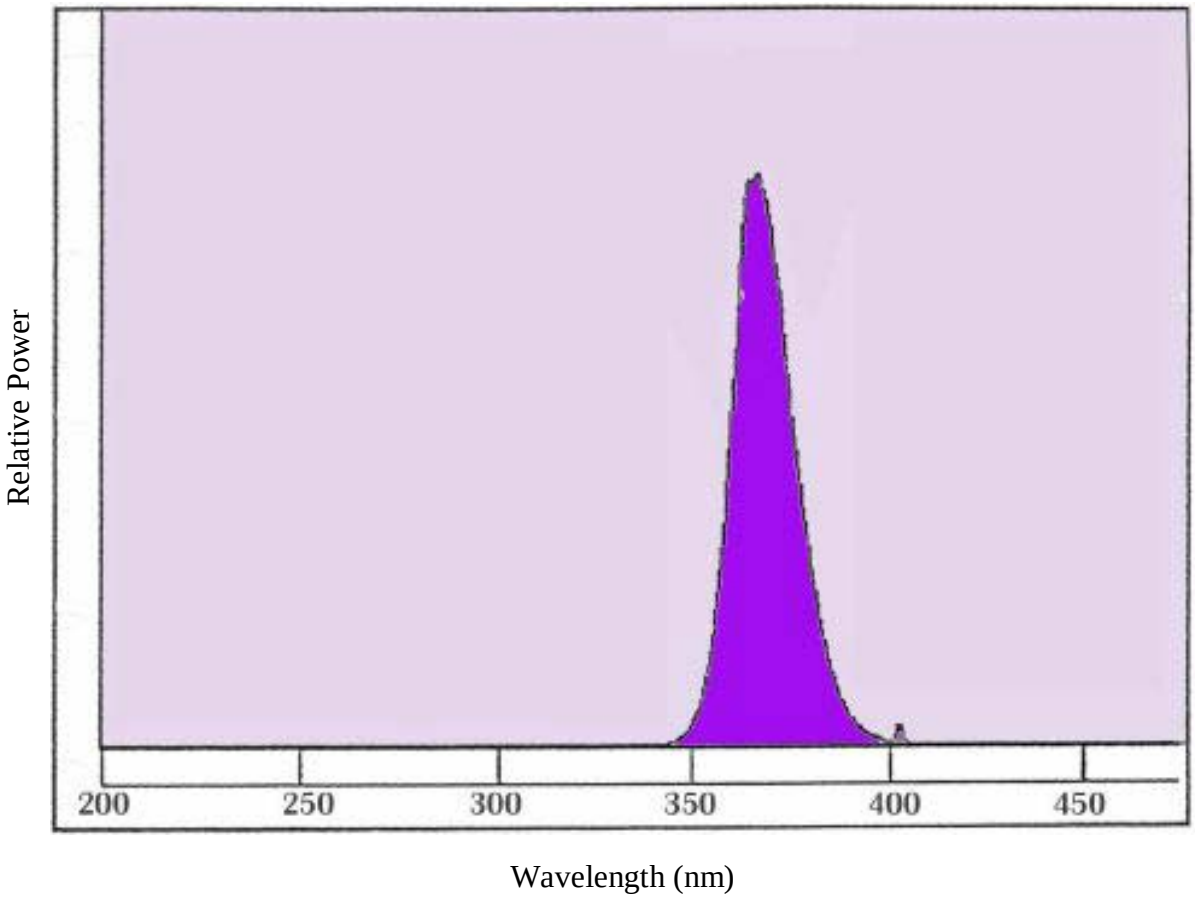

Figure A.2. Spectra emission wavelength range of 365nm with filter 8 Watt Lamp for UVA work, UVP, Inc., Upland, CA

APPENDIX B

B. XPS Spectral Graphs

XPS data table of PSS/PDDA (P) Sub-Coating

Quantification Report

Poly(styrenesulfonic acid), sodium salt (MW 70,000) (PSS) Aug 7 15:49:16 2009

State #0 : Etch Time 0.00 seconds

Peak	Position BE (eV)	FWHM (eV)	Raw Area (CPS)	RSF	Atomic Mass	Atomic Conc %	Mass Conc %
Na 1s	1067.000	2.093	1718.1	1.685	22.990	3.02	5.02
O 1s	529.000	2.371	6916.7	0.780	15.999	20.10	23.25
N 1s	400.000	1.474	1040.3	0.477	14.007	4.75	4.81
C 1s	283.000	2.093	8983.3	0.278	12.011	69.18	60.08
S 2p	166.000	2.074	923.6	0.668	32.065	2.95	6.84

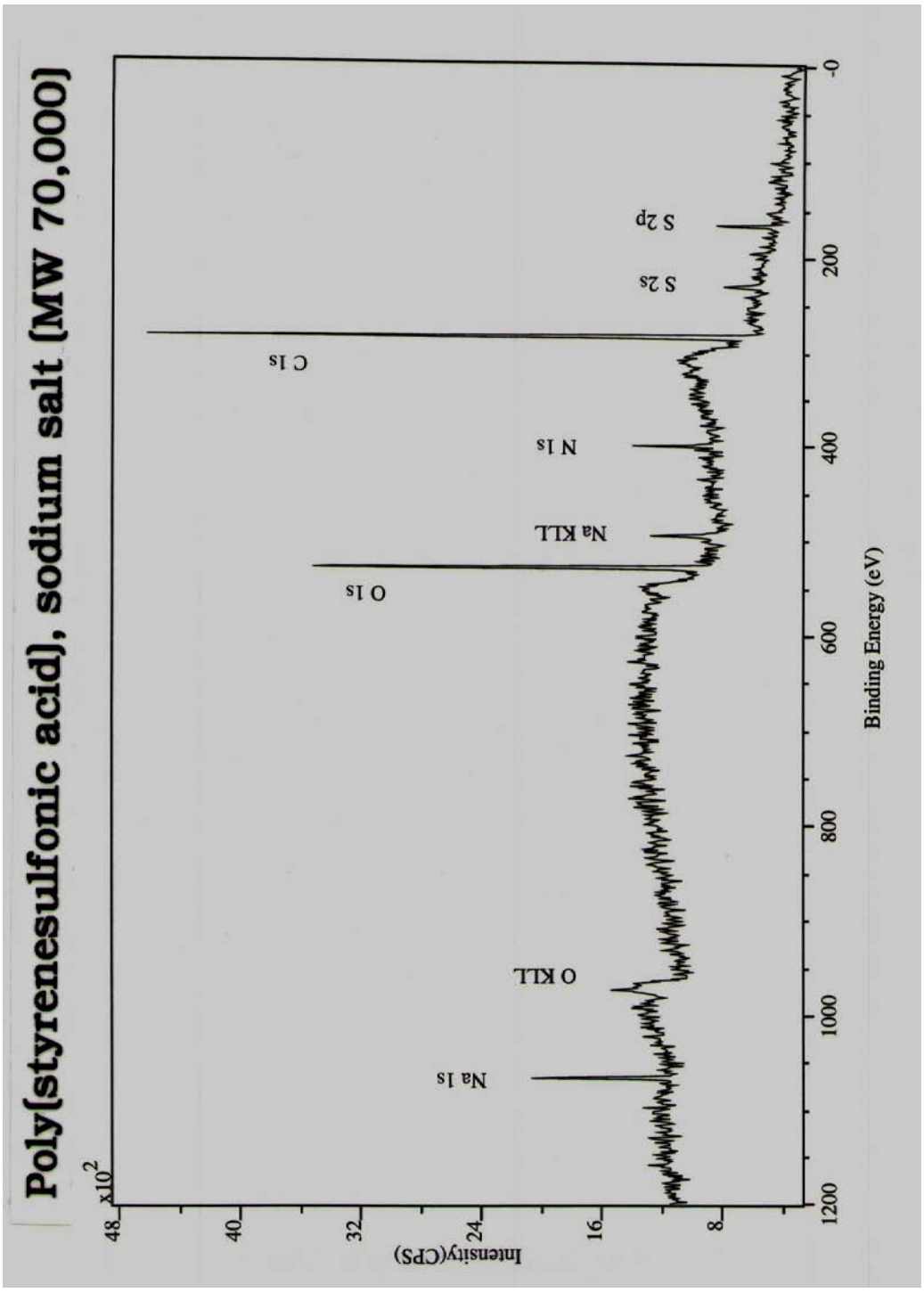

XPS spectral graph of PSS/PDDA Sub-Coating

XPS high resolution data table of PSS/PDDA Sub-Coating

Quantification Report

Poly(styrenesulfonic acid), sodium salt (MW 70,000) (PSS) e Aug 11 10:44:26 2009

State #0 : Etch Time 0.00 seconds

Peak	Position BE (eV)	FWHM (eV)	Raw Area (CPS)	RSF	Atomic Mass	Atomic Conc %	Mass Conc %
Na 1s 1	1066.817	1.394	1676.8	1.685	22.990	2.80	4.65
Na 1s 2	1067.600	0.991	156.1	1.685	22.990	0.26	0.43
Na 1s 3	1066.100	0.847	93.0	1.685	22.990	0.16	0.26
O 1s 1	528.488	1.475	5420.5	0.780	15.999	14.98	17.31
O 1s 2	529.597	1.452	1358.0	0.780	15.999	3.75	4.34
O 1s 3	527.765	0.797	300.0	0.780	15.999	0.83	0.96
O 1s 4	533.726	1.103	83.9	0.780	15.999	0.23	0.27
N 1s 1	400.019	1.108	648.9	0.477	14.007	2.82	2.85
N 1s 2	404.100	1.105	121.5	0.477	14.007	0.53	0.53
N 1s 3	400.600	0.851	87.6	0.477	14.007	0.38	0.39
N 1s 4	399.400	0.633	30.1	0.477	14.007	0.13	0.13
N 1s 5	393.939	1.154	38.5	0.477	14.007	0.17	0.17
N 1s 6	406.200	0.597	17.6	0.477	14.007	0.08	0.08
N 1s 7	399.400	0.732	18.8	0.477	14.007	0.08	0.08
N 1s 8	396.600	0.650	14.4	0.477	14.007	0.06	0.06
N 1s 9	402.900	0.490	7.1	0.477	14.007	0.03	0.03
C 1s 1	282.893	1.300	6587.7	0.278	12.011	48.26	41.87
C 1s 2	284.195	1.528	2688.2	0.278	12.011	19.70	17.09
C 1s 3	282.265	0.646	238.6	0.278	12.011	1.75	1.52
S 2p 1	166.235	1.256	615.4	0.668	32.065	1.87	4.33
S 2p 2	167.252	1.257	300.4	0.668	32.065	0.91	2.11
S 2p 3	165.650	0.695	57.7	0.668	32.065	0.18	0.41
S 2p 4	163.629	1.231	16.1	0.668	32.065	0.05	0.11

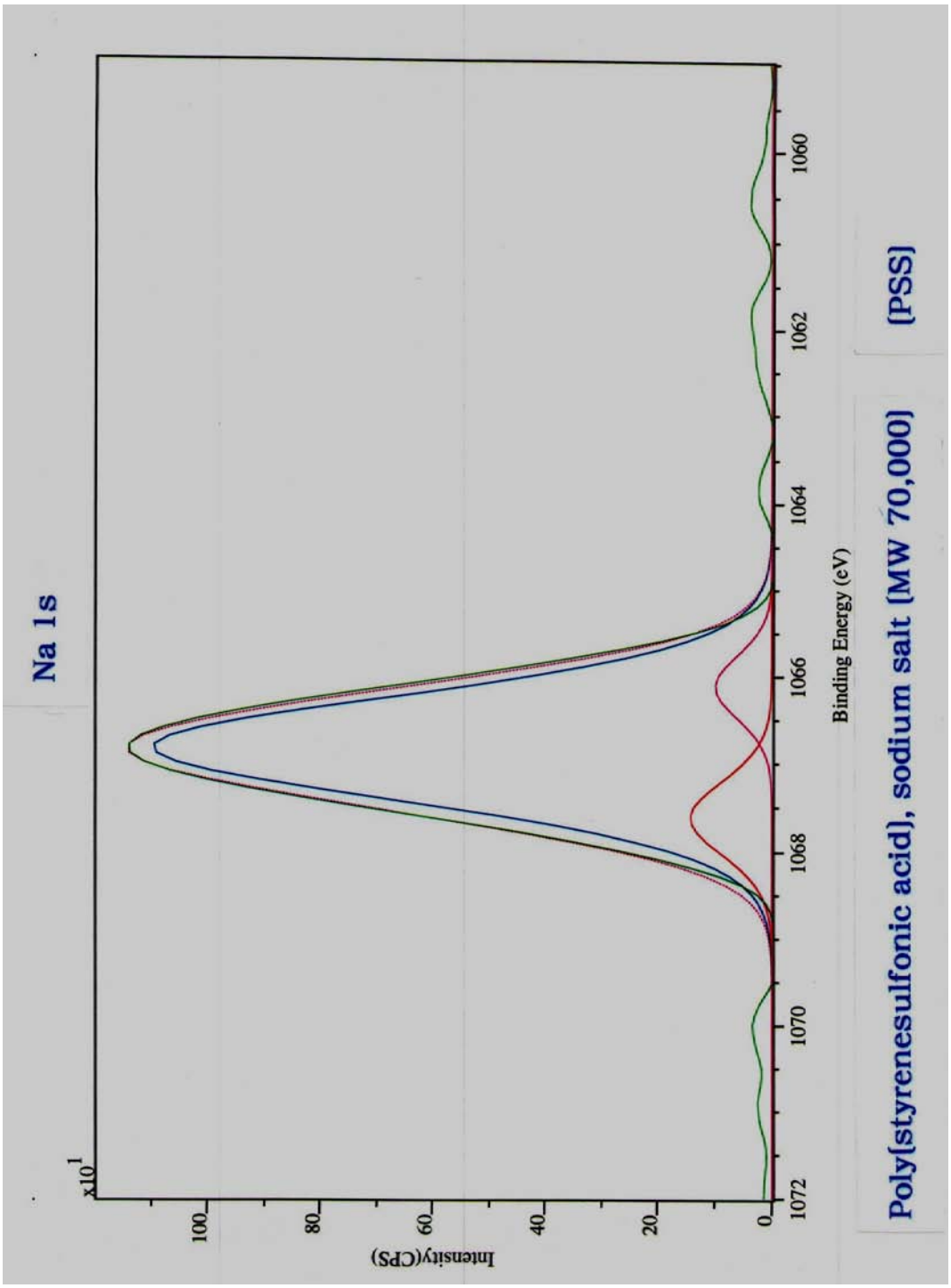

XPS high resolution spectral graph of Sodium 1s in PSS/PDDA Sub-Coating

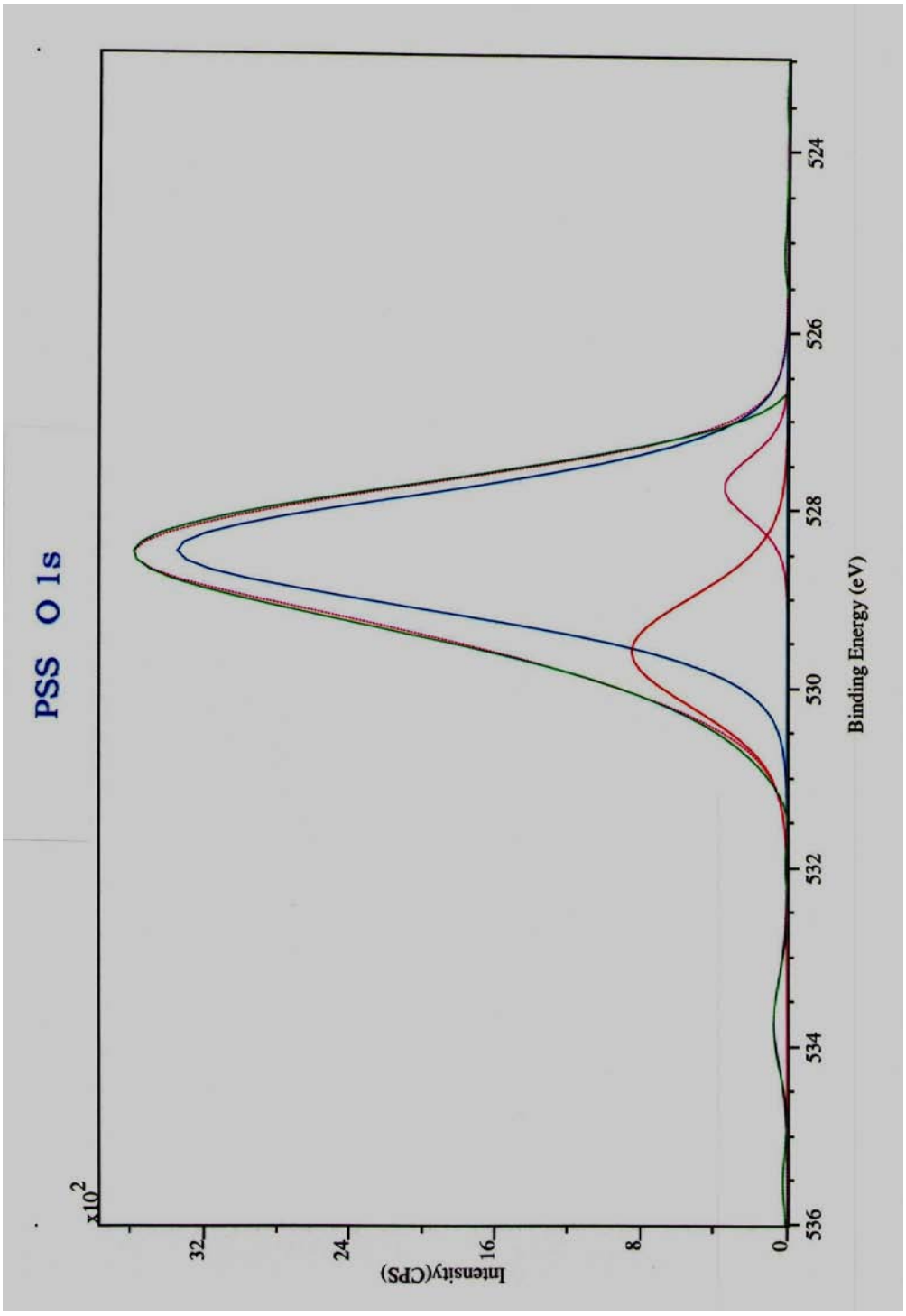

XPS high resolution spectral graph of Oxygen 1s in PSS/PDDA Sub-Coating

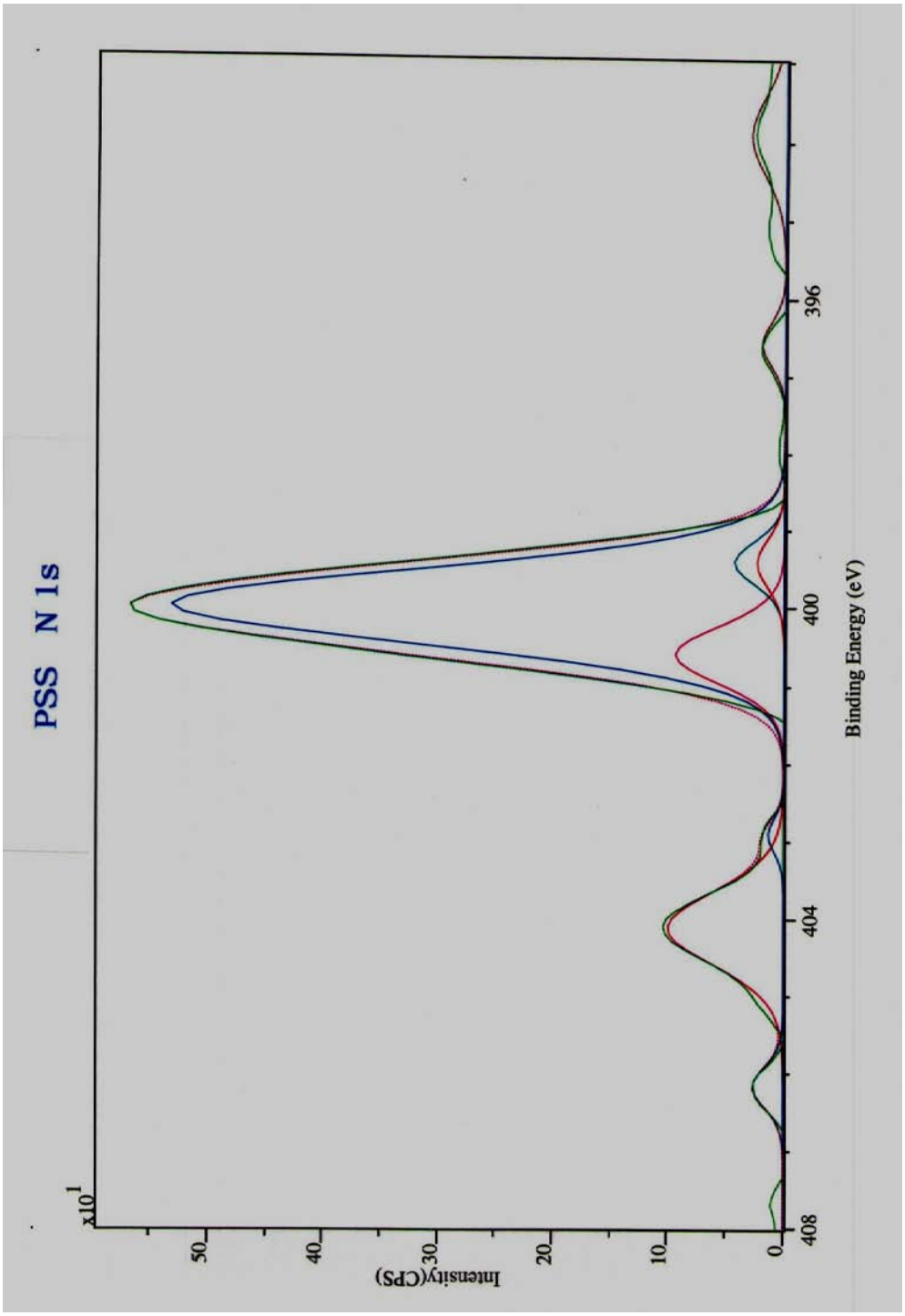

XPS high resolution spectral graph of Nitrogen 1s in PSS/PDDA Sub-Coating

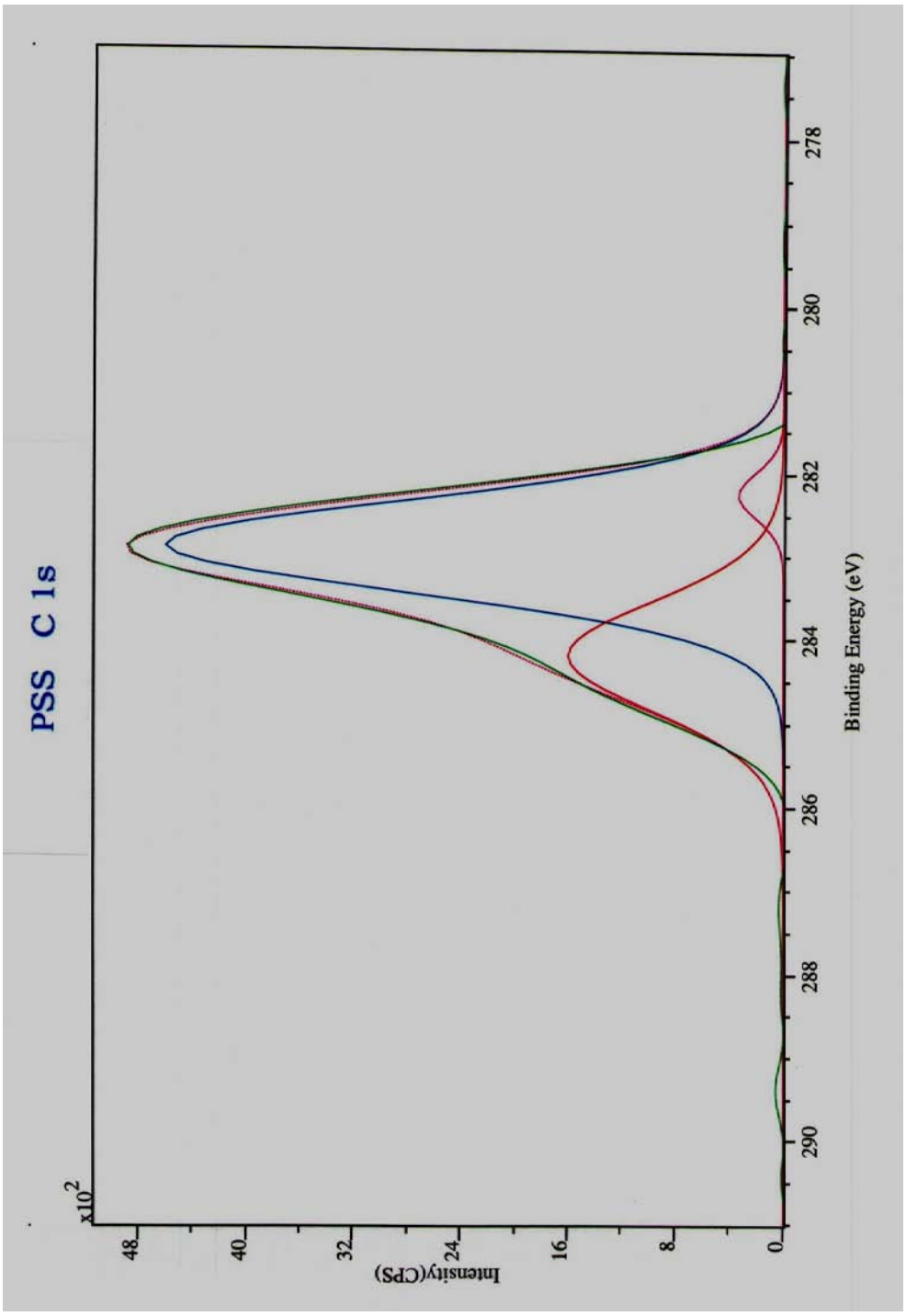

XPS high resolution spectral graph of Carbon1s in PSS/PDDA Sub-Coating

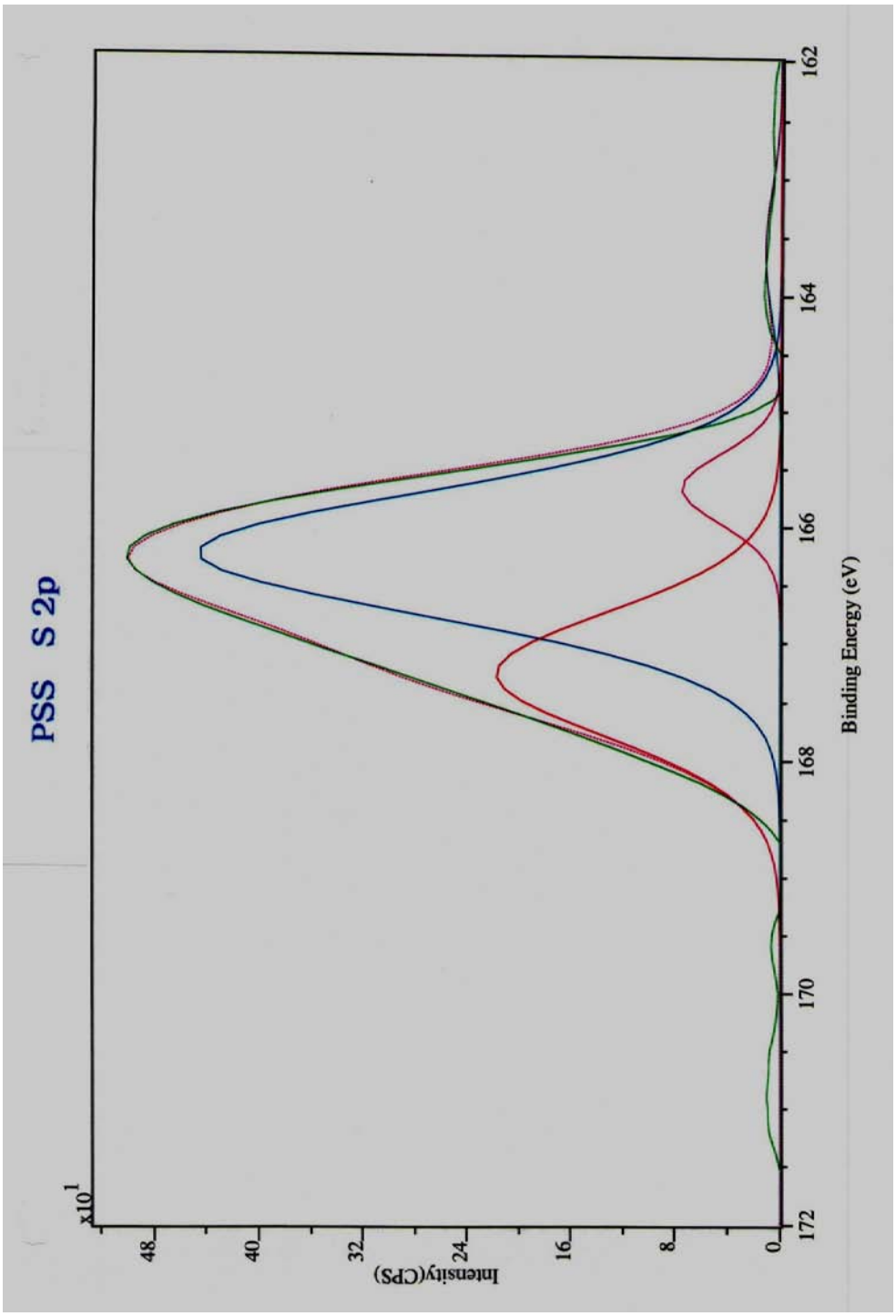

XPS high resolution spectral graph of Sulfur 2p in PSS/ PDDA Sub-Coating

XPS data table of P25 TiO_2 with PSS/PDDA Sub-Coating

PSS + P25

Quantification Report

Thu Aug 6 15:23:14 2009

State #0 : Etch Time 0.00 seconds

Peak	Position BE (eV)	FWHM (eV)	Raw Area (CPS)	RSF	Atomic Mass	Atomic Conc %	Mass Conc %
Na 1s	1066.000	2.332	2286.1	1.685	22.990	4.59	6.20
O 1s	529.000	4.232	11823.6	0.780	15.999	39.22	36.90
Ti 2p	456.000	1.397	3201.4	2.001	47.878	4.02	11.31
N 1s	400.000	1.977	808.3	0.477	14.007	4.22	3.47
C 1s	283.000	2.213	4537.5	0.278	12.011	39.89	28.18
S 2p	167.000	2.402	713.9	0.668	32.065	2.60	4.91
Si 2p	102.000	1.913	725.0	0.328	28.086	5.47	9.03

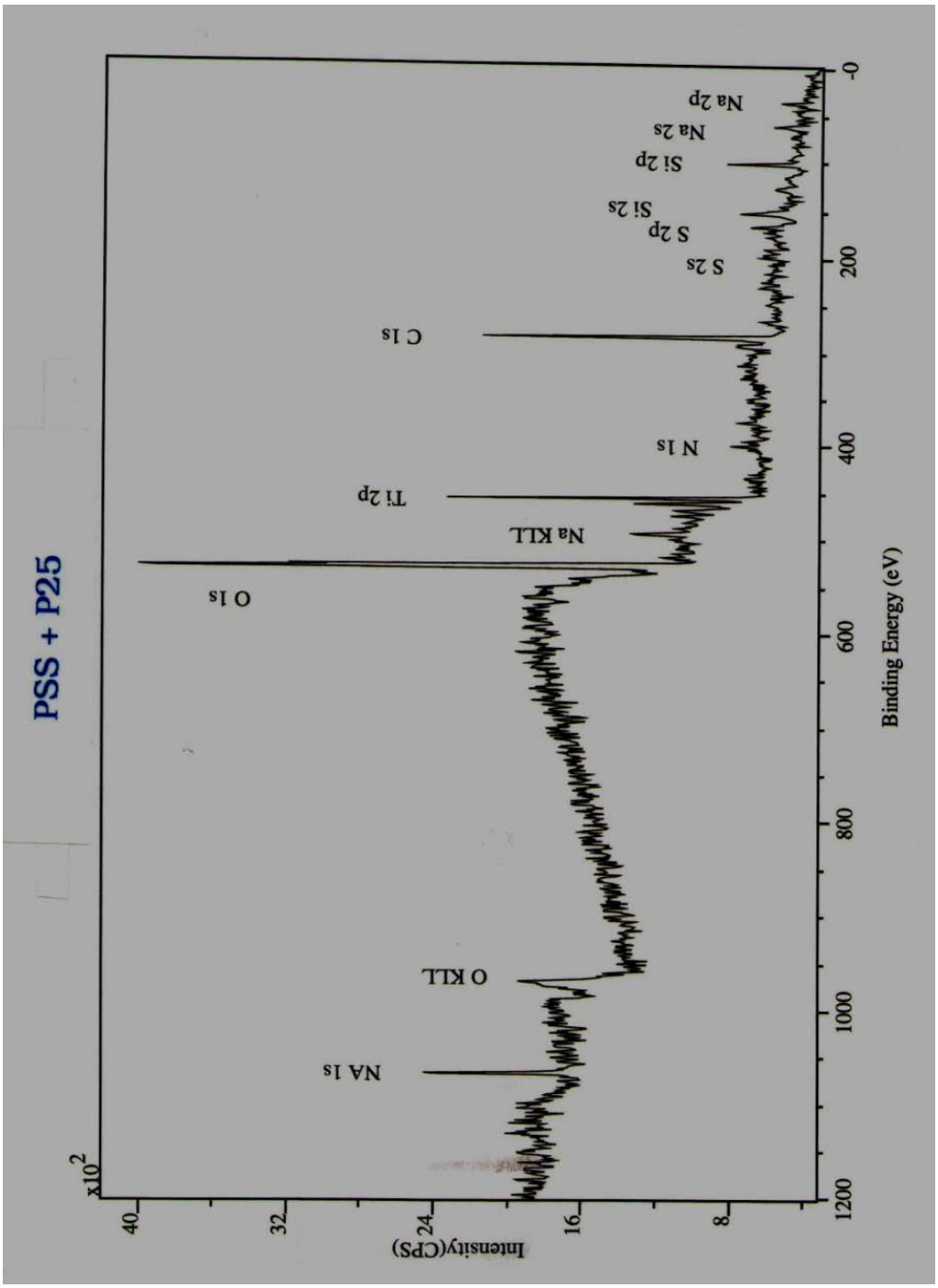

XPS spectral graph of P25 TiO_2 with PSS/PDDA Sub-Coating

XPS high resolution data table of P25 TiO_2 with PSS/PDDA Sub-Coating

PSS + P25 Quantification Report

Fri Aug 7 13:51:38 2009

State #0 : Etch Time 0.00 seconds

Peak	Position BE (eV)	FWHM (eV)	Raw Area (CPS)	RSF	Atomic Mass	Atomic Conc %	Mass Conc %
Na 1s 1	1066.800	1.420	1313.0	1.685	22.990	4.03	5.20
Na 1s 2	1067.500	1.157	135.8	1.685	22.990	0.42	0.54
Na 1s 3	1066.200	0.784	63.3	1.685	22.990	0.19	0.25
O 1s 1	529.657	1.490	3725.8	0.780	15.999	18.91	16.97
O 1s 2	526.915	1.216	2286.9	0.780	15.999	11.59	10.41
O 1s 3	528.472	1.294	1489.7	0.780	15.999	7.56	6.78
O 1s 4	530.525	1.046	654.7	0.780	15.999	3.32	2.98
O 1s 5	527.628	0.755	263.5	0.780	15.999	1.34	1.20
N 1s 1	400.254	1.033	147.6	0.477	14.007	1.18	0.93
N 1s 2	406.800	1.189	43.6	0.477	14.007	0.35	0.27
N 1s 3	403.227	0.874	29.0	0.477	14.007	0.23	0.18
N 1s 4	398.073	0.674	19.6	0.477	14.007	0.16	0.12
N 1s 5	408.927	0.919	28.1	0.477	14.007	0.22	0.18
N 1s 6	399.500	0.824	21.1	0.477	14.007	0.17	0.13
N 1s 7	405.581	0.743	16.3	0.477	14.007	0.13	0.10
N 1s 8	404.526	1.357	30.7	0.477	14.007	0.24	0.19
N 1s 9	392.354	0.818	19.9	0.477	14.007	0.16	0.12
N 1s 10	395.200	0.800	17.6	0.477	14.007	0.14	0.11
N 1s 11	401.900	0.683	10.1	0.477	14.007	0.08	0.06
N 1s 12	397.327	0.734	12.6	0.477	14.007	0.10	0.08
N 1s 13	400.800	0.624	9.2	0.477	14.007	0.07	0.06
N 1s 14	394.100	0.843	9.3	0.477	14.007	0.07	0.06
Ti 2p 1	456.000	1.092	1810.2	2.001	47.878	3.48	9.34
Ti 2p 2	461.700	1.631	702.5	2.001	47.878	1.35	3.63
Ti 2p 3	456.600	0.895	322.9	2.001	47.878	0.62	1.67
Ti 2p 4	455.400	0.705	122.1	2.001	47.878	0.23	0.63
Ti 2p 5	462.900	1.435	95.0	2.001	47.878	0.18	0.49
C 1s 1	283.158	1.245	1835.4	0.278	12.011	24.69	16.63
C 1s 2	284.209	1.480	598.2	0.278	12.011	8.05	5.42
C 1s 3	282.465	0.716	129.2	0.278	12.011	1.74	1.17
C 1s 4	285.044	0.788	44.2	0.278	12.011	0.59	0.40
S 2p 1	166.900	1.975	264.9	0.668	32.065	1.48	2.66
S 2p 2	170.700	0.783	26.2	0.668	32.065	0.15	0.26
S 2p 3	165.162	0.529	10.9	0.668	32.065	0.06	0.11
S 2p 4	161.880	0.911	17.3	0.668	32.065	0.10	0.17
S 2p 5	160.720	0.611	10.0	0.668	32.065	0.06	0.10
S 2p 6	172.700	1.196	18.5	0.668	32.065	0.10	0.19
S 2p 7	160.180	0.618	7.6	0.668	32.065	0.04	0.08
S 2p 8	169.300	0.480	4.5	0.668	32.065	0.03	0.05
S 2p 9	164.900	0.510	3.9	0.668	32.065	0.02	0.04
S 2p 10	165.000	0.552	2.9	0.668	32.065	0.02	0.03
Si 2p 1	102.000	1.337	431.7	0.328	28.086	4.98	7.85
Si 2p 2	105.682	0.862	40.3	0.328	28.086	0.46	0.73
Si 2p 3	102.900	1.246	50.8	0.328	28.086	0.59	0.92
Si 2p 4	104.859	0.788	14.8	0.328	28.086	0.17	0.27
Si 2p 5	101.300	0.768	12.9	0.328	28.086	0.15	0.23

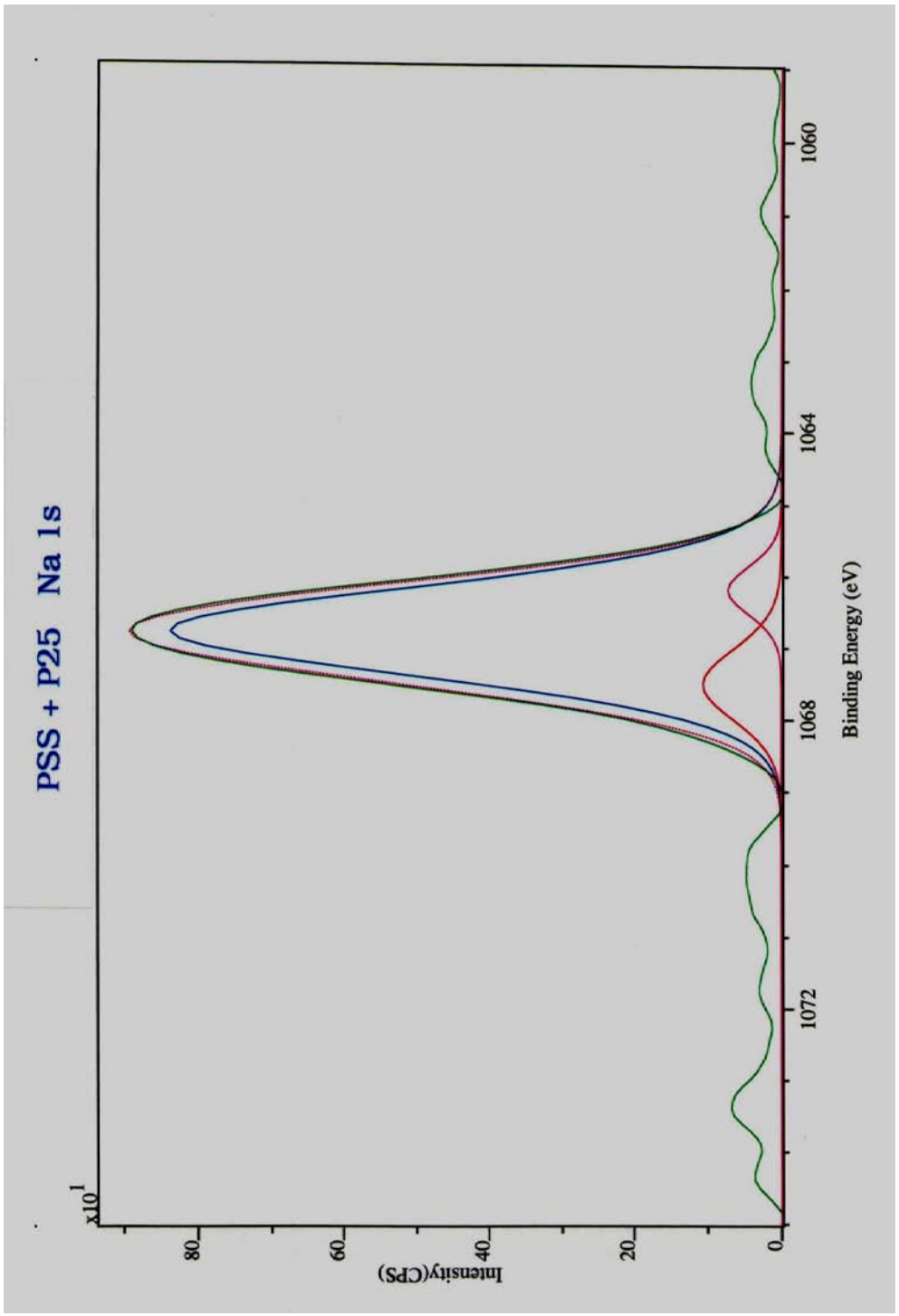

XPS high resolution spectral graph of Sodium 1s in P25 TiO_2 with PSS/PDDA Sub-Coating

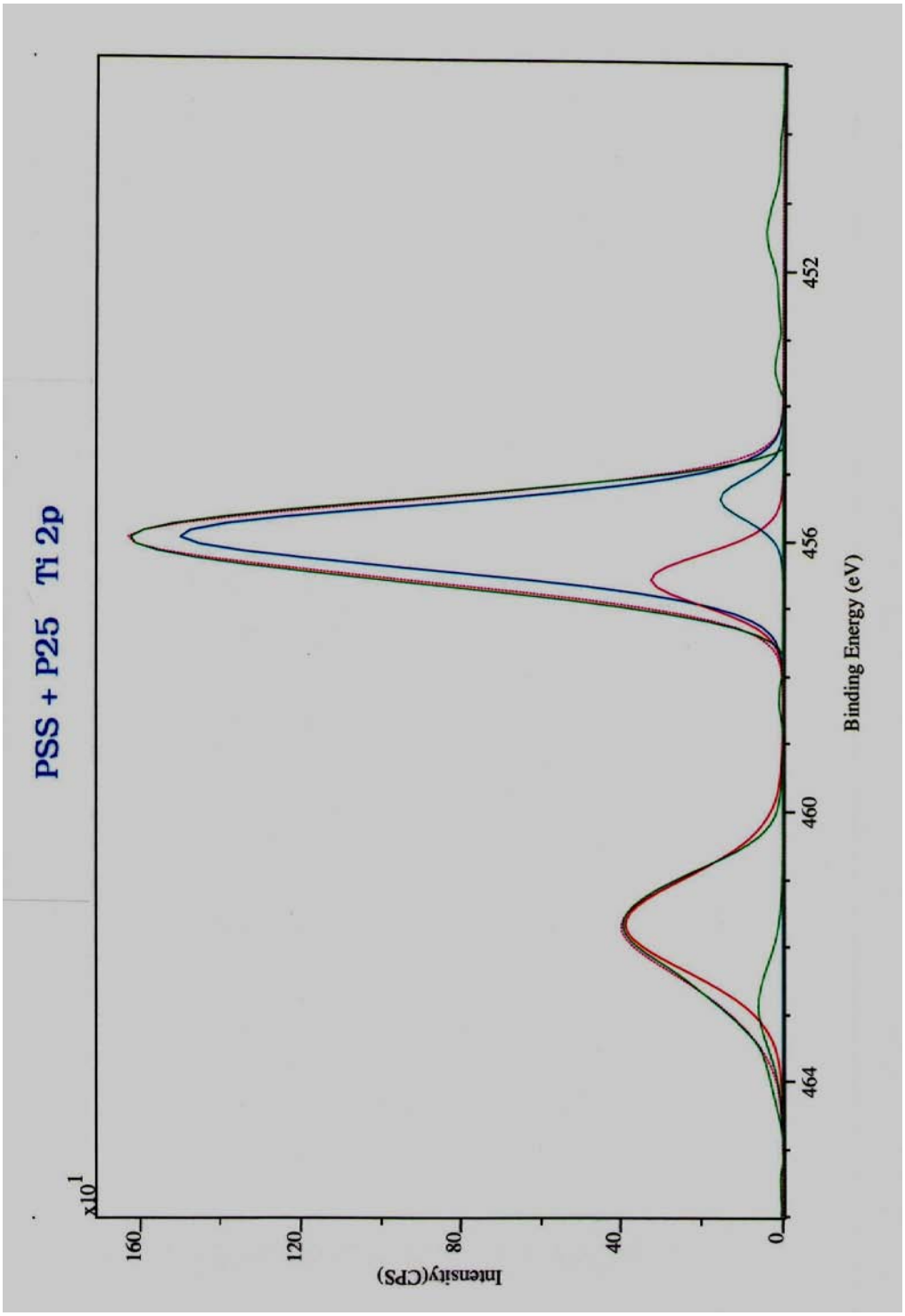

XPS high resolution spectral graph of Titanium 2p in P25 TiO_2 with PSS/PDDA Sub-Coating

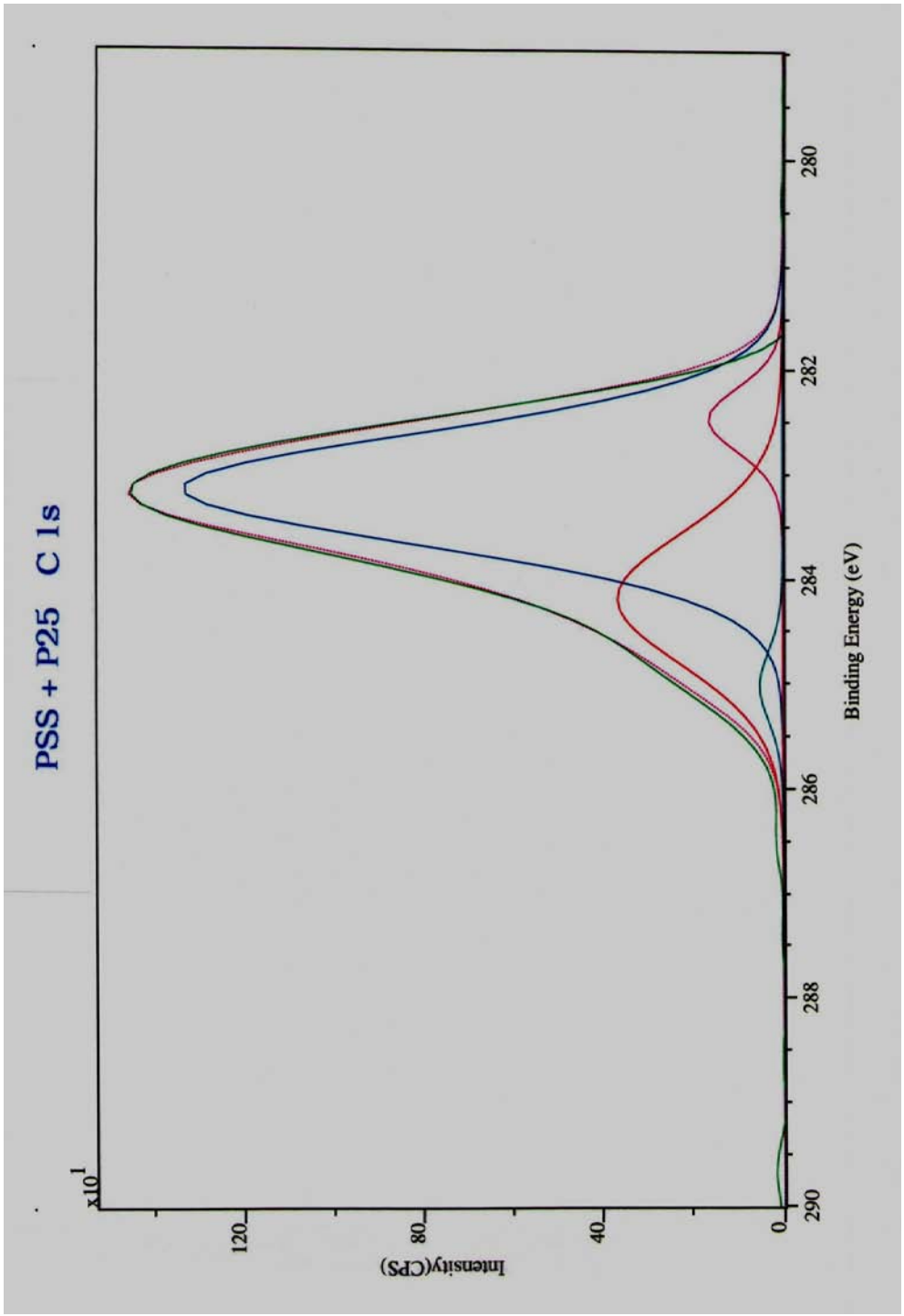

XPS high resolution spectral graph of Carbon 1s in P25 TiO_2 with PSS/PDDA Sub-Coating

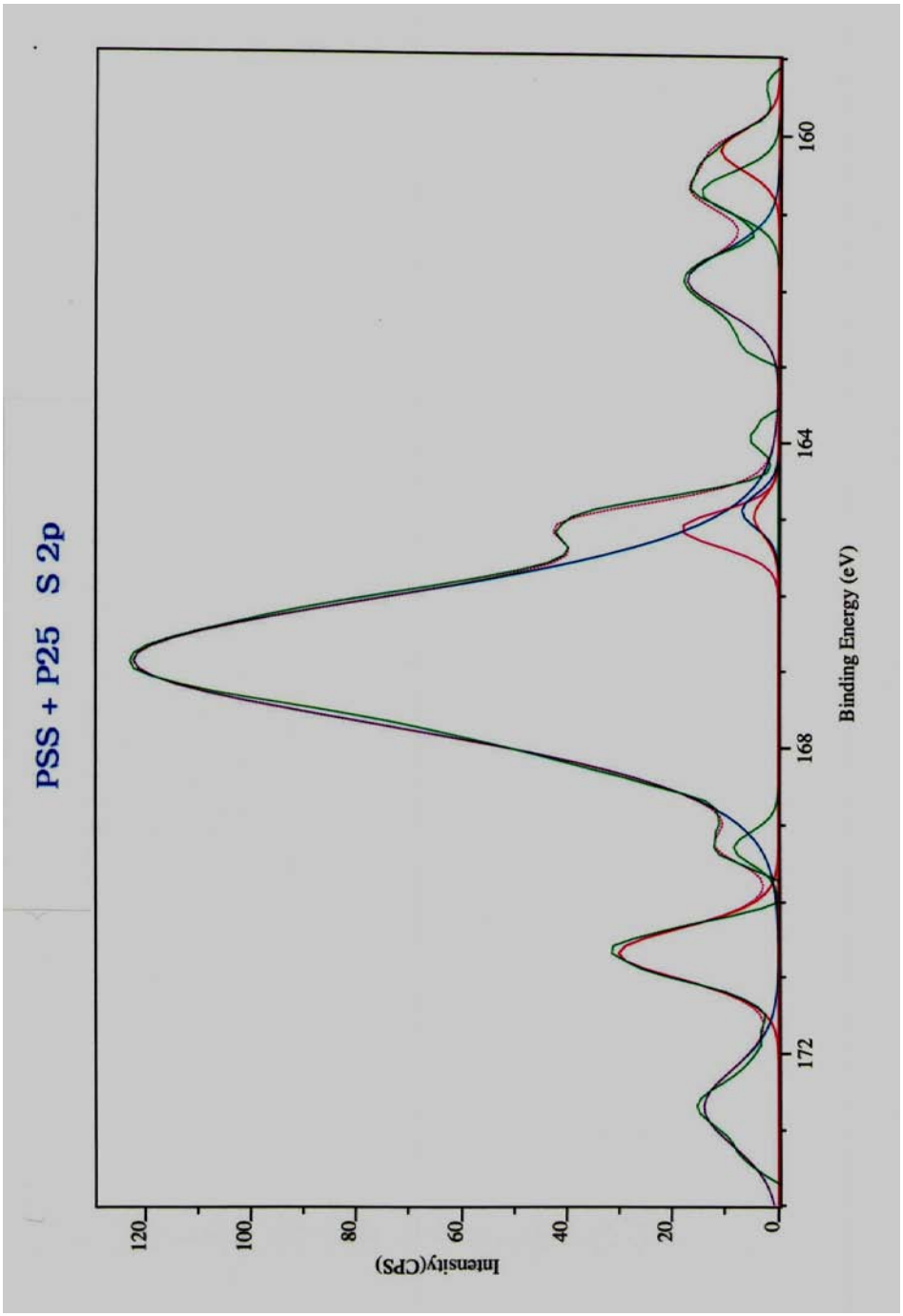

XPS high resolution spectral graph of Sulfur 2p in P25 TiO_2 with PSS/PDDA Sub-Coating

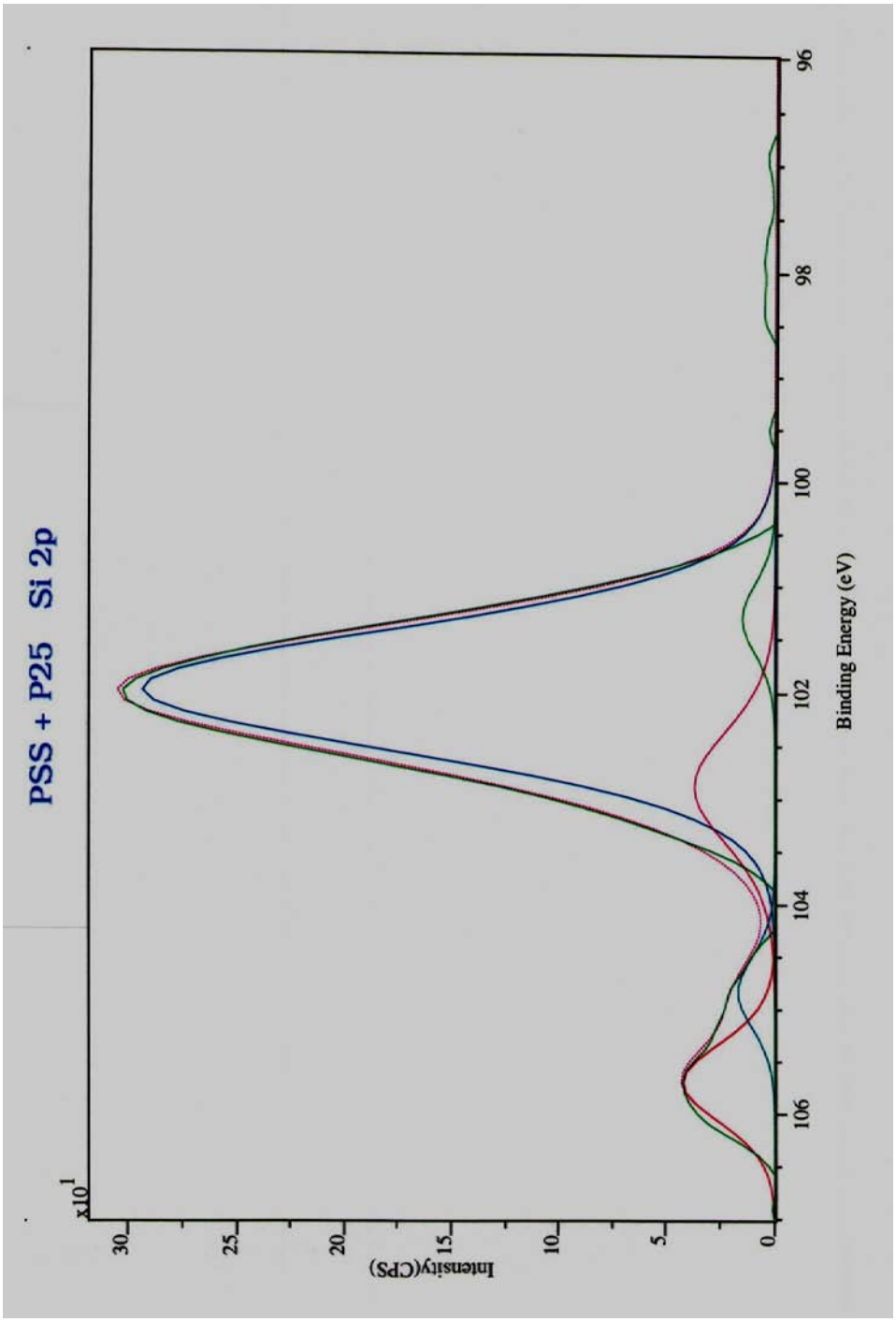

XPS high resolution spectral graph of Silicon 2p in P25 TiO_2 with PSS/PDDA Sub-Coating

XPS data table of Br200 TiO_2 with PSS/PDDA Sub-Coating

PSS + Br200 Quantification Report Thu Aug 13 17:21:33 2009

State #0 : Etch Time 0.00 seconds

Peak	Position BE (eV)	FWHM (eV)	Raw Area (CPS)	RSF	Atomic Mass	Atomic Conc %	Mass Conc %
Na 1s	1067.000	2.269	2565.3	1.685	22.990	5.43	8.13
O 1s	529.000	2.724	8087.5	0.780	15.999	28.30	29.49
Ti 2p	456.000	1.434	959.7	2.001	47.878	1.27	3.96
N 1s	400.000	2.107	869.4	0.477	14.007	4.78	4.36
C 1s	283.000	2.029	5808.3	0.278	12.011	53.87	42.15
S 2p	167.000	2.410	294.4	0.668	32.065	1.13	2.37
Si 2p	102.000	2.363	655.6	0.328	28.086	5.22	9.54

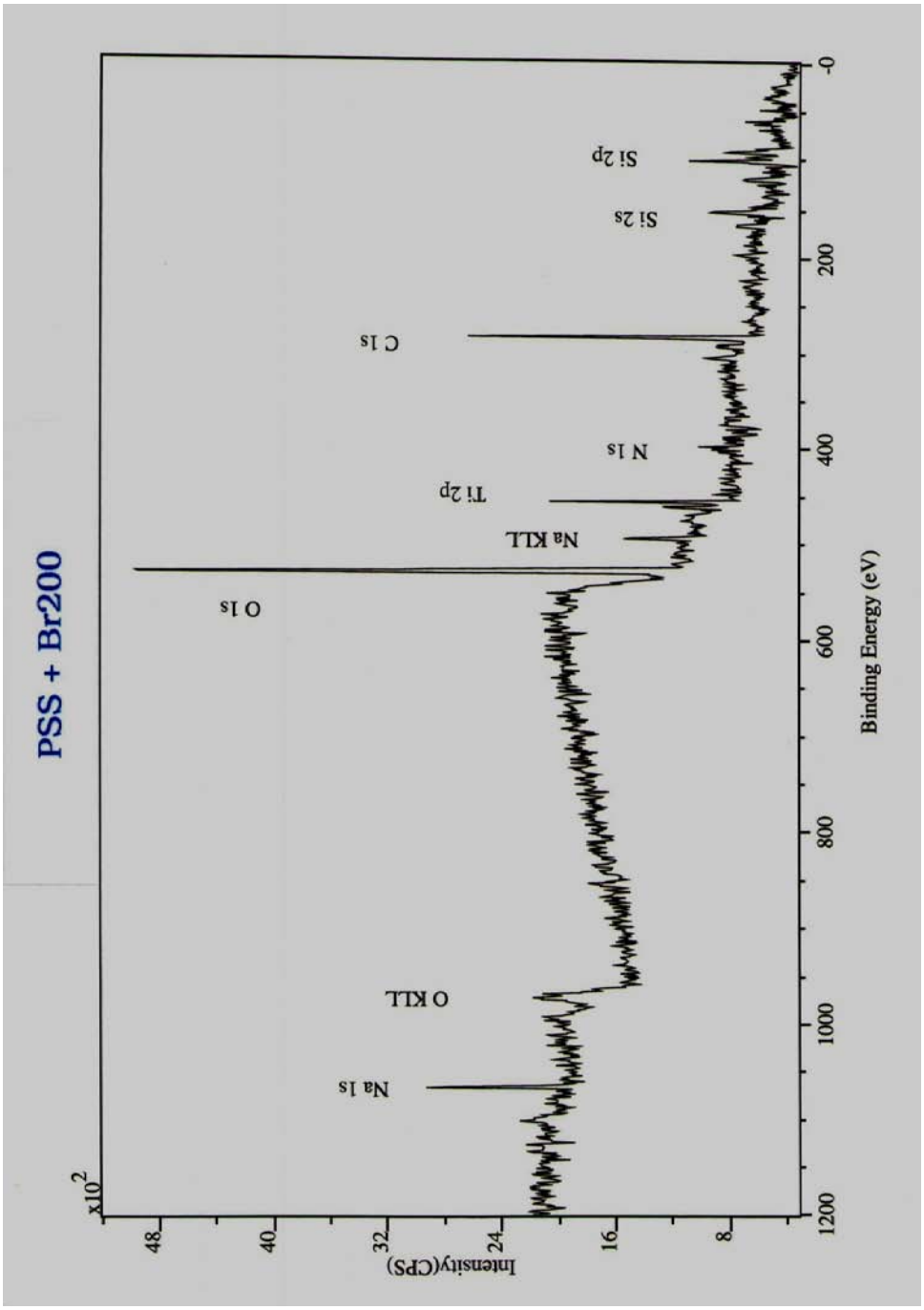

XPS spectral graph of Br200 TiO_2 with PSS/PDDA Sub-Coating

XPS high resolution data table of Br200 TiO_2 with PSS/PDDA Sub-Coating

PSS + Br200 Quantification Report

Thu Aug 13 17:36:10 2009

State #0 : Etch Time 0.00 seconds

Peak	Position BE (eV)	FWHM (eV)	Raw Area (CPS)	RSF	Atomic Mass	Atomic Conc %	Mass Conc %
Na 1s 1	1066.684	1.423	1796.1	1.685	22.990	4.92	7.13
Na 1s 2	1066.000	1.004	169.6	1.685	22.990	0.46	0.67
Na 1s 3	1067.600	0.958	95.0	1.685	22.990	0.26	0.38
O 1s 1	529.322	1.655	5054.8	0.780	15.999	22.91	23.10
O 1s 2	528.114	1.384	1194.3	0.780	15.999	5.41	5.46
O 1s 3	530.269	0.979	322.0	0.780	15.999	1.46	1.47
O 1s 4	526.798	1.295	263.4	0.780	15.999	1.19	1.20
O 1s 5	528.600	0.548	30.8	0.780	15.999	0.14	0.14
Ti 2p 1	455.888	1.332	381.2	2.001	47.878	0.65	1.97
Ti 2p 2	461.789	1.961	168.3	2.001	47.878	0.29	0.87
Ti 2p 3	465.669	0.990	31.2	2.001	47.878	0.05	0.16
Ti 2p 4	464.600	0.748	28.4	2.001	47.878	0.05	0.15
Ti 2p 5	449.900	0.665	19.7	2.001	47.878	0.03	0.10
Ti 2p 6	452.847	0.815	20.9	2.001	47.878	0.04	0.11
Ti 2p 7	466.476	0.657	16.8	2.001	47.878	0.03	0.09
Ti 2p 8	463.600	0.575	12.7	2.001	47.878	0.02	0.07
Ti 2p 9	467.818	0.987	21.0	2.001	47.878	0.04	0.11
Ti 2p 10	459.429	0.633	9.5	2.001	47.878	0.02	0.05
Ti 2p 11	451.324	0.817	10.8	2.001	47.878	0.02	0.06
Ti 2p 12	453.882	1.077	12.6	2.001	47.878	0.02	0.07
Ti 2p 13	458.300	0.570	6.3	2.001	47.878	0.01	0.03
N 1s 1	400.275	1.159	251.4	0.477	14.007	1.79	1.58
N 1s 2	401.000	0.759	19.5	0.477	14.007	0.14	0.12
N 1s 3	404.856	1.018	24.1	0.477	14.007	0.17	0.15
N 1s 4	399.600	0.763	16.8	0.477	14.007	0.12	0.11
N 1s 5	407.400	0.701	15.4	0.477	14.007	0.11	0.10
N 1s 6	397.744	1.166	21.2	0.477	14.007	0.15	0.13
N 1s 7	403.575	0.981	17.4	0.477	14.007	0.12	0.11
N 1s 8	402.300	0.656	9.6	0.477	14.007	0.07	0.06
N 1s 9	395.200	0.608	6.7	0.477	14.007	0.05	0.04
N 1s 10	393.500	0.676	7.5	0.477	14.007	0.05	0.05
C 1s 1	283.082	1.263	2798.1	0.278	12.011	33.62	25.45
C 1s 2	284.336	1.583	1207.4	0.278	12.011	14.51	10.98
C 1s 3	282.387	0.794	187.9	0.278	12.011	2.26	1.71
S 2p 1	166.709	1.368	269.5	0.668	32.065	1.34	2.71
S 2p 2	167.585	1.009	54.7	0.668	32.065	0.27	0.55
S 2p 3	165.986	0.733	28.9	0.668	32.065	0.14	0.29
Si 2p 1	102.015	1.414	544.0	0.328	28.086	5.61	9.92
Si 2p 2	101.033	1.105	99.1	0.328	28.086	1.02	1.81
Si 2p 3	102.777	0.874	40.4	0.328	28.086	0.42	0.74

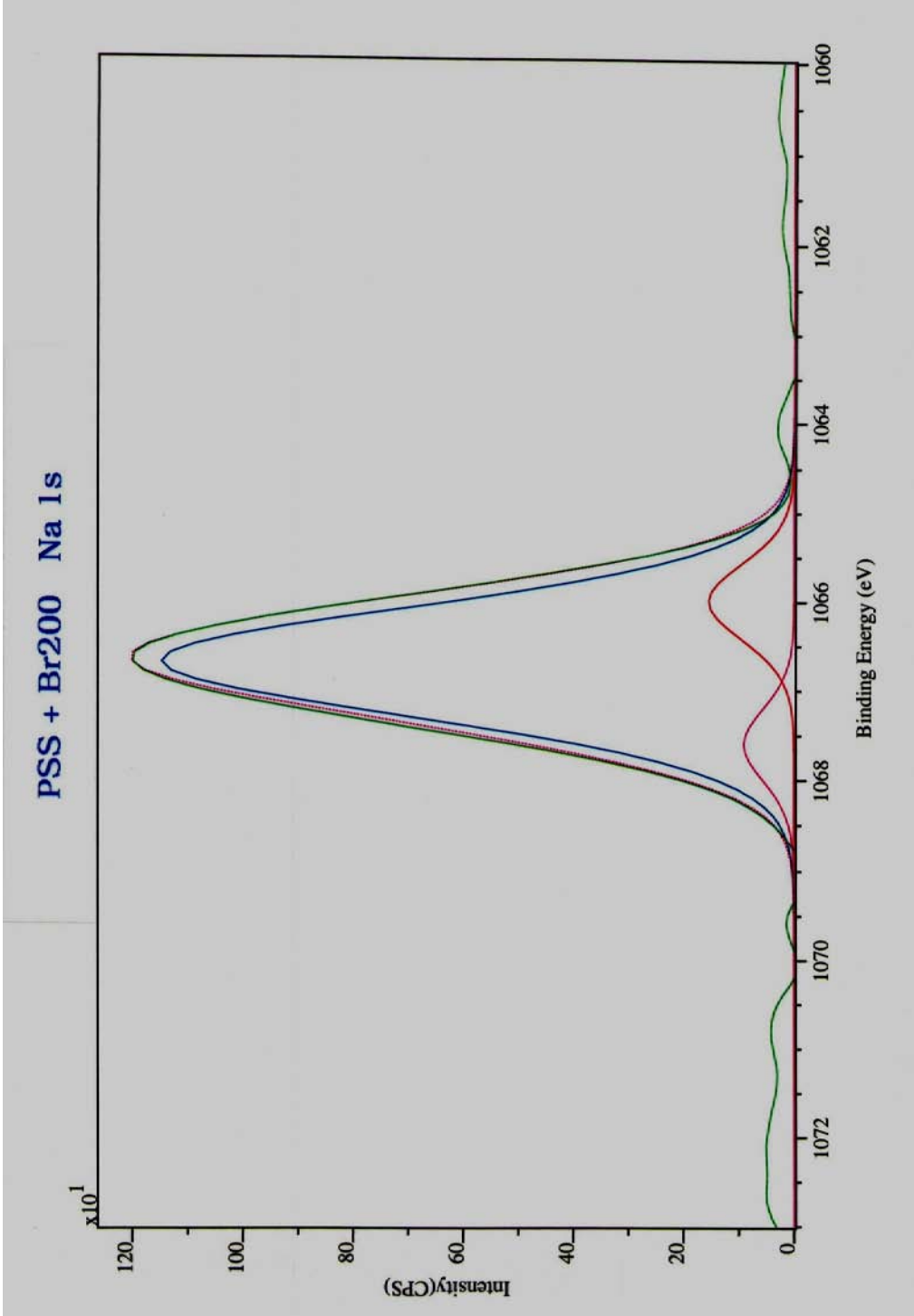

XPS high resolution spectral graph of Sodium 1s in Br200 TiO_2 with PSS/PDDA Sub-Coating

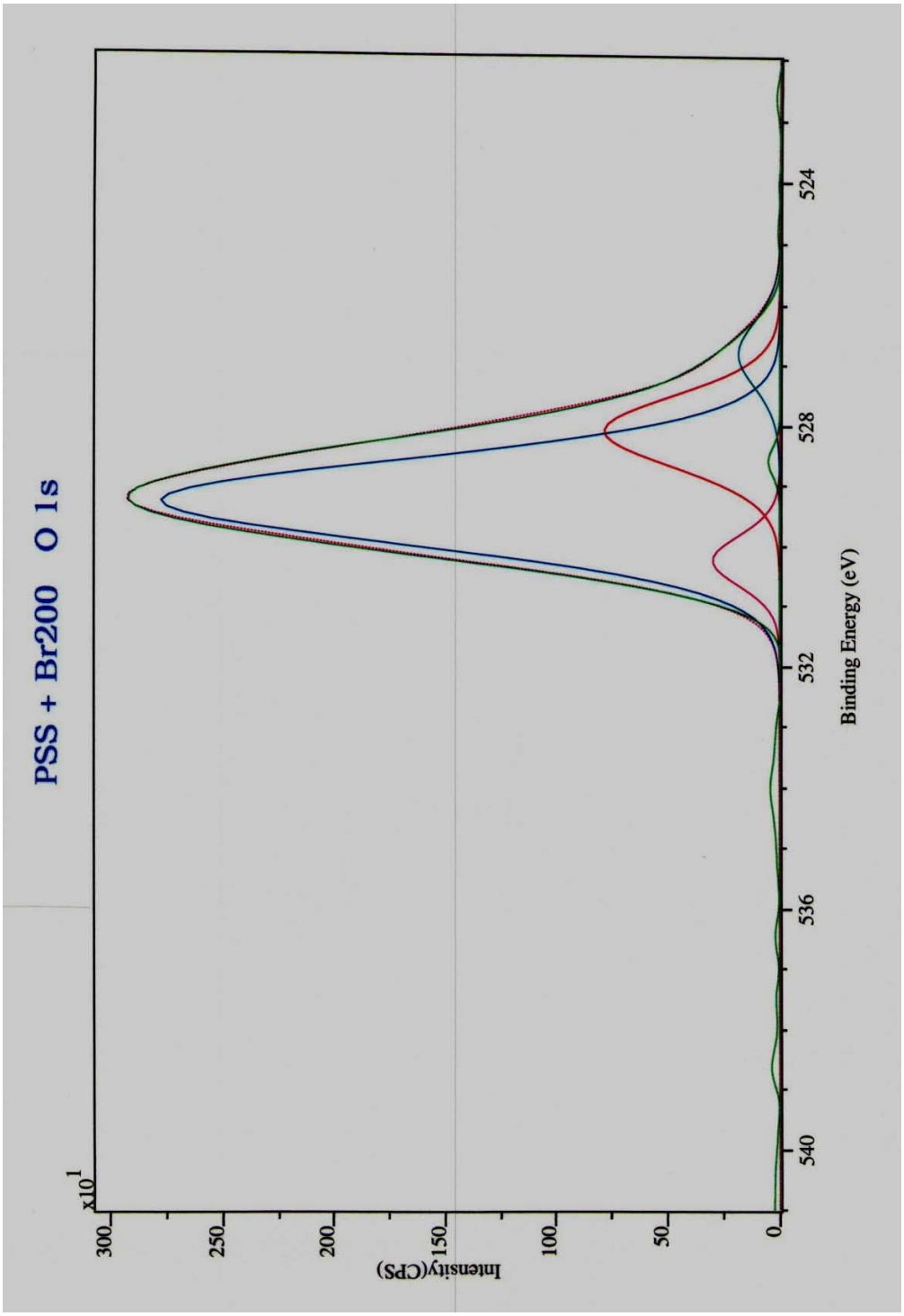

XPS high resolution spectral graph of Oxygen 1s in Br200 TiO_2 with PSS/PDDA Sub-Coating

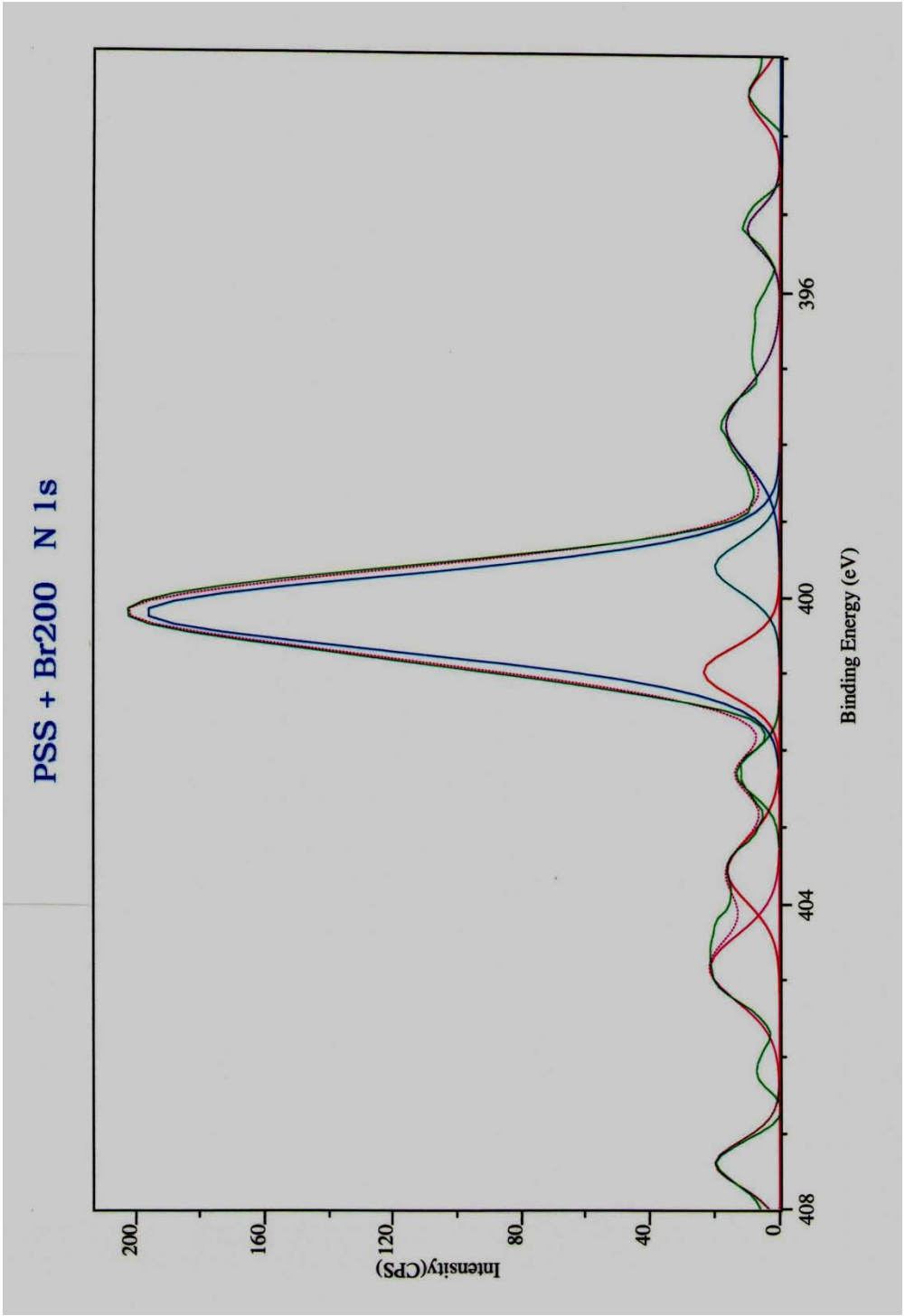

XPS high resolution spectral graph of Nitrogen 1s in Br200 TiO_2 with PSS/PDDA Sub-Coating

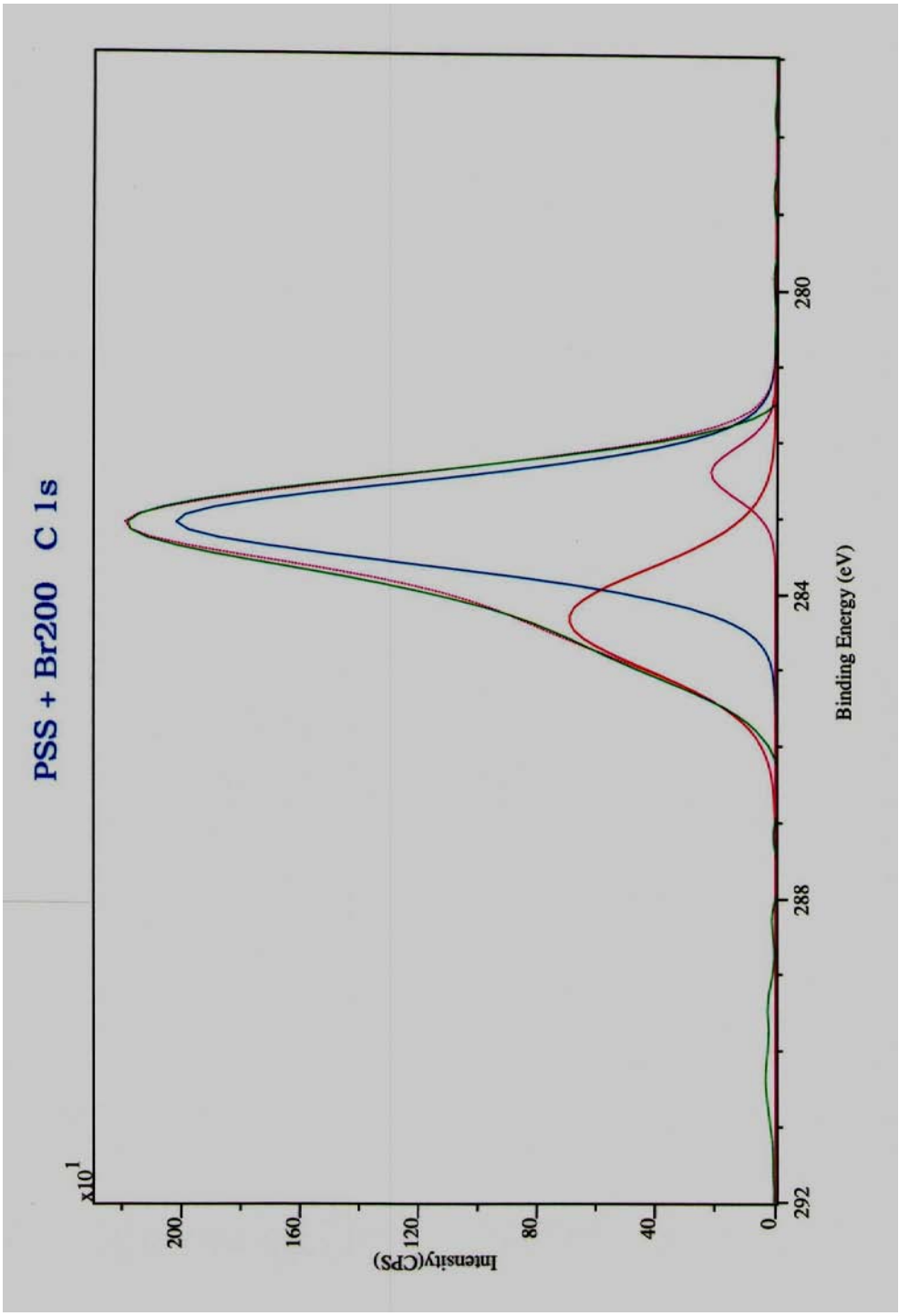

XPS high resolution spectral graph of Carbon 1s in Br200 TiO_2 with PSS/PDDA Sub-Coating

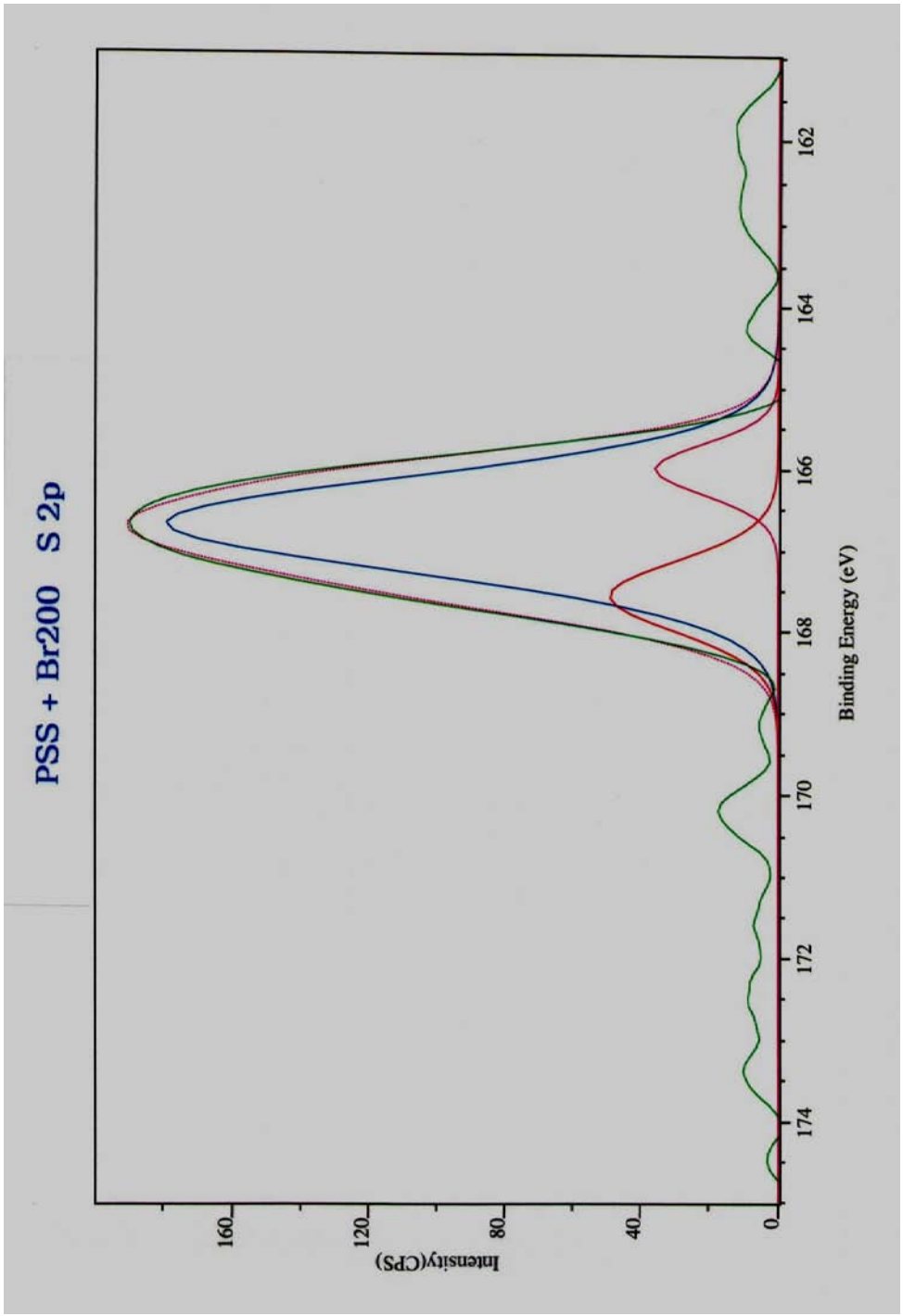

XPS high resolution spectral graph of Sulfur 2pin Br200 TiO_2 with PSS/PDDA Sub-Coating

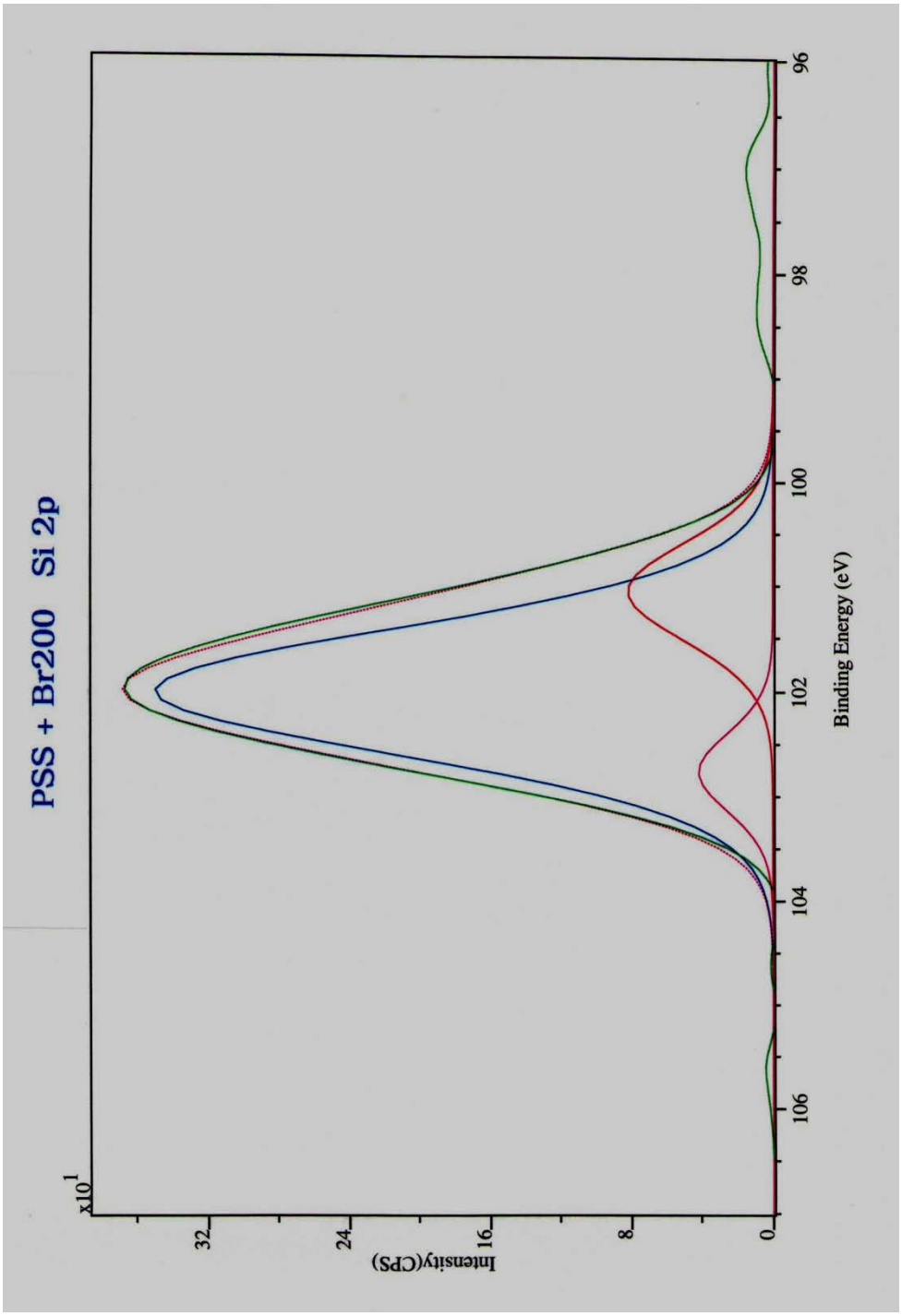

XPS high resolution spectral graph of Silicon 2p in Br200 TiO_2 with PSS/PDDA Sub-Coating

XPS data table of BrNMP TiO_2 with PSS/PDDA Sub-Coating

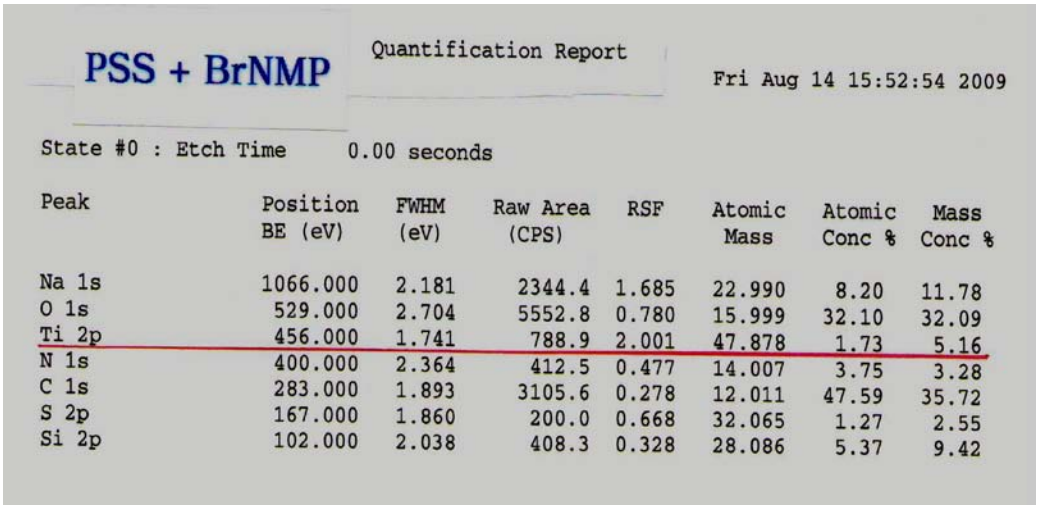

PSS + BrNMP

Quantification Report

Fri Aug 14 15:52:54 2009

State #0 : Etch Time 0.00 seconds

Peak	Position BE (eV)	FWHM (eV)	Raw Area (CPS)	RSF	Atomic Mass	Atomic Conc %	Mass Conc %
Na 1s	1066.000	2.181	2344.4	1.685	22.990	8.20	11.78
O 1s	529.000	2.704	5552.8	0.780	15.999	32.10	32.09
Ti 2p	456.000	1.741	788.9	2.001	47.878	1.73	5.16
N 1s	400.000	2.364	412.5	0.477	14.007	3.75	3.28
C 1s	283.000	1.893	3105.6	0.278	12.011	47.59	35.72
S 2p	167.000	1.860	200.0	0.668	32.065	1.27	2.55
Si 2p	102.000	2.038	408.3	0.328	28.086	5.37	9.42

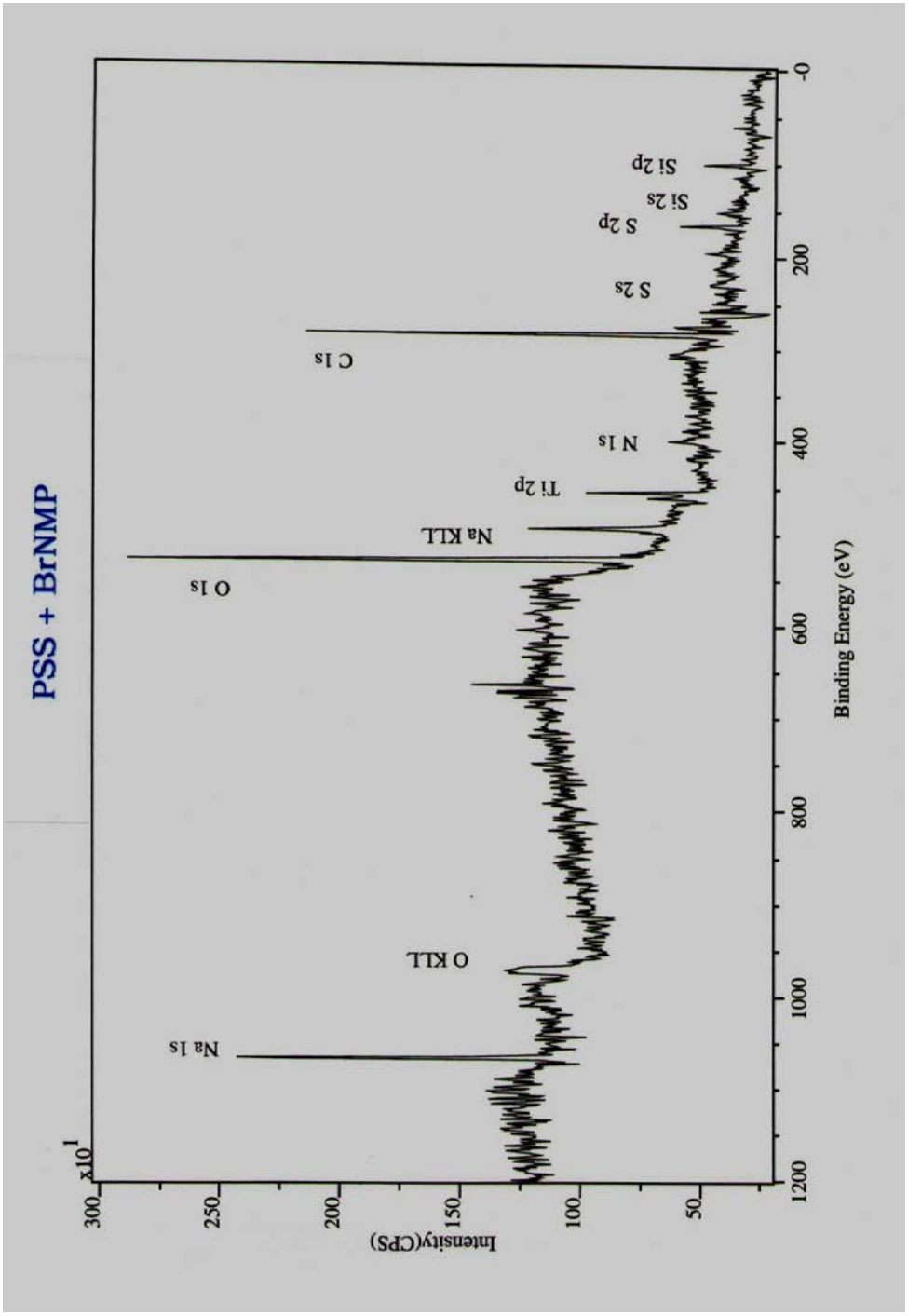

XPS spectral graph of BrNMP TiO_2 with PSS/PDDA Sub-Coating

XPS high resolution data table of BrNMP TiO_2 with PSS/PDDA Sub-Coating

PSS + BrNMP

Quantification Report

Mon Aug 17 12:19:47 2009

State #0 : Etch Time 0.00 seconds

Peak	Position BE (eV)	FWHM (eV)	Raw Area (CPS)	RSF	Atomic Mass	Atomic Conc %	Mass Conc %
Na 1s 1	1066.400	1.474	2771.8	1.685	22.990	10.27	14.50
Na 1s 2	1067.200	0.990	148.8	1.685	22.990	0.55	0.78
Na 1s 3	1065.500	0.990	127.1	1.685	22.990	0.47	0.66
O 1s 1	528.779	1.925	3662.8	0.780	15.999	22.44	22.05
O 1s 2	526.668	1.389	677.0	0.780	15.999	4.14	4.07
O 1s 3	529.820	1.211	170.3	0.780	15.999	1.04	1.03
O 1s 4	528.051	0.989	86.2	0.780	15.999	0.53	0.52
O 1s 5	532.600	1.196	43.4	0.780	15.999	0.27	0.26
Ti 2p 1	455.600	1.080	547.8	2.001	47.878	1.27	3.73
Ti 2p 2	461.221	1.539	236.9	2.001	47.878	0.55	1.62
Ti 2p 3	456.200	0.813	62.8	2.001	47.878	0.15	0.43
Ti 2p 4	466.700	0.787	32.0	2.001	47.878	0.07	0.22
Ti 2p 5	455.000	0.732	29.5	2.001	47.878	0.07	0.20
Ti 2p 6	465.700	0.644	19.0	2.001	47.878	0.04	0.13
Ti 2p 7	452.600	0.712	18.4	2.001	47.878	0.04	0.13
Ti 2p 8	458.100	1.237	27.3	2.001	47.878	0.06	0.19
Ti 2p 9	467.800	0.686	12.6	2.001	47.878	0.03	0.09
Ti 2p 10	464.100	0.837	15.4	2.001	47.878	0.04	0.11
N 1s 1	400.242	1.249	175.9	0.477	14.007	1.69	1.46
N 1s 2	404.437	1.090	48.4	0.477	14.007	0.47	0.40
N 1s 3	397.579	0.858	33.9	0.477	14.007	0.33	0.28
N 1s 4	403.221	0.855	29.5	0.477	14.007	0.28	0.24
C 1s 1	282.960	1.152	1808.7	0.278	12.011	29.38	21.67
C 1s 2	283.831	1.561	872.0	0.278	12.011	14.17	10.45
C 1s 3	282.265	0.465	121.1	0.278	12.011	1.97	1.45
C 1s 4	285.048	1.552	163.5	0.278	12.011	2.66	1.96
C 1s 5	289.738	1.485	64.4	0.278	12.011	1.05	0.77
C 1s 6	282.020	0.513	15.7	0.278	12.011	0.26	0.19
S 2p 1	166.458	1.502	233.9	0.668	32.065	1.58	3.10
S 2p 2	167.600	1.236	54.3	0.668	32.065	0.37	0.72
S 2p 3	173.458	0.637	15.1	0.668	32.065	0.10	0.20
S 2p 4	169.500	0.991	17.4	0.668	32.065	0.12	0.23
S 2p 5	171.600	0.750	8.7	0.668	32.065	0.06	0.12
S 2p 6	162.400	0.591	4.6	0.668	32.065	0.03	0.06
S 2p 7	163.600	0.449	3.5	0.668	32.065	0.02	0.05
S 2p 8	172.400	0.638	3.3	0.668	32.065	0.02	0.04
S 2p 9	167.600	0.964	5.0	0.668	32.065	0.03	0.07
S 2p 10	159.900	0.487	2.5	0.668	32.065	0.02	0.03
Si 2p 1	101.615	1.370	155.4	0.328	28.086	2.17	3.73
Si 2p 2	102.415	2.039	49.9	0.328	28.086	0.70	1.20
Si 2p 3	100.892	0.721	15.3	0.328	28.086	0.21	0.37
Si 2p 4	105.554	0.599	5.0	0.328	28.086	0.07	0.12
Si 2p 5	96.577	0.684	5.2	0.328	28.086	0.07	0.13
Si 2p 6	106.454	0.942	4.9	0.328	28.086	0.07	0.12
Si 2p 7	97.700	0.672	3.2	0.328	28.086	0.04	0.08
Si 2p 8	98.600	0.524	2.5	0.328	28.086	0.04	0.06

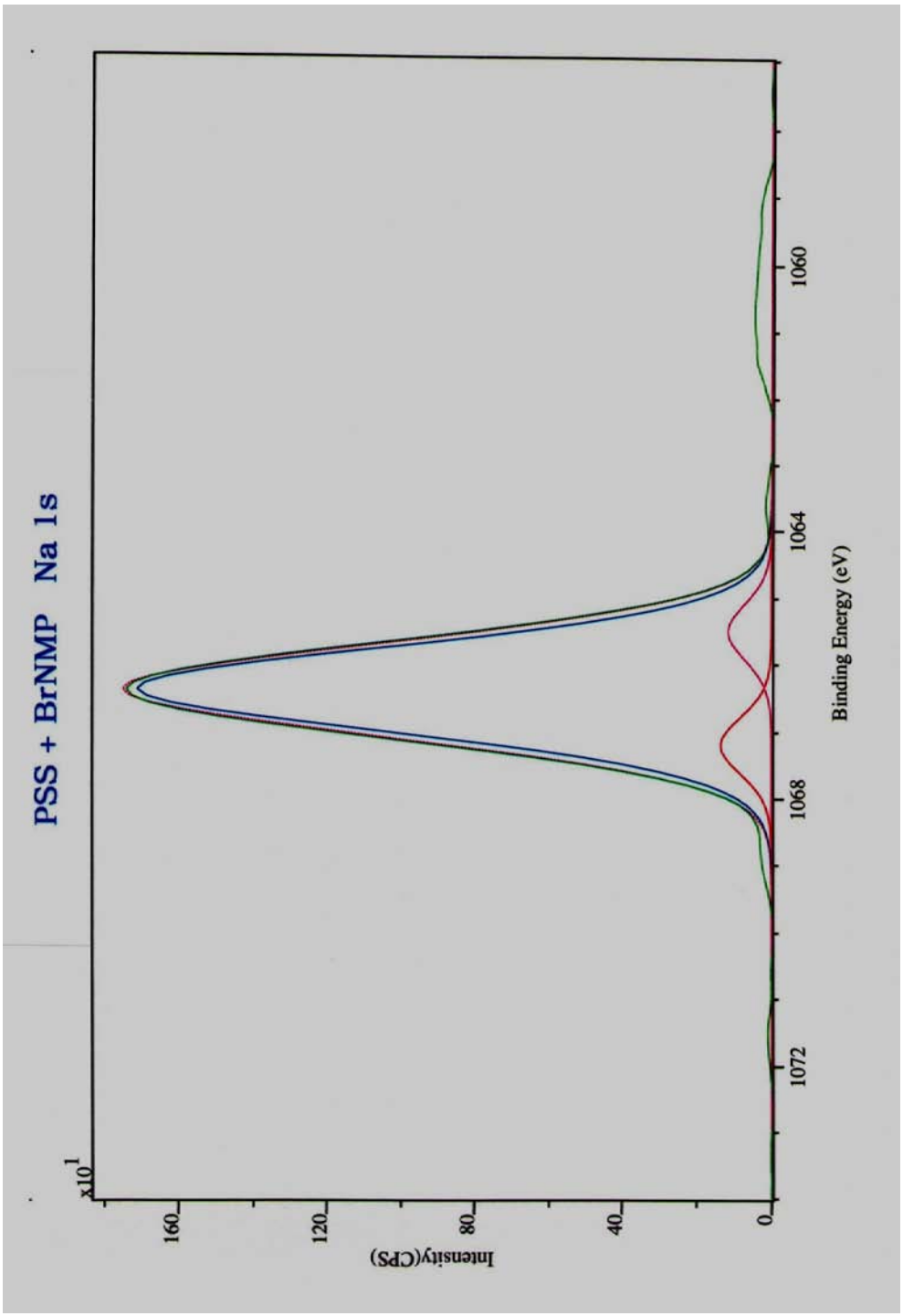

XPS high resolution spectral graph of Sodium 1s in BrNMP TiO_2 with PSS/PDDA Sub-Coating

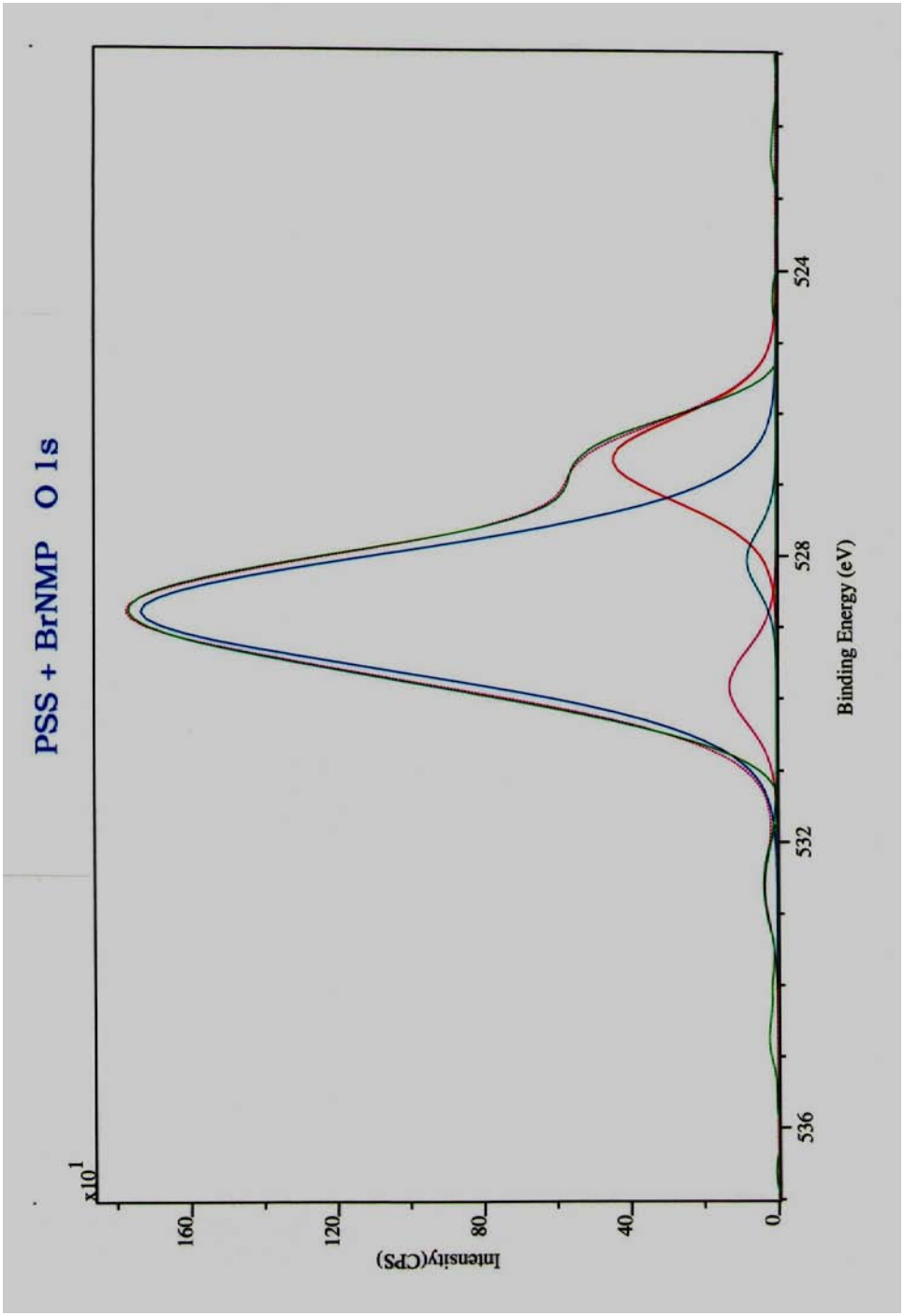

XPS high resolution spectral graph of Oxygen 1s in BrNMP TiO_2 with PSS/PDDA Sub-Coating

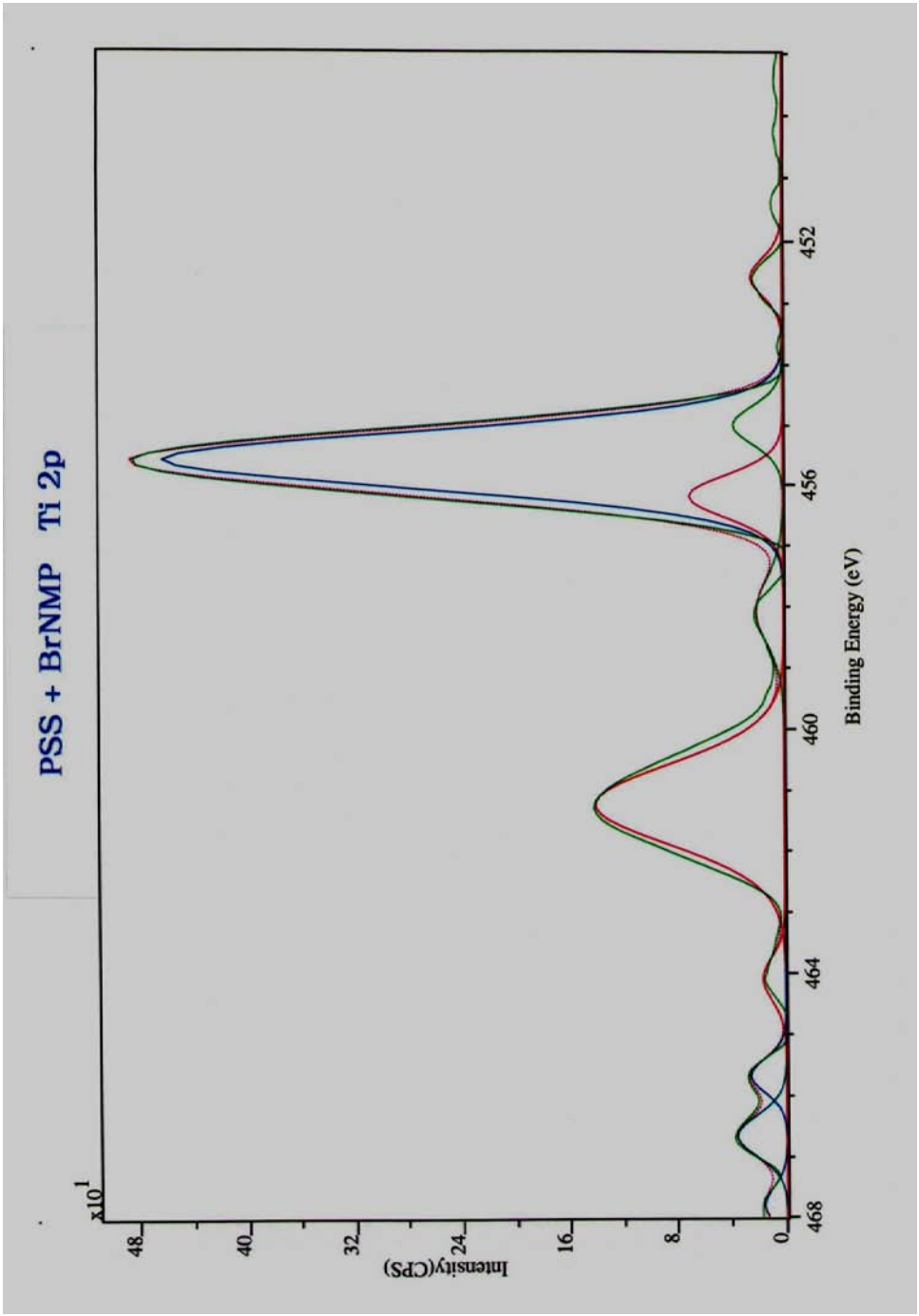

XPS high resolution spectral graph of Titanium 2p in BrNMP TiO_2 with PSS/PDDA Sub-Coating

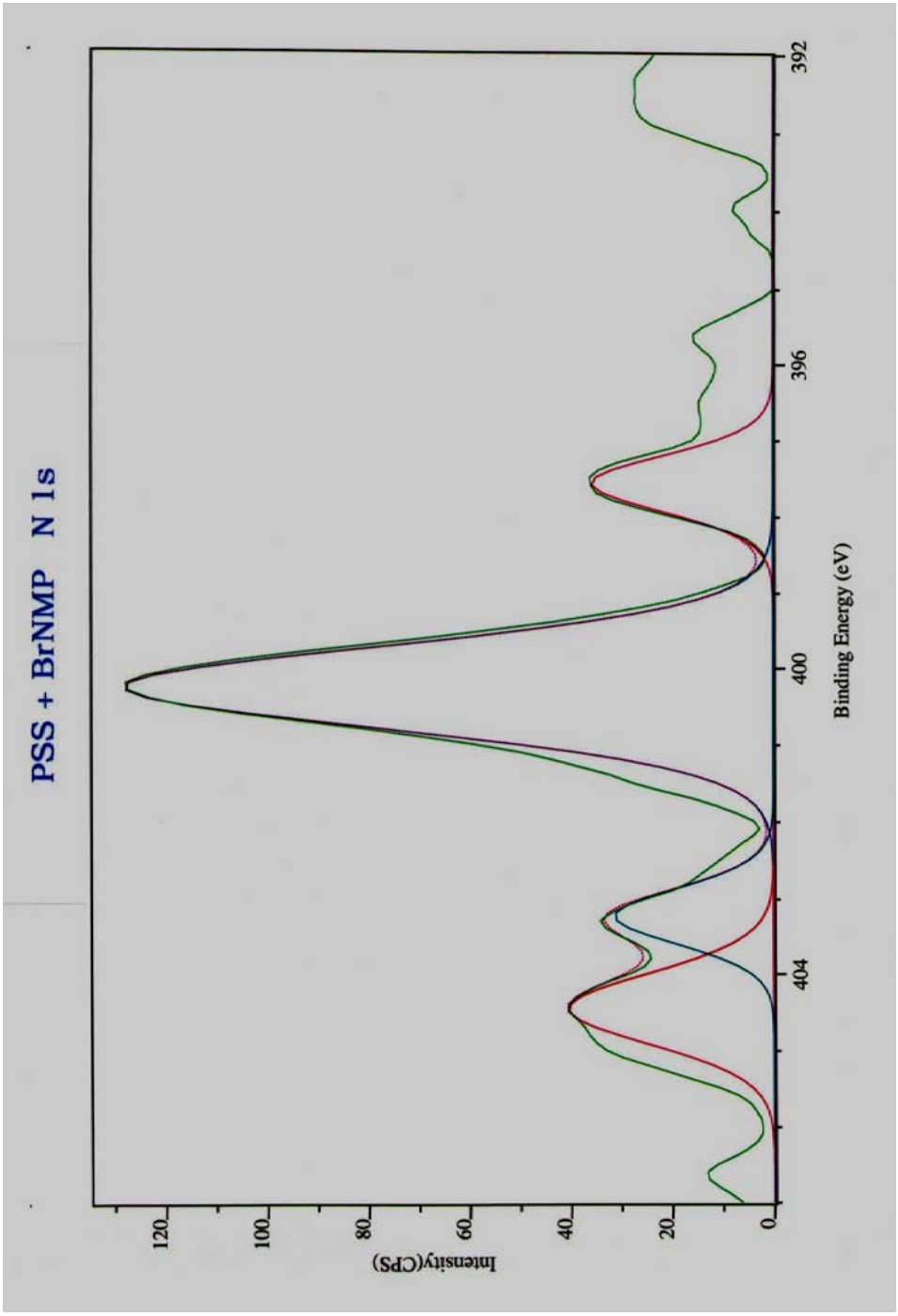

XPS high resolution spectral graph of Nitrogen 1s in BrNMP TiO_2 with PSS/PDDA Sub-Coating

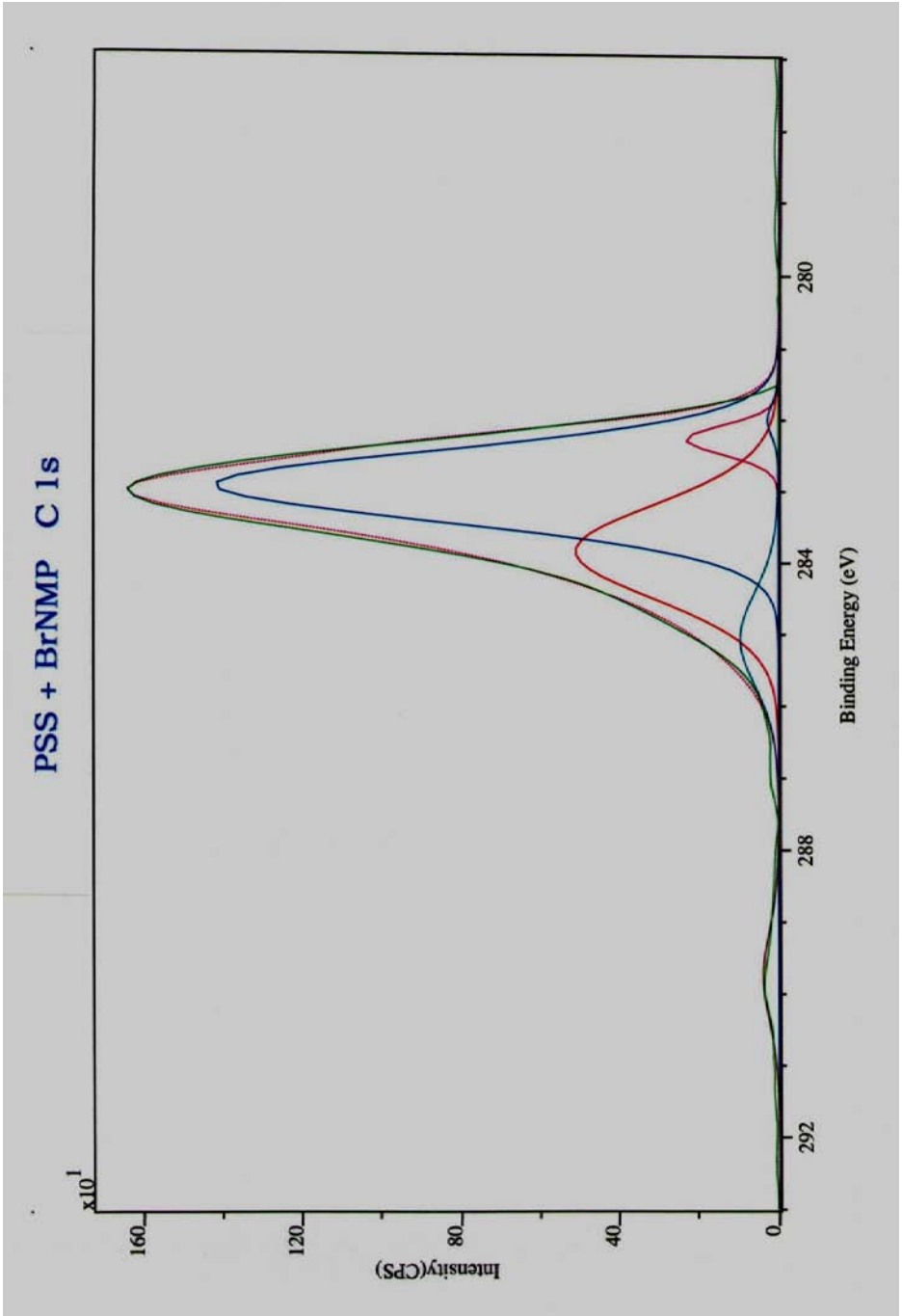

XPS high resolution spectral graph of Carbon 1s in BrNMP TiO_2 with PSS/PDDA Sub-Coating

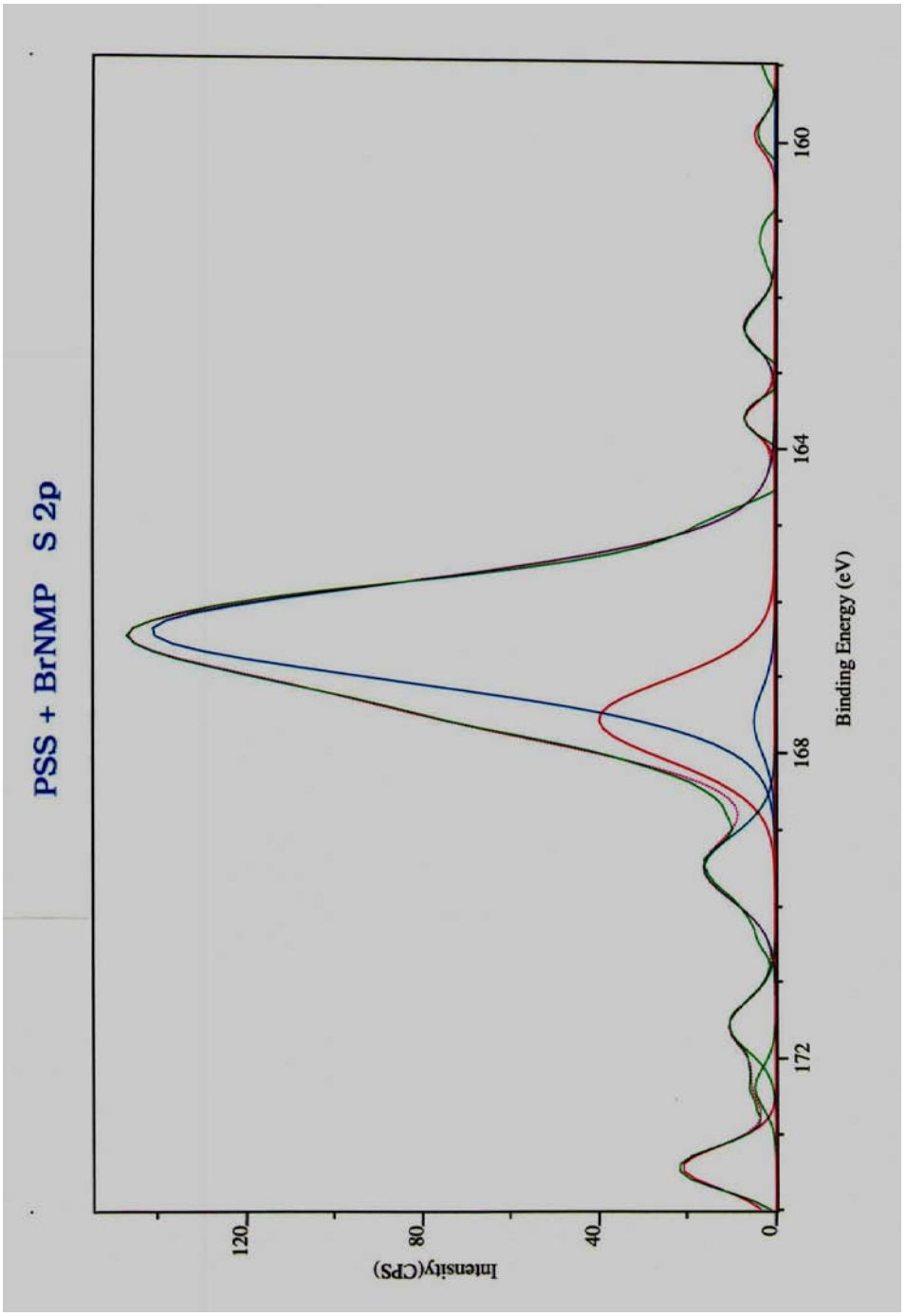

XPS high resolution spectral graph of Sulfur 2p in BrNMP TiO_2 with PSS/PDDA Sub-Coating

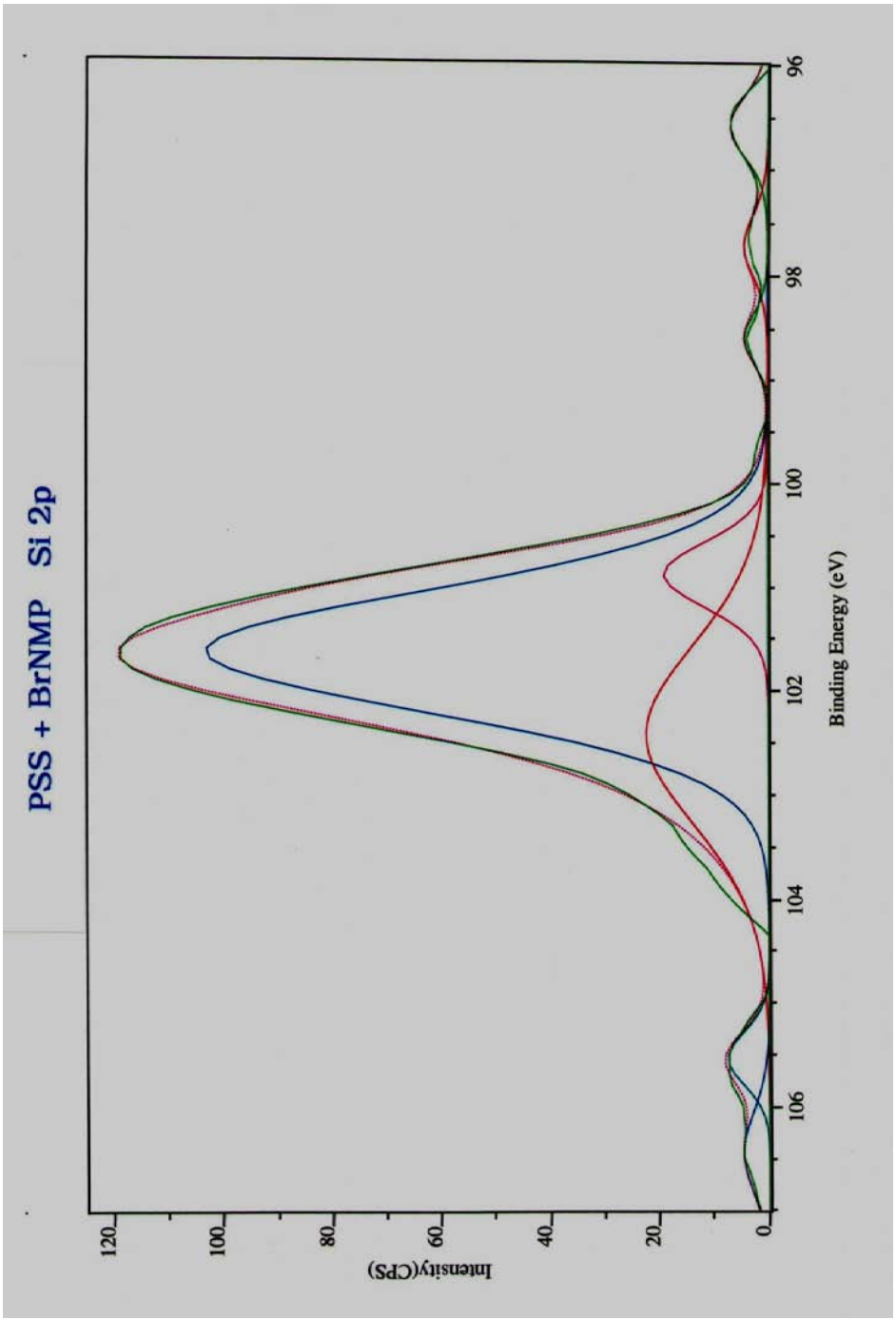

XPS high resolution spectral graph of Silicon 2p in BrNMP TiO_2 with PSS/PDDA Sub-Coating

XPS data table of vlp7000 TiO_2 with PSS/PDDA Sub-Coating

PSS + vlp7000 Quantification Report Thu Aug 20 17:20:01 2009

State #0 : Etch Time 0.00 seconds

Peak	Position BE (eV)	FWHM (eV)	Raw Area (CPS)	RSF	Atomic Mass	Atomic Conc %	Mass Conc %
Na 1s	1067.000	2.147	3166.7	1.685	22.990	4.50	6.45
O 1s	529.000	2.831	13316.7	0.780	15.999	31.32	31.22
Ti 2p	456.000	1.447	2701.4	2.001	47.878	2.40	7.17
N 1s	400.000	1.465	8.3	0.477	14.007	0.03	0.03
C 1s	283.000	1.941	8615.3	0.278	12.011	53.72	40.19
S 2p	167.000	1.927	666.7	0.668	32.065	1.72	3.44
Cl 2p	196.000	1.419	541.7	0.891	35.460	1.05	2.32
Si 2p	102.000	2.358	980.6	0.328	28.086	5.25	9.18

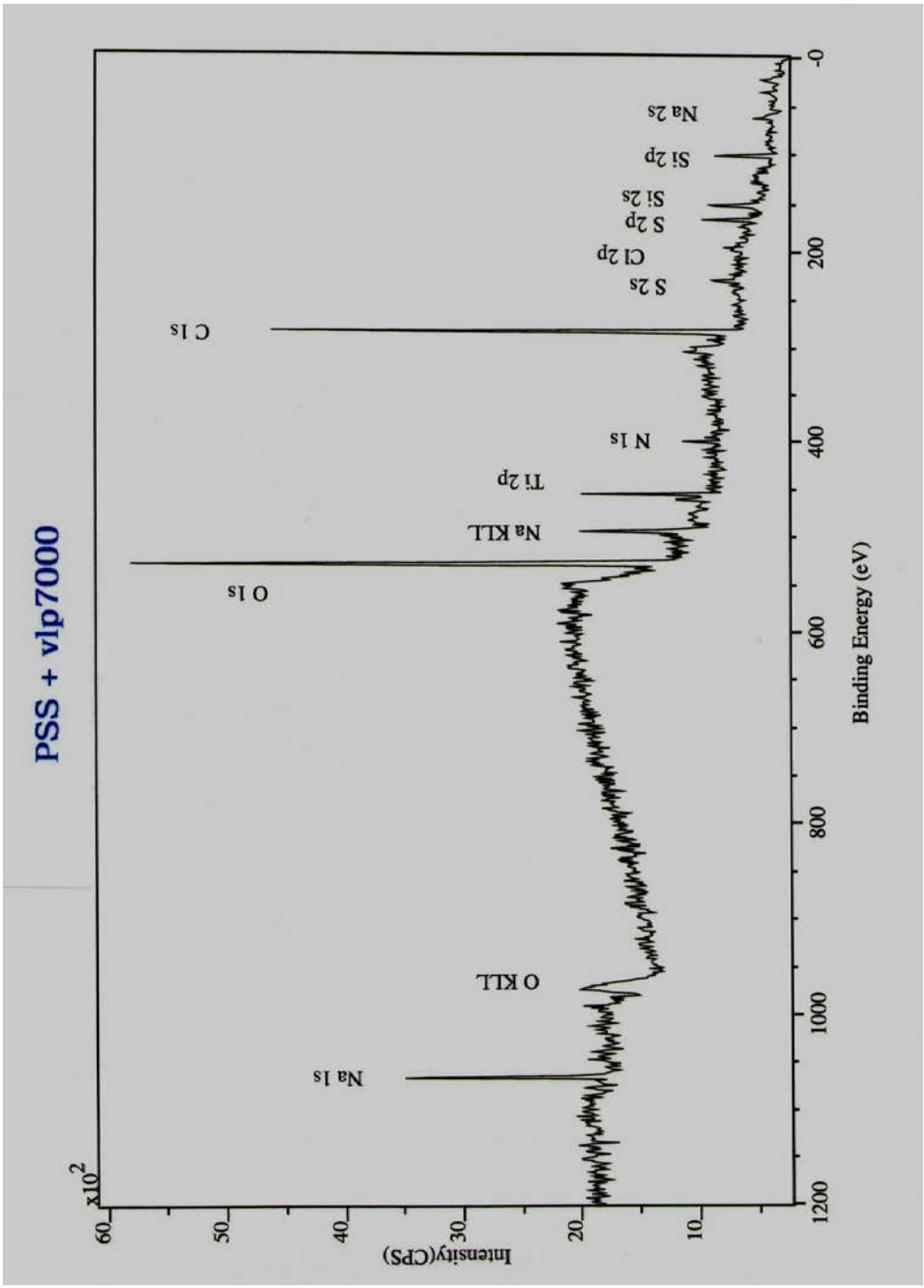

XPS spectral graph of vlp7000 TiO_2 with PSS/PDDA Sub-Coating

XPS data table of vlp7000 TiO_2 with PSS/PDDA Sub-Coating

PSS + vlp7000 Quantification Report — Thu Aug 20 17:52:54 2009

State #0 : Etch Time 0.00 seconds

Peak	Position BE (eV)	FWHM (eV)	Raw Area (CPS)	RSF	Atomic Mass	Atomic Conc %	Mass Conc %
Na 1s 1	1066.700	1.541	3117.8	1.685	22.990	4.82	6.82
Na 1s2	1067.700	1.284	306.7	1.685	22.990	0.47	0.67
Na 1s 3	1065.900	0.959	176.0	1.685	22.990	0.27	0.38
Na 1s 4	1075.600	1.315	169.1	1.685	22.990	0.26	0.37
Na 1s 5	1069.100	0.678	34.8	1.685	22.990	0.05	0.08
Na 1s 6	1063.800	0.972	46.5	1.685	22.990	0.07	0.10
Na 1s 7	1059.400	1.663	73.4	1.685	22.990	0.11	0.16
Na 1s 8	1071.800	0.820	36.2	1.685	22.990	0.06	0.08
Na 1s 9	1074.000	0.724	26.5	1.685	22.990	0.04	0.06
O 1s 1	529.098	1.759	8394.7	0.780	15.999	21.48	21.12
O 1s 2	526.888	1.427	1614.3	0.780	15.999	4.13	4.06
O 1s 3	530.159	1.161	938.7	0.780	15.999	2.40	2.36
O 1s 4	528.047	1.151	843.0	0.780	15.999	2.16	2.12
Ti 2p 1	455.900	1.065	1093.6	2.001	47.878	1.06	3.12
Ti 2p 2	461.600	1.503	458.9	2.001	47.878	0.45	1.31
Ti 2p 3	455.300	0.776	145.3	2.001	47.878	0.14	0.41
Ti 2p 4	456.600	0.707	83.1	2.001	47.878	0.08	0.24
Ti 2p 5	465.500	0.803	23.7	2.001	47.878	0.02	0.07
Ti 2p 6	462.700	0.895	26.4	2.001	47.878	0.03	0.08
Ti 2p 7	452.900	1.228	36.2	2.001	47.878	0.04	0.10
N 1s 1	400.900	0.765	429.2	0.477	14.007	1.73	1.49
N 1s 3	397.879	1.264	52.4	0.477	14.007	0.21	0.18
C 1s 1	283.085	1.255	5183.2	0.278	12.011	35.15	25.95
C 1s 2	284.286	1.539	1761.1	0.278	12.011	11.95	8.82
C 1s 3	282.410	0.731	362.5	0.278	12.011	2.46	1.81
C 1s 4	284.882	0.884	110.2	0.278	12.011	0.75	0.55
S 2p 1	166.557	1.303	549.6	0.668	32.065	1.55	3.05
S 2p 2	167.657	1.255	278.2	0.668	32.065	0.78	1.54
S 2p 3	165.900	0.614	23.8	0.668	32.065	0.07	0.13
S 2p 4	163.700	1.593	53.5	0.668	32.065	0.15	0.30
S 2p 5	162.021	0.899	16.2	0.668	32.065	0.05	0.09
S 2p 6	170.500	0.681	10.6	0.668	32.065	0.03	0.06
S 2p 7	173.400	0.571	8.8	0.668	32.065	0.02	0.05
S 2p 8	171.400	0.821	10.6	0.668	32.065	0.03	0.06
S 2p 9	161.300	0.605	4.7	0.668	32.065	0.01	0.03
Cl 2p 1	195.876	1.209	90.4	0.891	35.460	0.19	0.42
Cl 2p 2	198.900	1.006	40.4	0.891	35.460	0.09	0.19
Cl 2p 3	197.571	0.877	22.4	0.891	35.460	0.05	0.10
Cl 2p 4	190.400	0.750	21.6	0.891	35.460	0.05	0.10
Cl 2p 5	200.700	1.043	22.4	0.891	35.460	0.05	0.10
Cl 2p 6	205.676	0.888	18.6	0.891	35.460	0.04	0.09
Cl 2p 7	201.651	0.675	11.3	0.891	35.460	0.02	0.05
Cl 2p 8	192.700	0.738	9.8	0.891	35.460	0.02	0.04
Cl 2p 9	191.500	0.685	8.2	0.891	35.460	0.02	0.04
Cl 2p 10	204.124	0.641	7.3	0.891	35.460	0.02	0.03
Cl 2p 12	203.100	0.778	5.6	0.891	35.460	0.01	0.03
Cl 2p 13	196.993	0.918	10.2	0.891	35.460	0.02	0.05
Cl 2p 14	197.900	0.426	1.0	0.891	35.460	0.00	0.00
Si 2p 1	101.817	1.524	916.9	0.328	28.086	5.34	9.21
Si 2p 2	102.600	1.041	87.3	0.328	28.086	0.51	0.88
Si 2p 3	101.000	0.825	23.8	0.328	28.086	0.14	0.24
Si 2p 4	98.000	0.721	15.6	0.328	28.086	0.09	0.16
Si 2p 5	104.900	0.901	15.2	0.328	28.086	0.09	0.15
Si 2p 6	101.100	0.972	16.3	0.328	28.086	0.09	0.16
Si 2p 7	106.300	1.191	17.1	0.328	28.086	0.10	0.17

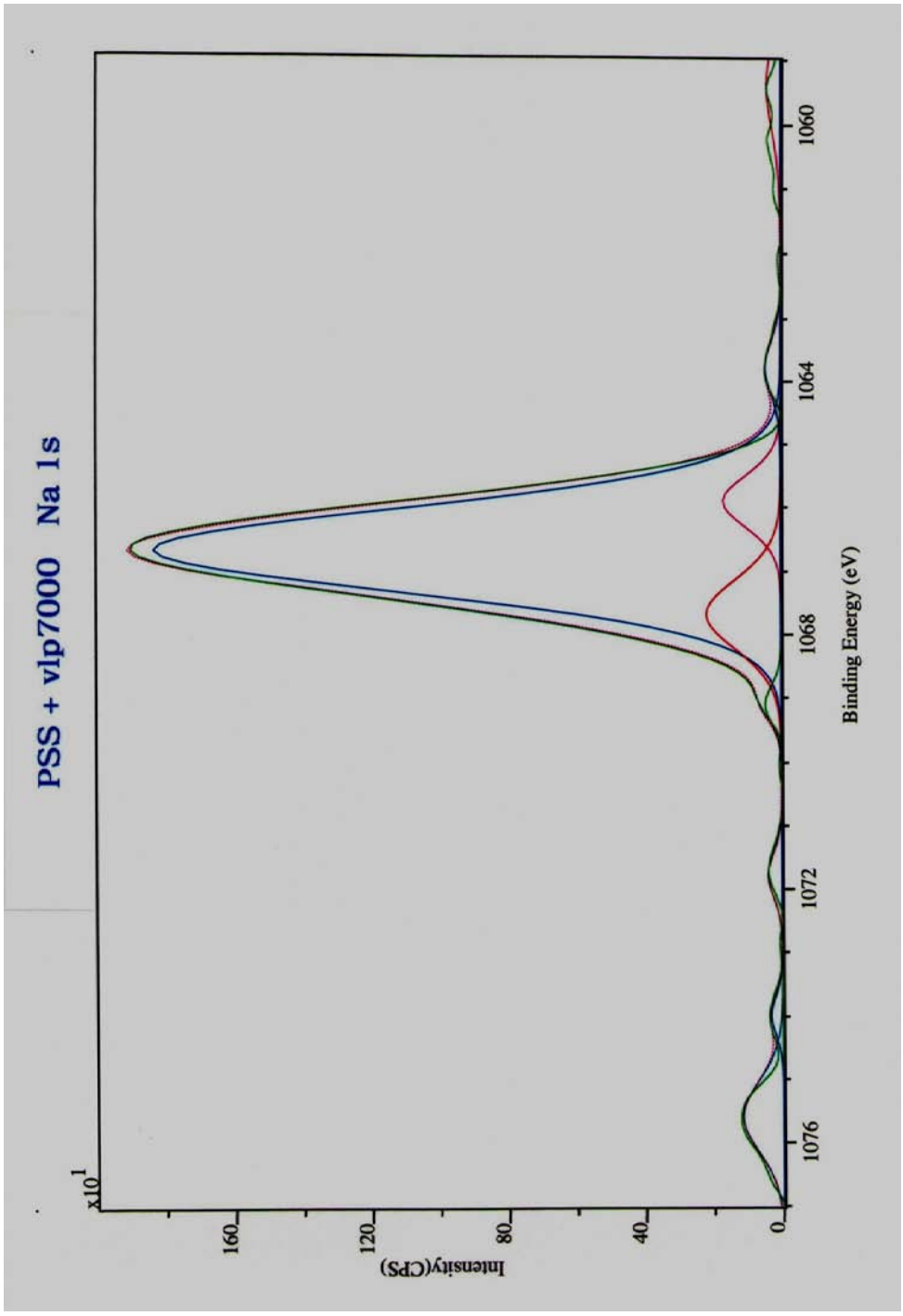

XPS high resolution spectral graph of Sodium 1s vlp7000 TiO_2 with PSS/PDDA Sub-Coating

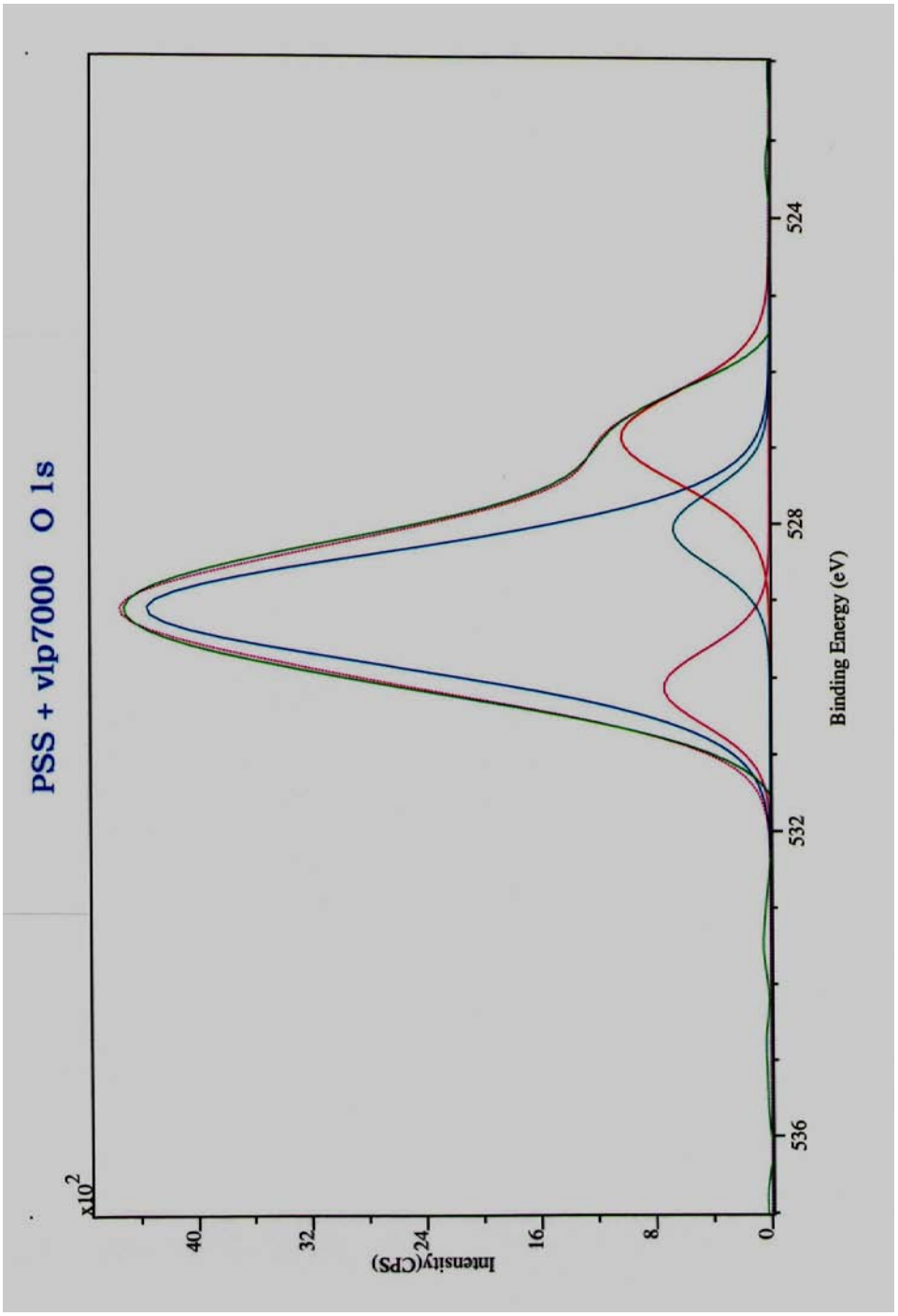

XPS high resolution spectral graph of Oxygen1s vlp7000 TiO_2 with PSS/PDDA Sub-Coating

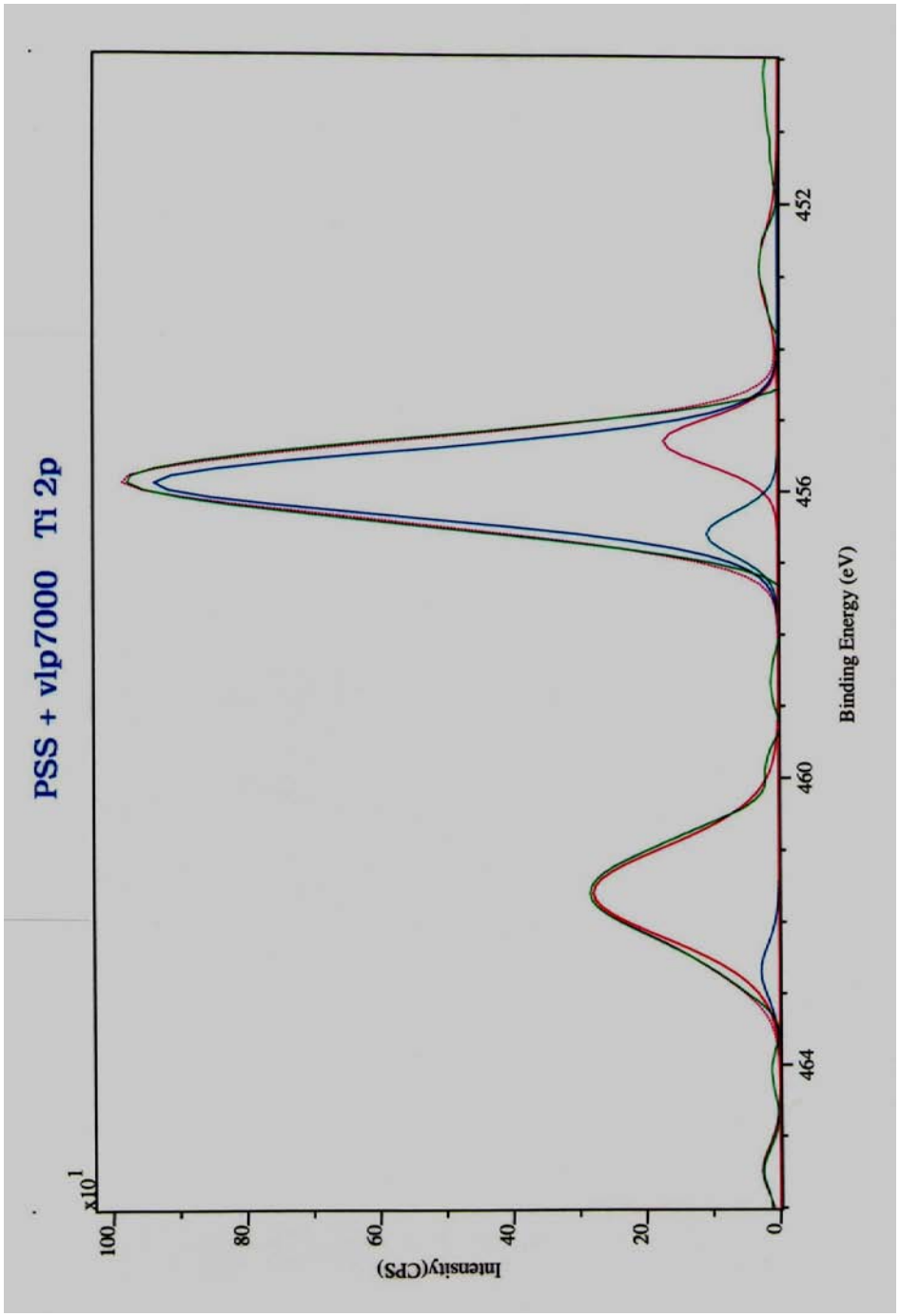

XPS high resolution spectral graph of Titanium 2p vlp7000 TiO_2 with PSS/PDDA Sub-Coating

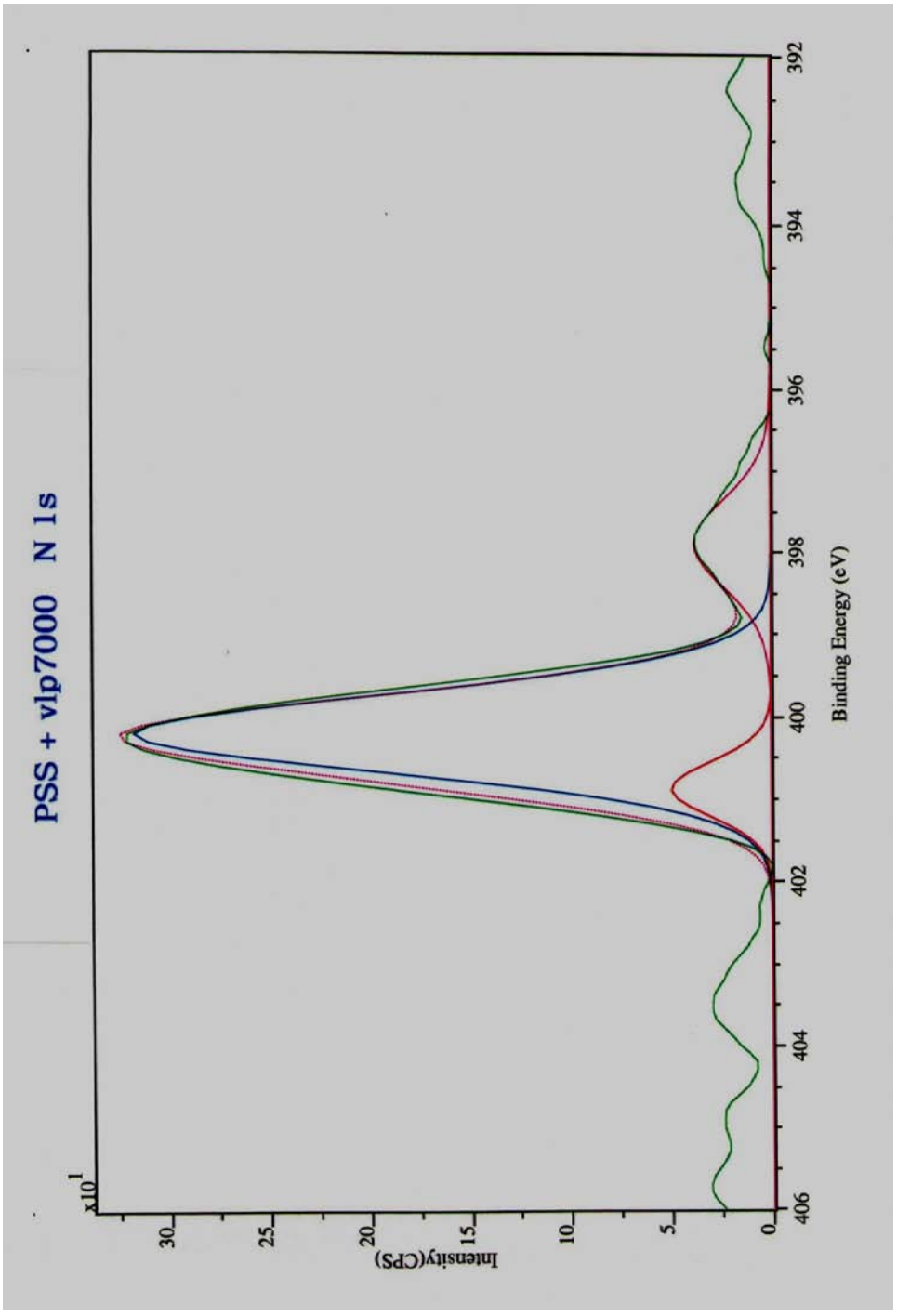

XPS high resolution spectral graph of Nitrogen 1s vlp7000 TiO_2 with PSS/PDDA Sub-Coating

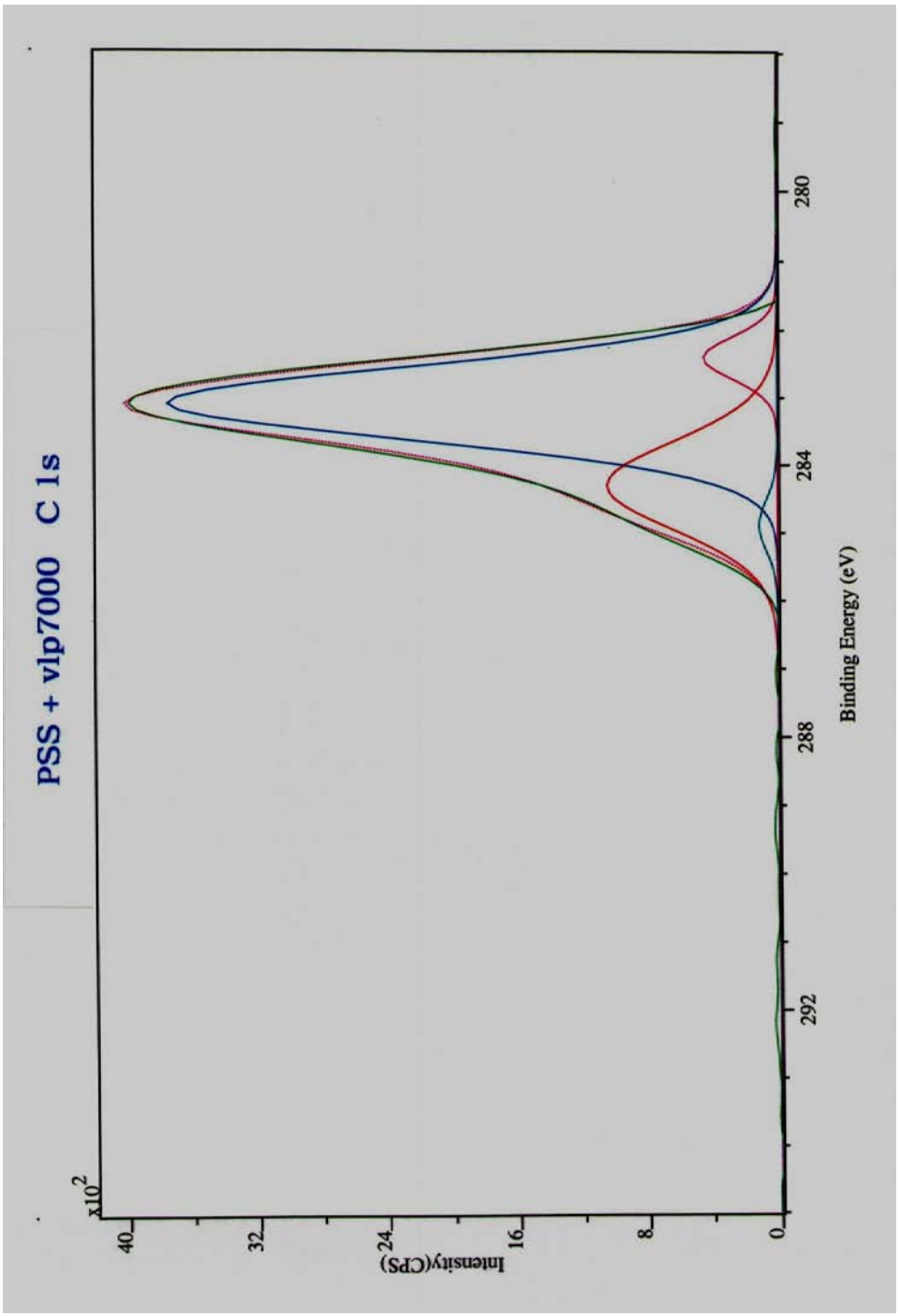

XPS high resolution spectral graph of Carbon 1s vlp7000 TiO_2 with PSS/PDDA Sub-Coating

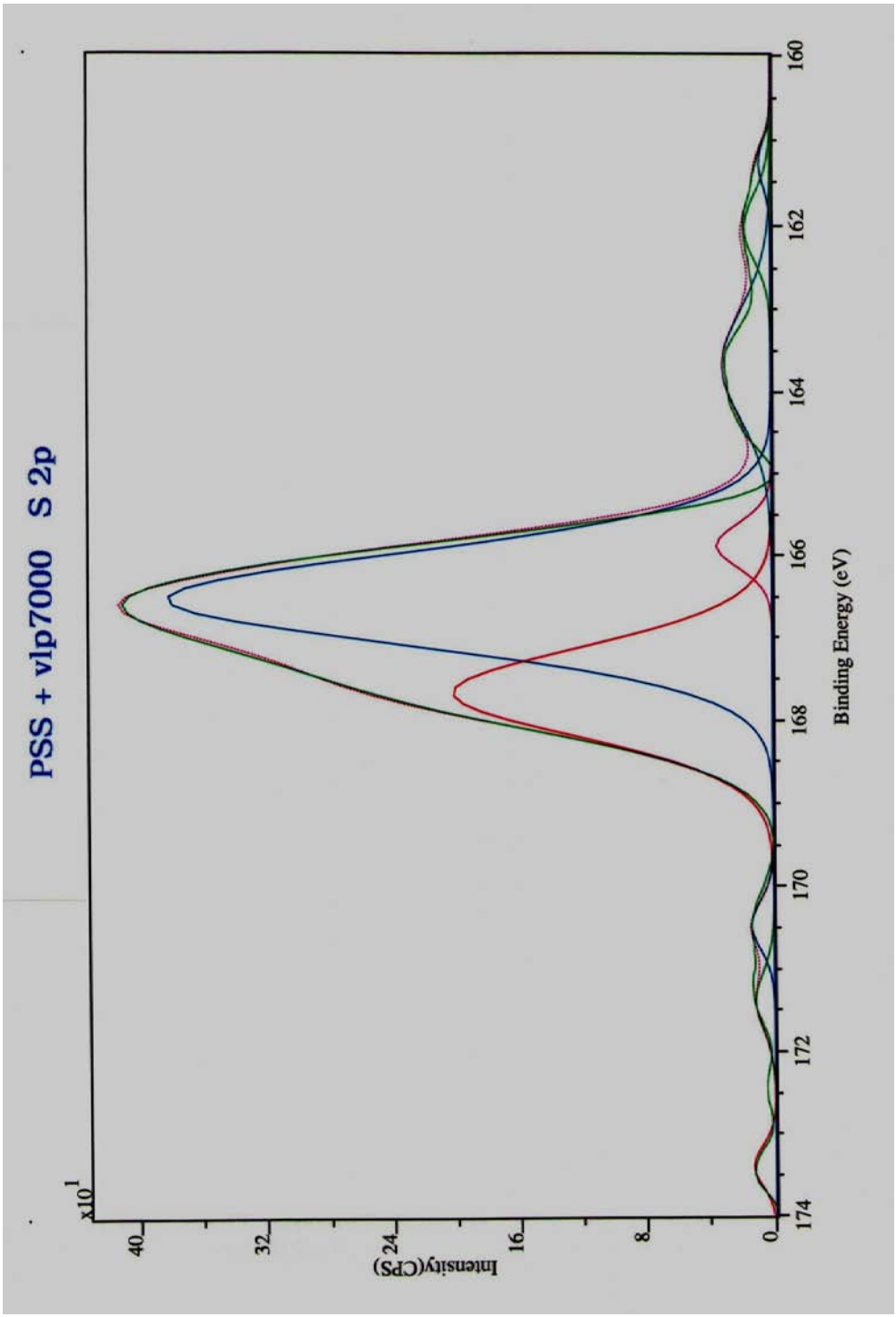

XPS high resolution spectral graph of Sulfur 2p vlp7000 TiO_2 with PSS/PDDA Sub-Coating

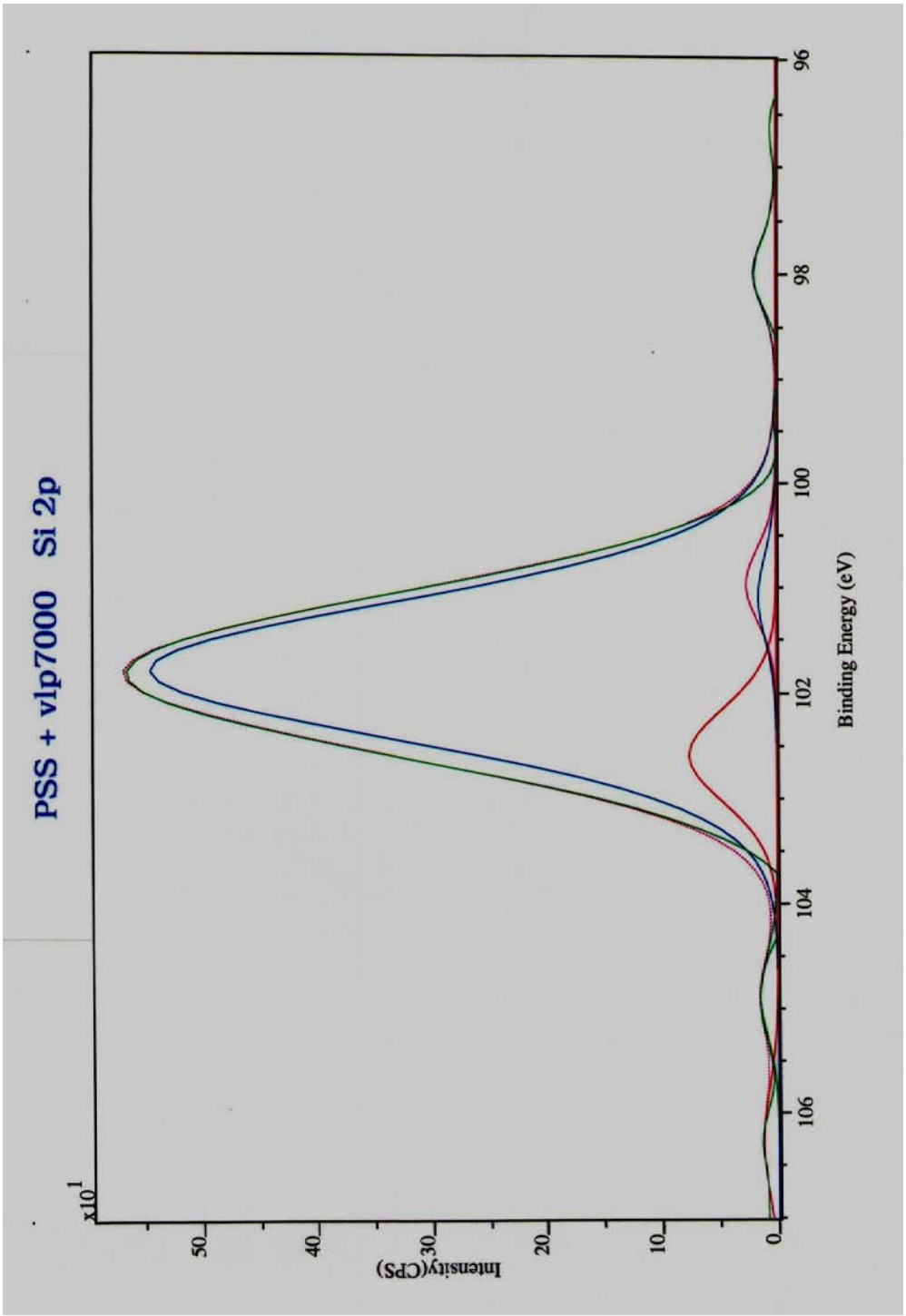

XPS high resolution spectral graph of Silicon 2p vlp7000 TiO_2 with PSS/PDDA Sub-Coating

XPS data table of vlp7001 TiO_2 with PSS/PDDA Sub-Coating

PSS + vlp7001 Quantification Report Mon Aug 24 11:51:39 2009

State #0 : Etch Time 0.00 seconds

Peak	Position BE (eV)	FWHM (eV)	Raw Area (CPS)	RSF	Atomic Mass	Atomic Conc %	Mass Conc %
Na 1s	1067.000	2.145	4702.8	1.685	22.990	6.34	9.29
O 1s	529.000	2.527	11777.8	0.780	15.999	26.26	26.77
Ti 2p	456.000	1.535	722.2	2.001	47.878	0.61	1.86
N 1s	400.000	1.877	1045.8	0.477	14.007	3.67	3.27
C 1s	283.000	2.040	9169.4	0.278	12.011	54.18	41.48
S 2p	167.000	2.488	686.1	0.668	32.065	1.68	3.44
Si 2p	102.000	2.085	1056.9	0.328	28.086	5.36	9.59
Cl 2p	196.000	2.541	1036.1	0.891	35.460	1.90	4.30

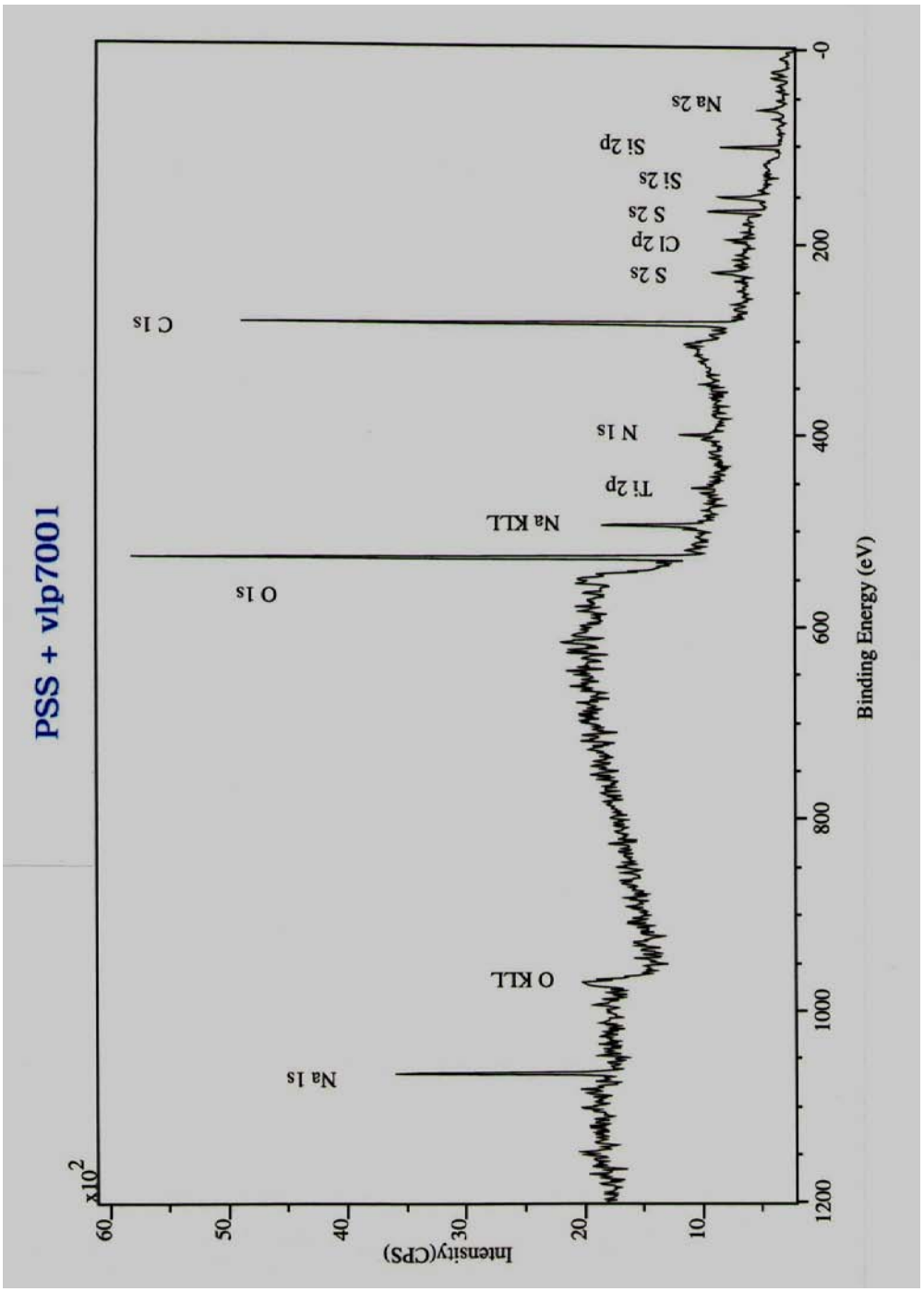

XPS spectral graph of vlp70001 TiO_2 with PSS/PDDA Sub-Coating

XPS data table of vlp7001 TiO_2 with PSS/PDDA Sub-Coating

PSS + vlp7001 Quantification Report

Mon Aug 24 16:13:00 2009

State #0 : Etch Time 0.00 seconds

Peak	Position BE (eV)	FWHM (eV)	Raw Area (CPS)	RSF	Atomic Mass	Atomic Conc %	Mass Conc %
Na 1s 1	1066.700	1.450	2739.8	1.685	22.990	4.80	7.14
Na 1s 2	1067.500	1.049	204.3	1.685	22.990	0.36	0.53
Na 1s 3	1066.000	0.860	138.8	1.685	22.990	0.24	0.36
Na 1s 4	1072.400	1.707	232.5	1.685	22.990	0.41	0.60
Na 1s 5	1073.800	0.850	56.3	1.685	22.990	0.10	0.15
Na 1s 6	1069.700	0.695	33.0	1.685	22.990	0.06	0.09
O 1s 1	529.118	1.965	7914.9	0.780	15.999	22.95	23.72
O 1s	530.100	1.250	758.9	0.780	15.999	2.20	2.28
O 1s 3	528.100	1.807	448.9	0.780	15.999	1.30	1.34
Ti 2p 1	455.962	1.326	317.1	2.001	47.878	0.35	1.08
Ti 2p 2	459.762	0.765	38.2	2.001	47.878	0.04	0.13
Ti 2p 3	461.662	1.022	42.1	2.001	47.878	0.05	0.14
Ti 2p 4	451.900	1.178	43.3	2.001	47.878	0.05	0.15
N 1s 1	400.318	1.269	402.3	0.477	14.007	1.83	1.66
N 1s 2	404.447	0.762	44.1	0.477	14.007	0.20	0.18
N 1s 3	400.900	1.032	34.2	0.477	14.007	0.16	0.14
N 1s 4	394.400	0.744	21.9	0.477	14.007	0.10	0.09
N 1s 5	397.324	1.172	37.6	0.477	14.007	0.17	0.16
N 1s 6	393.000	0.875	22.5	0.477	14.007	0.10	0.09
N 1s 7	402.853	0.529	13.7	0.477	14.007	0.06	0.06
N 1s 8	395.500	0.881	19.4	0.477	14.007	0.09	0.08
N 1s 9	403.636	0.706	17.2	0.477	14.007	0.08	0.07
N 1s 10	399.600	0.564	4.1	0.477	14.007	0.02	0.02
C 1s 1	283.131	1.268	4377.7	0.278	12.011	33.64	26.11
C 1s 2	284.184	1.655	2343.8	0.278	12.011	18.01	13.98
C 1s 3	282.501	0.706	274.3	0.278	12.011	2.11	1.64
C 1s 4	285.391	0.850	123.9	0.278	12.011	0.95	0.74
C 1s 5	285.000	0.836	113.0	0.278	12.011	0.87	0.67
Cl 2p 1	196.036	1.156	82.3	0.891	35.460	0.20	0.45
Cl 2p 2	198.400	0.975	22.7	0.891	35.460	0.05	0.12
Cl 2p 3	199.682	0.840	16.0	0.891	35.460	0.04	0.09
S 2p 1	166.767	1.409	565.3	0.668	32.065	1.80	3.73
S 2p 2	167.834	0.981	95.4	0.668	32.065	0.30	0.63
S 2p 3	166.100	0.864	60.3	0.668	32.065	0.19	0.40
S 2p 4	171.700	0.804	20.8	0.668	32.065	0.07	0.14
S 2p 5	163.400	0.846	21.7	0.668	32.065	0.07	0.14
S 2p 6	173.300	0.841	19.6	0.668	32.065	0.06	0.13
S 2p 7	169.600	0.872	18.0	0.668	32.065	0.06	0.12
S 2p 8	162.100	0.553	5.7	0.668	32.065	0.02	0.04
S 2p 9	167.400	0.864	4.5	0.668	32.065	0.01	0.03
Si 2p 1	101.900	1.589	768.4	0.328	28.086	5.07	9.19
Si 2p 2	102.700	1.007	38.7	0.328	28.086	0.26	0.46
Si 2p 3	101.100	0.851	24.5	0.328	28.086	0.16	0.29
Si 2p 4	96.800	0.922	19.8	0.328	28.086	0.13	0.24
Si 2p 5	98.700	0.667	12.8	0.328	28.086	0.08	0.15
Si 2p 6	104.500	0.691	11.6	0.328	28.086	0.08	0.14
Si 2p 7	105.600	0.638	9.2	0.328	28.086	0.06	0.11

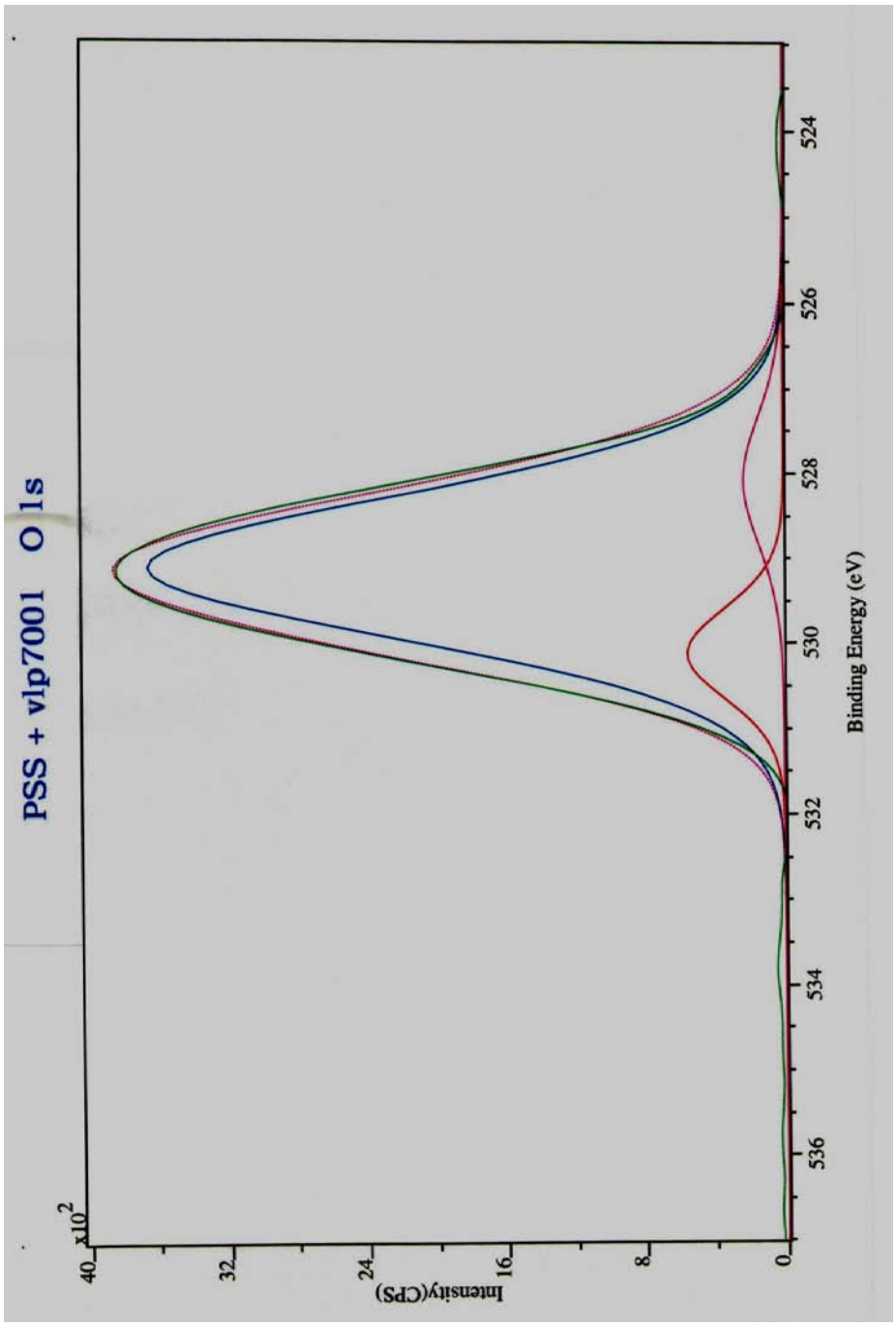

XPS high resolution spectral graph of Oxygen 1s vlp7001 TiO_2 with PSS/PDDA Sub-Coating

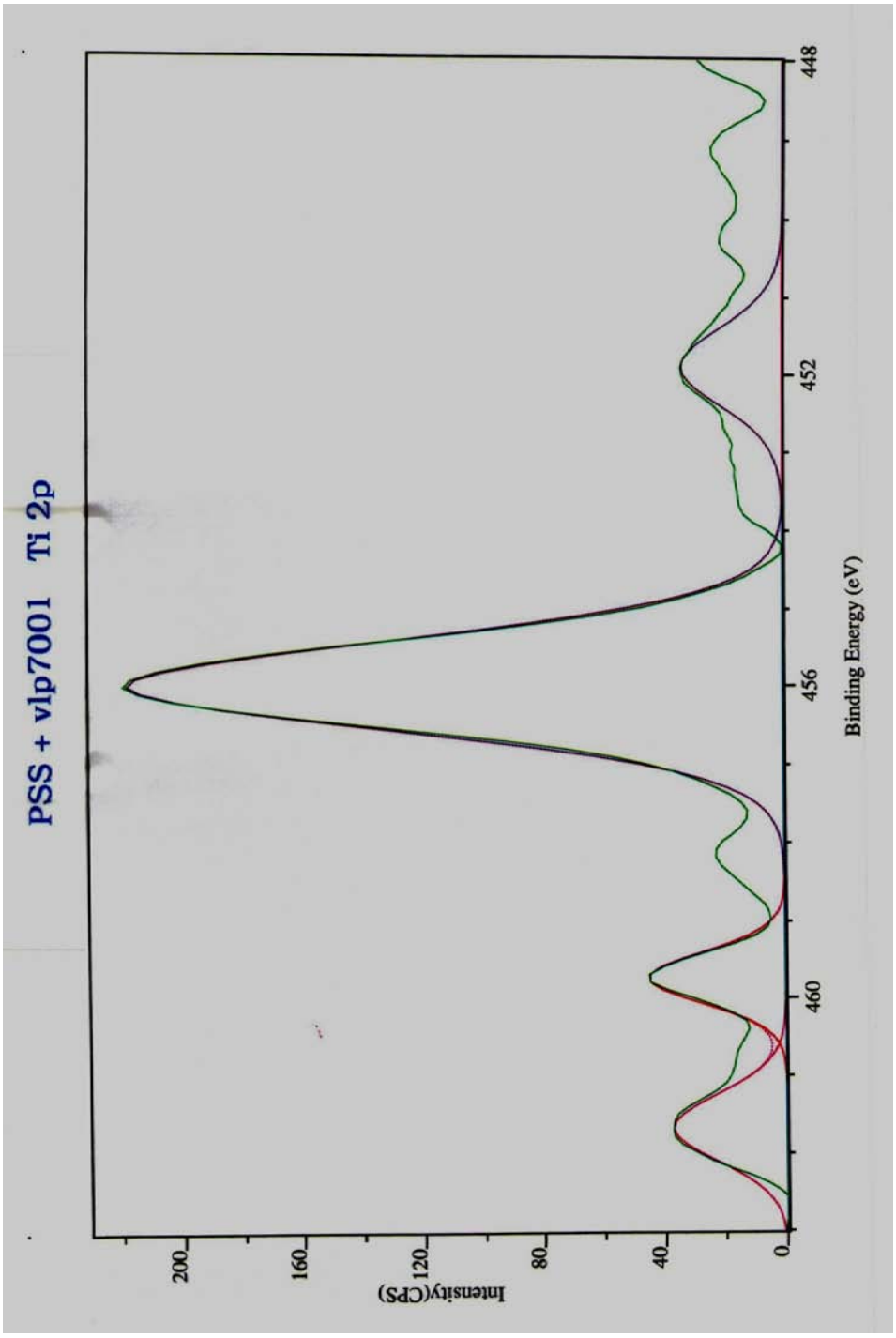

XPS high resolution spectral graph of Titanium 2p vlp7001 TiO_2 with PSS/PDDA Sub-Coating

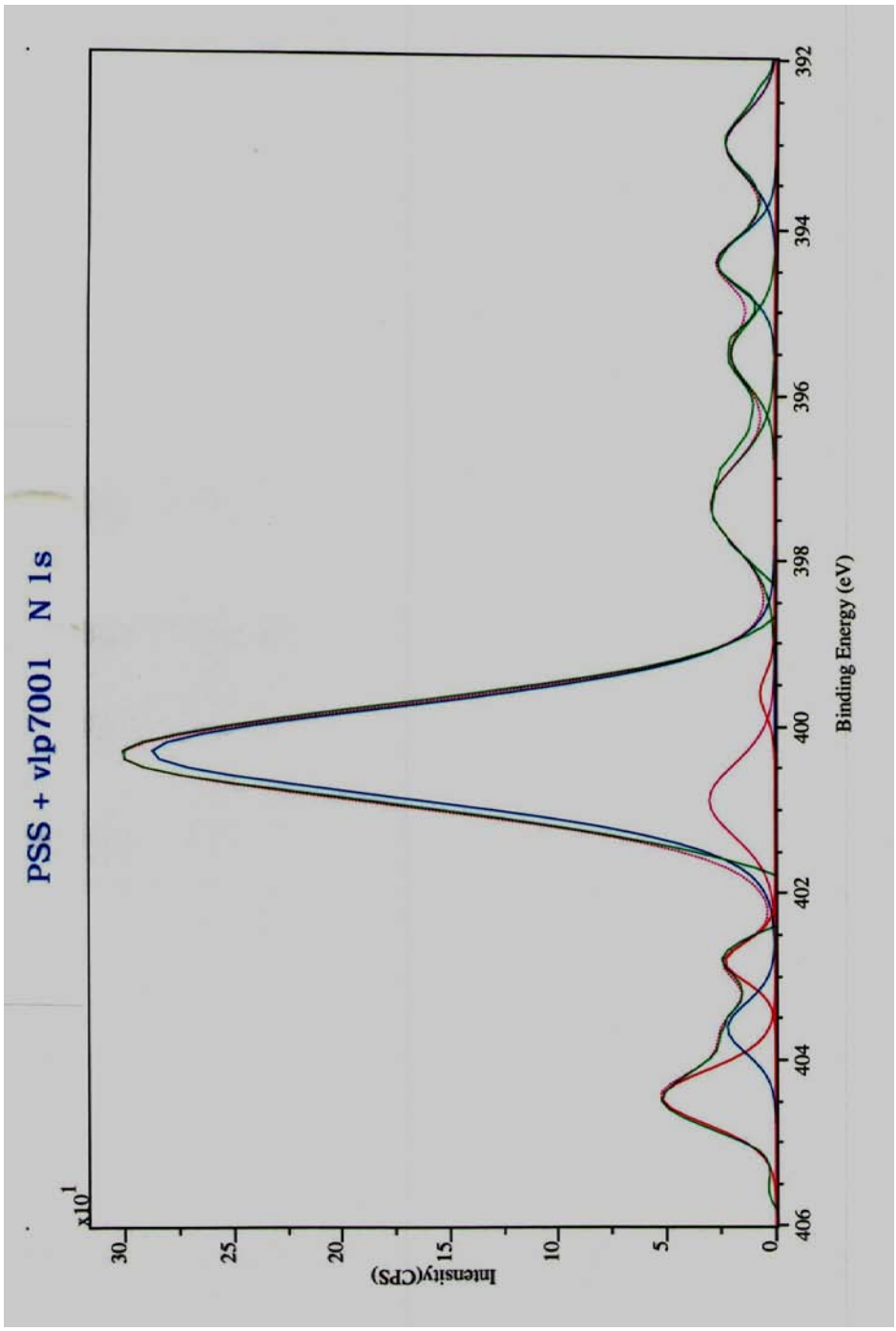

XPS high resolution spectral graph of Nitrogen 1s vlp7001 TiO_2 with PSS/PDDA Sub-Coating

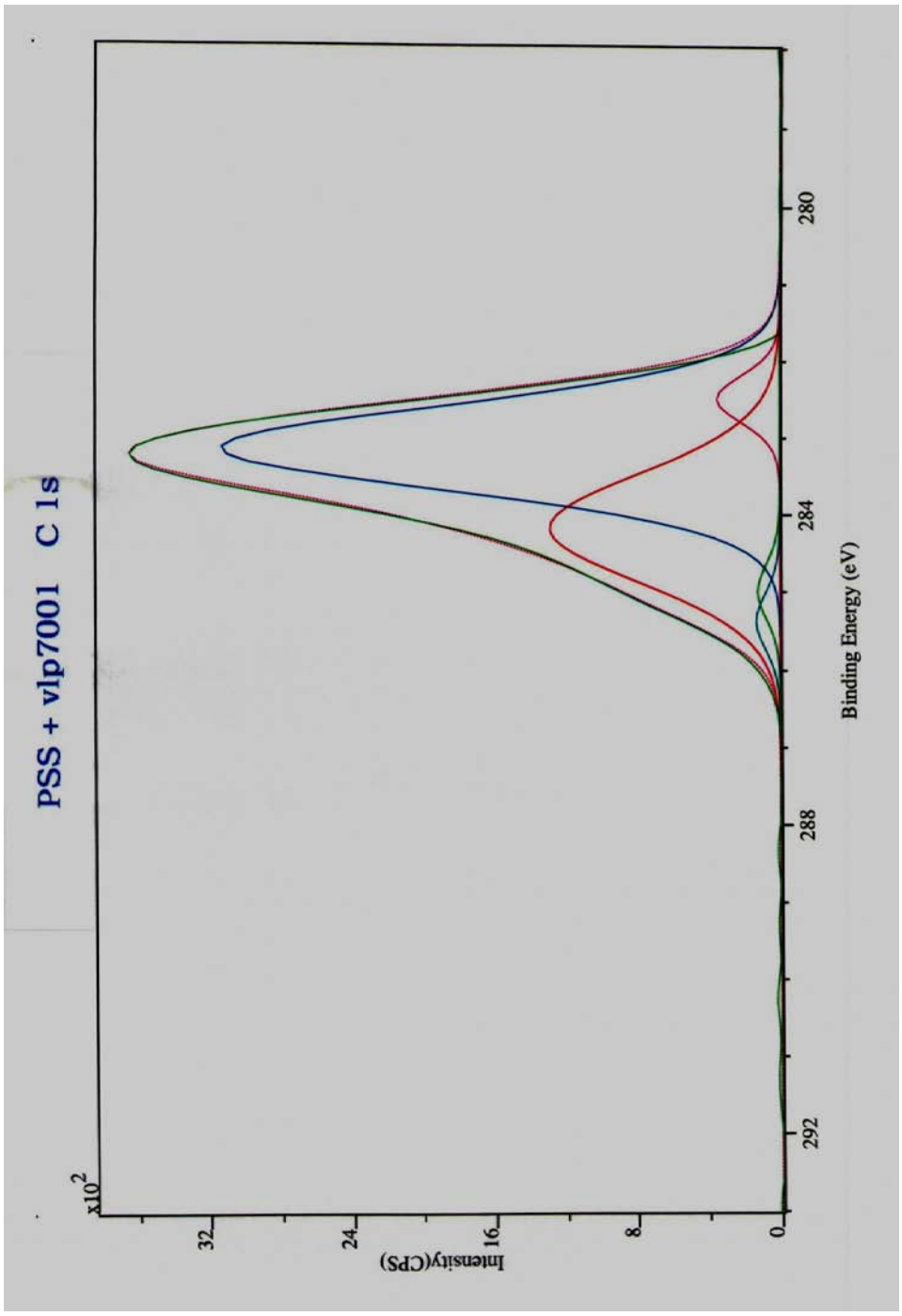

XPS high resolution spectral graph of Carbon 1s vlp7001 TiO_2 with PSS/PDDA Sub-Coating

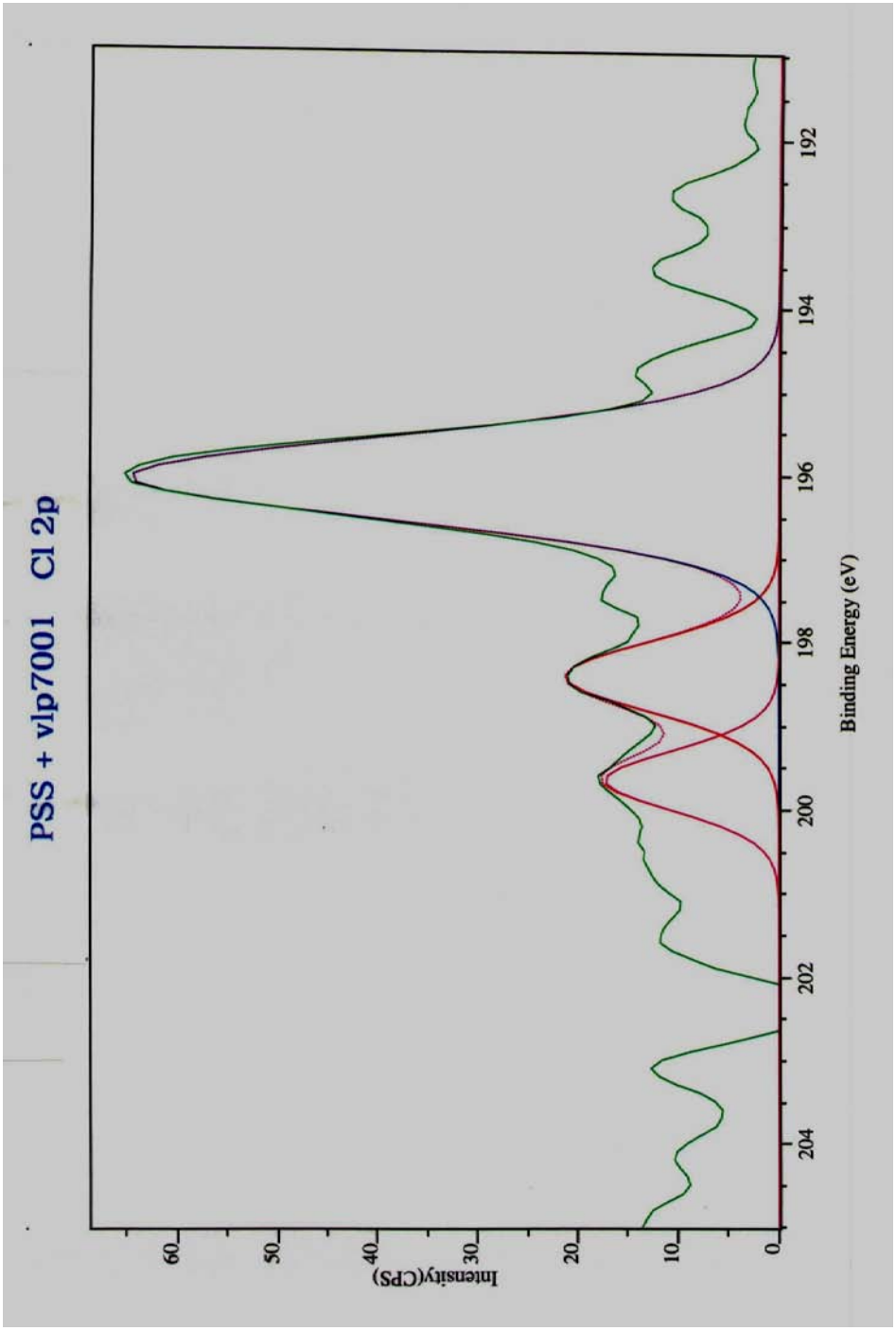

XPS high resolution spectral graph of Chlorine 2p vlp7001 TiO_2 with PSS/PDDA Sub-Coating

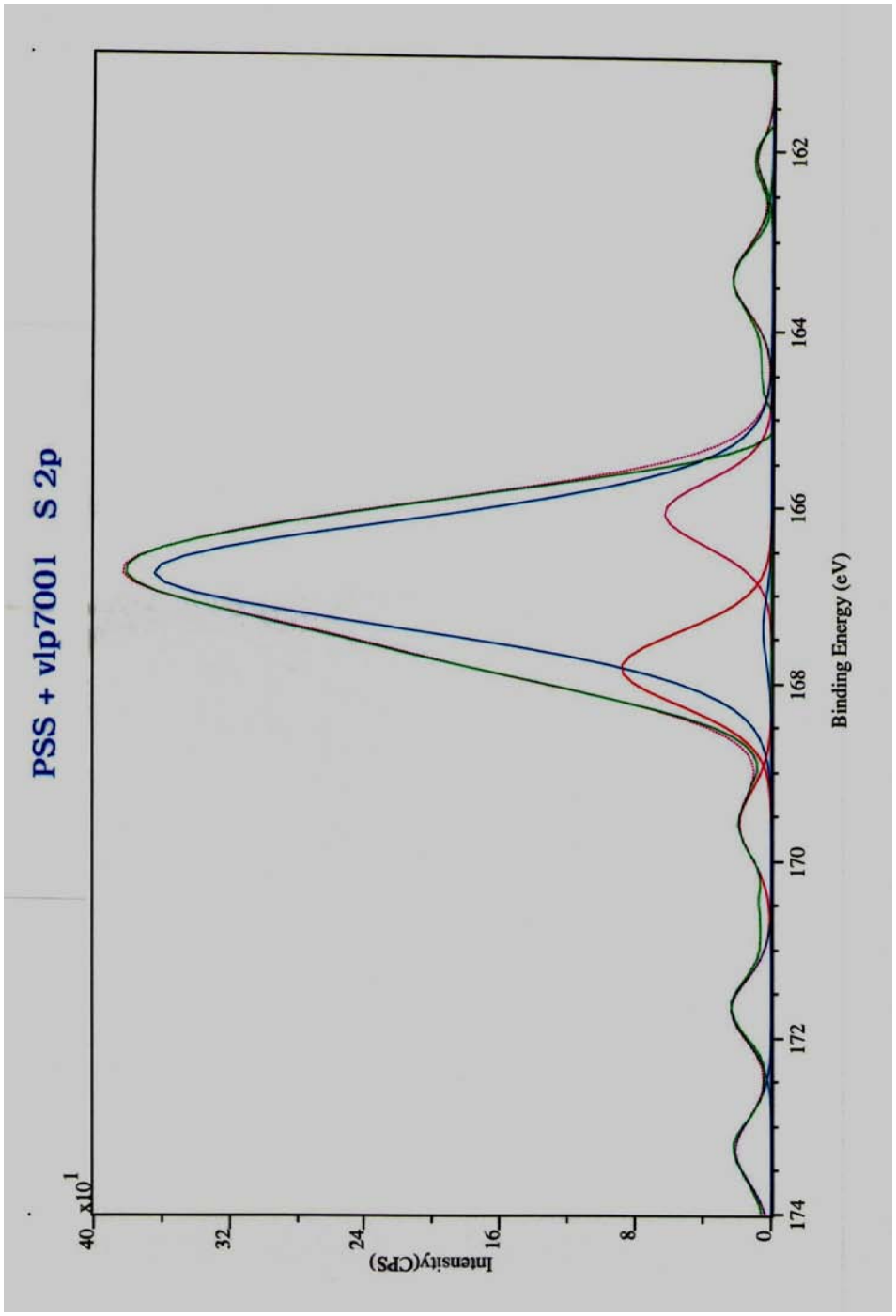

XPS high resolution spectral graph of Sulfur 2p vlp7001 TiO_2 with PSS/PDDA Sub-Coating

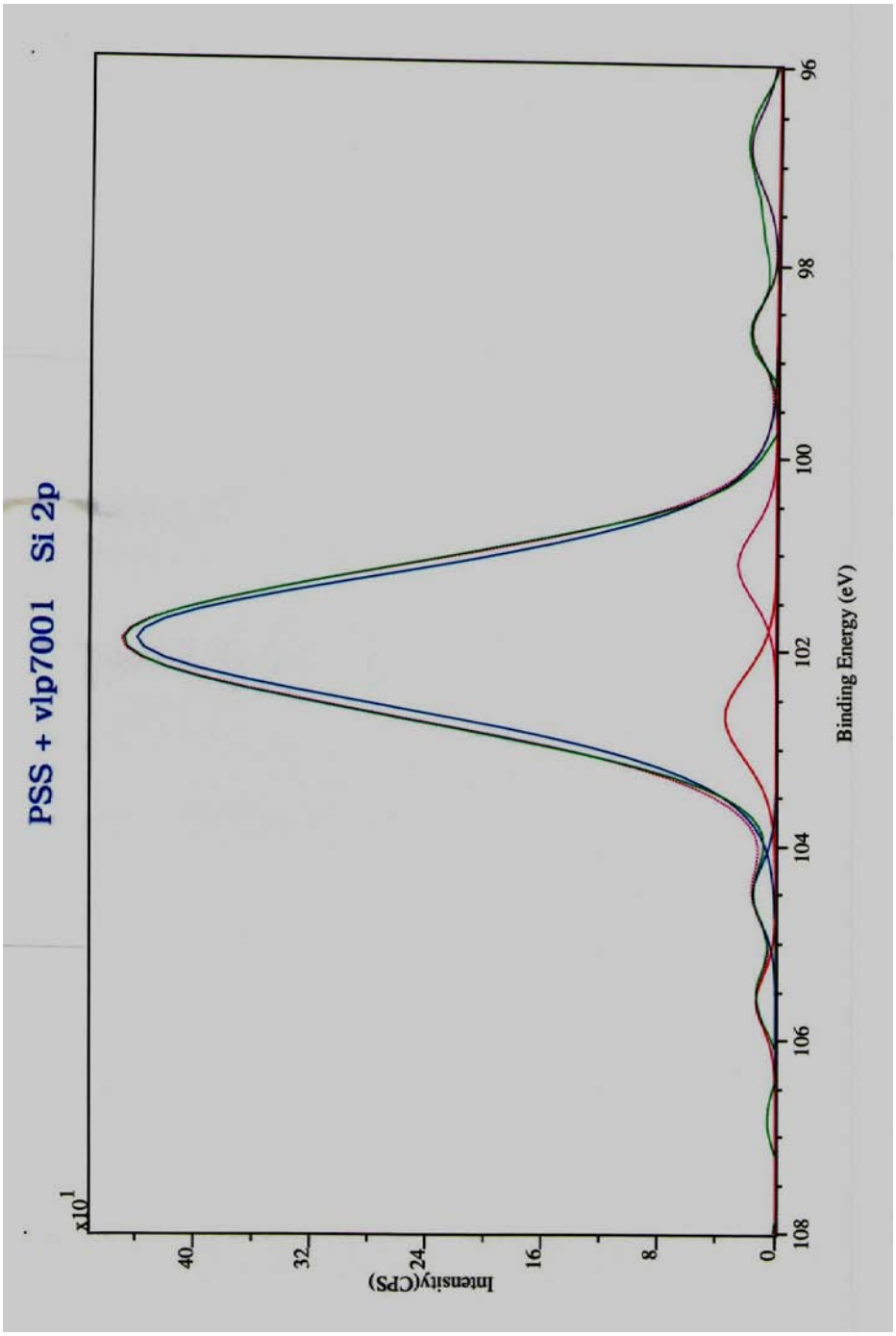

XPS high resolution spectral graph of Silicon 2p vlp7001 TiO_2 with PSS/PDDA Sub-Coating

XPS data table of Anatase TiO_2 with PSS/PDDA Sub-Coating

PSS + Anatase Quantification Report Thu Aug 20 13:37:14 2009

State #0 : Etch Time 0.00 seconds

Peak	Position BE (eV)	FWHM (eV)	Raw Area (CPS)	RSF	Atomic Mass	Atomic Conc %	Mass Conc %
Na 1s	1067.000	2.214	3968.1	1.685	22.990	6.34	8.89
O 1s	529.000	2.637	9611.1	0.780	15.999	25.40	24.78
Ti 2p	456.000	1.663	1488.9	2.001	47.878	1.49	4.35
N 1s	400.000	1.669	533.3	0.477	14.007	2.22	1.89
C 1s	283.000	2.046	7613.9	0.278	12.011	53.34	39.06
Cl 2p	197.000	1.848	1523.6	0.891	35.460	3.32	7.17
S 2p	167.000	2.434	488.9	0.668	32.065	1.42	2.78
Si 2p	102.000	2.306	1077.8	0.328	28.086	6.48	11.09

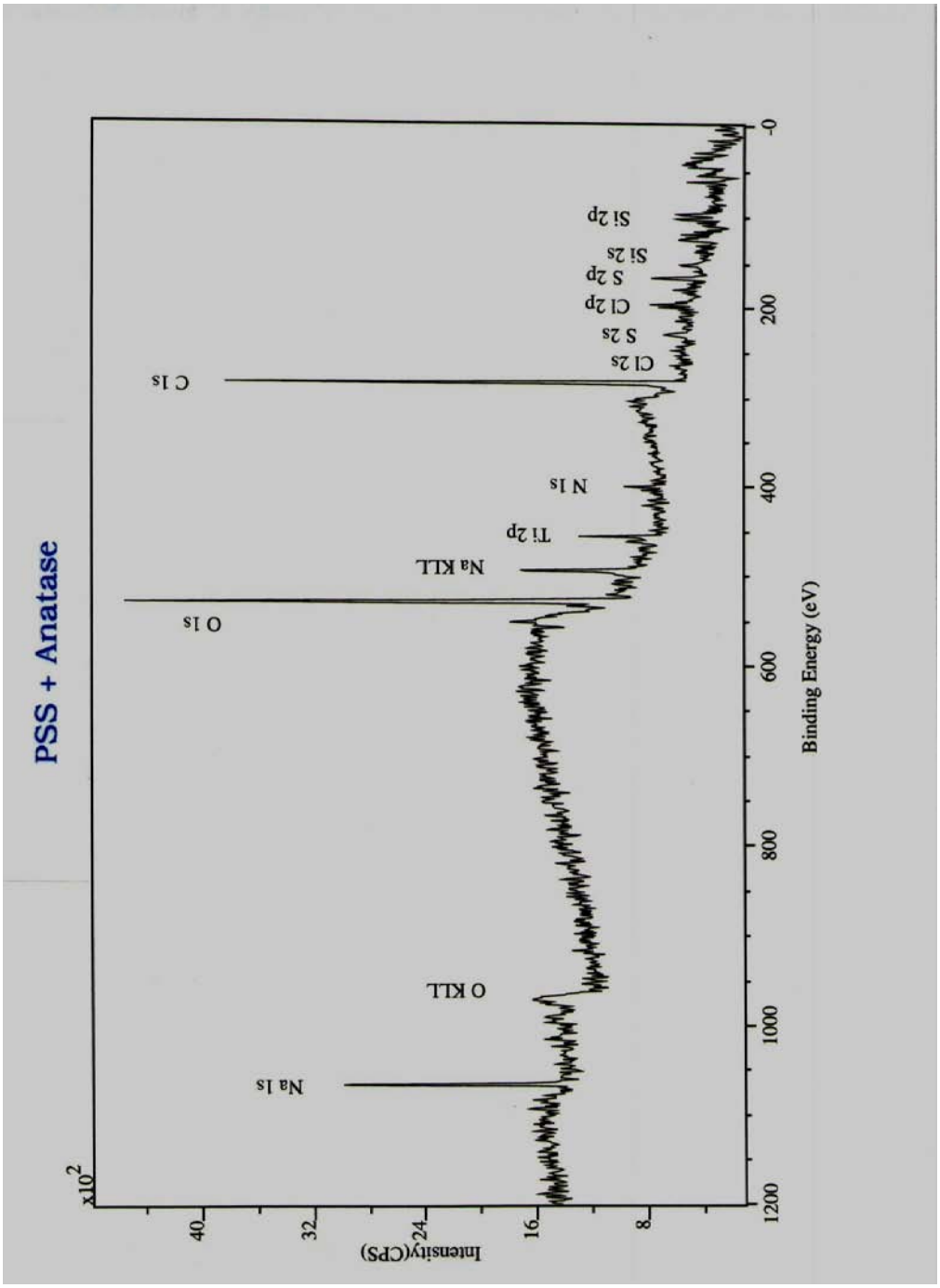

XPS spectral graph of Anatase TiO_2 with PSS/PDDA Sub-Coating

XPS high resolution data table of Anatase TiO_2 with PSS/PDDA Sub-Coating

PSS + Anatase — Quantification Report — Thu Aug 20 14:00:54 2009

State #0 : Etch Time 0.00 seconds

Peak	Position BE (eV)	FWHM (eV)	Raw Area (CPS)	RSF	Atomic Mass	Atomic Conc %	Mass Conc %
Na 1s 1	1066.690	1.316	3569.2	1.685	22.990	5.65	8.20
Na 1s 2	1065.974	0.874	446.6	1.685	22.990	0.71	1.03
Na 1s 3	1067.542	0.887	207.8	1.685	22.990	0.33	0.48
Na 1s 4	1071.305	1.121	132.7	1.685	22.990	0.21	0.30
O 1s 1	528.979	1.880	8497.0	0.780	15.999	22.26	22.47
O 1s 2	526.711	1.196	916.6	0.780	15.999	2.40	2.42
O 1s 3	530.061	1.165	549.7	0.780	15.999	1.44	1.45
O 1s 4	528.109	1.093	352.3	0.780	15.999	0.92	0.93
O 1s 5	529.800	0.958	104.6	0.780	15.999	0.27	0.28
O 1s 6	533.900	1.574	156.2	0.780	15.999	0.41	0.41
Ti 2p 1	455.800	1.160	944.3	2.001	47.878	0.94	2.83
Ti 2p 2	461.662	1.363	294.1	2.001	47.878	0.29	0.88
Ti 2p 3	455.200	0.831	70.0	2.001	47.878	0.07	0.21
Ti 2p 4	460.500	0.991	58.1	2.001	47.878	0.06	0.17
Ti 2p 5	456.400	0.785	43.1	2.001	47.878	0.04	0.13
Ti 2p 6	466.500	0.808	32.6	2.001	47.878	0.03	0.10
Ti 2p 7	464.438	1.897	50.3	2.001	47.878	0.05	0.15
Ti 2p 8	451.500	0.659	19.4	2.001	47.878	0.02	0.06
N 1s 1	400.317	1.121	390.7	0.477	14.007	1.61	1.42
N 1s 2	404.650	1.137	92.2	0.477	14.007	0.38	0.34
N 1s 3	402.500	0.669	22.1	0.477	14.007	0.09	0.08
N 1s 4	407.400	0.620	15.0	0.477	14.007	0.06	0.05
N 1s 5	397.850	1.040	33.6	0.477	14.007	0.14	0.12
N 1s 6	395.700	0.933	24.0	0.477	14.007	0.10	0.09
N 1s 7	399.700	0.667	14.7	0.477	14.007	0.06	0.05
N 1s 8	406.667	1.035	22.3	0.477	14.007	0.09	0.08
N 1s 9	401.000	0.813	14.9	0.477	14.007	0.06	0.05
N 1s 10	403.700	0.569	10.5	0.477	14.007	0.04	0.04
C 1s 1	283.072	1.175	4585.8	0.278	12.011	31.84	24.13
C 1s 2	284.076	1.594	2409.6	0.278	12.011	16.73	12.68
C 1s 3	282.369	0.633	450.8	0.278	12.011	3.13	2.37
C 1s 4	285.020	1.211	279.2	0.278	12.011	1.94	1.47
Cl 2p 1	196.200	1.309	144.0	0.891	35.460	0.31	0.70
Cl 2p 2	197.983	1.601	59.6	0.891	35.460	0.13	0.29
Cl 2p 3	201.750	0.745	17.9	0.891	35.460	0.04	0.09
Cl 2p 4	204.500	0.892	19.2	0.891	35.460	0.04	0.09
Cl 2p 5	194.234	0.601	7.8	0.891	35.460	0.02	0.04
Cl 2p 6	192.367	0.975	15.7	0.891	35.460	0.03	0.08
Cl 2p 7	199.399	0.655	7.7	0.891	35.460	0.02	0.04
Cl 2p 8	191.400	0.608	8.2	0.891	35.460	0.02	0.04
Cl 2p 9	203.100	1.014	12.1	0.891	35.460	0.03	0.06
Cl 2p 10	200.750	0.776	10.6	0.891	35.460	0.02	0.05
Cl 2p 11	193.784	0.618	7.4	0.891	35.460	0.02	0.04
Cl 2p 12	197.100	0.587	2.8	0.891	35.460	0.01	0.01
Cl 2p 13	201.800	0.549	2.6	0.891	35.460	0.01	0.01
Cl 2p 14	201.800	0.622	3.0	0.891	35.460	0.01	0.01
S 2p 1	166.644	1.396	605.4	0.668	32.065	1.74	3.53
S 2p 2	167.701	1.143	242.7	0.668	32.065	0.70	1.41
S 2p 3	165.959	0.679	22.7	0.668	32.065	0.07	0.13
S 2p 4	171.898	0.824	25.4	0.668	32.065	0.07	0.15
S 2p 5	170.155	0.846	21.7	0.668	32.065	0.06	0.13
S 2p 6	171.120	0.634	9.8	0.668	32.065	0.03	0.06
S 2p 7	162.102	1.392	19.6	0.668	32.065	0.06	0.11
Si 2p 1	101.700	1.552	560.9	0.328	28.086	3.34	5.92
Si 2p 2	102.500	1.002	60.1	0.328	28.086	0.36	0.63

XPS high resolution data table of Anatase TiO_2 with PSS/PDDA Sub-Coating (Continued)

Si 2p 3	100.800	0.906	34.7	0.328	28.086	0.21	0.37
Si 2p 4	108.300	1.089	15.6	0.328	28.086	0.09	0.16
Si 2p 5	104.600	0.674	8.1	0.328	28.086	0.05	0.09
Si 2p 6	105.700	0.739	8.8	0.328	28.086	0.05	0.09
Si 2p 7	107.100	0.787	7.6	0.328	28.086	0.05	0.08
Si 2p 8	101.100	0.747	5.4	0.328	28.086	0.03	0.06
Si 2p 9	97.400	0.675	4.9	0.328	28.086	0.03	0.05

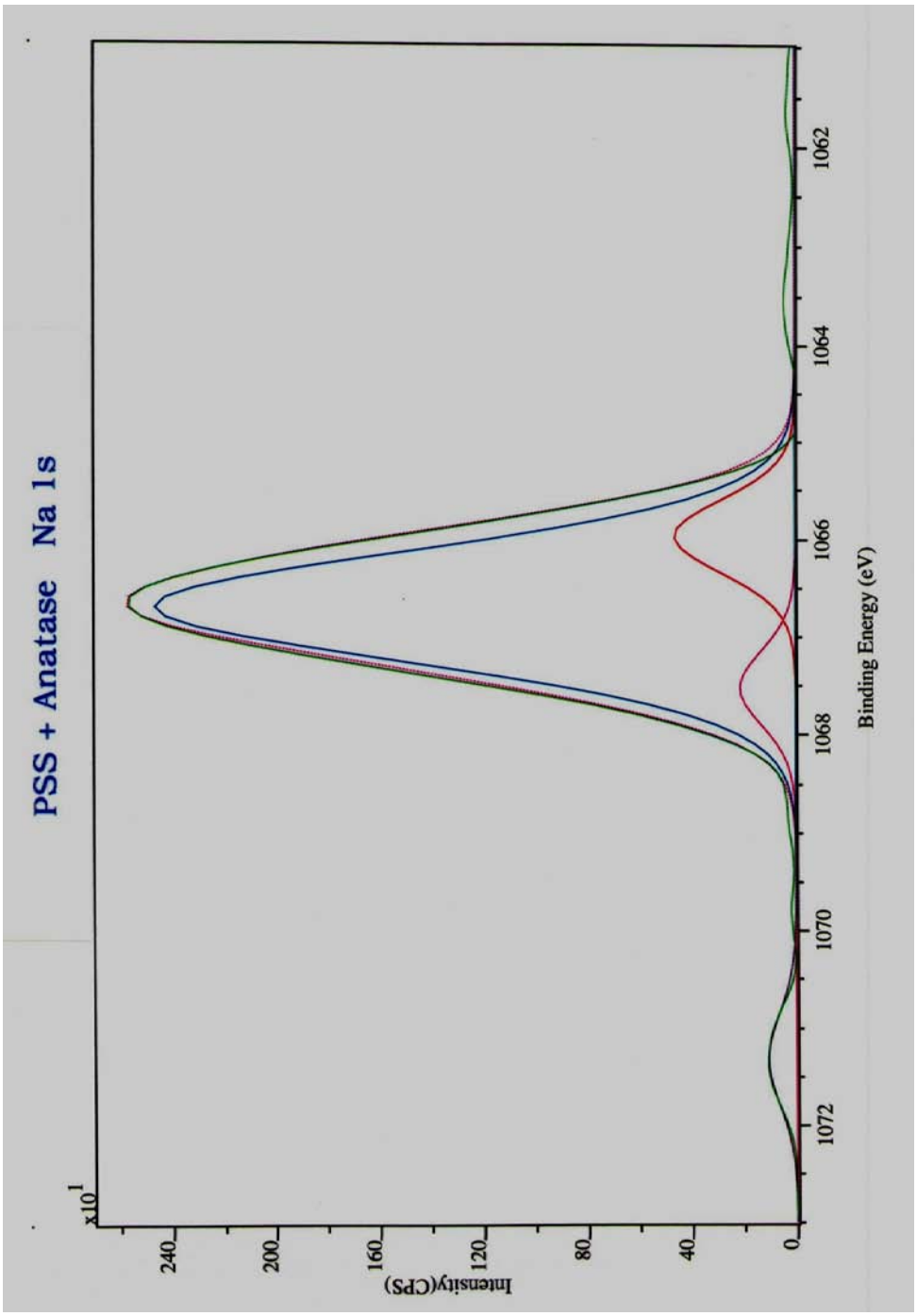

XPS high resolution spectral graph of Sodium 1s in Anatase TiO_2 with PSS/PDDA Sub-Coating

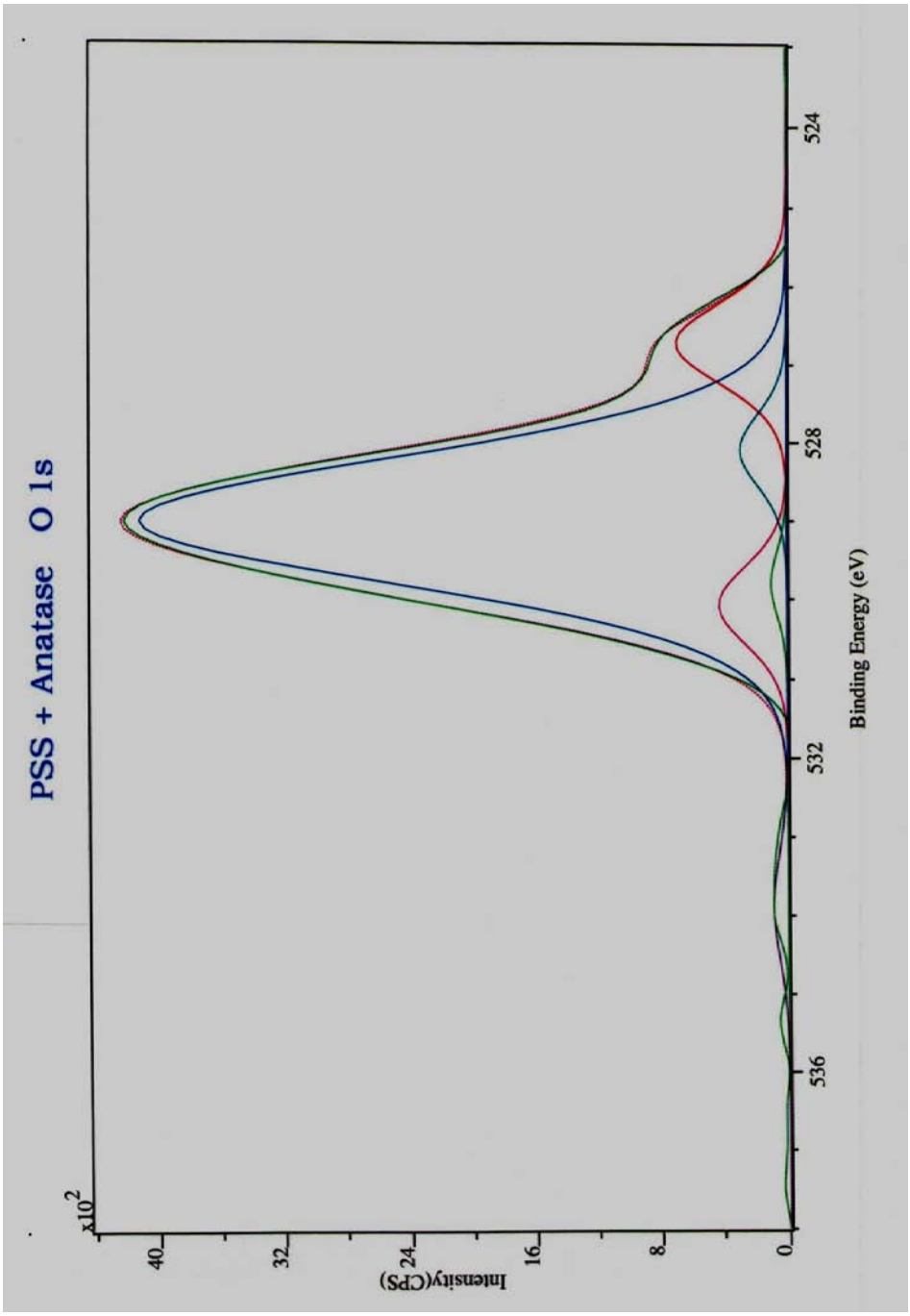

XPS high resolution spectral graph of Oxygen 1s in Anatase TiO_2 with PSS/PDDA Sub-Coating

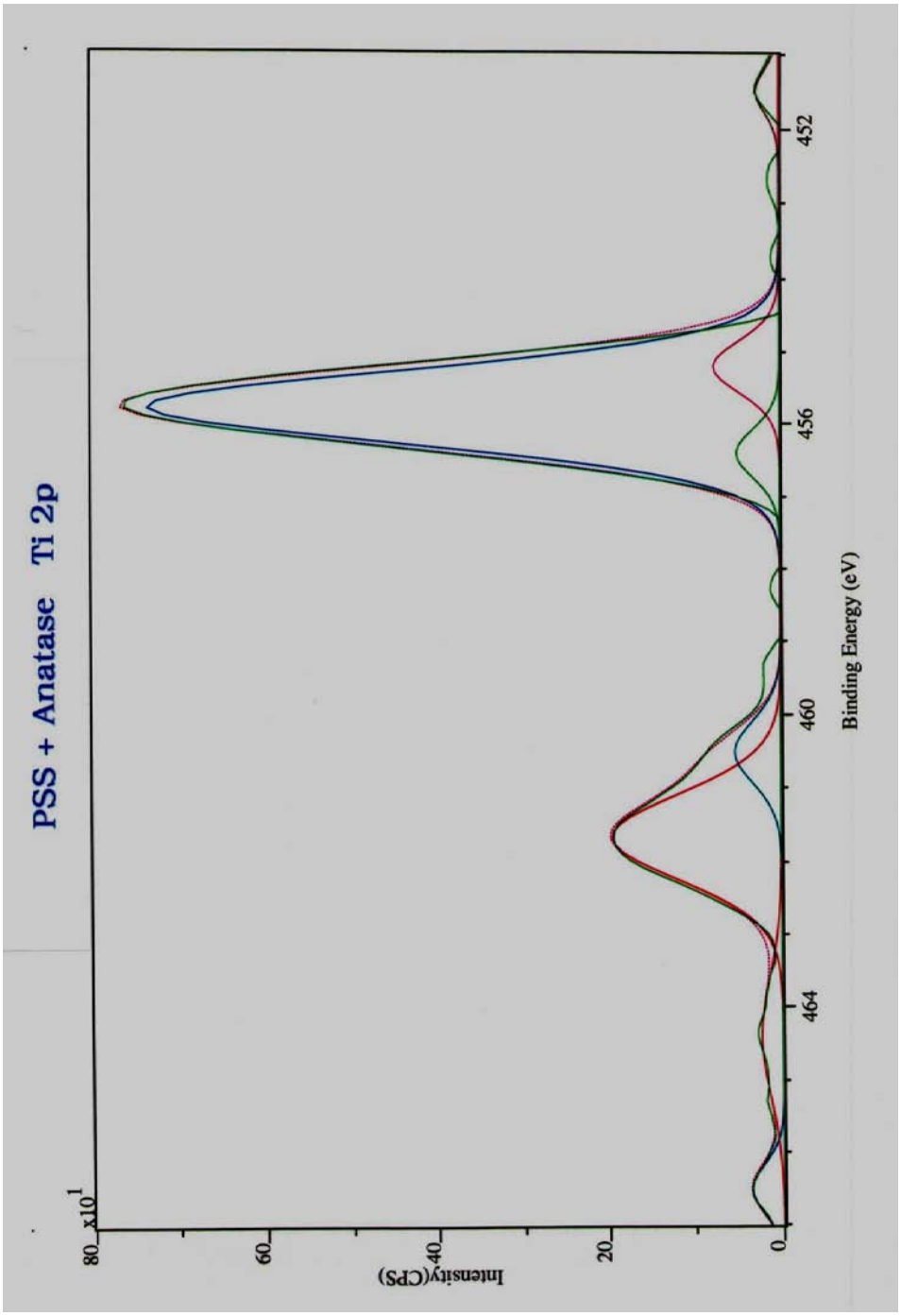

XPS high resolution spectral graph of Titanium 2p in Anatase TiO_2 with PSS/PDDA Sub-Coating

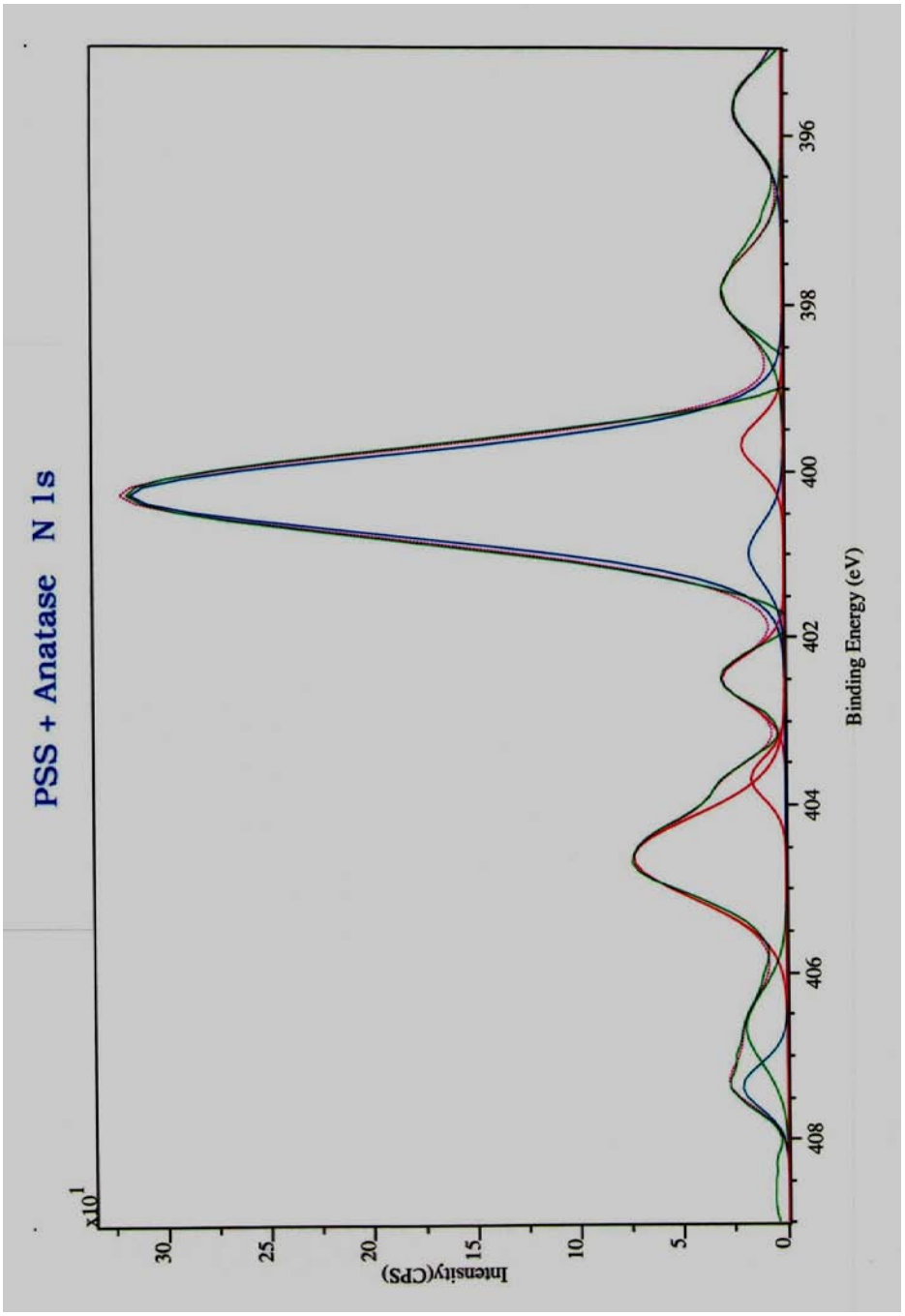

XPS high resolution spectral graph of Nitrogen 1s in Anatase TiO_2 with PSS/PDDA Sub-Coating

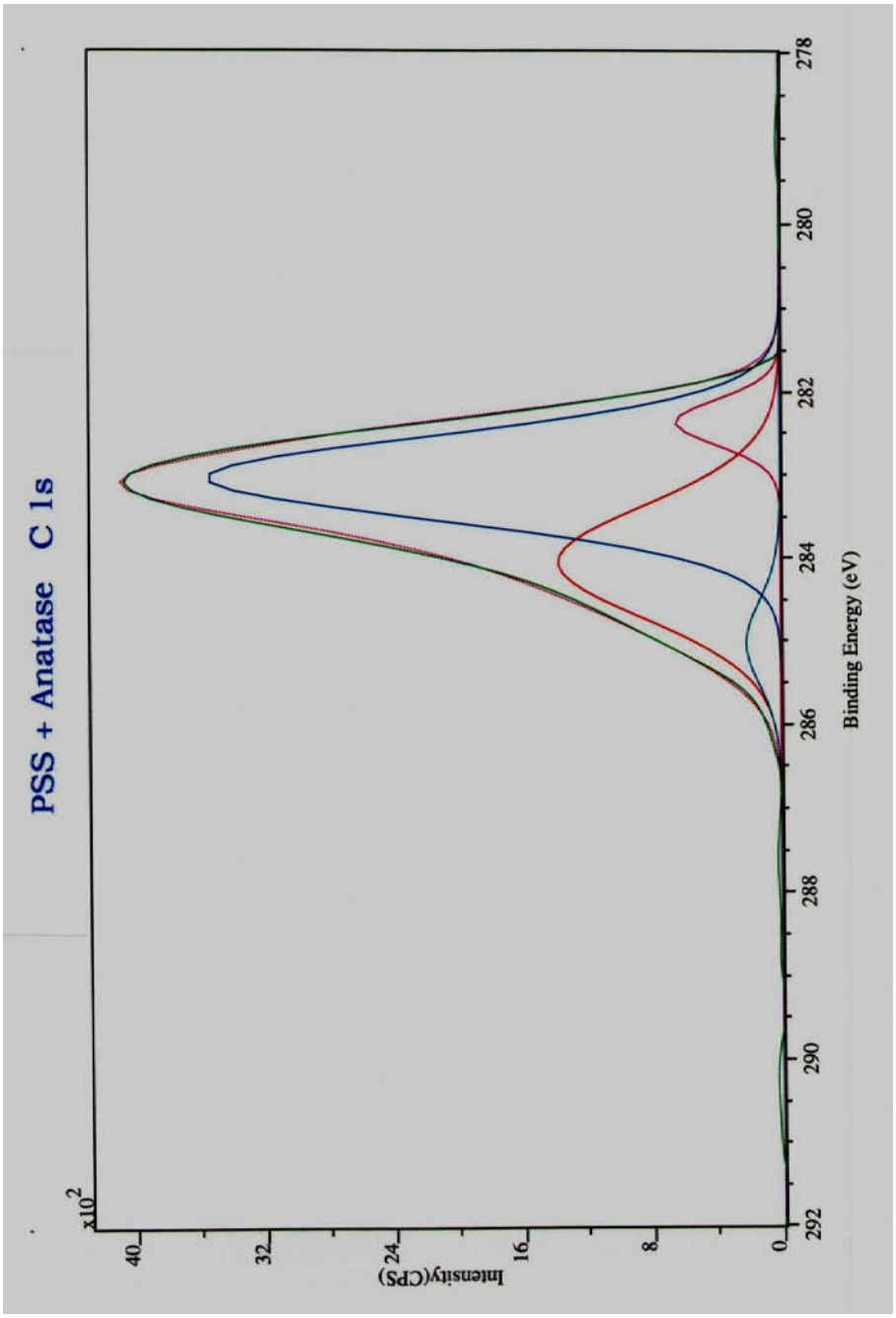

XPS high resolution spectral graph of Carbon 1s in Anatase TiO_2 with PSS/PDDA Sub-Coating

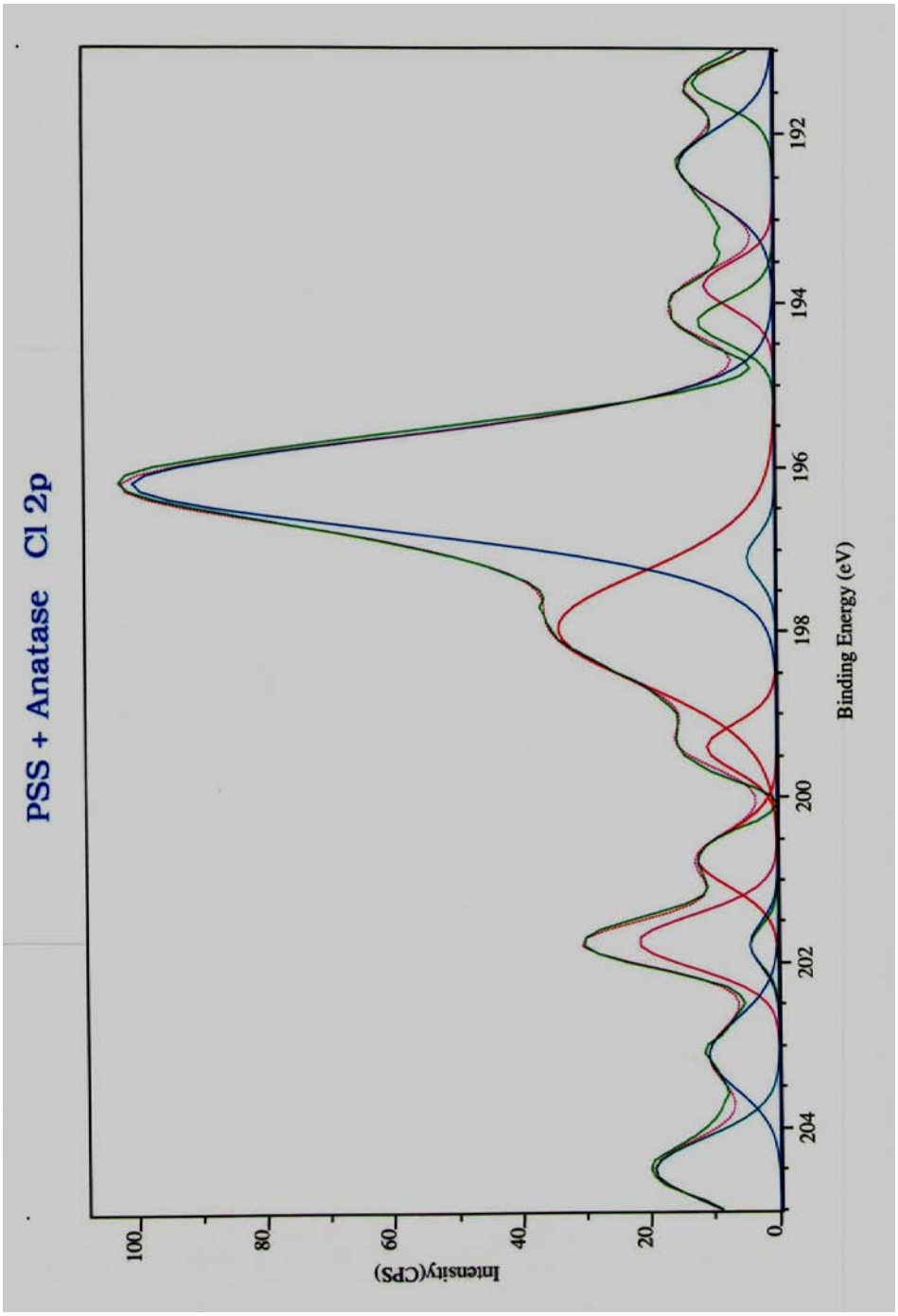

XPS high resolution spectral graph of Chlorine 2p in Anatase TiO_2 with PSS/PDDA Sub-Coating

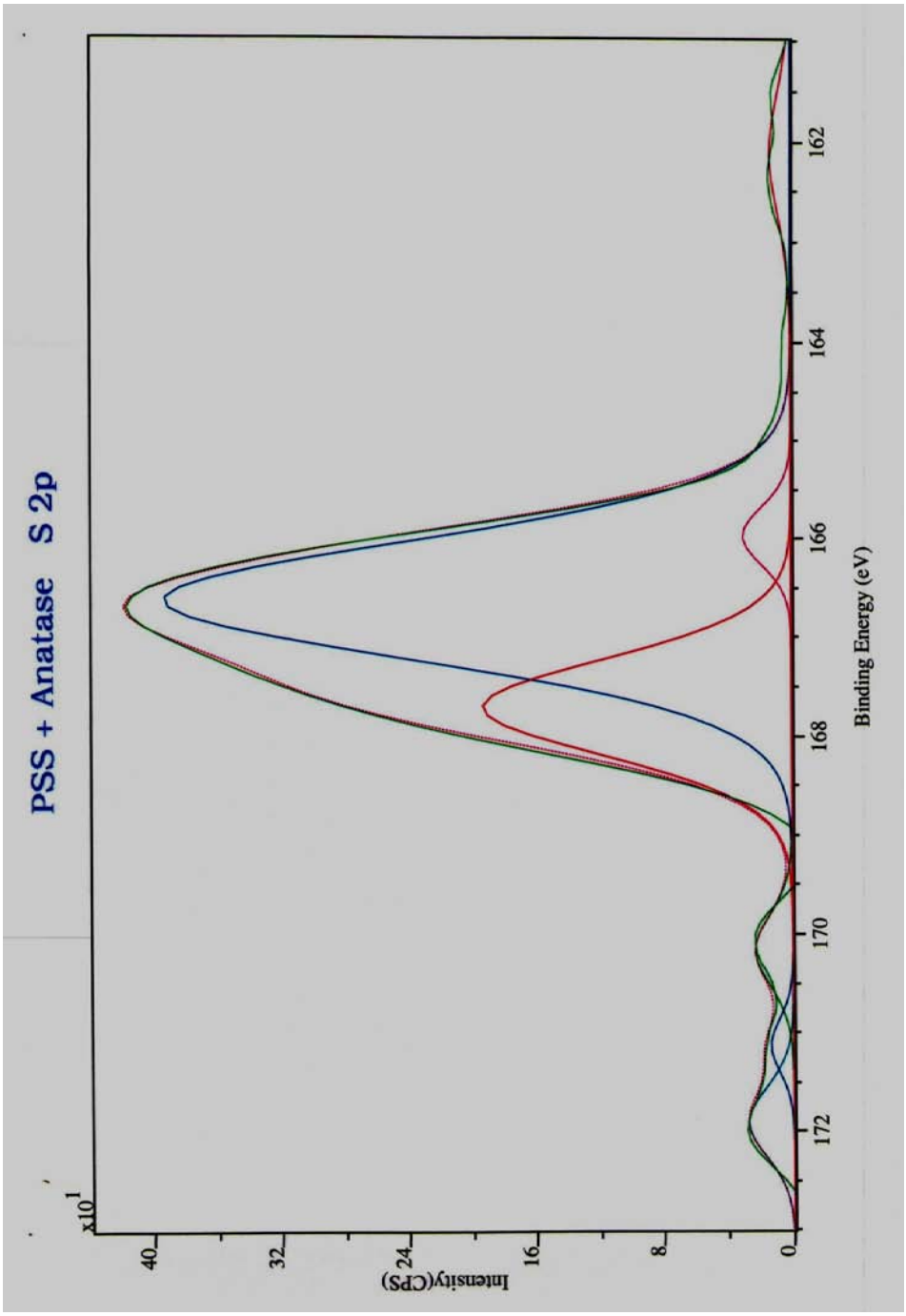

XPS high resolution spectral graph of Sulfur 2p in Anatase TiO_2 with PSS/PDDA Sub-Coating

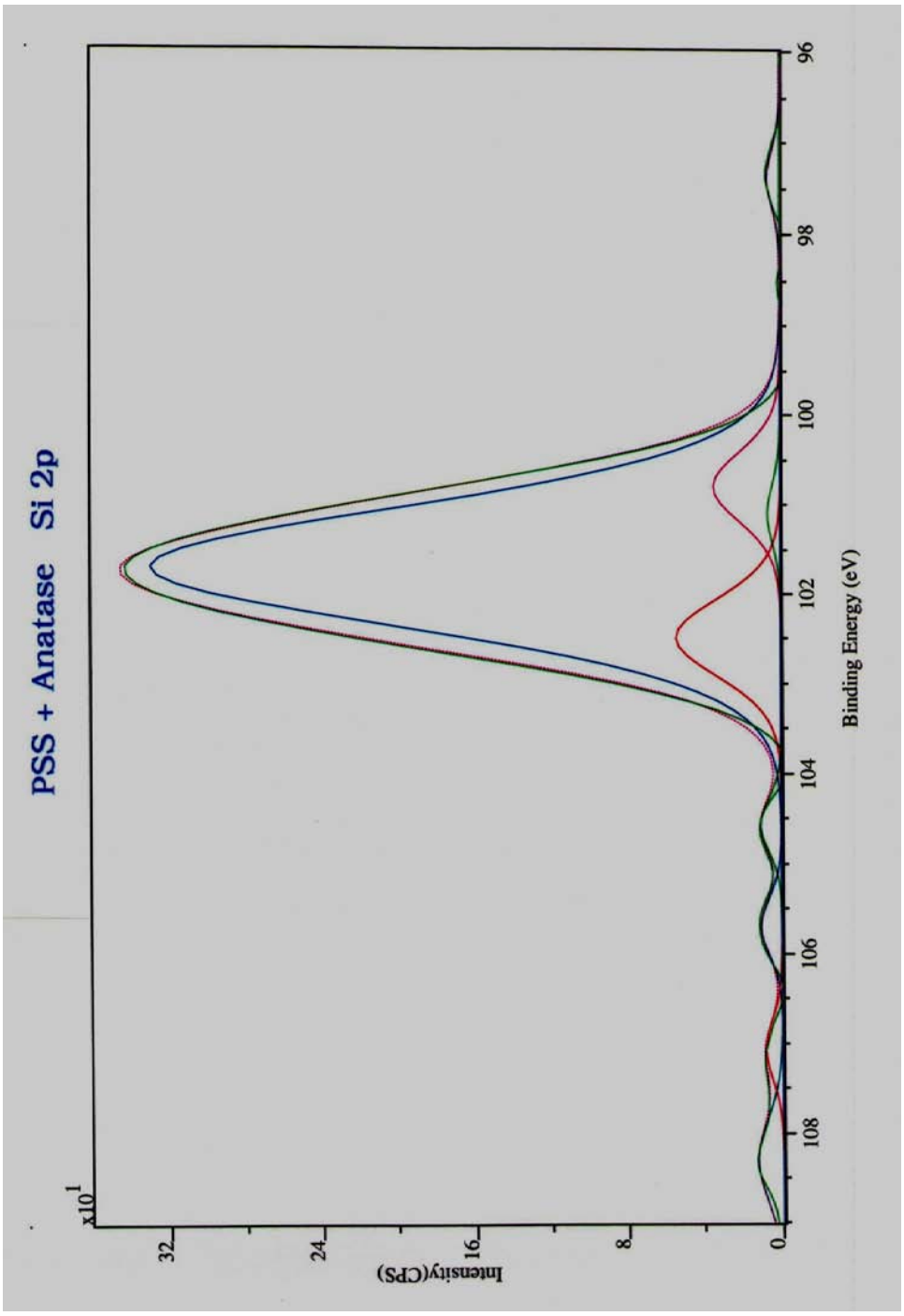

XPS high resolution spectral graph of Silicon 2p in Anatase TiO_2 with PSS/PDDA Sub-Coating

APPENDIX C

XRD SPECTRA GRAPHS OF TITANIA WITH P OR B SUB-COATINGS

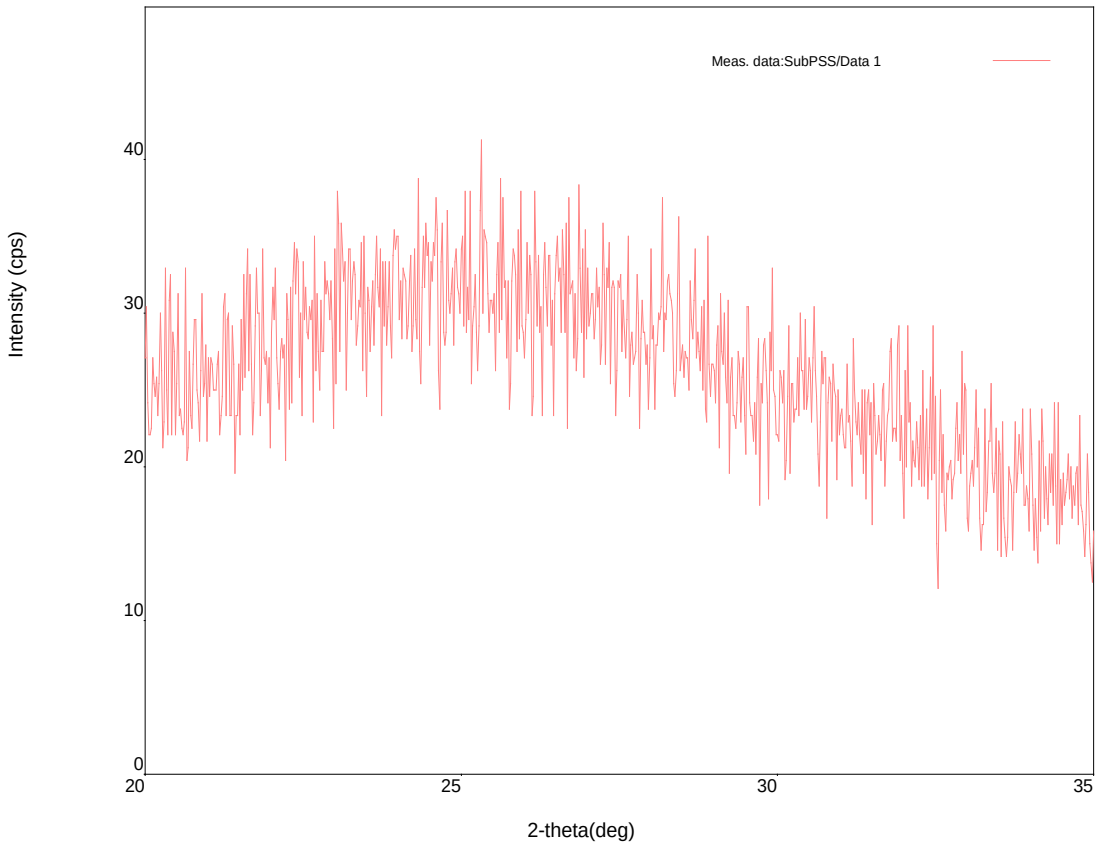

XRD spectral graph of PSS/PDDA alone on glass cover slip

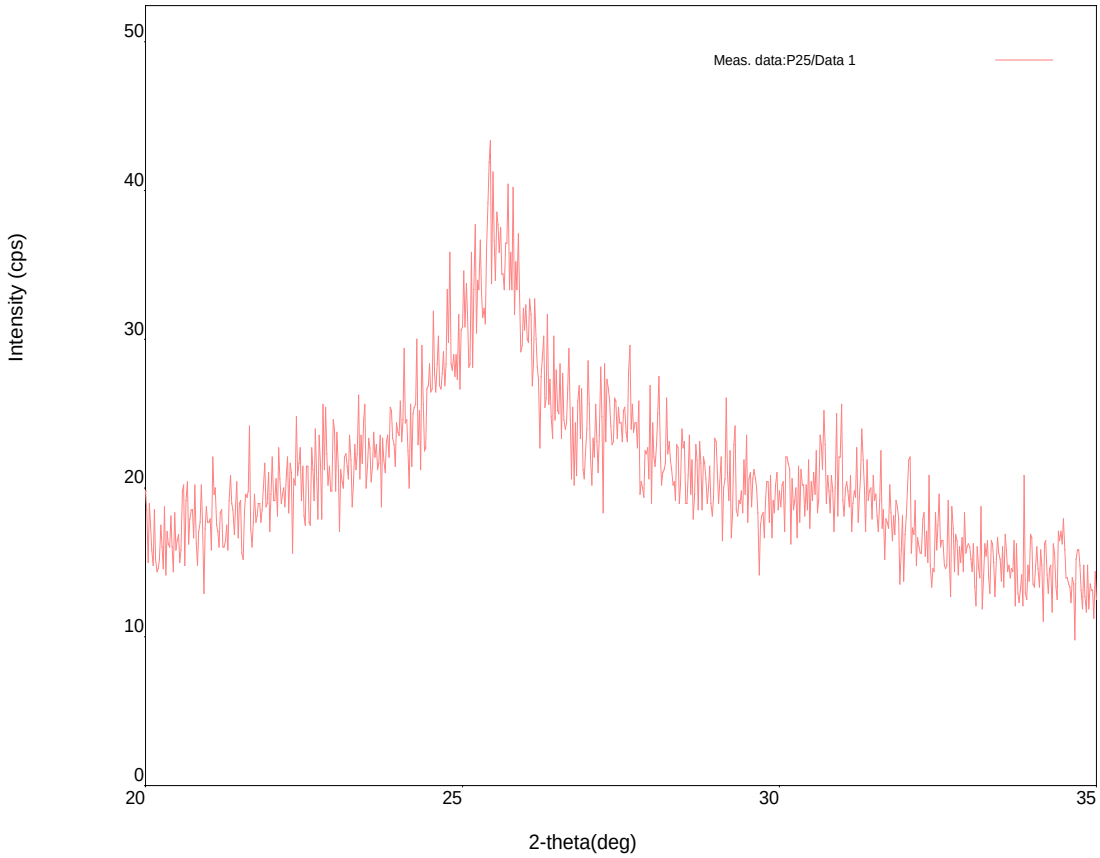

XRD spectral graph of PSS/PDDA with P25 TiO_2 on glass cover slip

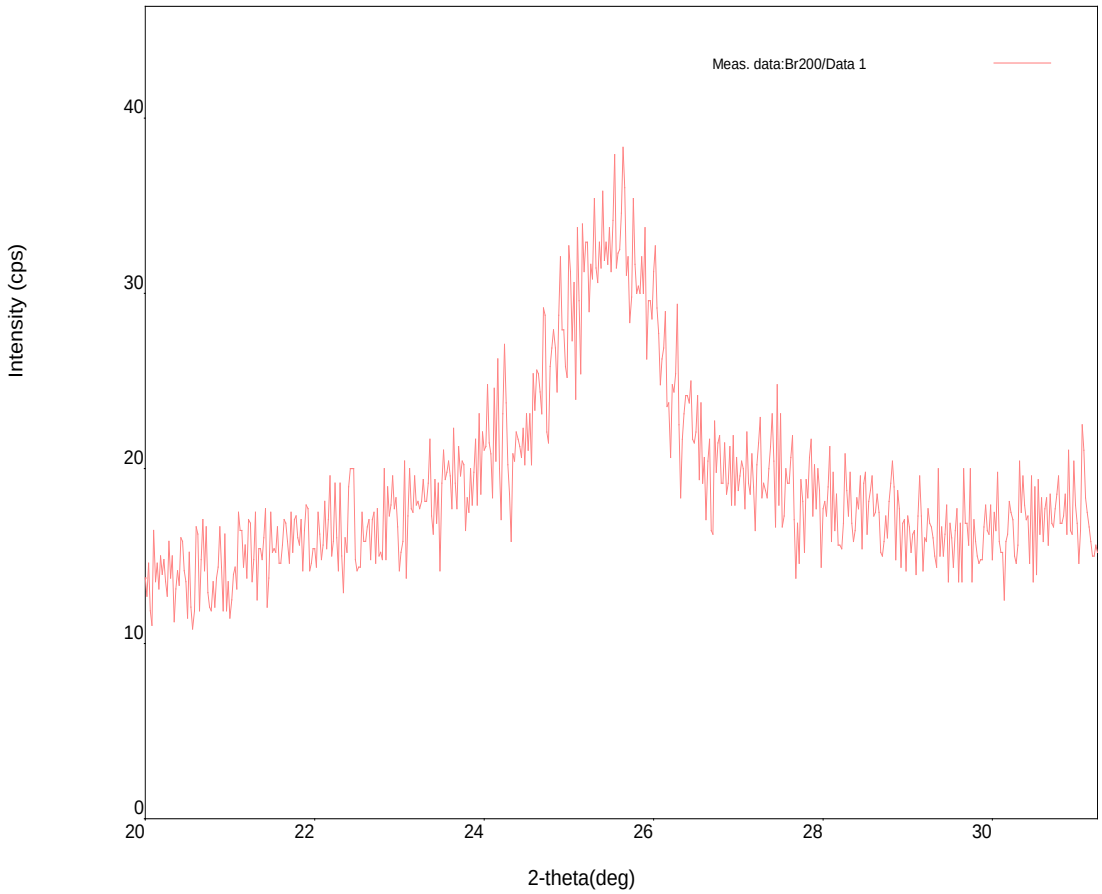

XRD spectral graph of PSS/PDDA with Br200 TiO_2 on glass cover slip

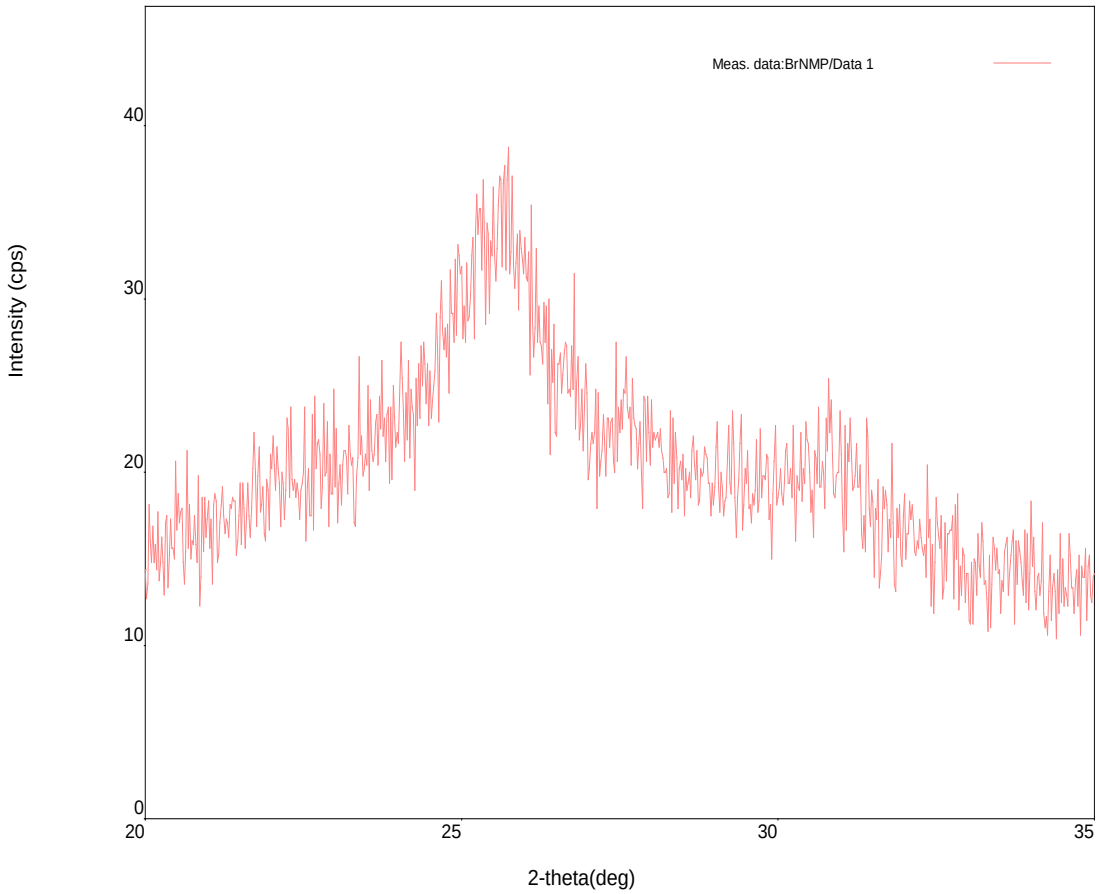

XRD spectral graph of PSS/PDDA with BrNMP TiO_2 on glass cover slip

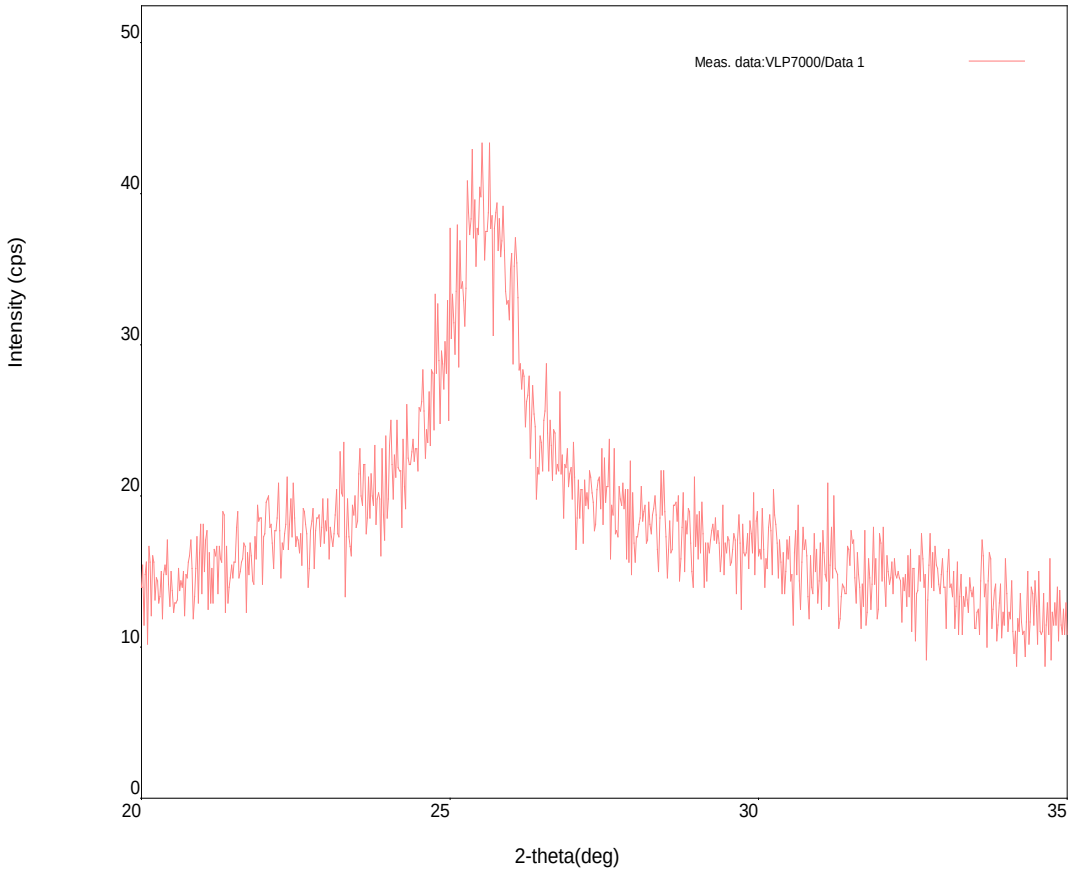

XRD spectral graph of PSS/PDDA with BrNMP TiO_2 on glass cover slip

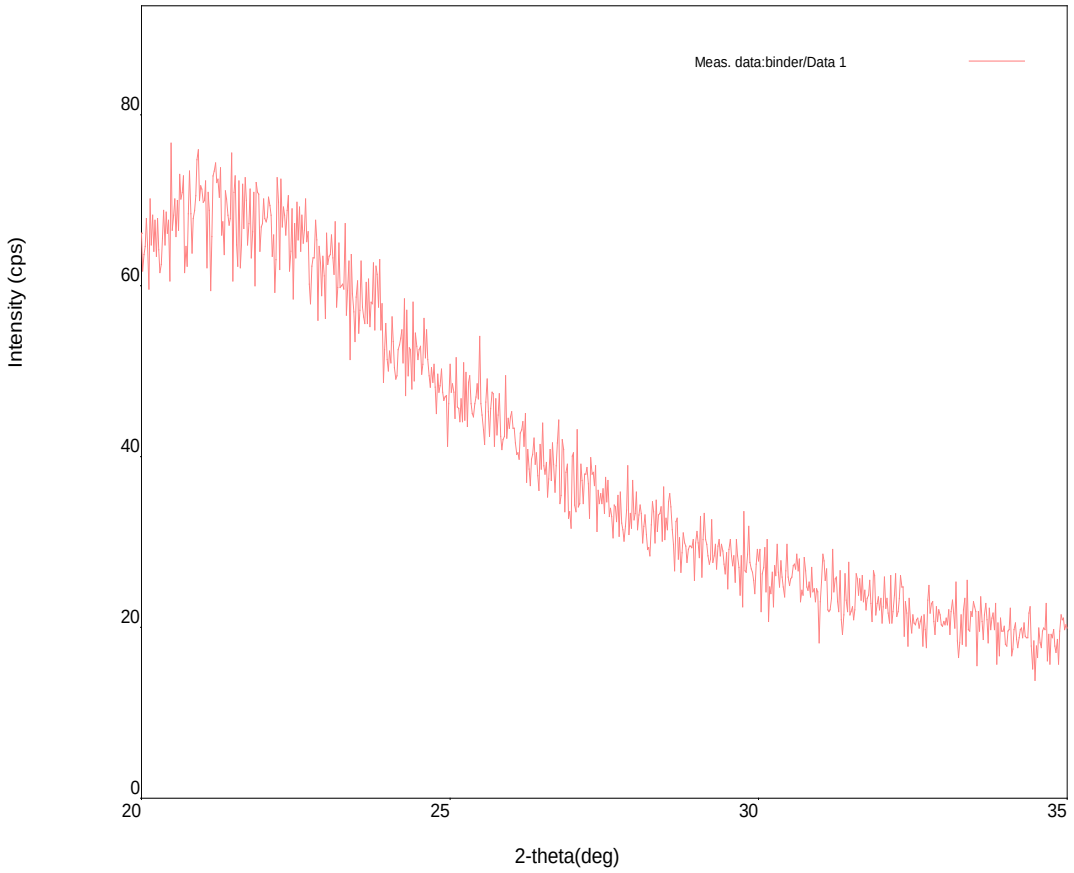

XRD spectral graph of Binder alone on glass cover slip

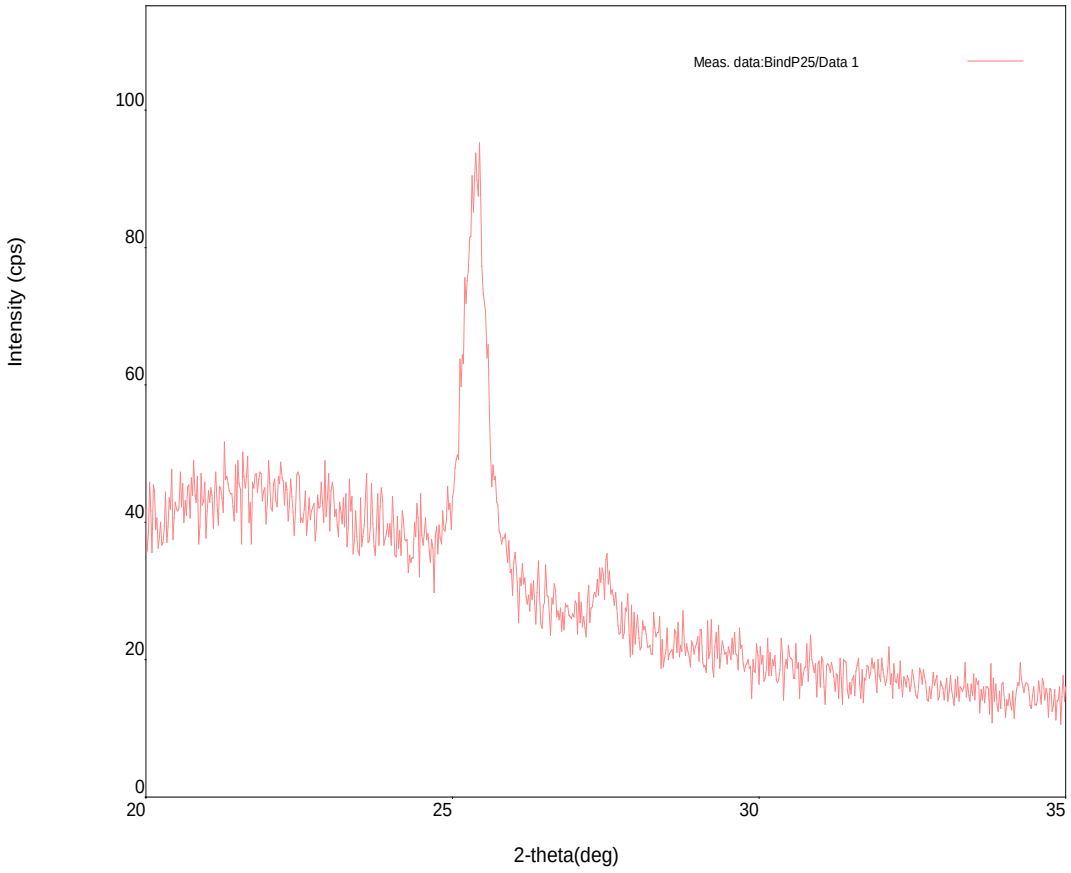

XRD spectral graph of Binder with P25 TiO_2 on glass cover slip

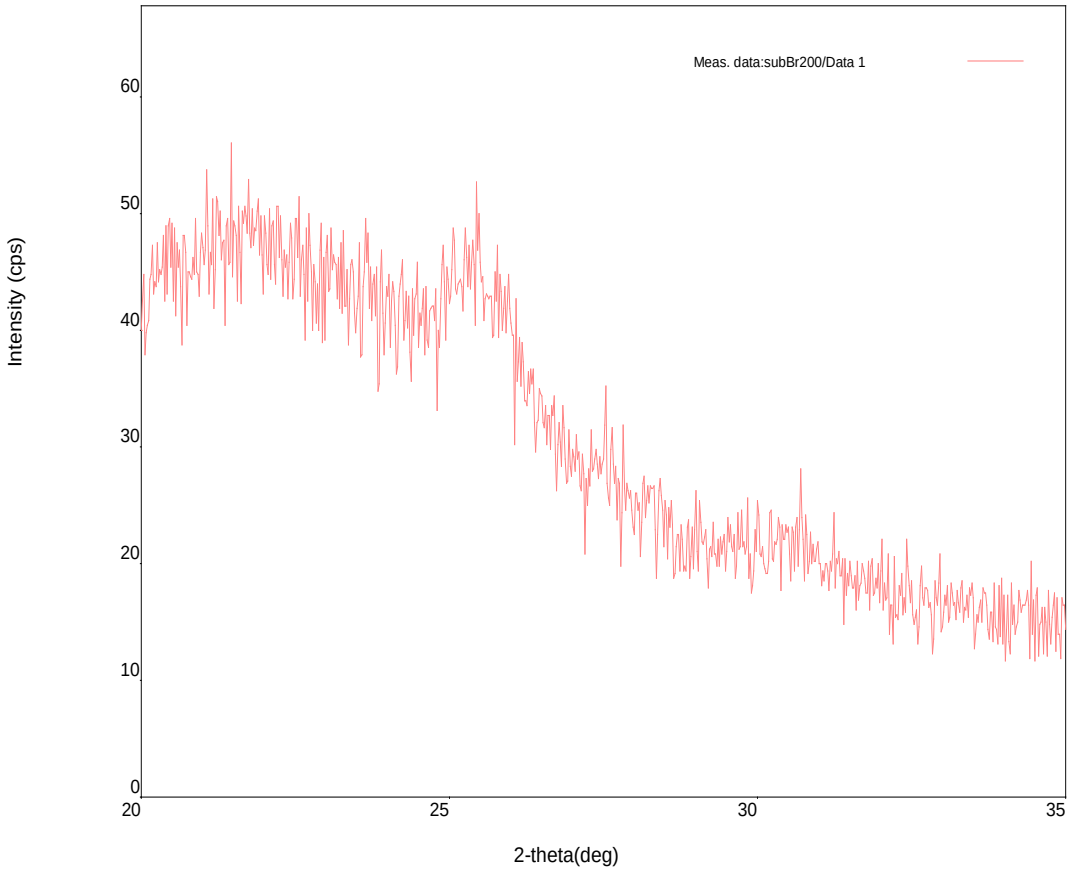

XRD spectral graph of Binder with Br200 TiO_2 on glass cover slip

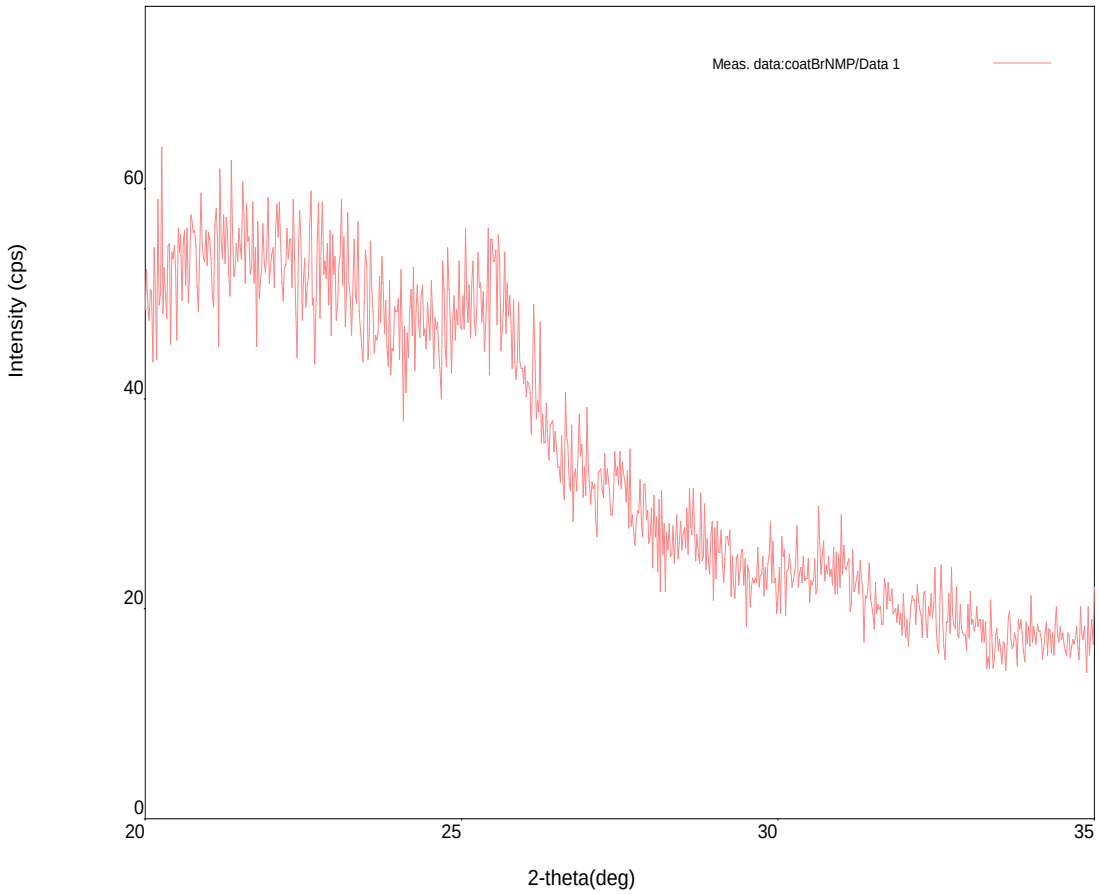

XRD spectral graph of Binder with BrNMP TiO_2 on glass cover slip

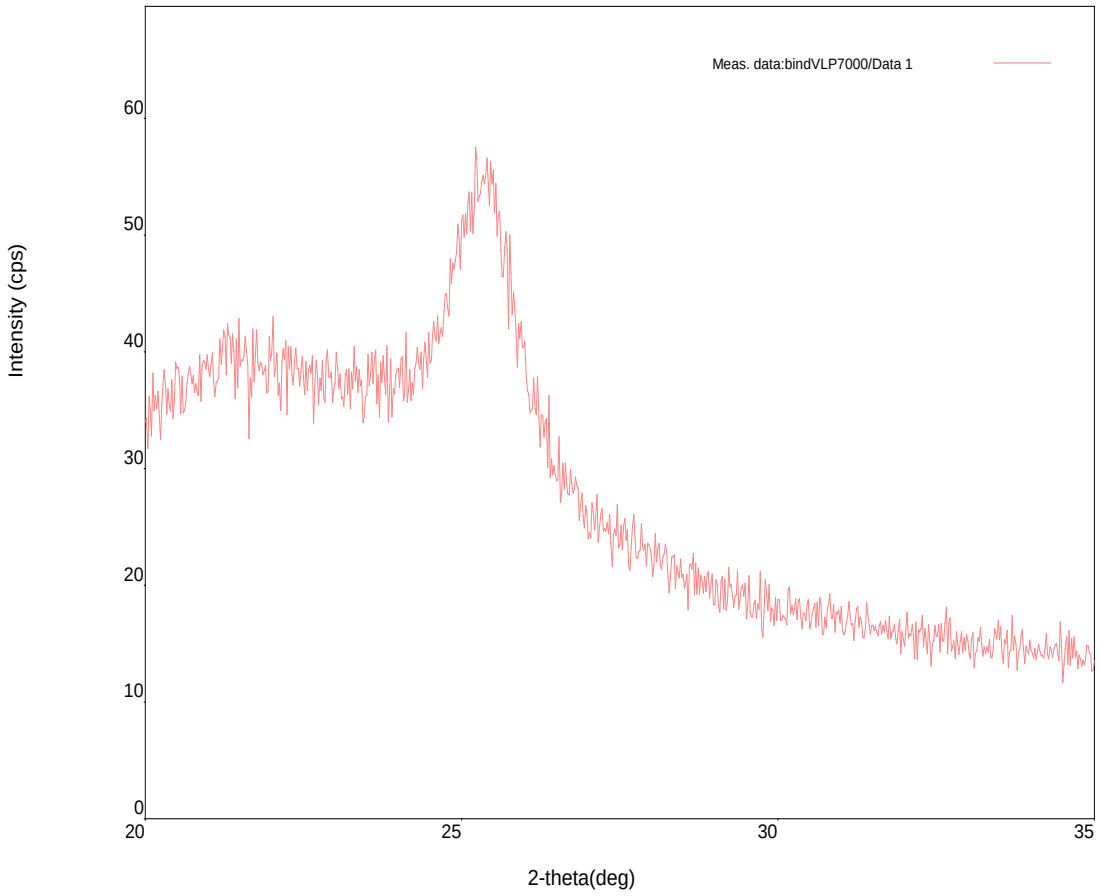

XRD spectral graph of Binder with vlp7000 TiO_2 on glass cover slip

APPENDIX D

P SUB-COATING STRUCTURES AND COMPONENTS

Poly(diallyldimethylammonium chloride) solution (PDDA)

Line formula: $(C_8H_{16}ClN)_n$

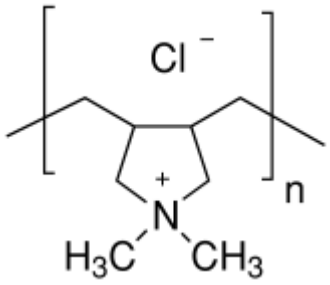

Poly(4-styrenesulfonic acid) solution (PSS)

Line formula: $(C_8H_8O_3S)_n$